THESIS

ON

PARAMETRIC APPROACH TO OPTIMIZE SUBMERGED ARC WELDING PROCESS FOR HSLA STEEL

Submitted in partial fulfillment of the requirement for the award of

degree of

MASTER OF ENGINEERING
IN
PRODUCTION & INDUSTRIAL ENGINEERING

Submitted by

GIANENDER
ROLL NO: 801182009

Under the Guidance of

Dr. AJAY BATISH
Professor
Mechanical Engineering Department

MECHANICAL ENGINEERING DEPARTMENT
THAPAR UNIVERSITY
PATIALA-147004, INDIA

JULY-2013

DECLARATION

I hereby declare that work done in this Thesis Report entitled, "**PARAMETRIC APPROACH TO OPTIMIZE SUBMERGED ARC WELDING PROCESS FOR HSLA STEEL**" submitted towards partial fulfilment of requirement for award of **Master of Engineering** degree in **Production & Industrial Engineering** in **Mechanical Engineering Department** of **Thapar University, Patiala,** is an authentic record of work carried out by me under the supervision and guidance of **Dr. AJAY BATISH, Professor & Head** of **Mechanical Engineering Department, Thapar University, Patiala.**

This matter embodied in this report has not been submitted in part or full to any other university or institute for the award of any degree.

Gianender

GIANENDER

This is to certify that above declaration made by the student concerned is correct to the best of my knowledge & belief.

DR. AJAY BATISH
PROFESSOR-MED
THAPAR UNIVERSITY, PATIALA

Countersigned by:

DR. AJAY BATISH
PROFESSOR & HEAD-MED
THAPAR UNIVERSITY, PATIALA

DR. S.K. MOHAPATRA
DEAN, ACADEMIC AFFAIRS
THAPAR UNIVERSITY, PATIALA

ACKNOWLEDGEMENT

I am highly grateful to the authorities of Thapar University, Patiala for providing this opportunity to carry out the thesis work.

I express my deep gratitude and respects to my supervisor ***Dr. Ajay Batish, Professor of Mechanical Engineering Department, Thapar University****,* ***Patiala*** *for his keen interest and valuable guidance, strong motivation and constant encouragement during the course of the work. I thank him for his great patience, constructive criticism and myriad useful suggestions apart from invaluable guidance to me.*

I also mention special thank to ***Mr. Anirban Bhattacharya****,* ***Assistant Professor of Mechanical Engineering Department, Thapar University****,* ***Patiala*** *for his technical and all other support extended to us. I would like to thank* ***Dr. O.P Pandey, Senior Professor of Material Science Department, Thapar University, Patiala*** *for helping me in metallurgical aspects of my research apart from their valuable time.*

I am highly grateful to the authorities of ***Defence Research & Development Organisation (DRDO)*** *and* ***Defence Material Research Laboratory (DMRL)****, Hyderabad for the support related to this work. I am also thankful* ***to Dr. S. Sankaran, Director, DMRL, Hyderabad*** *for providing the material used for the present study. I also thank to P.I. / Co-P.I. of DRDO sponsored project for providing me the financial support as 'Project Assistant' under the same project.*

The non teaching staff ***Mr. Mohinder Suri, Mr. Surinder kumar Tathgir, Mr. Lalit kumar Mr. Rath, Mr. Roashan, Mr. Rajinder, Mr. A. S. Cheema, Mr. Manoj, Mr. Narender, Mr. Sukhbir , Mr. Deshraj*** *deserve special thanks for their help during this period of this work.A would like to thank my friend* ***Manish Garg, Anupam Thakur, Geeta Bhatt, Mayank Singla, Parvesh Aggarwal, Gurjinder, Pardeep Sangwan*** *for their valorous help and co-operation. I am also thankful to faculty members of Mechanical Engineering Department and all the workshop staff of Department of Thapar University, Patiala for their everlasting support.*

GIANENDER

REGISTRATION NO. 801182009

ABSTRACT

The aim of the present work was to investigate the effect of various input process parameters i.e. current, travel speed, electrode diameter, flux composition, preheating of work piece, and electrode stick-out on desired response in submerged arc welding. The response measured were changes in quality of welds by radiography, impact strength, toughness at different temperature, micro hardness, weld bead height & width, chemical composition and metallurgical analysis of HSLA Steel. The effect of all the input parameters on the output response has been analyzed using the Taguchi experimental analysis. Bead geometry of the weld region was measured and bead width was mainly dependent on preheat temperature and travel speed. Bead height for HSLA steel was dependent on current and type of flux. Tensile strength of the welded specimen were studied and found that electrode diameter, welding current were the most dependent factors leading to changes in tensile strength. The tensile strength tended to increase significantly with the increase in electrode diameter from 3.2 to 4 mm and when increase in current from 450 to 500 A. Toughness at room temperature of the welded specimen were studied and found that electrode diameter, preheat temperature were the most significant factors and higher toughness at room temperature was observed when electrode diameter should be 4 mm, electrode stick-out should be 25 mm, welding current should be 450 A, preheat temperature should be 125^{o}C, electrode stick-out 25 mm and flux should be of type 1 i.e. GEEFLUX 541 (Basic) was used. Toughness at -40^{o}C of the welded specimens were studied and found that welding current and electrode stick-out were the most significant factors. The toughness at -40^{o}C tended to increase significantly with the increase in current from 400 to 500 A whereas tended to decrease significantly with the decrease in electrode stick-out from 25 to 35mm. The surface morphology of the welded plates was characterized by scanning electron microscopy with energy dispersive X-ray spectroscopy analysis (EDAX). EDX showed the nickel concentration was more significant affect the toughness at room temperature of welded region. The effect of variation in input parameters has been studied on the microstructure of the welded parts. Radiography test showed that welding was of very good quality and there were negligible amount of defects i.e. porosity, lack of penetration, slag at corner with low current used. It was also observed that no significant defect found with higher current in welded region. Welding current and electrode stick-out were found to be the most dependent factors leading to changes in micro hardness.

The micro hardness tended to decrease significantly with the increase of welding current from 400 to 500 A and as electrode stick-out increase from 25 to 35 mm, micro hardness will increase. Chemical composition of welding specimen was also studied and found that percentage change in Manganese and phosphorous was increasing in weld region but other element shows the mixed rend.

TABLE OF CONTENT

S.NO.	TOPIC	PAGE NUMBER
	List of Figures	xi-xv
	List of Tables	xvi-xvii
	Abbreviations	xviii

CHAPTER-1 INTRODUCTION **1-14**

1.1	Welding	1
1.2	Submerges Arc Welding (SAW)	1
1.3	Principle of SAW	2
1.4	Basic Equipment of SAW	3
1.5	Effect of Welding Parameters on SAW	4
1.5.1	Welding Current	4
1.5.2	Welding Voltage	5
1.5.3	Travel Speed	5
1.5.4	Electrode Size	5
1.5.5	Electrical Stick-Out	6
1.5.6	Preheating & Post heating of weldment	6
1.6	Advantage of SAW	6
1.7	Limitation of SAW	7
1.8	Application of SAW	7
1.9	High Strength Low Alloy Steel or Micro-Alloyed Steels	7
1.10	HSLA Steel Properties	8
1.11	Application of HSLA steel	9
1.12	Flux	10
1.13	Types of Fluxes	10
1.13.1	Fused Fluxes	10
1.13.2	Agglomerated Fluxes	11
1.13.3	Sintered fluxes	11

1.14	Defects in Welding	11
1.14.1	Cracks	11
1.14.2	Blowholes and Porosities	12
1.14.3	Shrinkage Cavity	12
1.14.4	Slag Inclusion	12
1.14.5	Incomplete Fusion and Penetration	12
1.14.6	Imperfect Shape	13
1.15	Effects of Alloying Elements in Steel	13
1.15.1	Carbon	13
1.15.2	Manganese	13
1.15.3	Chromium	13
1.15.4	Nickel	13
1.15.5	Molybdenum	14
1.15.6	Phosphorus	14
1.15.7	Sulphur	14
1.15.8	Silicon	14
1.15.9	Copper	14

CHAPTER-2 LITERATURE REVIEW 15-26

2.1	Review of Literature	15
2.2	Effect of Process Parameter and flux Consumption for HSLA Steel during SAW	15
2.3	Literature Summary	25
2.4	Gaps in literature	25
2.5	Objective of the Study	26

CHAPTER-3 DESIGN OF EXPERIMENTAL STUDY 27-54

3.1	Pilot Experimentation	28
3.2	Orthogonal Array	30
3.2.1	Selection of Orthogonal Array and Factor Assignment	32
3.3	Filler wire	32

3.4	Flux	33
3.5	Method of Preparation of Steel Plates	34
3.6	Testing of Weld Specimen	42
3.6.1	Tensile Test	42
3.6.2	Impact Test	44
3.6.3	Microhardness Test	46
3.6.4	Scanning Electron Microscope and EDAX	48
3.6.5	Chemical Composition of Weld Metal	49
3.6.6	Bead width and height of weld metal	50
3.6.7	Radiography Testing	51
3.7	Analysis of Results	52

CHAPTER-4 RESULTS AND ANALYSIS OF TENSILE TEST 55-71

4.1	Tensile Test	55
4.2	ANOVA for Tensile Strength	67
4.3	Optimal Design for Tensile Strength	68
4.4	Discussion of Tensile Test Results	69
4.5	Regression Analysis for Tensile Test Results	69
4.6	Residual Analysis	70

CHAPTER-5 RESULTS AND ANALYSIS OF BEAD GEOMETRY 72-82

5.1	ANOVA Analysis	72
5.2	ANOVA for Bead Height	72
5.3	Optimal Design for Bead Height	75
5.4	Analysis of S/N Ratio for Bead Height	76
5.5	ANOVA for Bead Width	77
5.6	Optimal design for bead width	80
5.7	Analysis of S/N Ratio for Bead Width	81

CHAPTER-6 RADIOGRAPHY TESTING 83-94

6.1	Introduction	83
6.2	Radiography Image	84
6.3	Discussion of Radiography Images	93

CHAPTER-7 RESULTS AND DISCUSSIONS OF CHEMICAL COMPOSITION 95-107

7.1	Chemical Composition of Weld Metal	95
7.2	Percentage Change in Chemical Composition	101
7.3	Discussion of Chemical Composition	107

CHAPTER-8 MICROSTRUCTURAL ANALYSIS 108-130

8.1	Introduction	108
8.2	Micro structural Analysis	108
8.3	Discussion	128

CHAPTER-9 RESULTS AND ANALYSIS OF TOUGHNESS TEST 131-140

9.1	Toughness Test	131
9.2	ANOVA for Toughness at Room Temperature	133
9.3	Optimal Design for Toughness at Room Temperature	135
9.4	ANOVA for Toughness at -40 ^{o}C	136
9.5	Optimal Design for Toughness at -40 ^{o}C	139
9.6	Discussion of Toughness Test Results	140

CHAPTER-10 RESULTS AND ANALYSIS OF MICROHARDNESS TEST 141-147

10.1	Microhardness Test	141
10.2	ANOVA for Microhardness at Weld Region	146
10.3	Discussion of Microhardness	147

CHAPTER-11 SUMMARY, CONCLUSIONS & FUTURE SCOPE 148-152

11.1	Results	148
11.1.1	Tensile Strength	149
11.1.2	Bead Width	149
11.1.3	Bead height	149
11.1.4	Toughness at Room Temperature	150
11.1.5	Toughness at -40 ^{o}C	150
11.1.6	Microhardness at weld centre	150
11.1.7	Chemical Composition	151
11.1.8	Radiography Testing	151
11.1.9	Micro structural study	151
11.2	Conclusions	151
11.3	Future Scope	152

CHAPTER-12 REFERENCES 153-155

LIST OF FIGURES

FIGURE NO.	DESCRIPTION	PAGE NUMBER
1.1	Submerged arc Welding	1
1.2	Equipment set up for SAW machine	3
1.3	Influence of welding parameters on bead shape	4
1.4	Influence of electrode size on weld bead	5
3.1	Chemical composition of base metal by using spectroscopy	27
3.2	SAW setup for experimental work	28
3.3	Burn through defect was observed due to higher current and lower speed	29
3.4	Flow chart of experimental plan	31
3.5	Filler wire AWS code F7A2-EH14	33
3.6	Flux used for experimental work	34
3.7	Cutting of steel plates through oxy-acetylene gas cutting	35
3.8	Cutting of steel strip through power hacksaw	35
3.9	Double-V Groove geometry (a) Front view (b) Top view (All dimensions are in mm)	36
3.10	Making chamfer on corner of plate	36
3.11	Double-V groove between two plates (i) Front view (ii) Top View	37
3.12	(i) Tacking and Rooting on double-V groove plates through SMAW (ii) Back side penetration observation on plates	37
3.13	Submerged arc welding of plates after single layer	38
3.14	Multi layer joint of double V-groove plates after welding	39
3.15	Welding on all specimens through SAW	39
3.16	Orientation of cutting of plates after welding	40
3.17	(i) Cutting of plates according to required tensile specimen size on surface grinding machine (ii) Cutting of weld region by power hacksaw	41
3.18	(i) Cutting of plates after power hacksaw (ii) Machining on welding	41

	region for reducing thickness approximately to 10-12 mm on vertical milling machine	
3.19	(i) Grinding of plates using centre less grinding machine (ii) Plates after grinding from welding area	41
3.20	Computerised universal testing machine	43
3.21	Tensile test specimens according to ASTM E8-11 standard	43
3.22	Specimen for tensile testing	43
3.23	Standard charpy test specimen	44
3.24	Charpy test specimen	45
3.25	Charpy test machine	45
3.26	(i) Infrared thermometer used for the measurement of temperature (ii)Apparatus for liquid nitrogen	45
3.27	Belt grinder	46
3.28	(i) Polishing with emery paper of grit size 400,600,800,1000,2500 (ii)Polisher with using kerosene and diamond paste solution	47
3.29	Specimens for microhardness testing	47
3.30	(i) Microhardness test machine (ii) Diamond indent shown at 40X on the screen and its measurement	48
3.31	Scanning electron microscope	49
3.32	Atomic absorption spectrometer	49
3.33	Samples for chemical composition testing	50
3.34	(i) & (ii) Measurement of bead width using Leica microscope or digital vernier calliper (iii) Measurement of bead height using vernier height gauge	51
3.35	(i) Radioactive source i.e. gamma-rays (ii) Exposing radioactive source on weld region through negative film	52
4.1	Specimen after tensile test	55
4.2	Load vs displacement and stress vs strain curve base metal	56
4.3	Variation of maximum tensile load of different specimens	58
4.4	Variation of maximum tensile strength of different specimens	58
4.5 (a-r)	Load vs displacement and stress vs strain curve for tensile test for trial no.1-18	66

4.6	Main effect plot for tensile strength	68
4.7	Residual plots for mean tensile strength	71
5.1	Main effect plot for bead height	75
5.2	Main effect plot for S/N ratios of bead height	77
5.3	Main effect plot for mean of bead width	80
5.4	Main effect plot for S/N ratios of bead width	82
6.1	Schematic of radiography testing	84
6.2 (a-r)	Radiography image of a weld revealing defects of trial no. 1-18	93
7.1	Specimen after checking composition	95
7.2 (a)	Variation in %age composition of iron at weld centre	96
7.2 (b)	Variation in %age composition of carbon at weld centre	96
7.2 (c)	Variation in %age composition of silicon at weld centre	97
7.2 (d)	Variation in %age composition of manganese at weld centre	97
7.2 (e)	Variation in %age composition of phosphorus at weld	98
7.2 (f)	Variation in %age composition of sulphur at weld centre	98
7.2 (g)	Variation in %age composition of chromium at weld centre	99
7.2 (h)	Variation in %age composition of copper at weld centre	99
7.2 (i)	Variation in %age composition of chromium at weld centre	100
7.2 (j)	Variation in %age composition of cobalt at weld centre	100
7.3 (a)	Variation in %age change in composition of carbon at weld centre	102
7.3 (b)	Variation in %age change in composition of silicon at weld centre	102
7.3 (c)	Variation in %age change in composition of manganese at weld centre	103
7.3 (d)	Variation in %age change in composition of phosphorus at weld centre	104
7.3 (e)	Variation in %age change in composition of sulphur at weld centre	105
7.3 (f)	Variation in %age change in composition of nickel at weld centre	105
7.3 (g)	Variation in %age change in composition of copper at weld centre	106
7.3 (h)	Variation in %age change in composition of chromium at weld centre	107
8.1	SEM &EDX micrograph of parent metal (i)500x (ii)1000x (iii)EDX image of parent metal (iv) Chemical composition of parent metal resulting from EDX analysis	109

8.2	SEM &EDX micrograph of welding region with trial no.1 (i) 500x (ii) 1000x (iii) EDX image of trial no. 1 (iv) Chemical composition of trial no.1 resulting from EDX analysis	110
8.3	SEM &EDX micrograph of welding region with trial no.2 (i) 250x (ii)500x (iii) EDX image of trial no. 2 (iv) Chemical composition of trial no.2 resulting from EDX analysis	111
8.4	SEM &EDX micrograph of welding region with trial no.3 (i) 500x (ii) 1000x (iii) EDX image of trial no. 3 (iv) Chemical composition of trial no.3 resulting from EDX analysis	112
8.5	SEM &EDX micrograph of welding region with trial no.4 (i) 250x (ii) 500x (iii) EDX image of trial no. 4 (iv) Chemical composition of trial no.4 resulting from EDX analysis	113
8.6	SEM &EDX micrograph of welding region with trial no.5 (i) 500x (ii) 1000x (iii) EDX image of trial no. 5 (iv) Chemical composition of trial no.5 resulting from EDX analysis	114
8.7	SEM &EDX micrograph of welding region with trial no.6 (i) 500x (ii) 1000x (iii) EDX image of trial no. 6 (iv) Chemical composition of trial no.6 resulting from EDX analysis	115
8.8	SEM &EDX micrograph of welding region with trial no.7 (i) 500x (ii) 1000x (iii) EDX image of trial no. 7 (iv) Chemical composition of trial no.7 resulting from EDX analysis	116
8.9	SEM &EDX micrograph of welding region with trial no.8 (i) 250x (ii) 500x (iii) EDX image of trial no. 8 (iv) Chemical composition of trial no.8 resulting from EDX analysis	117
8.10	SEM &EDX micrograph of welding region with trial no.9 (i) 500x (ii) 1000x (iii) EDX image of trial no. 9 (iv) Chemical composition of trial no.9 resulting from EDX analysis	118
8.11	SEM &EDX micrograph of welding region with trial no.10 (i) 500x (ii) 1000x (iii) EDX image of trial no. 10 (iv) Chemical composition of trial no.10 resulting from EDX analysis	119
8.12	SEM &EDX micrograph of welding region with trial no.11 (i) 500x (ii) 1000x (iii) EDX image of trial no. 11 (iv) Chemical	120

	composition of trial no.11 resulting from EDX analysis	
8.13	SEM &EDX micrograph of welding region with trial no.12 (i) 500x (ii) 1000x (iii) EDX image of trial no. 12 (iv) Chemical composition of trial no.12 resulting from EDX analysis	121
8.14	SEM &EDX micrograph of welding region with trial no.13 (i) 500x (ii) 1000x (iii) EDX image of trial no. 13 (iv) Chemical composition of trial no.13 resulting from EDX analysis	122
8.15	SEM &EDX micrograph of welding region with trial no.14 (i) 500x (ii) 1000x (iii) EDX image of trial no. 14 (iv) Chemical composition of trial no.14 resulting from EDX analysis	123
8.16	SEM &EDX micrograph of welding region with trial no.15 (i) 500x (ii) 1000x (iii) EDX image of trial no. 15 (iv) Chemical composition of trial no.15 resulting from EDX analysis	124
8.17	SEM &EDX micrograph of welding region with trial no.16 (i) 500x (ii) 1000x (iii) EDX image of trial no. 16 (iv) Chemical composition of trial no.16 resulting from EDX analysis	125
8.18	SEM &EDX micrograph of welding region with trial no.17 (i) 500x (ii) 1000x (iii) EDX image of trial no. 17 (iv) Chemical composition of trial no.17 resulting from EDX analysis	126
8.19	SEM &EDX micrograph of welding region with trial no.18 (i) 500x (ii) 1000x (iii) EDX image of trial no. 18 (iv) Chemical composition of trial no.18 resulting from EDX analysis	127
9.1	Specimen after toughness test at -40 ^{o}C &room temperature (twice study for each temperature)	131
9.2	Variation in toughness at room temperature	133
9.3	Main effect plot for tensile test at room temperature	135
9.4	Variation in toughness at -40 ^{o}C	138
9.5	Main effect plot for mean at -40 ^{o}C	139
10.1	Microhardness of base metal	141
10.2	Variation of microhardness of different trials (i-xviii) at weld parts	145
10.3	Main effect plot for microhardness at weld region	147

LIST OF TABLES

TABLE NO.	DESCRIPTION	PAGE NUMBER
1.1	Technical parameters of welding	2
3.1	Chemical composition of base metal	27
3.2	Process parameters and their parameters for pilot study	28
3.3	Process parameters and their levels that effects welding	30
3.4	Orthogonal arrays for experimentation	31
3.5	DOF allocated to various factor combinations	32
3.6	Concentration of different percent composition in fluxes	34
3.7	Chemical composition of SMAW electrode wire	38
3.8	Value for input process parameters for SMAW	38
4.1	Maximum tensile load & strength value of base metal	55
4.2	Maximum tensile load & tensile strength readings	57
4.3	Analysis of variance for mean tensile strength	67
4.4	Response table for means of tensile strength	68
4.5	Regression table for mean tensile strength	70
4.6	Analysis of variance for regression of mean tensile strength	70
5.1	Results for bead height	73
5.2	Analysis of variance for mean bead height	74
5.3	Response table for means of bead height	74
5.4	Analysis of variance for S/N ratio	76
5.5	Response table for signal to noise ratio	76
5.6	Results for bead width	78
5.7	Analysis of variance for means bead width	79
5.8	Response table for means of bead width	79
5.9	Analysis of variance for S/N ratio	81
5.10	Response table for signal to noise ratio	82
6.1	Welding imperfection found in the radiography test	94
7.1	Percentage change in chemical composition of carbon and silicon	101

	w.r.t. base metal	
7.2	Percentage change in chemical composition of manganese and phosphorus w.r.t. base metal	103
7.3	Percentage change in chemical composition of sulphur and nickel w.r.t. base metal	104
7.4	Percentage change in chemical composition of copper and chromium w.r.t. base metal	106
9.1	Toughness values of base metal	131
9.2	Toughness value at room temperature	132
9.3	Analysis of variance for means toughness at room temperature	134
9.4	Response table for means of toughness at room temperature	134
9.5	Toughness at -40 ^{o}C temperature	137
9.6	Analysis of variance for means toughness at 40 ^{o}C temperature	138
9.7	Response table for means of toughness at 40 ^{o}C temperature	138
10.1	Microhardness values of base metal at different region	141
10.2	Microhardness values at weld region (indent load 1 kg and dwell time 20s)	142
10.3	Response table for mean of microhardness at weld region	147
11.1	Tables for mean value of results	148

ABBREVATIONS

SAW	Submerged Arc Welding
HVN	Vickers hardness number
EDX	Energy Dispersive X-ray
BI	Basicity Index
HSLA	High Strength Low Alloy
ASTM	American Society for Testing and Materials
A	Ampere
HAZ	Heat Affected Zone
ANOVA	Analysis of Variance
SEM	Scanning Electron Microscope
DOE	Design of Experiments
DOF	Degree of Freedom
PWHT	Post Weld Heat Treatment
SMAW	Shielded Metal Arc Welding
CCT	Centre Cracked Tension
S/N Ratio	Signal to Noise Ratio

CHAPTER-1
INTRODUCTION

1.1 WELDING

It is a process which produces coalescence of materials by heating them to suitable temperature with or without the application of pressure or by the application of pressure alone, and with or without the use of filler. Hence joining process is called positive process (addition of metal). Arc welding in its present form appeared on the industrial scene in 1880's.Arc welding however, was not accepted for fabrication of critical component till about 1920 by which time coating for electrodes had been well developed. The successful development of submerged arc welding in 1930's almost simultaneously both in USSR and USA. SAW sometimes also referred to as 'Sub-Arc Welding' [1].

1.2 SUBMERGED ARC WELDING

SAW is an arc welding process in which heat is generated by an arc which is produced between bar consumable electrode wire and the work piece. The arc and the weld zone are completely covered under a blanket of granular, fusible flux, which melts and provides protection to the weld pool from the atmospheric gases.

Alloy ingredients in the flux may be present to enhance the mechanical properties and crack resistance of the weld deposits. The molten flux flow down continuously and fresh flux melts around the arc. The molten flux reacts with the molten metal forming slag and improves the properties and later floats on the molten/solidifying metal to protect it from atmospheric gas contamination ad retards cooling rate as in figure 1.1.

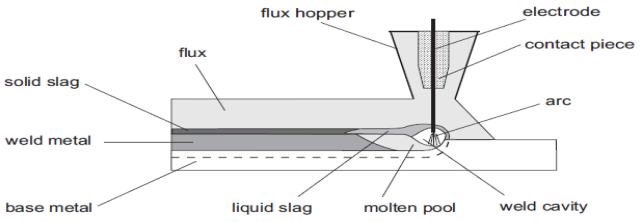

FIGURE1.1 Submerged Arc Welding [2]

1.3 PRINCIPLE OF SAW

In SAW have a continuous electrode is being fed into the joint by Mechanically powered drive rolls electrical current, which produce the arc, is supplied to the electrode through the contact tube. Both AC and DC power source are used and they may be of constant current (CC) or Constant Voltage (CV) type for single arc, DC power source with CV is almost invariably employed while AC power source are most often used for multi-electrode SAW. After welding is completed and the weld metal has solidified, unfused flux and slag are removed by chipping hammer. The layer of flux is to protect the weld region from the ill effect of atmospheric gases and its sufficient depth is used to avoid spatter and it protect from crack defect. Then finally result in a smooth weld bead. The unmelted flux acts as an insulator and is reclaimed for reuse purpose. SAW is mainly two types that one is automatic type and another one is semi-automatic type. The welding gun for automatic SAW is attached to the wire feed motor and includes current pick up tip for providing the electrical contact to the wire electrode. The flux hopper is attached to welding head and it may be magnetically operated through valves so that they can be opened or closed by control system but in semi-automatic SAW employs no carriage or automatic head system. To increase deposition rate or welding speed, more than one wire can be fed simultaneously into the same weld pool. In twice arc welding, two electrodes are fed into the same weld pool while sharing a common power source and contact tip. In tandem Arc SAW, multiple electrodes are arranged with one in front of the other. Each electrode has an independent power supply and contact tip. The main parameter uses in Submerged Arc Welding are given below. [3]

TABLE 1.1 Technical Parameters of Welding

Wire Feeding Rate	0.5 m/min-2.5m/min
Electrode Diameter	2.4-6mm
Welding current	150 A-1200 A
Welding Voltage	22V-35V
Travel Speed	20-600m/h

1.4 BASIC EQUIPMENT OF SAW

The basic equipment of a SAW consists of-

- A Welding power source i.e. AC type or DC type to supply current to the electrode at the contact tube. For large diameter electrode used constant type power source. A constant voltage power source is used for small diameter electrode. In DC operation, the electrode is normally connected to the positive terminal. Electrode negative (Direct current electrode negative) polarity can be used to increase deposition rate but depth of penetration is reduced by between 20 and 25%. AC power sources usually have a constant-current output characteristic and are therefore not self-regulating. The arc with this type of power source is controlled by sensing the arc voltage and using the signal to control wire feed speed
- Welding Head consists of wire spool (long consumable electrode is rapped in the form of spool), wire feed unit or contact nozzle/tube.
- Flux handling system is used for holding the flux and feeding it ahead of the arc. In small welding systems, flux is usually held in a small hopper above the welding torch. It is fed automatically (by gravity or mechanized feed) ahead of the arc. In larger installations the flux is stored in large hoppers and is fed with compressed air or by manually.[5]

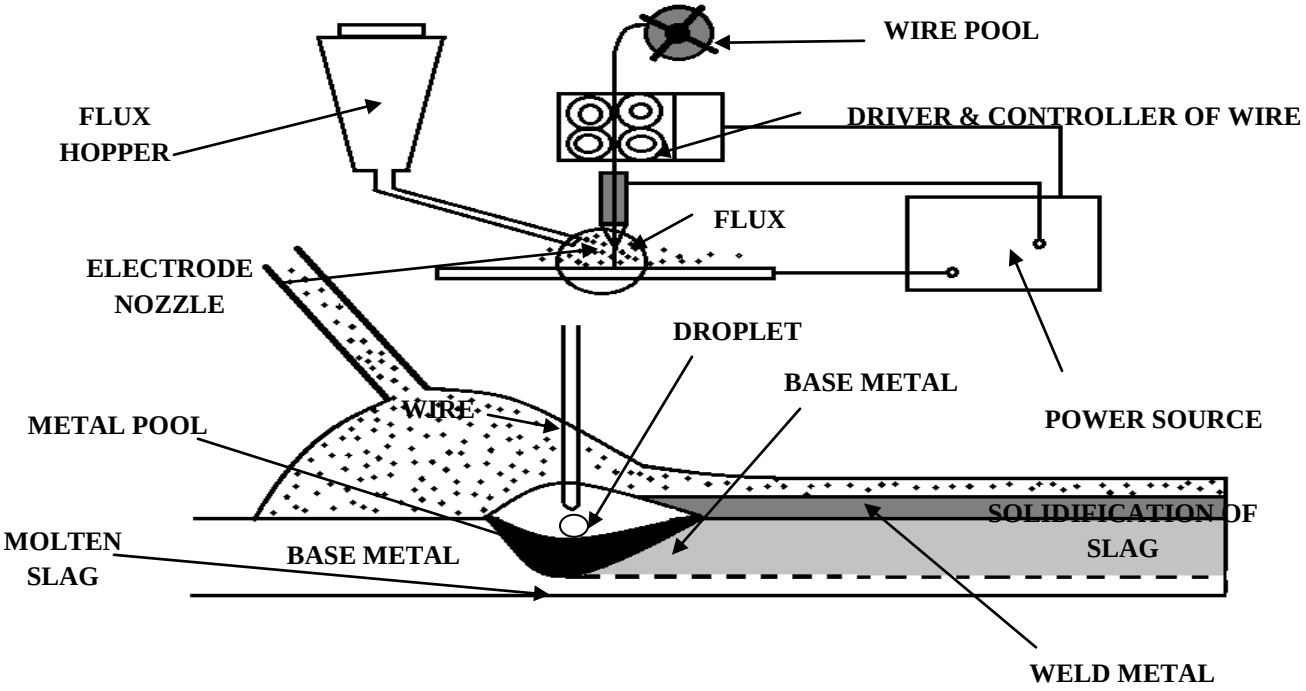

FIGURE 1.2 Equipment set up for SAW Machine

1.5 EFFECT OF WELDING PARAMETERS ON SAW

The SAW process can provide high deposition rate and produces a very smooth bead with good penetration and excellent fusion which mainly depends upon welding current, Arc-voltage, Speed and different flux composition.

1.5.1 Welding Current

The increase in welding current the pressure exerted by the arc increases which drives out the molten metal from beneath the arc and that leads to increased depth of penetration. but the width of weld remains almost unaffected. SAW process usually employs wire of 2 to 6 mm diameter, thus for deeper penetration at low current a wire of diameter 2 to 3mm is best suited. In welding, with high current shall lead to too much penetration resulting into burn through in the weld being joined, Excessive Reinforcement and therefore larger amount of distortion whereas to insufficient penetration, lack of fusion and instability shall lead to low current.[3]

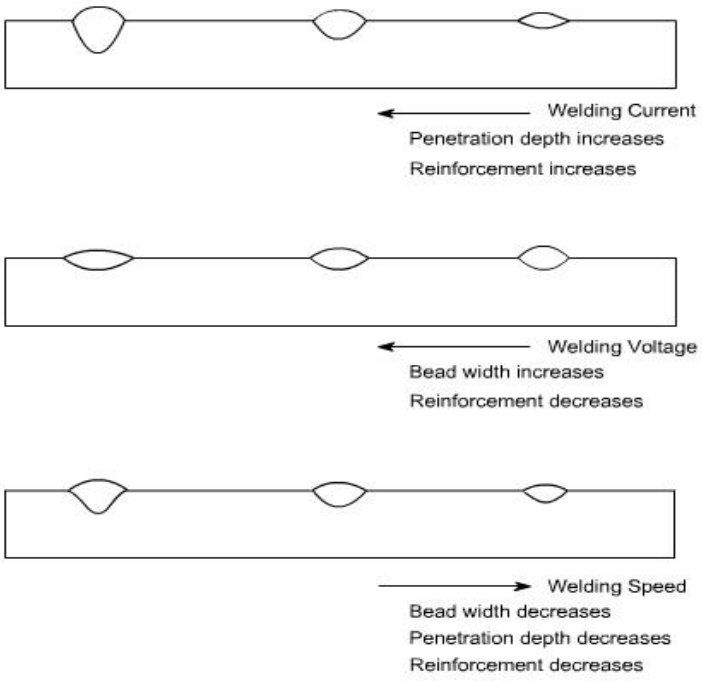

FIGURE 1.3 Influence of Welding Parameters on Bead Shape [3]

1.5.2 Welding Voltage

Arc voltage varies indirect proportion to the arc length with the increase in arc length the arc voltage increase and thus more heat is available to melt the metal and the flux. However, increased arc length means more spread of arc column, this leads to increase in weld width and volume of reinforcement while the depth of penetration decreases. The arc voltage varies with welding current and wire diameter, and in SAW it usually ranges between 25 to 50 volts. Welding voltage has significant effect on the electrode wire melting rate but higher voltage leads to flatter and wider bead, increased flux composition and resistance to porosity caused by rust or scale and help bridge gap when fit up is poor. Lower voltage produces resistance to arc blow but high narrow bead with poor slag removal [3].

1.5.3 Travel Speed

In welding the travel speed is increase, the width of weld decreases. However, if the increase in speed is small the depth of penetration increase because the layer of molten metal is reduced which leads to higher heat conduction towards the bottom the plate. If the welding speed is increased, heat input per unit length of weld is decreased, less welding material is applied per unit length of weld, and consequently less weld reinforcement results and penetration decreases. Excessive high travel speed decrease melting action, increase tendency for undercut, arc blow, porosity and uneven bead shapes while slower travel speed reduces the tendency to porosity and slag inclusion [3].

1.5.4 Electrode Size

The electrode size principally affects the depth of penetration for fixed current. Smaller wire is generally used in semiautomatic equipment to provide flexibility, to the welding gun. The small wires are also used in multiple electrodes, parallel wire setups. The layer electrodes are generally used to take advantage of higher current and consequently higher deposition rates. [3]

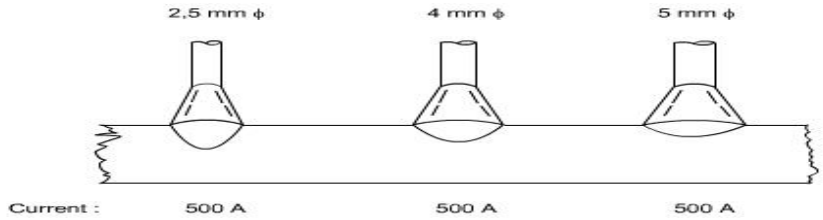

FIGURE 1.4 Influence of electrode size on weld bead [3]

1.5.5 Electrode Stick-Out

The longer the electrode stick-out then the greater amount of heating and the higher the deposition rate. Hence, when the electrode stick-out is increased to obtain higher deposition rate, then up to 25-50% but it reduce the penetration up to 10% and excessive overheating of the wire leads to electrode pulsation, arc instability and stubbing.[3]

1.5.6 Preheating & Post heating of weldment

Pre and post heating is a heat treatment process before and after welding primarily to improve the micro structural and mechanical properties of the weldment and is often used to improve the properties of a weldment.

Post heating is used to minimize the potential for hydrogen induced cracking. Stress relief heat treatment is used to reduce the stresses that remain locked in a structure as a consequence of manufacturing processes. Different causes and effects of residual stresses are described in the previous lecture. Some design guidelines for PWHT are given below:

1. Welding of carburized or hardened steels requires controlled conditions and proper equipment and supplies. Designers should not specify such welding unless it is unavoidable.
2. Welding removes or reduces the hardness of carburized or nitride steels in the area of welding. So, if it is possible, hardening has to be done after the welding.
3. Carbon in welded areas will affect the physical and chemical characteristics of the weld bead, resulting in possible cracking or weld failure in or adjacent to the weld.[4]

1.6 ADVANTAGES OF SUBMERGED ARC WELDING

The advantages of SAW are following:

- Higher deposition rate have been reported and distortion is much less.
- The arc is under a blanket of flux, which virtually eliminates arc flash, spatter and fume (this making the process attractive from an environmental standpoint).
- The flux act as a scavenger and deoxidizer to remove contaminants such as oxygen, nitrogen and sulphur from the molten weld pool. This help to produce sound weld with excellent Mechanical properties.
- Weld produced is sound, uniform ductile, corrosion resistance and have good impact value.

- It provides deep weld penetration and cost per unit length of joint is relatively low.

1.7 LIMITATION OF SUBMERGED ARC WELDING

The limitations of SAW are following:

- Process can be used only in flat positions.
- Plate of lesser thickness (lesser than 5mm) cannot be welded due to risk of burn through.
- Smaller diameter component cannot be welded because the fluxes fall among away from groove area.
- It is mainly used for join more than 6mm thick plates.
- Limited to ferrous (steel or stainless steel) and some nickel based alloy.

1.8 APPLICATION OF SUBMERGED ARC WELDING

The application of SAW is following:

- It is widely used in ship building, offshore, structural and pressure vessel industries, locomotives etc.
- General fabrication of pipes, penstocks, LPG cylinder, bridge girders and other structures are produced by submerged arc welding.
- Hard facing for steel mills, earthmoving equipment, mining etc.

1.9 HIGH STRENGTH LOW ALLOY STEEL OR MICRO-ALLOYED STEELS

- High Strength Low Alloy (HSLA) Steel is a type of alloy steel that provides better mechanical properties or greater resistance to corrosion than carbon steel. HSLA steels vary from other steels in that they are not made to meet a specific chemical composition, but rather to specific mechanical properties. They have carbon content between 0.05–0.25% to retain formability and weldability. Other alloying elements include up to 2.0% manganese and small quantities of copper, nickel, niobium, nitrogen, vanadium, chromium, molybdenum, titanium, calcium, rare earth elements, or zirconium.
- Copper, titanium, vanadium, and niobium are added for strengthening purposes. These elements are intended to alter the microstructure of carbon steels, which is usually a ferrite-pearlite aggregate, to produce a very fine dispersion of alloy carbides in an almost pure ferrite matrix.

- This eliminates the toughness-reducing effect of a pearlite volume fraction, yet maintains and increases the material's strength by refining the grain size, which in the case of ferrite increases yield strength.
- The yield strengths vary between 250–655MPa. Due to their higher strength and toughness HSLA steels usually require 25 to 30% more power to form, as compared to carbon steels.
- Copper, silicon, nickel, chromium, and phosphorus are added to increase corrosion resistance.
- Zirconium, calcium, and rare earth elements are added for sulphide-inclusion shape control which increases formability. These are needed because most HSLA steels have directionally sensitive properties. Formability and impact strength can vary significantly when tested longitudinally and transversely to the grain.
- HSLA steels are also more resistant to rust than most carbon steels, due to their lack of pearlite – the fine layers of ferrite.[6]

1.10 HSLA STEEL PROPERTIES

- High Strength Low Alloy (HSLA) Steels provide increased strength-to-weight ratios over conventional low-carbon steels for only a modest price premium. Because HSLA alloys are stronger, they can be used in thinner sections, making them particularly attractive for transportation-equipment components where weight reduction is important. HSLA steels are available in all standard wrought forms - sheet, strip, plate, structural shapes, bar-size shapes, and special shapes.
- Typically, HSLA steels are low-carbon steels with up to 1.5% manganese, strengthened by small additions of elements, such as columbium, copper, vanadium or titanium and sometimes by special rolling and cooling techniques. Improved-formability HSLA steels contain additions such as zirconium, calcium, or rare-earth elements for sulphide-inclusion shape control.
- HSLA steels can have thinner cross sections than equivalent parts made from low-carbon steel; corrosion of HSLA steel can significantly reduce strength by decreasing the load-bearing cross section. While additions of elements such as copper, silicon, nickel, chromium, and phosphorus can improve atmospheric corrosion resistance of these alloys, they also increase cost.

- Galvanizing, zinc-rich coatings, and other rust-preventive finishes can help protect HSLA-steel parts from corrosion.
- Improved-formability HSLA steels were developed primarily for the automotive industry to replace low-carbon steel parts with thinner cross-section parts for reduced weight without sacrificing strength and dent resistance.
- Forming, drilling, sawing, and other machining operations on HSLA steels usually require 25 to 30% more power than do structural carbon steels. They are used to handle large amounts of stress or a good strength-to-weight ratio. HSLA steels are usually 20 to 30% lighter than carbon steel with the same strength. HSLA steels usually have densities of around 7800 kg/m^3.
- HSLA alloys have directionally sensitive properties. For some grades, formability and impact strength vary significantly depending on whether the material is tested longitudinally or transversely to the rolled direction. For example, bends parallel to the longitudinal direction are more apt to cause cracking around the outside, tension-bearing surface of the bend. This effect is more pronounced in thick sheets. This directional characteristic is substantially reduced in HSLA steels that have been treated for sulphide shape control.[6]

1.11 APPLICATION OF HSLA STEEL

- Improved-formability HSLA steels were developed primarily for the automotive industry to replace low-carbon steel parts with thinner cross-section parts for reduced weight without sacrificing strength and dent resistance. Typical passenger-car applications include door intrusion beams, chassis members, reinforcing and mounting brackets, steering and suspension parts, bumpers, and wheels.
- Trucks, construction equipment, off-highway vehicles, mining equipment, and other heavy-duty vehicles use HSLA sheets or plates for chassis components, buckets, grader blades, and structural members outside the body. For these applications, sheets or light-gage plates are specified. Structural forms (alloys from the family of 45,000 to 50,000 psi minimum yield strength HSLA steels) are specified in applications such as offshore oil and gas rigs, single-pole power-transmission towers, railroad cars, and ship construction. [6]

1.12 FLUX

The flux protects the molten pool and the arc against atmospheric oxygen and nitrogen creating an envelope of molten slag. The slag also cleanses the weld metal (i.e. Deoxidizes it and remove impurities such as sulphur) modifies its chemical composition and controls the profile of the weld bead. It is a chemical cleaning agent which facilitates welding by removing oxidation from the metals to be joined ammonium chloride, rosin, hydrochloric acid, zinc chloride, borax are commonly flux is used. Its main purpose is to prevent oxidation of the base and filler materials and react with the weld pool to provide clean high quality weld metal with the desired properties. [5]

The most convenient method of classifying, however, is by reference to the 'Basicity Index'(BI) of the flux. The basicity Index is calculated by dividing the sum of the percentage of the basic constituents by the sum of the acid constituents. Calcium, Magnesium, Sodium, Potassium and Manganese Oxide, Calcium Carbonate and Calcium Fluoride are the basic constituents of a flux, Silica and alumina the acid constituents. It has a major effect on the weld bead mechanical properties, most importantly the notch toughness. As a general rule, the higher the basicity, the higher the notch toughness. If the basicity index is less than 1 then it is called as Acidic flux and if BI is vary between '1 to 1.5' then it will be neutral fluxes. In the Basic flux having BI range between '1.5 to 2.5' or if this range more than 2.5 then it is called high basic index. The standard formula for finding the basicity index is:

$$\mathbf{BI} = \frac{\mathbf{CaO+MgO+CaF2Na2O+K2O+BaO+0.5(MnO+FeO)}}{\mathbf{SiO2+0.5(Al2O3+TiO2+ZrO2)}}$$

1.13 TYPES OF FLUXES

There are two types of submerged arc fluxes are available, depending on the method of manufacture i.e. fused and agglomerated.

1.13.1 Fused Fluxes

Typical ingredient are quartz, manganese ore or slag and clay fused fluxes are made by dry mixing the raw material, melting (fusion) in a furnace and cooling which is accomplished by using large chill block or a stream of water. The glassy flux material is then crushed, screened for particles sizing and packaged for shipment. It have less moisture pick up than other flux manufacturing method and can by recycling through flux recovery system without losing particles sizing or composition but it have major disadvantages is the difficulty in

adding deoxidizers and alloy during manufacture. Particles are non-hygroscopic and do not absorb moisture, therefore only a low temperature (300°F/150°C) drying cycle is required to remove surface moisture/condensation, providing increased protection against hydrogen cracking. Fused fluxes provide smooth, stable performance even welding currents (up to 2,000 amps).[3] [4]

1.13.2 Agglomerated Fluxes

This type of flux are made from raw material that are powdered, dry mixed and bonded together with either a potassium silicate or sodium silicate binder or combination of both. It is more beneficial than the fused flux because it in easy adding of deoxidizers and alloying elements and produce weld deposits of better ductility and impact strength as compared with fused fluxes.[3] [4]

1.13.3 Sintered fluxes

They are produced by grinding the dry charge together, pressing into small balls, and heating to1,000-1,100°C (just below melting point) in gas-fired furnaces. The solid mass produced then has the characteristics of a fused flux. It is crushed to the desired fineness, sieved, sized and packed in suitable containers. [3] [4]

1.14 DEFECTS IN WELDING

The performance of welded structure in service depends on presence or absence of defects in weld joints. Weld defects impair the strength of welded joints and may results in the failure of a complete assembly / structure in service. In a general sense, the term weld defect refers to any departure in welded structure or welded joints from the specified requirements. According to the International Institute of Welding, the weld defects are classified into six groups as follows: (i) Cracks (ii) Cavities (blowholes, porosity, shrinkage, etc.) (iii) Solid Inclusion (iv) incomplete fusion (v) Imperfect Shape (vi) miscellaneous defects. [1]

1.14.1 Cracks

Cracks are the most dangerous amongst all types of defects as it reduce the performance of a welded joint drastically and can also cause catastrophic failure. Depending on the position, location and orientation these can be categorized as longitudinal cracks, transverse cracks, crater cracks, under-bead cracks and toe cracks. These cracks are usually visible and hence, referred to surface defects in weld joints. In general, the cracks in weld joints occur due to

high concentration stresses during solidification of weld, poor fit-up and incorrect welding procedures, and poor edge quality. Formation of cracks can be controlled by preheating the joints, reducing the cooling rate, taking proper precautions during post weld heat treatment. [1]

1.14.2 Blowholes and Porosities

These are usually subsurface defects in weld joints and are actually voids, holes or cavities formed by the entrapped gases by the solidified weld metal. The source of the trapped gas may be un cleaned rust, dirt, paint, etc. on the parent metal or electrode, damp flux (in shielded metal or submerged arc welding), impurities and moisture in the shielding gas.
Normally, porosity is not considered as serious a defect as cracks since the porosity cavities usually have rounded ends which are not expected to propagate as cracks .[1]

1.14.3 Shrinkage Cavity

It is referred to the cavities which are formed due to shrinkage of weld metal during its solidification. The shrinkage cavity usually occurs during welding of thick plates in a single pass using submerged arc welding or electro slag welding processes. Proper amount of filler material has to be supplied for compensation during shrinkage to avoid this king of defect. [1]

1.14.4 Slag Inclusion

The slag inclusion refers to the solidified flux comprising of oxides, phosphorous compounds and nitrides, which fail to float out to the surface and get entrapped in the weld. When gas tungsten arc welding is carried out with direct current electrode positive polarity and at high current, tungsten inclusion from the tungsten electrode into the weld can occur. Such inclusions can be continuous, intermittent or very randomly paced. Slag inclusions reduce the mechanical strength, in particular, the ductility, of the welds. [1]

1.14.5 Incomplete Fusion and Penetration

Incomplete fusion can occur due to inadequate welding current, offset of electrode from the axis of the weld, too high a weld speed, improper joint preparation and fit-up. It occurs between the parent metal and the weld metal and also between intermediate layers in multi-pass welding reducing the weld strength. [1]

1.14.6 Imperfect Shape

Dimensional deviations, undercut, under fill, overlap, excessive reinforcement, excessive penetration, bead shape are the examples of Imperfect shape. Under fills and Suck backs refer to uneven depression (such as a concave contour) respectively, on the face or on the root surface of the weld extending below the surface of the adjacent base metal. Both of these defects reduce the cross-sectional area of the weld below the designed amount and thus, a point of weakness and or stress raiser where failure may occur.

Excessive penetration and / or reinforcement are also undesirable in weld joints. Both are usually caused by poor fit-up, too wide a root gap or too small a root face, improper welding technique and excessive welding current. [1]

1.15 EFFECTS OF ALLOYING ELEMENTS IN STEEL

Steel is basically iron alloyed to carbon with certain additional elements to give the required properties to the finished melt. Listed below is a summary of the effects of various alloying elements in steel.

1.15.1 Carbon

The basic metal, iron, is alloyed with carbon to make steel and has the effect of increasing the hardness and strength by heat treatment but the addition of carbon enables a wide range of hardness and strength.

1.15.2 Manganese

Manganese is added to steel to improve hot working properties and increase strength, toughness and hardenability.

1.15.3 Chromium

Chromium is added to the steel to increase resistance to oxidation. This resistance increases as more chromium is added. When added to low alloy steels, chromium can increase the response to heat treatment, thus improving hardenability and strength.

1.15.4 Nickel

Nickel has a tendency to form austenite which is responsible for a great toughness and high strength at both high and low temperatures. Nickel also improves resistance to oxidation and corrosion. It increases toughness at low temperatures when added in smaller amounts to alloy steels.

1.15.5 Molybdenum

Molybdenum when added to low alloy steels, molybdenum improves high temperature strengths and hardness.

1.15.6 Phosphorus

Phosphorus is usually added with sulphur to improve machinability in low alloy steels, phosphorus, in small amounts, aids strength and corrosion resistance.

1.15.7 Sulphur

Sulphur improves machinability when added in small amount.

1.15.8 Silicon

Silicon is used as a deoxidising (killing) agent in the melting of steel; as a result, most steels contain a small percentage of silicon. Silicon contributes to hardening of the ferritic phase in steels.

1.15.9 Copper

Copper is normally present in stainless steels as a residual element. However it is added to a few alloys to produce precipitation hardening properties. [6]

CHAPTER-2
LITERATURE REVIEW

2.1 REVIEW OF LITERATURE

This chapter covers a detailed review of literature on the various aspects of Submerged Arc Welding (SAW) mainly on High Strength Low Alloy (HSLA) Steel. The literature review includes the research carried out on SAW process, effect of weld parameters like welding current; pre and post weld heat treatment, electrode stick-out, travel speed, electrode diameter or different flux composition and metallurgical behaviour effects on HSLA steel.

2.2 EFFECT OF PROCESS PARAMETER AND FLUX CONSUMPTION FOR HSLA STEEL DURING SAW

Kanjilal *et al.* [7] investigated the combined effect of flux mixture and welding parameters on submerged arc weld metal chemical composition and mechanical properties. It showed that two factors interaction effects are higher than the individual effect of mixture related variable. Among the welding parameter, polarity is found to be important for all response; viz. weld metal chemical composition and mechanical properties. In EP (electrode positive) polarity, gain of manganese and silicon at cathode (weld pool) take place due to electrochemical reduction reaction otherwise it loss due to oxidation reaction. SAW fluxes are generally characterized by their BI (Basicity Index), the interaction between flux and welding parameter have been tried to establish in term of B.I (i.e. using different flux chemical composition) and predominant welding parameter (i.e. electrode positive polarity) and then finally found carbon, manganese, silicon and nickel are higher as well as oxygen content is lower in EP Polarity than in EN Polarity of weld metal. It showed the formation of microstructure such as acicular ferrite which ultimately improves the mechanical properties.

Dwivedi *et al.* [8] investigated the influence of welding parameter (i.e. current, speed) on the microstructure, hardness and toughness of HSLA Steel weld joints. In this paper 16 mm thick HSLA steel plates with heat input limit between (3.0 to 6.3 KJ/mm) by varying welding current (500-700A) and welding speed (200-300mm/min) is used. They found that toughness increased linearly by increasing welding current from 500A to 600A at a given welding speed (200 mm/min or 300mm/min) and further increasing in welding current up to 700 A lowered the toughness. Scanning electron microscopy (SEM) of the fractured surface of impact test specimen was carried out to study the fracture modes. Electron probe micro analysis (EPMA)

was carried out to investigate the variation in wt. % of different element in the weld centre line to the base metal. Weld joint produced using 3.0 kJ/mm heat input do not exhibit the coarse columnar grains while weld joint produced using higher input (3.6kJ/mm, 4.2kJ/mm and 6.3kJ/mm) revealed columnar grain. The Hardness has been found to vary from the weld centre line to base metal was largely uniform.

Mercado *et al.* [9] studied the effect of flux composition for the microstructure and tensile properties of a Submerged arc welded steel. Microstructure and macrostructure of weld were observed with light and scanning electron microscopes (SEM). They found that higher content of TiO_2 leads in chemical composition help to acicular ferrite (i.e. providing a good toughness and tensile strength to the weld region because its fine grain size has a higher resistance to the crack propagation). In this paper different flux compositions were selected in order to analyse the effect of SiO_2, MnO and TiO_2 on weld properties. In the Present study the welding parameters like welding current (600A), welding voltage (30V) and welding speed (0.118m/s) in SAW and their effect on Mechanical properties were studied. The chemical analysis of weld was performed by the X-ray fluorescence spectrometer. In summary, this work showed the importance of the selection for the flux composition in order to improve the Mechanical Properties of steel welds.

Karaoglu *et al.* [10] studied about the sensitivity analysis of process parameters such as welding current; welding voltage and welding speed is used as design variable. The objective function is formed using width, height and penetration of the weld bead. Experimental study is based on 3-Level factorial design of three process parameter and a mathematical model is constructed by using multiple curvilinear regression analysis. Sections of weld were examined using an optical microscope. Magnified photograph were taken and images were processed digitally to measure the weld metal geometry parameter including bead width, bead height and depth of penetration. Sensitivity information should be interpreted using mathematical definition of derivatives. Namely, positive sensitivity values imply an increment in the objective function by a small change in design parameter whereas negative value states the opposite. It used the current range between 400 to 600A; welding speed 6.6667 to 13.3 mm/s and 20V to 30V are welding voltage. They found that bead width is very sensitive to current, voltage and speed variation than that of bead height and penetration. The penetration is almost non-sensitive to variation in voltage and speed. In summary, this work showed the maximum bead width was found at lower current (400A), welding voltage (30V) and welding speed value 6.6667mm/s in the current sensitivity condition. The maximum

voltage sensitivity of bead width is observed at higher current (600A), lower voltage (20V) and lower welding speed value (6.6667mm/s). In the welding speed sensitivity of bead width, bead height and penetration are found in negative sense. Negative welding speed sensitivity of bead width increase with increasing current and voltage, whereas it found maximum decrement with increasing speed at 600A, 30V and 6.6667mm/s welding process parameter.

Chandel *et al.* [11] studied the effect of submerged arc welding parameters on the size of the heat affected zone (HAZ) and heat size to bead size ratio. Among the welding parameter, the welding current has the greatest influence on HAZ size and HAZ to bead size ration, higher current caused smaller heat affected zone (HAZ) and HAZ to bead size ratio. Other parameters like heat input, polarity also affect HAZ to bead size ration while voltage, electrode diameter have no significant effect on HAZ size. The HAZ is undesirable but unavoidable region of a fusion welded joint. A large wide HAZ indicated poor toughness and larger grain thus coarse grain size due to maximum Soaking time.

Bhole *et al.* [12] carried out the effect of alloy addition of Ni (Nickel), Molybdenum (Mo) in the weld metal decreasing the volume fraction of grain boundary ferrite (GBF) and promoted formation of higher toughness of acicular ferrite (AF). They found that decreasing micro-structural defect and increasing the inter phase bond strength and phase uniformity. It showed that the addition of Mo in the range 0.817-0.881 wt. % resulted in a decreasing of fracture appearance transition Temp. (FATT) and an increasing of impact toughness, GBF in weld metal. But the combination of both Ni (2.03-2.91 wt.%) and Mo (0.7-0.995 wt.%) in the weld metal with produced fine AF (Acicular Ferrite) with good toughness and grain boundary ferrite (GBF) are reduced. When Ni is added alone in the range (2.03-3.75 wt. %) the weld metal showed a lower toughness. The weld metal microstructures (tested by scanning electron microscope with X-rays microanalysis) showed the optimum impact toughness at 45ºC of 77% acicular ferrite and 20% granular bainite.

Sahni *et al.* [13] studied that slag generated during submerged arc welding can be recycled by mixing varying percentage of crushed slag with fresh flux to use in further operation. The influence of using flux-slag mixture on weld chemistry has been investigated. According to AWS requirement carbon content should be 0.015-0.15% and then chemical analysis indicates that carbon content decreased with addition of slag in fresh flux and they showed that decreasing the amount of deoxidizers in the flux weld metal Finally, it was found slag mixed with fresh flux up to 60% can produce sound weld. The use of slag flux mixture

reduced sulphur and phosphorous in weld metal which is beneficial regarding toughness of the weld.

Nowacki and Pawel [14] discussed the influence of heat input SAW duplex (double) steel on kind and quantity of welded butt joint and its defect identify. It used the heat input between 2.5 to 4.5 KJ/mm to affect the mechanical and metallurgical properties on weld bead of 10-32mm steel thickness plate. It was shown that SAW of duplex steel with the heat input from 2.5 up to 4.0 KJ/mm has no negative influence on mechanical properties of joint. It was also observed that slightly less welding defect (i.e. slag, and crack propagations, lack of a joint penetration for plates of thickness of 10-23 mm) found with heat input up to 3.0 KJ/mm. It used the radiography method to identify the defects in welding region. It was observed that increase of plate thickness increased weld defectiveness of duplex steel but increased heat input reduce the welding imperfection in joint, which reduced the cost of testing and repairs. Formula used for finding out Percentage index of welding defectiveness was (W) =RN×100/RC, Here RN is the quantity of radiograph with negative result, RC the complete quantity of radiograph.

Shen *et al.* [15] showed how variation in heat input achieved using single and double wires affected bead reinforcement, bead width or other bead geometry. The level of dilution and different melting efficiency were calculated and their variation with heat input. In the present study showed that penetration and HAZ increased as well as heat input increased but bead contact angle decreased with it. The electrode melting efficiency increased with increasing heat input for single wire welding, but plate melting efficiency did not change much for both single wire and tandem wire welding.

Beidokhti *et al.* [16] studied the effect of titanium addition on the SAW weld metal microstructure of pipeline steel. The microstructure and toughness of weld metal can be studied by means of full metallographic, longitudinal tensile, charpy V notch test on the specimen cut transversely to the weld bead. The best combination of microstructure (i.e. increase acicular ferrite) and impact properties or increase Percentage of shear fracture area was obtained in the range of 0.02-0.05% titanium .The increased Ti content in the weld metal leads to an increase in the titanium content of inclusions. It used flux (alumina flux has basicity index of about 1.3),0.5% Mn and 0.2% Si transfer to the weld deposit. With the addition of Ti to the flux, the recovery of Mn and Si was increased and the amounts of these elements in the weld metal were promoted. They showed that high content of Ti, the

difference of manganese percentage between the weld metal and base metal was about 0.7%. It also found that Ti addition greater than 0.09%, the high manganese content will be found in the weld metal but it is the negative effect.

Yayla *et al.* [17] used different welding techniques to evaluate the Mechanical performance of weldment of HV-80 steel. Its main objective is to determine the optimum welding method for steel. The effect of welding method on the weld metal microstructure and mechanical properties including weld metal tensile strength and charpy V-notch impact toughness over the temperature Range -20°C to 200°C was investigated. The different welding method has remarkable effect on the fracture resistance and hardness of HAZ of 22mm thickness steel is used. It was investigated that the entire tensile test carried out on the sample extracted from the weldment, the rupture occurs at the main material. The charpy V-notch impact test results have shown that, due to higher input, the SAW have better HAZ toughness than the GMAW (Gas Metal Arc Welding) process. Moreover, the hardness tests results have shown than the SAW welding method have given slightly higher hardness profile across weld metal and HAZ than the GMAW.

Tusek *et al.* [18] investigated the multiple-wire Submerged-arc welding and cladding with metal-powder addition. It was found that the use of metal powder increased the deposition rate and the welding arc efficiency and reduced the shielded flux consumption. The metal powder is supplied through a tube mounted between the wires, the arc of the first wire will also melt the parent metal and the arc of second wire will melt the metal powder and shape the final run. Finally, it was shown that the energy efficiency and deposition rate could be increased by even 60% while the shielding-flux consumption is very low. Mainly alloy of weld is used in the metal-powder addition.

Gulenc *et al.* [19] observed worn roller parts welding using the SAW process with different wires and fluxes were used for this purpose. This welded part was subjected to wear test under different load and changes in the hardness and metallurgical behaviour were examined. The result showed that the hardest weld metal showed the highest wear resistance while the least hard weld metal showed the least wear resistance. The specimens were then subjected to wear test on a pin-on-disk test apparatus. It appeared that increasing carbon, manganese and chromium in the weld wire, wear resistance increased and wear resistance is also depending upon the chemical composition of the weld wire and flux. Finally it showed that the fine-

grained structure exhibited better wear resistance than a coarse-grained structure by help of Metallographic investigation.

Ravi *et al.* [20] investigated the influence of post weld heat treatment (PWHT) on fatigue life prediction of different Mis-Match Ratio (MMR), under Matched (UM), even Matched (EM) and over Matched (OM) weld metals. A Centre Cracked Tension (CCT) specimen has been used to evaluate the fatigue crack growth behaviour of the welded joints. Mis-Matched Welded joints are joints in which the yield strength or microstructure of the weld metal will be different from that of the base metal and HAZ. The MMR is the ratio between the yield strength of weld metal and yield strength of base metal. Post weld heat treatment is used because it reduce the effect of any stresses induced by the welding process and tempers the heat affected zone and did not affect the strength and impact toughness of weld metal greatly but decreased the hardness and increased the percentage of elongation. Finally, it found the fatigue crack growth rate is much faster in the case of under match joint when compared to over match joint because mis-match ration is having inversely proportional relationship with fatigue crack growth exponent.

Shan-Ping Lu *et al.* [21] observed the wear resistance of Fe-Mn-Cr-Mo-V alloy cladding deposited on SM45C Substrate (Carbon steel) by automatic SAW using stoody 105 alloy wires. In this paper the microstructure and surface hardness of the cladding were investigated under different welding condition and the results showed that the retained austenite in the cladding increase with the increased welding current and reduced travel speed because that time cooling rate is decreased as well as increased current so the austenite to martensite transformation was partially prevented and the retained Austenite is increased. The wear behaviour of the clad was studied using ball on disk tribometer and wear mechanism was analysed based on the analysis of the worn surface both the clad and ball by scanning electron Microscope (SEM) equipped with an Energy Dispersive Spectrometer (EDS).Cladding technique improved the surface properties, such as wear and the corrosion or oxidation resistance. Cladding is the deposition of dissimilar material on the surface of substrate to obtain desired properties, which using special heat source such as arc, flame, induction heat etc. Finally, it also found that Comparing to other welding process, submerged arc cladding offer high deposition rate, higher layering capacity and better bead characteristics. Finally, the more is the retained austenite; the lower is the surface hardness.

Pandey *et al.* [22] investigated of SAW and flux basicity index of the weld chemistry and transfer of element manganese, silicon, carbon and sulphur. It used different type of flux

composition and welding parameters. They found that weld metal has minor influence by basicity index of flux but strength, toughness and solidification cracking behaviours are mainly affected by chemical composition. It also found that welding parameters influenced by both weld metal and weld composition. The weld parameter composition showed, in general, gain of silicon and loss of carbon, manganese and sulphur element.

Kumaresh *et al.* [23] studied an experimental work carried out to evaluate and compare corrosion of carbon steel boiler weldment by SAW process with four different heat input exposed to hydrochloric acid medium at 0.1 M, 0.5 M and 1.0 M concentration at 100°C. Electrochemical polarization technique such as tafel line extrapolation (Tafel), Linear polarization Resistance (LPR) method have been used to measure the corrosion current and finally it found corrosion rate for weld metal and HAZ decrease with increase in heat input and corrosion rate increase if the level of concentration is going to increase.

Datta *et al.* [24] carried out application of the Taguchi method in combination with grey relational analysis for solving multiple objective optimization problems in Submerged Arc Welding (SAW). Taguchi's L9 Orthogonal array design has been adopted and experiment have been according conducted with three different level of conventional process parameter using welding current and flux basicity index to obtain bead-on-plate weld on mild steel plates. The slag, generated during welding, has been consumed in further runs by mixing it with fresh unmelted flux and fresh flux has been defined as slag mix percentage welding has been performed by using varying slag mix percentage, treated as another process variable, in order to obtain the optimum amount of slag-mix that can be used without any alarming adverse effect on bead geometry an HAZ.

It showed that 10% slag-mix can be used obtain optimum bead width and depth of HAZ, whereas 15% and 20% would yield optimal reinforcement and depth of penetration respectively.

Chandel *et al.* [25] studied that by adding the powder in SAW, a better use of heat can be made; thus, for a given heat input, the no. of passes required to fill a joint can be reduced and therefore, it showed that the total energy supplied to the joint can be reduced. Finally, They found the higher deposition rate can be achieved by lowering heat input per pass without losing its mechanical properties weld metal produced under faster cooling rates are also superior in mechanical properties. It showed the width of HAZ is less in the case of powder addition. Thus the process of powder addition may become attractive for welding HSLA

because it not only cost effective but they also found acicular type grain structure of welded region.

Bang Kook-Soo *et al.* [26] studied that submerged arc welding was performed using cored wire and fluxes with different composition. The effect of flux composition on the different process parameters i.e. chemical composition, tensile strength and impact toughness of weld metal were investigated and interpreted in term of element transfer between the slag and the weld metal, i.e. quantity. Both carbon and Manganese show negative quantity in most combination, indicating the transfer of the elements from the weld metal to the slag during welding. The amount of transfer however is different depending on the flux composition. More basic flux give less negative ΔC and ΔMn through the reduction of oxygen content in the weld metal and presumably higher Mn activity in the slag. The transfer of silicon however is influenced by Al_20_3, TiO_2 and ZrO_2 contents in the flux. The value of Si increases if these oxides content in the flux increase.

It showed the P_{cm} Index calculated from the chemical composition of weld metal, according to varies, depending upon different combination (i.e. here use two different composition metal core wire and three type of flux with basicity index is 0.62, 1.82, 1.90 is used. They found that tensile strength of weld metal increased almost linearly with an increased in the P_{cm} Index. P_{cm} Index is equal to C+Si/30 Mn/20+Cu/20+Ni/60+Cr/20+Mo/15+V/10+5B.The impact toughness of the weld metal increased with an increase of flux Basicity through a reduction of oxygen content in the weld metal.

Vera *et al.* [27] discussed the Post weld Heat Treatment (PWHT) frequently applied to steel pressure vessel, following the requirement of the ASME code which establishes the parameter of the PWHT based on the thickness and chemical composition of the welded section. After welding process, the plate was cut into two piece and one of the part was subjected to PWHT at 650^{o}C during 5 hour and after light and scanning electron microscopy technique examine the microstructures of the base metal, HAZ and weld metal and toughness of the weld metal, HAZ and base metal was evaluated by means of a charpy impact test. Finally result showed that this PWHT practice promoted a reduction in the mechanical properties of the base metal and the HAZ but toughness of the weld metal is increased.

Kumar *et al.* [28] investigated that the chemical composition and mechanical properties of the all weld metal prepared from the developed flux (acidic and basic agglomerated flux) prepared from the waste flux dust.Approx.10-15% of the flux get converted into fine particles

termed as flux dust before and after welding, due to transportation and handling. If welding is performed without removing these very fine particles from the flux, the gases generated during welding are not able to escape, thus it may result into surface pitting (pocking) and even porosity. If the fine particles are removed by sieving, the cost of welding will be increased significantly and if the flux dust is damped/ thrown will create pollution.

It prepared two agglomerated cost effective flux (first is acidic and another one is basic) with addition of potassium silicate as binder (it have high arc stability capacity) and aluminium powder as deoxidizer and it was mixed for 10 minute and after dried in air for 24 hours and then baked in the muffle furnace between 650^{o}C-700^{o}C for nearly 3 hours. Finally it showed the welded joints were also found to be radio graphically sound. Therefore the developed fluxes prepared from the waste flux dust can be used without any compromise in mechanical properties and quality of the welded joint. It reduced the cost of welding and pollution.

Zrilic *et al.* [29] investigated the toughness and crack properties of the welded joint, both in the weld metal and the heat affected zone (HAZ). Experimental investigation of toughness and crack resistance parameter through static and impact test of a high strength low alloy steel (HSLA) with a nominal yield strength of 700 MPa and its welded joint were performed on charpy-sized specimen, V-notched and pre-cracked of the parent metal, weld metal and HAZ. The result showed that the toughness and crack resistance of the weld metal were significantly lower than those of the parent metal and the HAZ. The heterogonous microstructure present in the HAZ show sufficient cracking resistance. It showed that WM cracking resistance can be further improved by selecting consumables with higher nickel percentage.

Bhattacharya *et al.* [30] studied the effect of process parameters like effect of flux, welding current, arc voltage and travel speed on changes in micro hardness and microstructure of the HAZ (heat affected zone) and to optimize the process so that minimal changes occur in the material properties after completion of a SAW following suitable Taguchi experimental design. Welding current and type of flux were found to be the most significant factor leading to changes in micro hardness and metallurgical properties.

By Taguchi experiment taking four factors i.e. flux with two level (i.e. BI is 0.8 and 1.6), current in ampere with three level 350,400 and450, travel speed (m/h) is also with three level 27,29 and 31 and voltage variation (i.e. 28,30 and 32V), experiments were conducted. Flux index with 0.8 showed a significantly higher micro hardness as compared to flux with B.I of 1.6 because due to lower amount of CaO and Mgo present in flux 2 has a tendency to pick up

carbon from steel work piece, and then reduce the production of martensite so that finally hardness decreased with change of flux from level 1 to level 2 while ferrite content increased and if current (A) is increased from 350 to 450 as well as hardness increased but ferrite count decreased. The result are as expected as higher ferrite content mean less hardness thus correlating the two response to each other.

Yun *et al.* [31] studied the microstructure and properties of the welding HAZ of laboratory-produced HCM12A steel with thickness14 mm using welding thermal simulation method. The microstructure of HAZ of the steel are insensitive to cooling rate but can be changed remarkably by Post welding heat treatment (PWHT). It applied the welding thermal cycles are 800°C, 850°C, 900°C, 950°C, 1000°C, 1150°C and1300°C and the holding time at the peak temperature was 5 sec. for all thermal cycles and the specimen were cooled down to below 200°C with cooling rates of 5°C/s, 20°C/s and 50°C/s and then these samples were taken out from the jaw and cooled down to room temperature. After the above welding thermal cycles, some of these samples were heat-treated with the processes of 740°C holding 2 hrs. and air cooled. Optical microscope and micro hardness apparatus were used for microstructure observation and hardness examination. It showed when the peak temperature of the simulated HAZ is up to 1300°C, the test steel is overheated, and the austenite grain will grow up rapidly. It showed that the hardness of the simulated HAZ at this peak temp. is reduced after PWHT, all the hardness value exceed HV460 if no PWHT is carried out. When the PWHT is used, the hardness value of are decreased to below HV300. The decrease of the hardness for this area is beneficial for improving its ductility and toughness and if no PWHT is performed, the microstructure of the simulated HAZ, at the peak temperature i.e. 800°C, 850°C and 900°C is mainly composed of tempered sorbite, fine low-carbon martensite, carbide and nitride and the microstructure of the simulated HAZ at higher peak temp.

Singh *et al.* [32] investigated that the reuse of slag can be very economical and also ensure that no maximum change in chemical composition and mechanical properties of weld metal according to AWS (American Welding Society) .The flux used in SAW is convert into slag during welding which is presently a waste. This slag is brittle or glassy material so that it cannot be used as a filling material in building construction or other ways. The recycling slag is prepared by adding of alloying element/deoxidizers were added and 20% solution of potassium silicate binder was added to wet the dry mixed powder (powder is prepared by ball or roller mill).It was found that reuse of slag has minor effect on mechanical properties of weld metal.

Shafeek *et al.* [33] introduced a computer vision system is investigated to detect the welding defect of gas pipe line from the radiography technique. It used computer vision algorithms to detect the welding cracks, defects and also to calculate the size of defects such as length, width, area and perimeter of the defects It used automatic welding defects assessment (AutoWDA) software was totally based on Microsoft visual C++ to measure the radiography films.

2.3 LITERATURE SUMMARY

After studying the literature it can be concluded that a lot of work has been done in the field of submerged arc welding, in one way or another. Some investigators have focused on effect of using different SAW welding parameters on weld bead geometry, chemical composition and mechanical testing of Submerged Arc Weld metal. Some investigators have studied the effect of flux composition or mixture of flux-slag for the microstructure, size of HAZ and tensile properties of submerged-arc welded steel. Some other researchers studied the effect of alloying element or metal powder addition on the mechanical properties with microstructure of weld metal in HSLA steel. Some other researchers studied the effect of process parameters for parametric optimization on bead geometry, micro hardness, microstructure of HAZ in SAW by using Taguchi philosophy. Some investigators have studied the influence of PWHT on fatigue life prediction, microstructure and properties of the welding HAZ of steel. Many studies have been done to detect the quality of weld by radiography film through computer vision system.

It can be concluded from literature review that the main process parameter are welding current, preheat temperature, travel speed, electrode stick-out, electrode diameter which affect the properties like strength, toughness, micro hardness and quality of welded joints during SAW.

2.4 GAPS IN LITERATURE

- It was also observed that very few comprehensive studies have been reported for HSLA material which was welded with multi-pass submerged arc welding process.
- Radiography tests are very important test for HSLA steels during Submerged Arc Welding which is being used for showing the crack & Defects but very less emphasis have been given to it and also rarely reported.

- After literature survey it was found that very few comprehensive studies has been reported for HSLA material with thicker plate and also some, not all, factors have been studied for process optimization using design of experiment.
- None of the study reported in the literature comprehensively cover all the welding parameters for HSLA material greater than 28 mm thickness during SAW.
- In the present study it is proposed to carry out the above tests along with other mechanical tests like micro hardness, impact Strength (toughness), change in microstructure, chemical composition, study of heat affected zone, tensile strength and study of bead geometry of welded joint i.e. bead height and bead width will be reported.

2.5 OBJECTIVE OF THE STUDY

The objective of this study is to investigate the effects of welding parameters such as welding current, travel speed, different flux compositions, electrode stick-out, pre-heating of work piece and filler wire diameter on quality inspected of weld region by radiography, tensile strength, bead geometry i.e. bead width and bead height, impact strength at different temperature, micro hardness, chemical composition, metallurgical behaviour of the weld metal of HSLA work piece using submerged arc welding (SAW).Design of experiments and analysis of variance (ANOVA) using MINITAB 16 software were used to optimize the process parameters. In the present work SAW process was carried out by using three levels of welding current, speed, flux, electrode stick-out, preheating of workpiece. Electrode wire of 3.2 and 4 mm diameter were used as filler wire.

CHAPTER-3
DESIGN OF EXPERIMENTAL STUDY

The literature review showed that any change in the parameter of submerged arc welding affect the properties of welding. So, in this study it was proposed to find out the effect of changing different welding parameters on microstructure, quality of welds, weld geometry (bead height and bead width), tensile strength, and toughness at different temperature, micro hardness and change in chemical composition. The high strength low alloy steel plate of dimension 100 x 125 x 28 (lxbxh) mm was used as a work material.

Table 3.1 shows the composition of base metal was found by using atomic absorption spectrometer.

FIGURE 3.1 Chemical Composition of base metal by using spectroscopy

TABLE 3.1 Chemical composition of base metal

C	Si	Mn	P	S	Ni	Cu	Cr
0.13	0.25	0.39	0.003	0.01	1.76	0.5	0.41

Taguchi experiments have been conducted on Submerged Arc Welding Machine (Tornado Saw M-800 transformer and FD 10-200T welding tractor) available at Central Workshop, Thapar University, Patiala as shown in Figure 3.2.

The main parts of the machine are control box panel, flux hopper, wire reel, electrode wire, wire feeder, power source and auto torch flux. Digital Control box panel is provided on the machine for control the welding current, voltage and travel speed. Electrode wire and flux is passing through electrode gun on the work piece as shown in figure ahead. SAW process can be manual or can be automatic. There is also welding head site adjustment function it make the gun move horizontally and vertically.

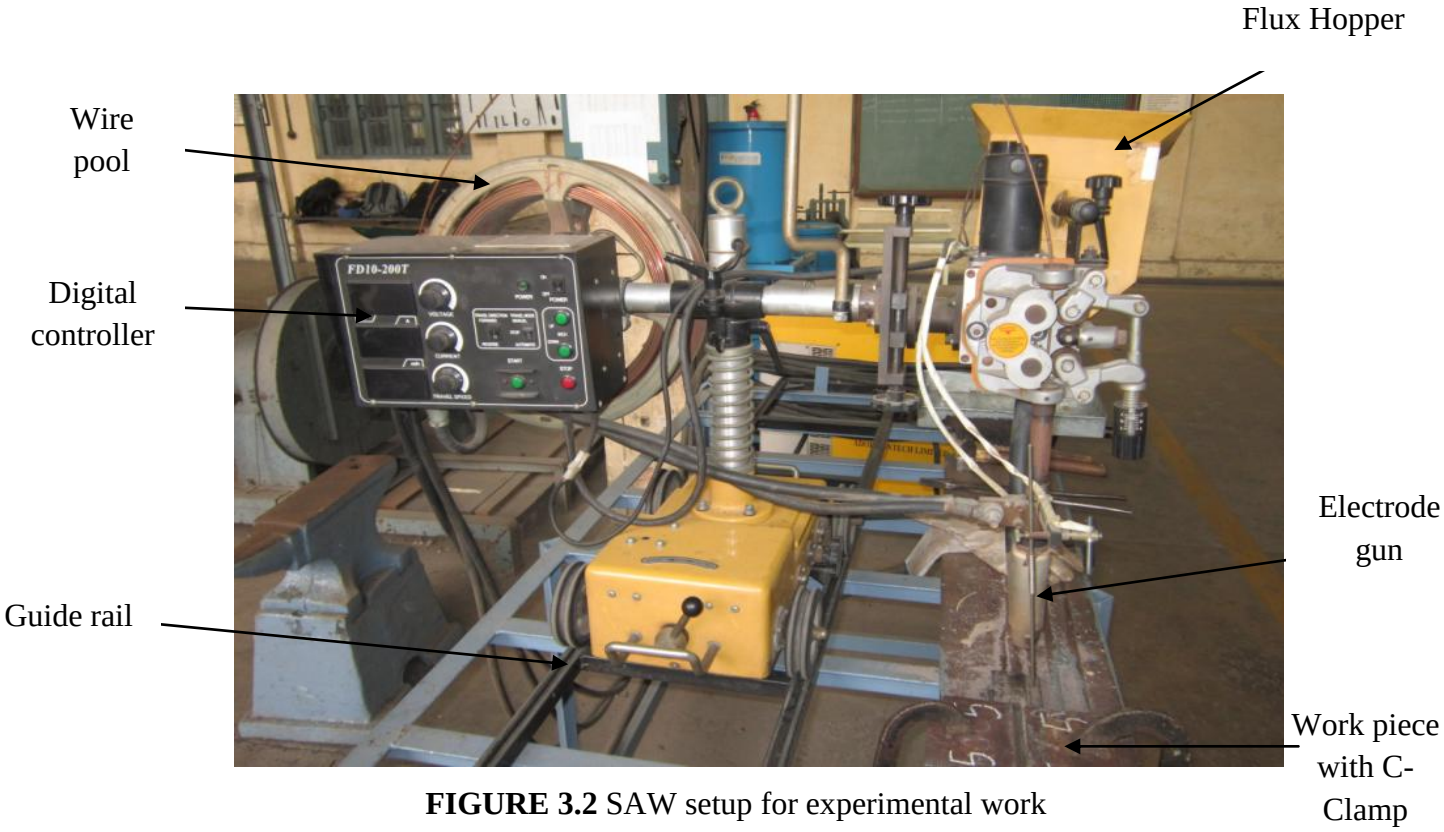

FIGURE 3.2 SAW setup for experimental work

(**Courtesy:** Central Workshop, Thapar University, Patiala)

3.1 PILOT EXPERIMENTATION

In order to study the contributing factors that affect the response parameters, pilot experiment was carried out on the SAW machine. For the pilot experiment current, voltage, travel speed, electrode stick out, edge including angle, preheating of work piece and different flux composition were varied at three levels each and electrode diameter were varied at two levels as shown in table 3.2.

TABLE 3.2 Process parameters and their parameters for pilot study

Serial No.	Contributing Factors	Units	Level 1	Level 2	Level 3
1	Welding current	Amp.	350	400	450
2	Voltage	V	28	30	32
3	Speed of arc travel	m/hr	15	18	20
4	Electrode stick-out	mm	20	28	35
5	Edge including angle	degree	60	75	90
6	Pre heating of workpiece	^{O}C	No Preheat	100	150
7	Different flux composition		1	2	3
8	Electrode diameter	mm	3.2	4	---

Based on the above experiment it was observed that edge including angle and voltage had no significant impact on optimal conditions for SAW through pilot study so that voltage has taken 30 V constant values in further study. It was also observed from the above study tensile strength and micro hardness is continuously increasing with increasing the welding current and decreasing the travel speed. But in the pilot study burn through defect was observed then it used higher current value (500A) with lower value of travel speed as shown in figure.3.3. It was concluded that 400A to 500A current,18 to 22 m/hr travel speed, 25 to 35 mm electrode stick-out and room temperature to 200^{O}C preheat temperature were chosen for the present experiment work. In the present experimental setup, there are five factors varied at 3-level and one factor varied at 2-level were chosen through pilot study for the SAW. Hence only six factors were taken up for the detailed Taguchi experiment. Taguchi design has been used for the design of experiments, because it reduces the number of iterations and used to optimize the known parameters.

A literature review and based on above experiment suggested that when doing SAW machine on HSLA steel plates above 28mm thickness the values of different parameters should be given in Table 3.3.

FIGURE 3.3 Burn through defect was observed due to higher current and lower travel speed

TABLE 3.3 Process parameters and there levels that effects welding

Serial No.	Contributing Factors	Units	Level 1	Level 2	Level 3
1	Welding current	Amp.	400	450	500
3	Speed of arc travel	m/hr	18	20	22
3	Electrode stick-out	mm	25	30	35
4	Pre heating of workpiece	^{O}C	No Preheat (30)	125	200
5	Different flux composition		1	2	3
6	Electrode diameter	mm	3.2	4	---

3.2 ORTHOGONAL ARRAY

The Taguchi method involves reducing the variation in a process through robust design of experiments. The main objective of taguchi method is to produce high quality product at low cost to the manufacturer. It was developed by Dr. Genichi Taguchi of Japan who maintained that variation. To select an appropriate orthogonal array for experiments, the total degrees of freedom must be computed. The degrees of freedom are defined as the number of comparisons between process parameters that must be made to determine which level is better and, specifically, how much better it is. For example, a two-level process parameter counts for one degree of freedom. The degrees of freedom associated with interaction between two process parameters are given by the product of the degrees of freedom for the two process parameters. In the present study, once the degrees of freedom are known, the next step is to select an appropriate orthogonal array to fit the specific task. The degrees of freedom for the orthogonal array should be greater than, or at least equal to, those for the process parameters. In this study, Taguchi L18 orthogonal array with six columns and eighteen rows was used. Each welding parameter was assigned to a column and eighteen welding parameter combinations were tested. Therefore, only eighteen experiments were required to study the entire welding parameter space using the L18 orthogonal array. The experimental layout for the welding parameters using the L18 orthogonal array is shown in Table 3.4.

EXPERIMENTAL PLAN

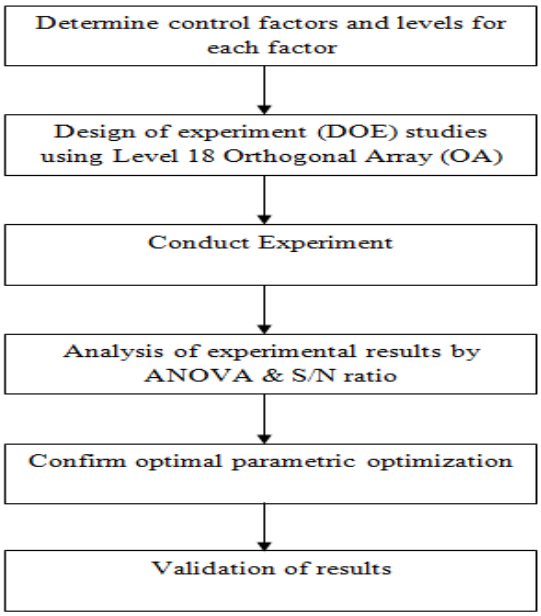

FIGURE 3.4 Flow chart of experimental plan

TABLE 3.4 orthogonal arrays for experimentation

Exp. No.	Electrode Diameter 'Ø' (mm)	Current 'C' (Amp)	Electrode Stick-Out 'D' (mm)	Preheat Temperature 'T' (^{o}C)	Travel Speed 'S' (m/hr)	Flux 'F'
1	3.2	400	25	30	18	1
2	3.2	400	30	125	20	2
3	3.2	400	35	200	22	3
4	3.2	450	25	30	20	2
5	3.2	450	30	125	22	3
6	3.2	450	35	200	18	1
7	3.2	500	25	125	18	3
8	3.2	500	30	200	20	1
9	3.2	500	35	30	22	2
10	4	400	25	200	22	2
11	4	400	30	30	18	3
12	4	400	35	125	20	1
13	4	450	25	125	22	1
14	4	450	30	200	18	2
15	4	450	35	30	20	3
16	4	500	25	200	20	3
17	4	500	30	30	22	1
18	4	500	35	125	18	2

3.2.1 Selection of orthogonal array and factor assignment

In this experimental study, five factors were varied to three levels each and one factor were varied to two levels. The degree of freedom (DOF) to a three level parameter is 2 (because DOF = number of levels -1), similarly DOF for two level parameter is 1. Hence total DOF for the experiment is 11. So the Orthogonal Array (OA) which could be used was L18. Degree of freedom allocated to various factors is given in table 3.5

TABLE 3.5 DOF allocated to various factor combinations

Serial No.	Parameter	Units	DOF
1	Welding current	Ampere	2
2	Flux	----	2
3	Travel Speed	m/hr	2
4	Preheat Temperature	^{O}C	2
5	Electrode stick-out	mm	2
6	Electrode Diameter	mm	1
	Total		**11**

3.3 FILLER WIRE

The filler wire used for root layer on the both side of double-V butt joint in the experiment work was EH14 of diameter 3.2 mm and 4 mm. According to American welding standards its AWS code is F7A2-EH14.

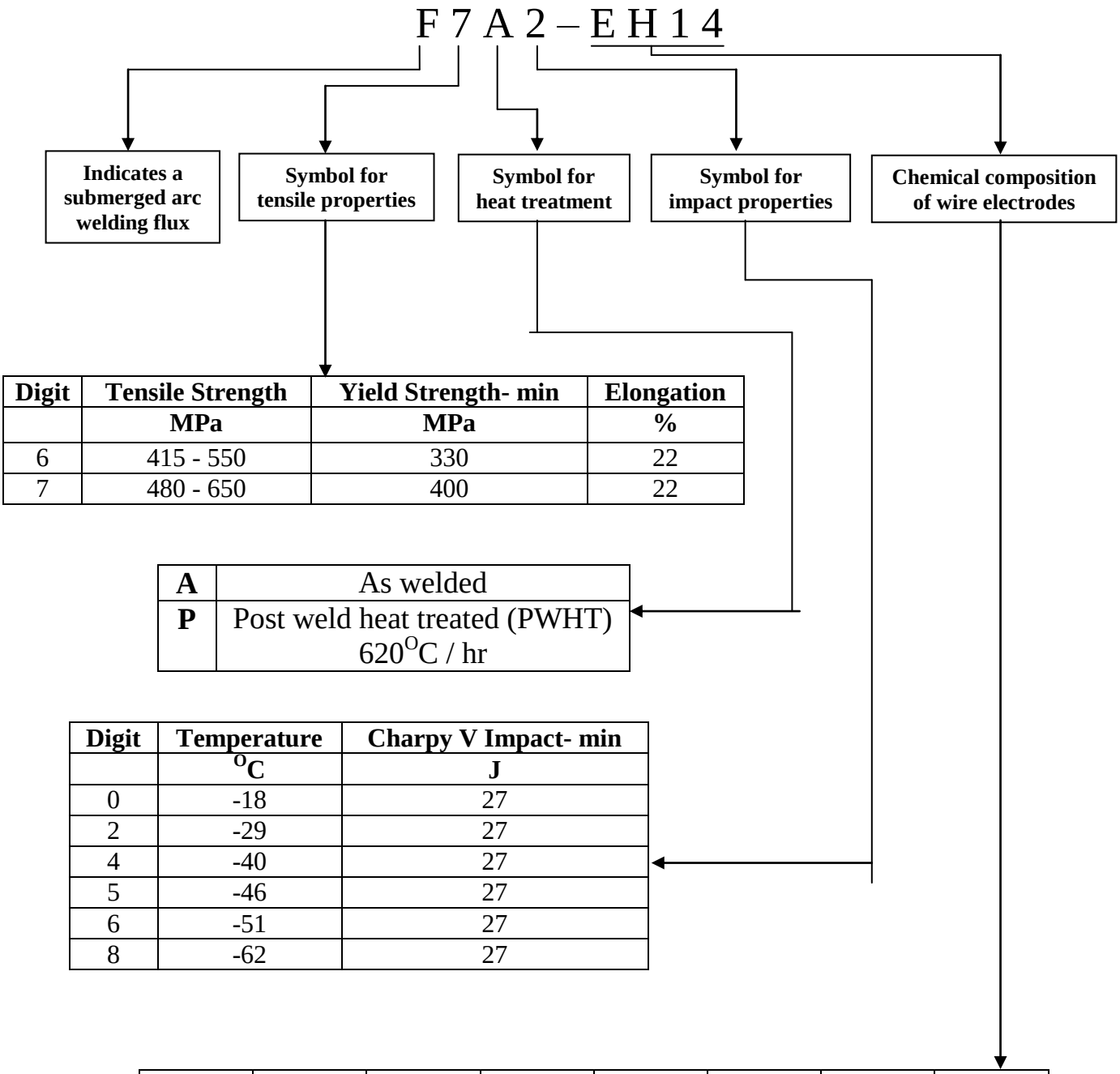

Digit	Tensile Strength	Yield Strength- min	Elongation
	MPa	MPa	%
6	415 - 550	330	22
7	480 - 650	400	22

A	As welded
P	Post weld heat treated (PWHT) $620^{O}C$ / hr

Digit	Temperature	Charpy V Impact- min
	^{O}C	J
0	-18	27
2	-29	27
4	-40	27
5	-46	27
6	-51	27
8	-62	27

C	Si	Mn	P	S	Ni	Cu	Cr
0.12	0.08	1.88	0.019	0.016	0.03	0.14	0.08

FIGURE 3.5 Filler wire AWS code F7A2-EH14

3.4 FLUX

Three different types of flux were used in this study i.e. AUTOMELT B31, GEE FLUX 544 and GEE FLUX 541 (Make: ADOR Welding Ltd. and GEE Ltd.) which was compatible with EH14 SAW filler wire as shown in Figure 3.6. In which Gee flux 541 and Gee flux 544 fluxes were of basic in nature and Automelt B31 is neutral in nature. Table 3.6 shows the

basic detail and percent composition of different element present in the fluxes that used in this experiment work.

TABLE 3.6 Concentration of different percent composition in fluxes

S. No.	Flux Name	Flux Type	SiO_2 + TiO_2	CaO + MgO	Al_2O_3 + MnO	CaF_2	C	Mn	Si	S	P	Cu
1	GEE FLUX 541	Basic	-	-	-	-	0.07	1.64	0.33	0.015	0.021	0.12
2	GEE FLUX 544	Basic	15 %	35 %	20 %	30 %	-	-	-	-	-	-
3	AUTO MELT B31	Neutral	15 %	20 %	30 %	35 %	-	-	-	-	-	-

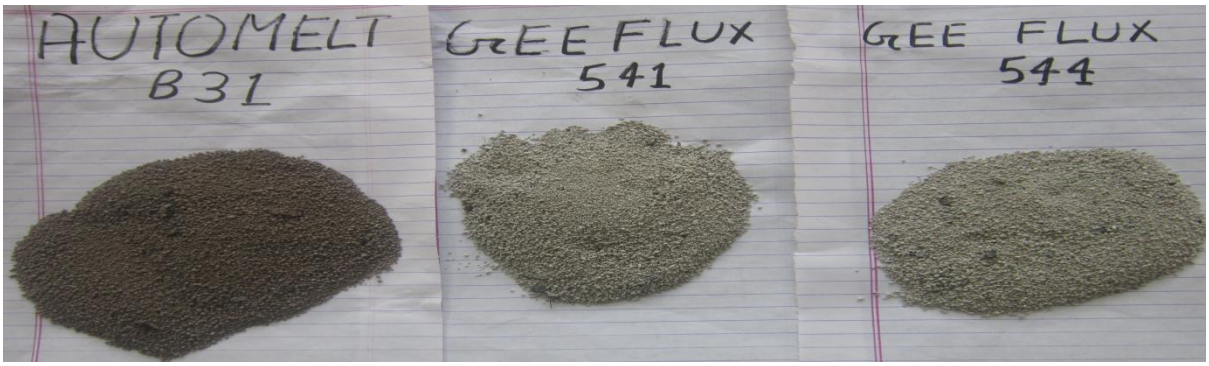

FIGURE 3.6 Flux used for experimental work

3.5 METHOD OF EDGE PREPARATION OF STEEL PLATES

The HSLA steel plates available for the study were of size 1000 x 500 x 28 mm. These were first cut to strip of size 1000 x 125 x 28 mm using oxy-acetylene gas cutting as shown in Figure 3.6. Then these HSLA steel strips were cut to the required size of 100 x 125 x 28 mm with power hacksaw (Make: Jaura, India) as shown in Figure 3.7.

FIGURE 3.7 Cutting of steel plates through oxy-acetylene gas cutting

FIGURE 3.8 Cutting of steel strip through power hacksaw

(**Courtesy:** Central Workshop, Thapar University, Patiala)

In this study L18 was chosen as the preferred array, 36 plates were cut to size of dimension 100 x 125 x 28 mm for experiment because two plates were required for welding in each trial. Edge preparation was completed on each of the 36 plates as per the requirement of 18 trial condition given by taguchi orthogonal array. The edge preparation of 60^{o} on both side of work piece was made on 125 mm side as shown in figure 3.7. Edge preparation was done on shaper as shown in Figure 3.9. Groove between two plates is shown in figure 3.10. After edge preparation, the plates were tacked through manual arc welding to avoid misalignment as shown in figure 3.9.

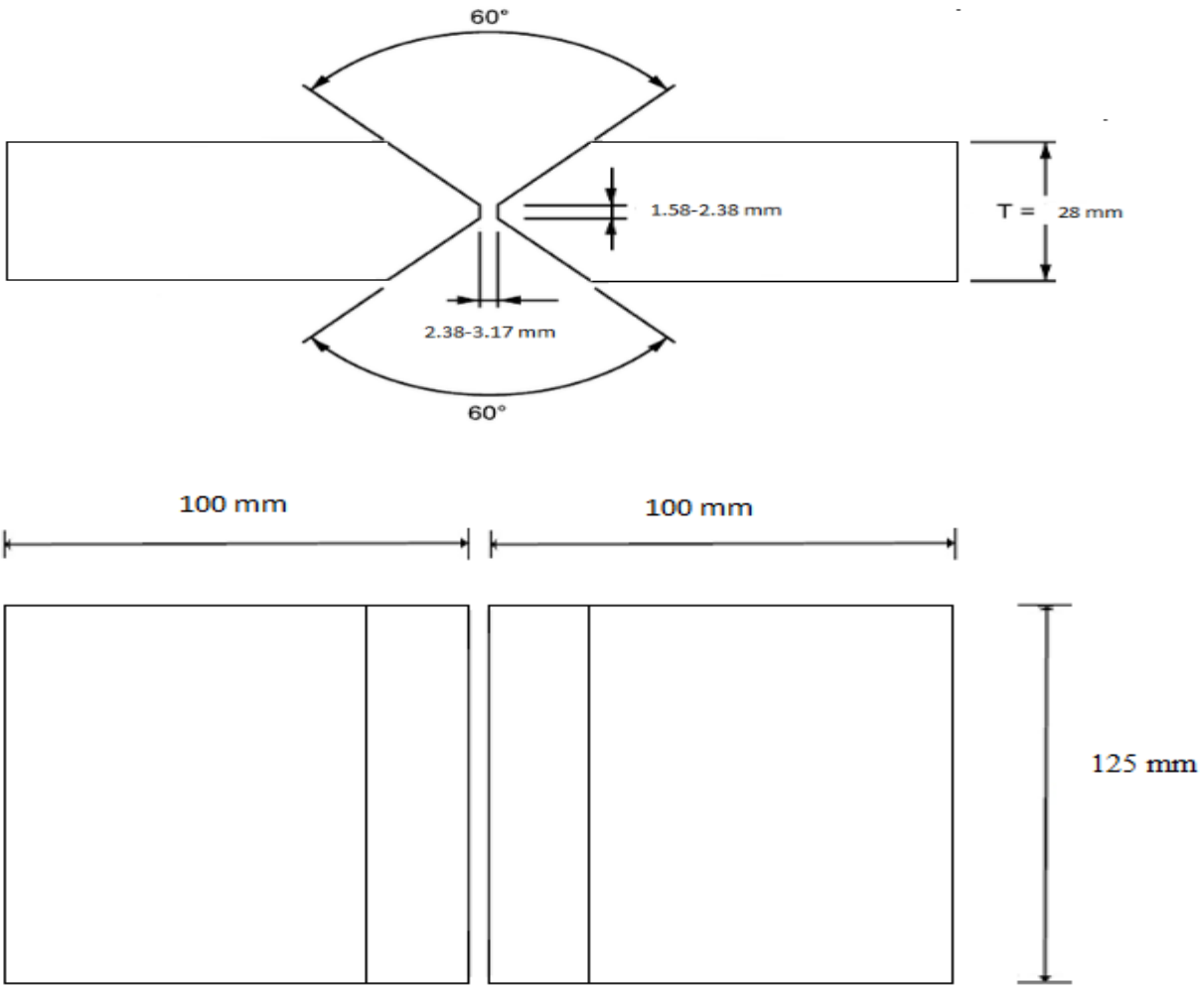

FIGURE 3.9 Double-V Groove geometry (a) front view and (b) top view (all dimensions are in mm)

FIGURE 3.10 Making chamfer on corner of plate

(i)

(ii)

FIGURE 3.11 Double-V Groove between two plates **(i)** front view **(ii)** top view

(i) **(ii)**

FIGURE 3.12 (i) Tacking and Rooting on Double-V Groove plates through SMAW (ii) Back side penetration observation on plates

After tacking, the specimens were put on the base plate of SMAW (Shielded Metal Arc Welding) and were clamped with base plate. Finally a root layer was deposited by filler wire as shown in Figure 3.11. The electrode used for SMAW was E7018 for the root layer purpose on the both side of plate. Table 3.7 and 3.8 shows the composition of electrode and value of input process parameter for SMAW.

TABLE 3.7 Chemical composition of SMAW Electrode wire

C	Si	Mn	P	S	Ni	Mo	Cr
0.12	0.75	1.6	0.04	0.03	0.3	0.3	0.2

TABLE 3.8 Value for input process parameter for SMAW

Serial No.	Parameter	Units	Value
1	Current	Ampere	140
2	Travel Speed	m/hr.	8-10
3	Electrode Diameter	mm	3.15

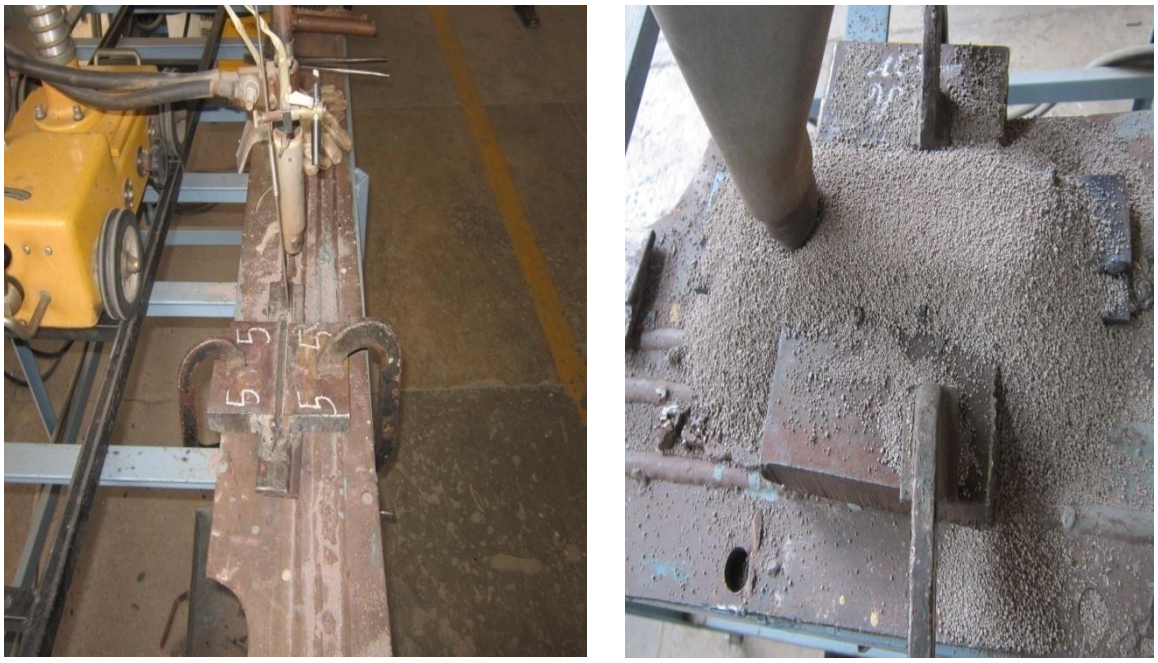

FIGURE 3.13 Submerged arc welding of plates after single layer

FIGURE 3.14 Multi layer Joint of double V-groove plates after welding

FIGURE 3.15 Welding on all specimens through SAW

After welding the parts were cut to size as per the requirement for tensile test, toughness, micro hardness, metallurgical structure and chemical composition

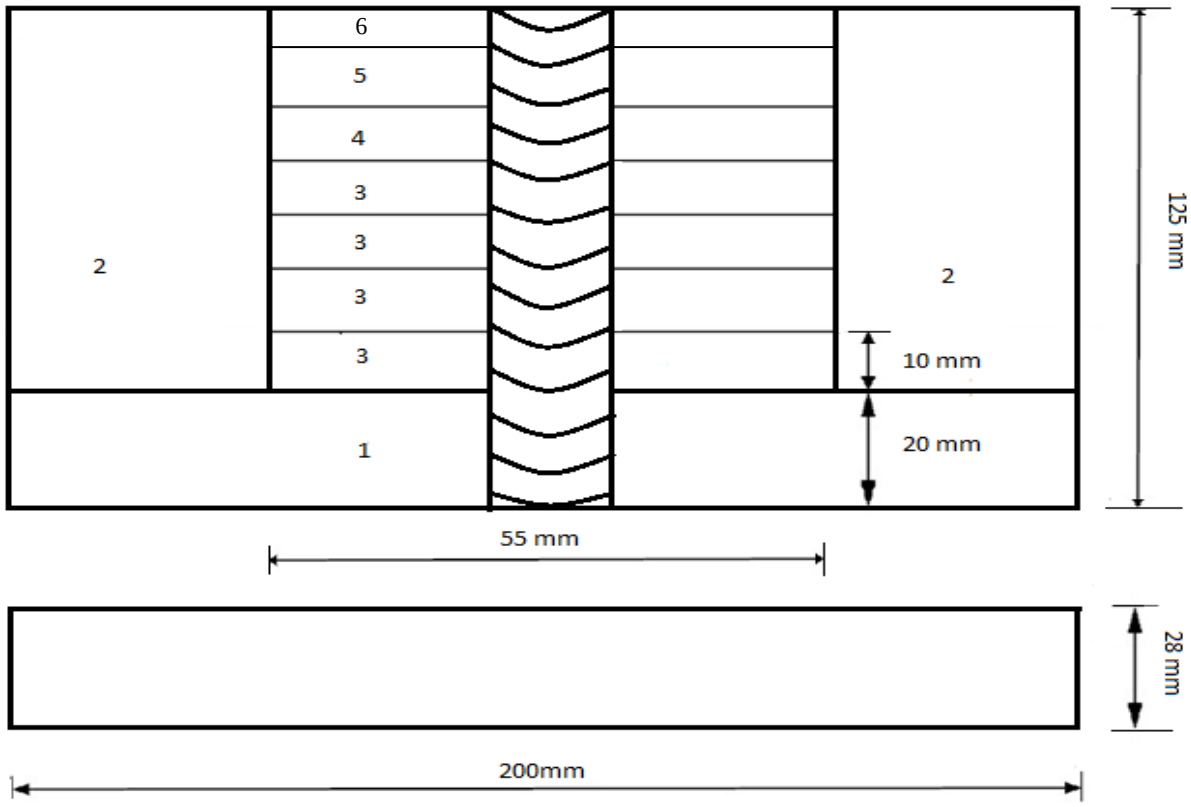

FIGURE 3.16 Orientation of Cutting of plates after welding

Orientation of cutting of specimens after welding is shown in Figure 3.15, (1) represents tensile test specimen (2) represents waste material, (3) represents toughness test specimen, (4) represents micro hardness and microstructure test specimen, (5) represents composition test specimen, (6) represents waste material due to defect region is found at corner part of welded region measured by radiograph film

Figure 3.16 shows the cutting of plates with the help of surface grinding machine (Make: Himlitz Products, India and motor speed-2800 rpm) and the cutter used for cutting of plates was of dimension 200 x 1.5 x 31.75 mm. Figure 3.16 (ii) shows the cutting of weld region with the help of power hacksaw and weld region specimen as shown in figure 3.17c (i). The thickness of welding region is reduced by vertical milling machine as shown in figure 3.17 (ii)

(i) **(ii)**

FIGURE 3.17 (i) Cutting of plates according to required tensile specimen size on surface grinding machine (ii) Cutting of weld region by power hacksaw

(**Courtesy:** Central Workshop, Thapar University, Patiala)

(i) **(ii)**

FIGURE 3.18 (i) Cutting of plates after power hacksaw (ii) Machining on welding region for reducing thickness approximately to 10-12 mm on vertical milling machine

(i) **(ii)**

FIGURE 3.19 (i) Grinding of plates using centre less grinding machine (**Courtesy:** Central Workshop, Thapar University, Patiala), **(ii)** Plates after grinding from welding area

3.6 TESTING OF WELD SPECIMENS

As proposed in this experimental work, following tests and measurements were conducted on the weld specimens during SAW:

- Tensile Test
- Weld bead geometry
- Impact test at room temperature
- Impact test at -40^0C temperature
- Microhardness test
- Chemical composition
- Scanning Electron Microscope & EDX Analysis
- Radiography testing

3.6.1 Tensile Test

Ratio of the maximum load a material can support without fracture when being stretched to the original area of a cross section of the material. When stresses less than the tensile strength are removed, a material completely or partially returns to its original size and shape. As the stress approaches that of the tensile strength, a material that has begun to flow forms a narrow, constricted region that is easily fractured. Tensile strengths are measured in units of force per unit area.

The testing would be carried on Computerised Universal Testing Machine (Make: Blue Star Ltd. - New Delhi, India, Load capacity-1000 Ton) as shown in Figure 3.20. Figure 3.21 and 3.22 shows the schematic of tensile test specimen and the specimens before machining and the machining was done on lathe (Make: Gujarat Lathe Manufacturing Co. Pvt. Ltd. Rajkot, India).

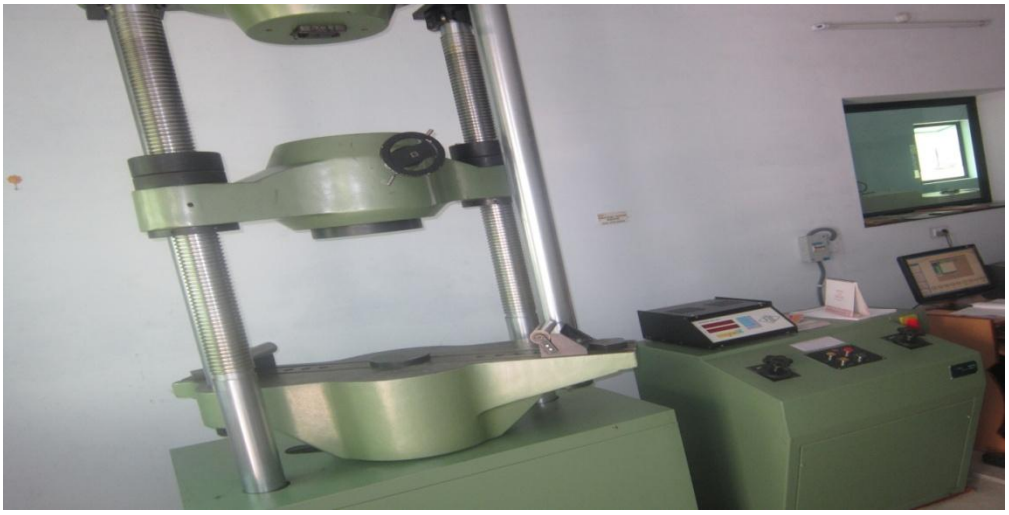

FIGURE 3.20 Computerised universal testing machine

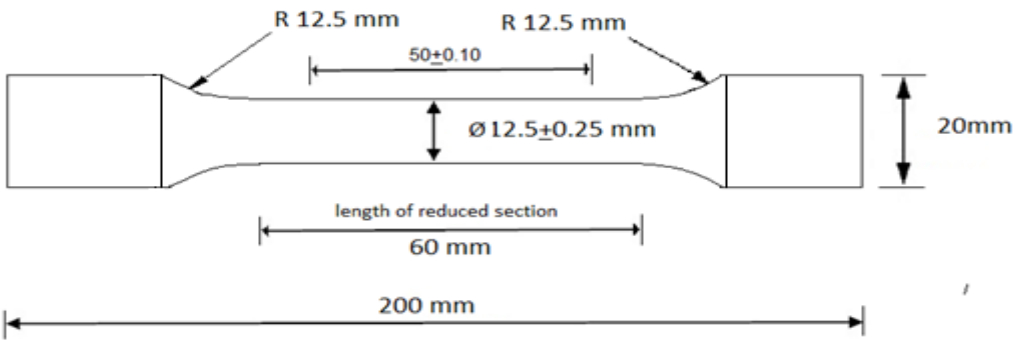

FIGURE 3.21 Tensile test specimens according to ASTM E8-11 Standard [34]

FIGURE 3.22 Specimen for tensile testing

3.6.2 Impact Test

It is ability of a metal to rapidly distribute within itself both the stress and strain caused by a suddenly applied load or the ability of a material to withstand shock loading. It is the exact opposite of "brittleness" which carries the implication of sudden failure. A brittle material has little resistance to failure once the elastic limit has been reached.

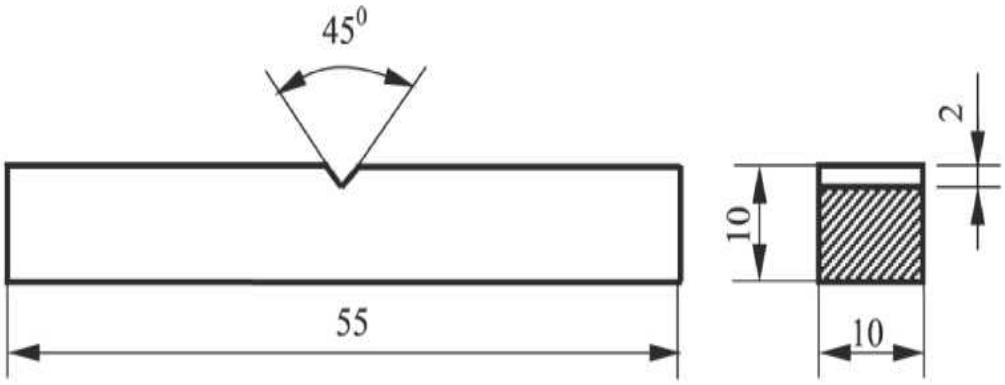

FIGURE 3.23 Standard charpy test specimen

Specimen were prepared according to IS 3613-1974 (1993) standard shown in figure 3.22, 72 specimens were make as shown in figure 3.23, 4 from each plate of dimension 55x10x10mm for charpy impact test and test them on machine as shown figure 3.24.The thickness of material is removed from both side of specimen take place on vertical milling machine (Make: HMT Limited, Pinjore India) and after machining the specimen thickness left was 10 mm. The length and width of charpy test specimen was prepared by surface grinding machine.

The apparatus consists of a pendulum axe swinging at a notched sample of material. The energy transferred to the material can be inferred by comparing the difference in the height of the hammer before and after a big fracture. Impact test on the weld specimen is performed on the impact testing machine (Make: Alfred J. Amsler & Co., Switzerland) having a range of 0-30 Kg-m or 0-300 Joules as shown in the figure ahead

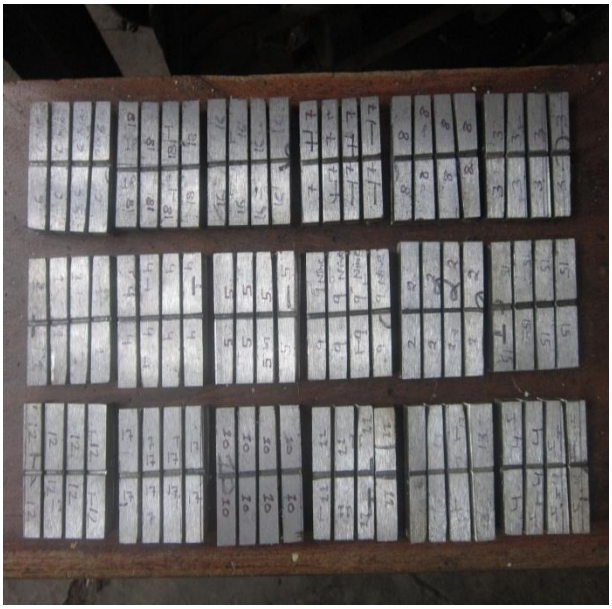

FIGURE 3.24 Charpy Test specimen

FIGURE 3.25 Charpy test machine

(**Courtesy:** Strength of Material Lab, Thapar University, Patiala)

The temperature of specimens below room temperature (30^0C),-20 ^{0}C, -40^0C and pilot study was generated by using liquid nitrogen and the specimens were put in the same for 5-10 minutes as shown in the figure ahead. An infrared thermometer (shown in the figure ahead) was used for the measurement of temperature of test specimens.

(i) **(ii)**

FIGURE 3.26 (i) Infrared thermometer used for the measurement of temperature (ii) Apparatus for liquid nitrogen

3.6.3 Microhardness Test

The samples measuring for micro hardness were firstly ground on the belt grinder, then rubbed with emery paper size no. 400, 600, 800, 1000 and then polished on polishing wheel (Make: Scientific, India) as shown in Figure ahead. Microhardness of the weld region was measured by using the computer interfaced micro hardness tester (Make: Metatech Industries, Pune, India) as shown in Figure 3.29. The measurement was dependent on the size of indentation on the samples. The diagonals of the indents formed by a pyramid- shaped diamond indenter was measured with the help of Quantimet software at 40X magnification, which gave a direct hardness Vickers number (HVN) for microhardness. The hardness values obtained were useful indicators of material properties. The load applied on the indenter was 1000g and the dwell time was 20 second. Figure 3.28 shows the specimen which was used for microhardness test.

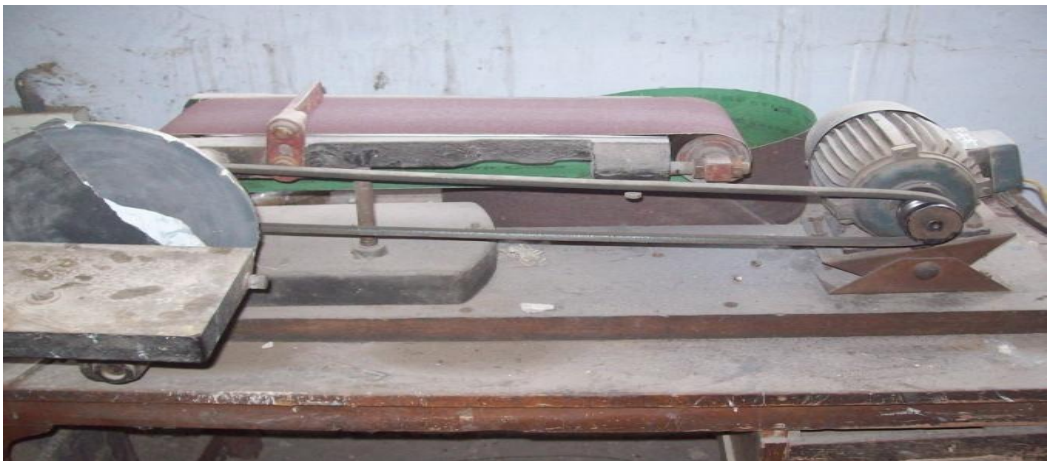

FIGURE 3.27 Belt grinder

(**Courtesy:** Machine Tool Lab, Thapar University, Patiala)

Figure ahead shows the suface finish on the specimens finally achieved to carry out the microhardness test.

(i) **(ii)**

FIGURE 3.28 (i) Polishing with emery paper of grit size 400, 600,800,1000,2500 **(ii)** Polisher with using kerosine and Diamond paste solution (**Courtesy:** Texture Laboratory, Metallurgical Deptt., IIT Bombay)

FIGURE 3.29 Specimens for microhardness testing

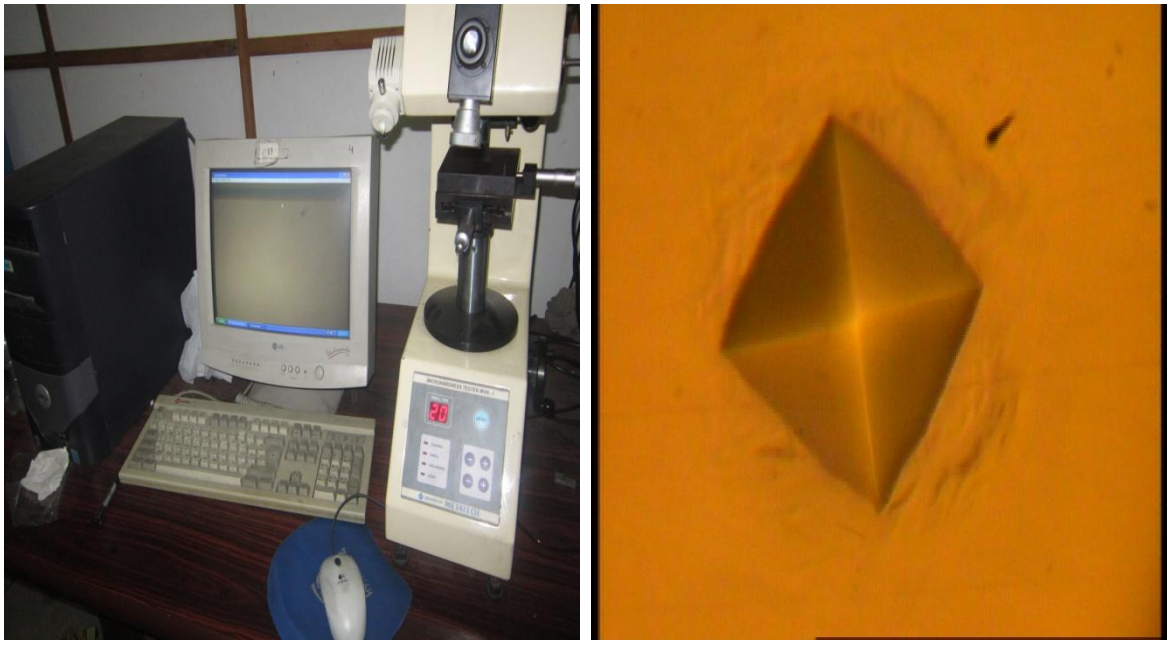

(i) **(ii)**

FIGURE 3.30 (i) Microhardness test machine (**Courtesy:** Central Workshop, Thapar University, Patiala) **(ii)** Diamond indent shown at 40X on the screen and its measurement

3.6.4 Scanning Electron Microscope (SEM) and EDAX

Scanning electron microscope (SEM) is an important tool for microstructural analysis. The microstructural characteristic of the sample correlate the effect of different processing condition with properties and behavior of materials that involves their microstructural changes. The SEM provides information relating to topographical features, morphology, phase distribution, compositional differences, crystal orientation and presence of defects and their location. The strength of SEM lies in its inherent versatility due to the multiple signals generated, simple image formation process, wide magnification range and excellent depth of field. Structural analyses were carried out to see the morphological features of grain formation. Elemental Dispersive Analysis by X-rays (EDAX) is used for the quantitative approach. When a beam of electron strikes a specimen, a fraction of the incident electrons excites the atoms of the specimen, which then emit X-rays when they return to their ground state. The energy of these X-rays is strictly related to the atomic number of the elements excited and therefore their detection forms the basis of elemental analysis in the electron microscope. [35]

FIGURE 3.31 Scanning Electron Microscope

(**Courtesy:** OIM Laboratory, Metallurgical Department, IIT Bombay)

3.6.5 Chemical Composition of Weld Metal

The composition of base metal and welded metal was found by using atomic absorption spectrometer (Figure 3.33) in which Argon gas pressure was maintained at 60 litre/min and the software used for finding chemical composition was Worldwide Analytical System (WAS). Figure 3.33 shows the specimen for composition test.

FIGURE 3.32 Atomic absorption spectrometer

(**Courtesy:** Central Workshop, Thapar University, Patiala)

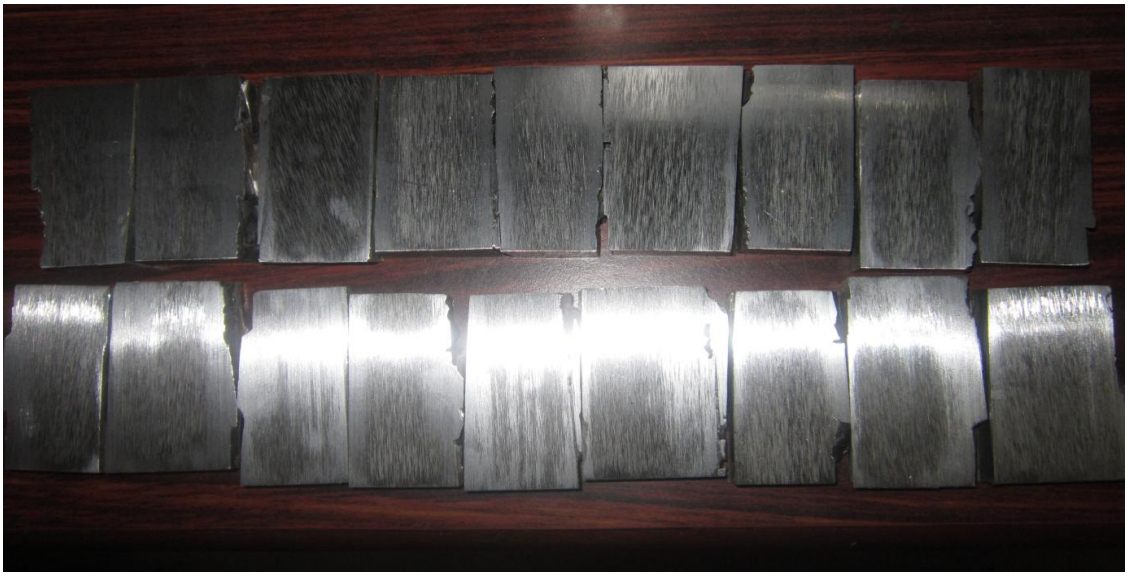

FIGURE 3.33 Samples for chemical composition testing

3.6.6 Bead Width & Height of Weld Metal

Bead width and bead height of all the specimens were measured in the metrology lab of Thapar University by keeping all the specimens on the surface plate as shown in the figure ahead. Four readings at different points were taken to take a better overall average. Bead width was measured using digital vernier caliper (Make: Starrett No. 723, American and least count = 0.01 mm) or leica Microscope and bead height was measured using vernier height gauge (Make: Mitutoyo, Japan and least count = 0.02 mm).

(i)

(ii) (iii)

FIGURE 3.34 (i) & (ii) Measurement of bead width using Leica Microscope or digital vernier calliper (iii) Measurement of bead height using vernier height gauge (**Courtesy:** Metrology lab, Thapar University, Patiala)

3.6.7 Radiography Testing

Radiographic testing is a non-destructive method of inspecting materials for hidden flaws by using the ability of short wavelength electromagnetic radiation (high energy photons) to penetrate various materials. It is helped we could find any type of defect in weld region i.e porosity, lack of fusion, blow holes etc.. In this method the part is placed between the radiation source and a piece of film**.** A pattern will be generated on the film depending on the thickness of the inspected part. Where ever there is a defect, the amount of radiation absorbed will be different and corresponding pattern will be generated**.** Detection of subsurface defects is the major advantage of this test but proper safety measures have to be taken to prevent exposure to these radiations. Either a Gamma-Rays Machine or radioactive source (Ir-192) is using as a source of photons as shown in figure 3.35.

The beam of radiation must be directed to the middle of the section under examination and must be normal to the material surface at that point, except in special techniques where known defects are best revealed by a different alignment of the beam. The length of weld under examination for each exposure shall be such that the thickness of the material at the diagnostic extremities, measured in the direction of the incident beam, does not exceed the actual thickness at that point by more than 6%. The specimen to be inspected is placed between the source of radiation and the detecting device, usually the film in a light tight holder or cassette, and the radiation is allowed to penetrate the part for the required length of time to be adequately recorded.

(i) (ii)

FIGURE 3.35 (i) Radioactive source i.e.gamma-rays (ii) Exposing radioactive source on weld region through negative film (**Courtesy:** Northern Industrial radiography services, Industrial Area, Yamuna Nagar)

3.7 ANALYSIS OF RESULTS

ANOVA is a statistical technique which can infer some important conclusions based on analysis of the experimental data. The method is very useful for revealing the level of significance of influence of factor(s) or interaction of factors on a particular response. It separates the total variability of the response (sum of squared deviations about the grand mean) into contributions rendered by each of the parameter/ factor and the error. Thus

$\mathbf{SS_T = SS_F + SS_E}$

Where, $SS_T = \sum_{J=1}^{P} \left(\gamma_j - \gamma_m\right)^2$

Where, SS_T = Total sum of squared deviations about the mean.

γ_j = Mean response for j^{th} experiment.

γ_m = Grand mean of the response.

SS_F = Sum of squared deviations due to each factor.

SS_E = Sum of squared deviations due to error.

In the ANOVA table mean square deviation is defined as:

MS = Mean Square

$$\mathbf{MS} = \frac{\mathbf{SS\ (Sum\ of\ squared\ division)}}{\mathbf{DOF\ (Degree\ of\ Freedom)}}$$

F-value of Fisher's F ratio (Variance ratio) is defined as:

$$\mathbf{F} = \frac{\mathbf{MS\ for\ a\ term}}{\mathbf{MS\ for\ the\ error\ term}}$$

Depending on F value, P-value (probability of significance) is then calculated. If P-value for a term appears less than 0.05 (For 95% confidence level) then it can be concluded that the effect of the factors / interaction of factors is significant on the selected response. Significance of all the dependent variables has been completed using statistical software MINITAB 15. These dependent variables studied in this study are (1) Tensile strength (2) Toughness at room temperature (3) Toughness at -40 ^{o}C (4) Microhardness.

In the ANOVA table, the degrees of freedom are used to calculate the mean square (MS). In general, the degrees of freedom measure how much "independent" information is available to calculate each sum of squares (SS).

Total DOF = DOF for all factors + DOF for all interactions + DOF for error

Where n is the total number of observations and,

DOF for factor = $k-1$

Where k is the number of the factor levels.

DOF for Interaction = $(k_1-1) \times (k_2-1)$

Where k_1 is the number of levels of factor one, and k_2 is the number of levels of factor two. The same rule applies to interactions of more than two factors. In the present study, the interaction of factors has not been studied. The sequential sum of squares for each term in the model (factor or interaction) measures the amount of variation in the response that is explained by adding each term to the model sequentially in the order listed under. Thus, the sequential sums of squares for terms are specific to the order of the terms specified in the linear model. The adjusted sum of squares for a term in the model (factor or interaction) measures the amount of additional variation in the response that is explained by the term, given that all the other terms are already in the model. Thus, the values for the adjusted sums of squares do not depend on the order of the terms listed under source. The adjusted mean square for a term is simply the adjusted sum of squares (Adj. SS) divided by the degrees of freedom.[36]

For this experimental work, the following response characteristics have been studied-

1. Response Name	:	Bead height
Response type	:	Lower-the-better
Units	:	mm
2. Response Name	:	Tensile strength
Response type	:	Higher-the-better
Units	:	N/mm^2
3. Response Name	:	Toughness at room temperature (30 ^oC)
Response type	:	Higher-the-better
Units	:	Joule
4. Response Name	:	Toughness at -40 ^oC
Response type	:	Higher-the-better
Units	:	Joule
5. Response Name	:	Microhardness at weld region
Response type	:	Higher-the-better
Units	:	HVN
6. Response Name	:	Bead width
Response type	:	Lower-the-better
Units	:	mm

CHAPTER-4

RESULT AND ANALYSIS OF TENSILE TEST

4.1 TENSILE TEST

Universal tensile testing machine was used to carry out tensile tests. Ultimate Tensile Load for the base metal is 84.35 KN. Tensile round specimen were prepared according to ASTM E8-11 which specifies acceptance tests for wire-flux combinations for submerged arc welding of HSLA steel. Then readings for various specimens made using different types of parameters are taken on UTM. Ratio of the maximum load a material can support without fracture when being stretched to the original area of a cross section of the material. Specimens broken after tensile test is shown in figure 4.1.

FIGURE 4.1 Specimen after tensile test

The tensile test details for base metal are shown in Table 4.1 and corresponding tensile test plot is shown in Figure 4.2 for comparison.

TABLE 4.1 Maximum tensile load & strength value of base metal

	Maximum Tensile Load (kN)	**Maximum Tensile Strength (N/mm^2)**
Base Metal	84.35	687.06

PLOT - Load vs Displacement **PLOT -** Stress vs Strain

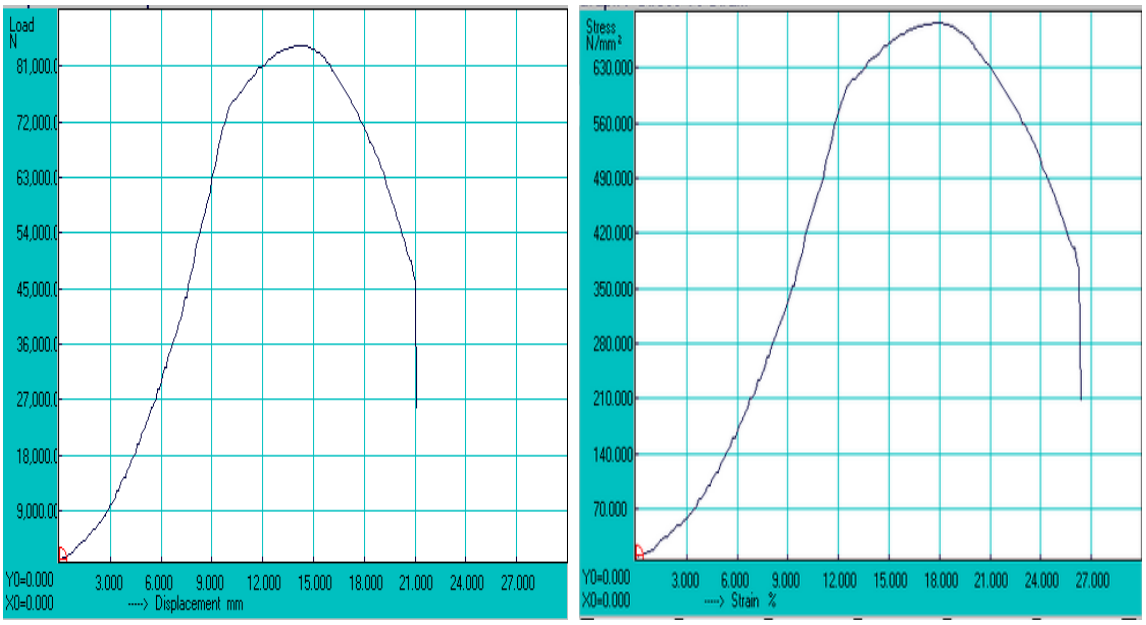

FIGURE 4.2 Load vs displacement and stress vs strain curve base metal

For all the 18 sets of experiment, the tensile test summary is shown in table 4.2 and corresponding load vs displacement and stress vs strain plots are shown below sequentially in figure 4.3 (a-r).

TABLE 4.2 Maximum tensile load & tensile strength readings

Experiment No.	Contributing Factors	Maximum Tensile Load (kN)	Maximum Tensile Strength (N/mm^2)
1	Ø1, C1, D1, T1,S1, F1	82.65	550.22
2	Ø1, C1, D2,T2,S2, F2	80.85	558.56
3	Ø1, C1, D3, T3,S3, F3	71.35	581.18
4	Ø1, C2, D1, T1, S2, F2	65.45	533.12
5	Ø1, C2, D2, T2, S3, F3	73.65	599.91
6	Ø1, C2, D3, T3, S1, F1	65.05	530.15
7	Ø1, C3, D1, T2, S1, F3	77.65	632.50
8	Ø1, C3, D2, T3, S2, F1	75.30	613.35
9	Ø1, C3, D3, T1, S3, F2	76.40	622.31
10	Ø2, C1, D1, T3, S3,F2	77.90	634.53
11	Ø2, C1, D2, T1, S1, F3	66.50	541.67
12	Ø2, C1, D3, T2, S2, F1	73.35	597.47
13	Ø2, C2, D1, T2, S3, F1	76.80	625.57
14	Ø2, C2, D2, T3, S1, F2	66.65	542.90
15	Ø2, C2, D3, T1, S2, F3	75.65	616.20
16	Ø2, C3, D1, T3, S2, F3	72.15	640.70
17	Ø2, C3, D2, T1, S3, F1	78.30	637.79
18	Ø2, C3, D3, T2, S1, F2	81.30	662.23

Where,

- Ø1 and Ø2 represents electrode diameter vary at two different levels namely (I) 3.2 mm and (II) 4 mm.
- C1, C2 and C3 represents current vary at three different levels namely (I) 400 Amp, (II) 450 Amp and (III) 500 Amp.
- D1, D2 and D3 represents electrode stick-out vary at three different levels namely (I) 25 mm, (II) 30 mm and (III) 35 mm.
- S1, S2 and S3 represents travel Speed vary at three different levels namely (I) 18 m/hr, (II) 20 m/hr and (III) 22 m/hr.
- T1, T2 and T3 represents preheat temperature vary at three different levels namely (I) No-Preheat, (II) 125 ^{o}C and (III) 200 ^{o}C.
- F1, F2 and F3 represents flux vary at three different levels namely (I) GEE FLUX 541, (II) GEE FLUX 544 and (III) AUTOMELT B31.

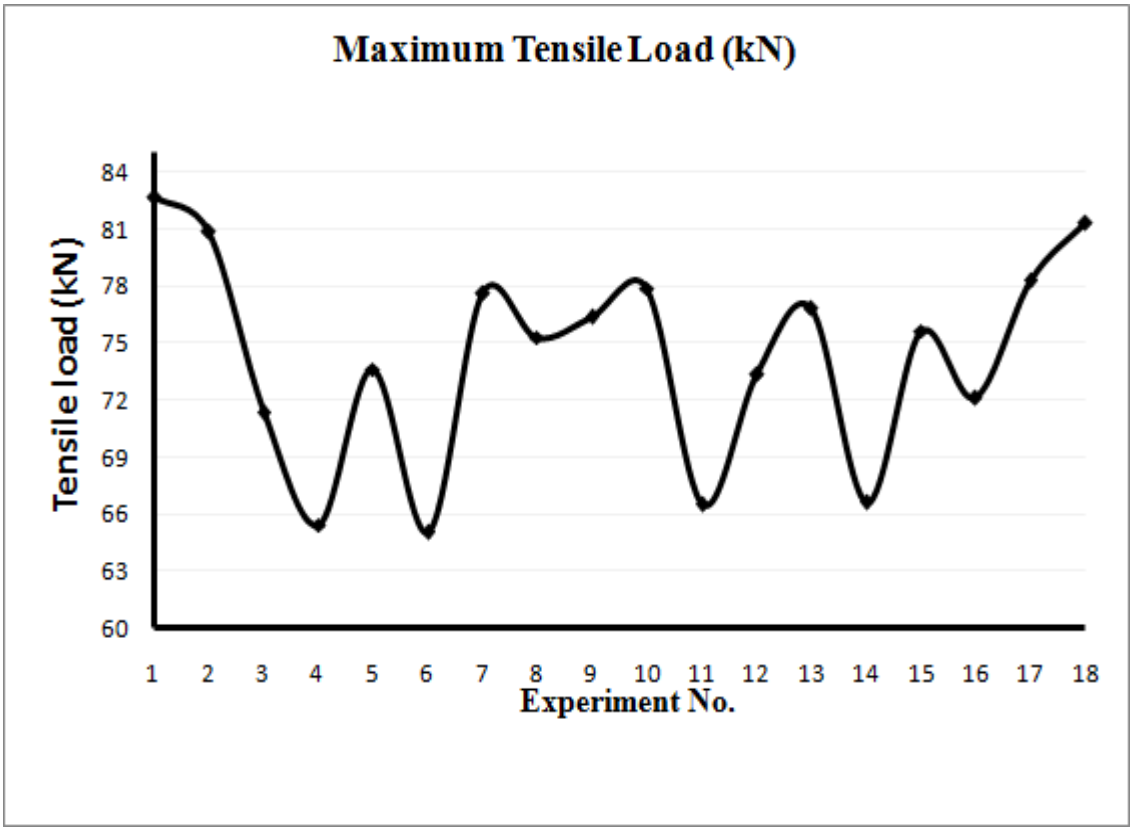

FIGURE 4.3 Variation of maximum tensile load of different specimens

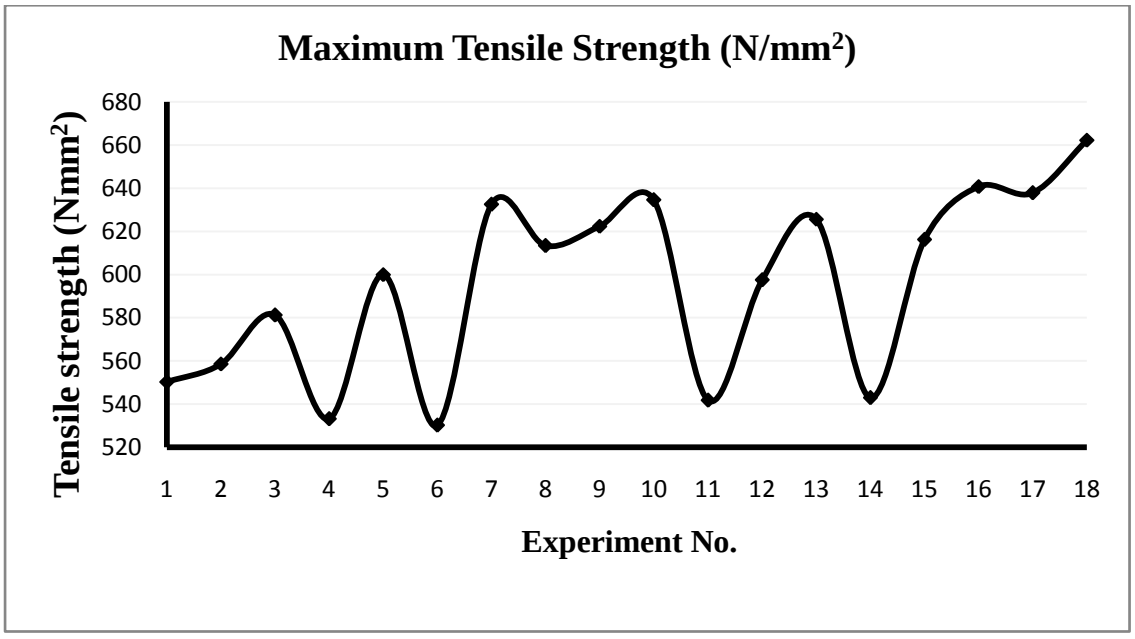

FIGURE 4.4 Variation of maximum tensile strength of different specimens

PLOT - Load vs Displacement

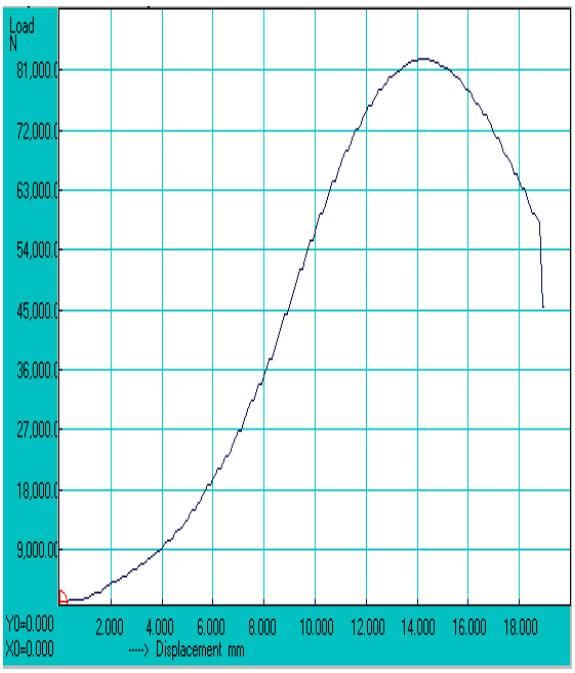

(a)

PLOT - Load vs Displacement

(b)

(a) & (b) Specimen No.1 &2 with contributing factor **(Ø1, C1, D1, T1, S1, F1) & (Ø1, C1, D2, T2,S2, F2)**

PLOT - Load vs Displacement

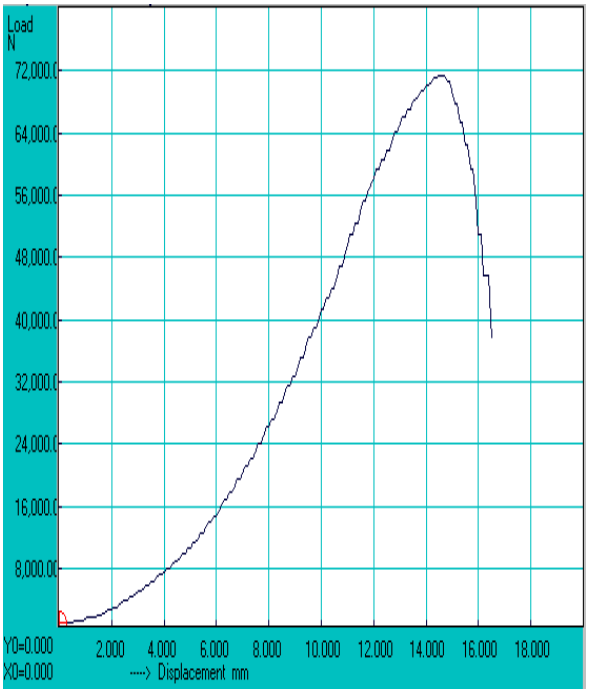

PLOT – Stress vs Strain

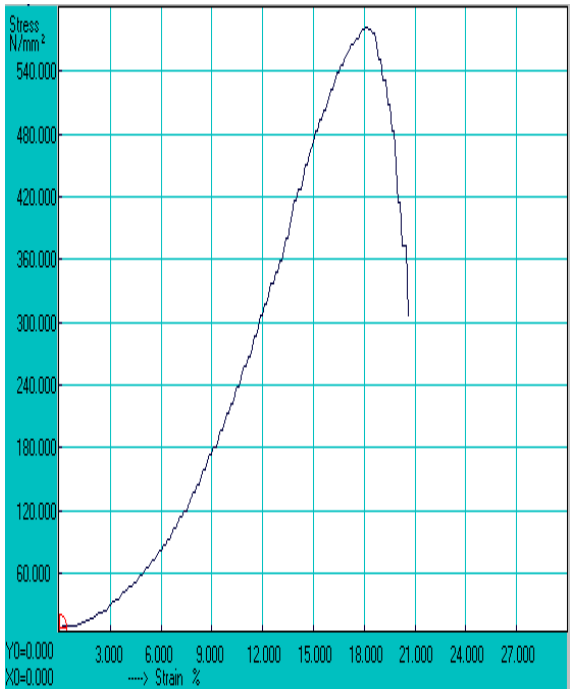

(c) Specimen No.3 with contributing factor **(Ø1, C1, D3, T3, S3, F3)**

PLOT - Load vs Displacement

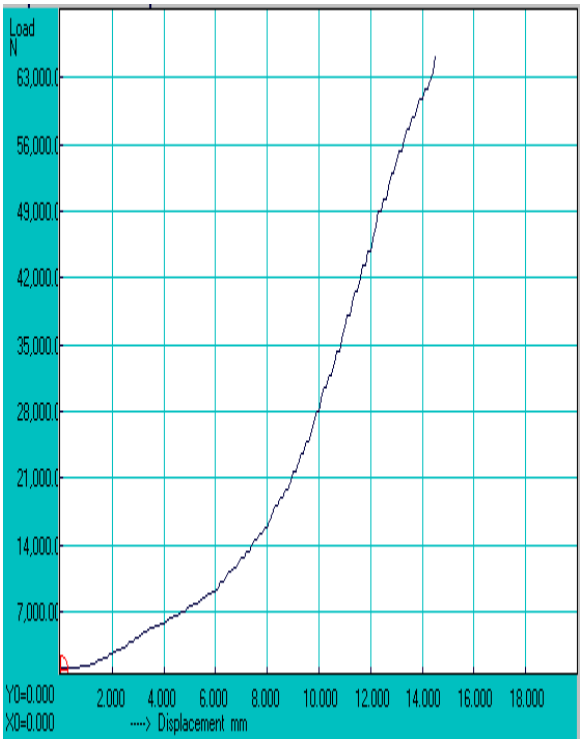

PLOT - Stress vs Strain

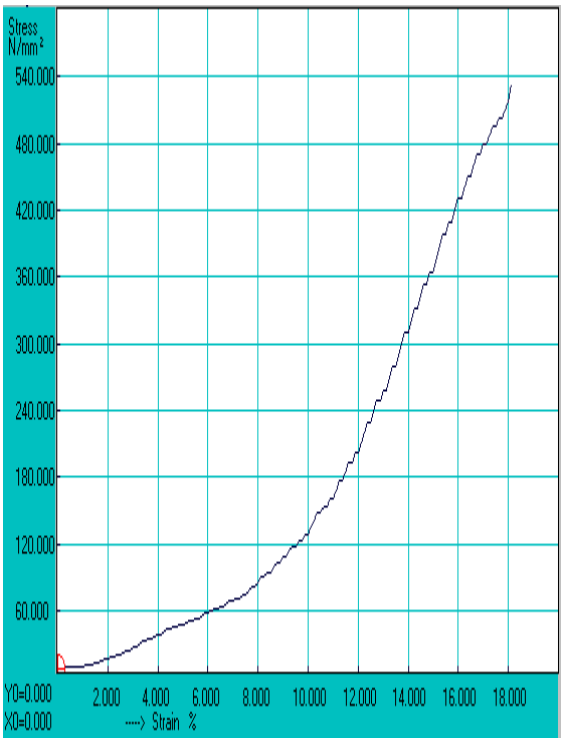

(d) Specimen No.4 with contributing factor **(Ø1, C2, D1, T1, S2, F2)**

PLOT - Load vs Displacement

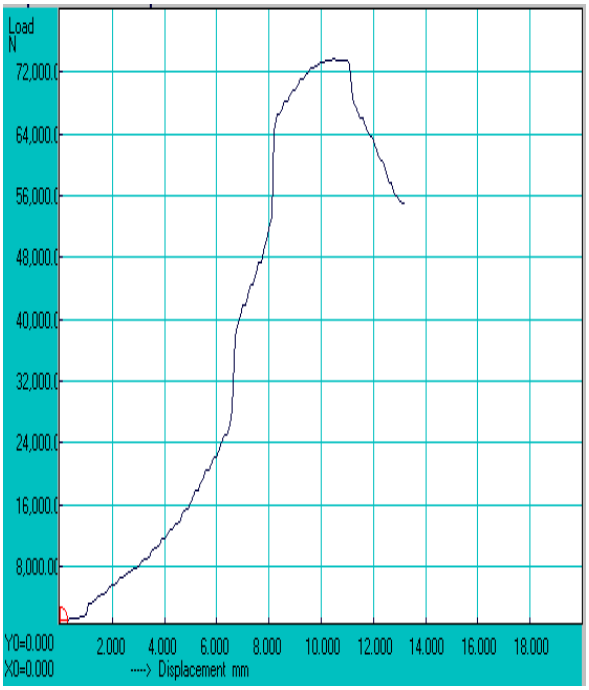

PLOT - Stress vs Strain

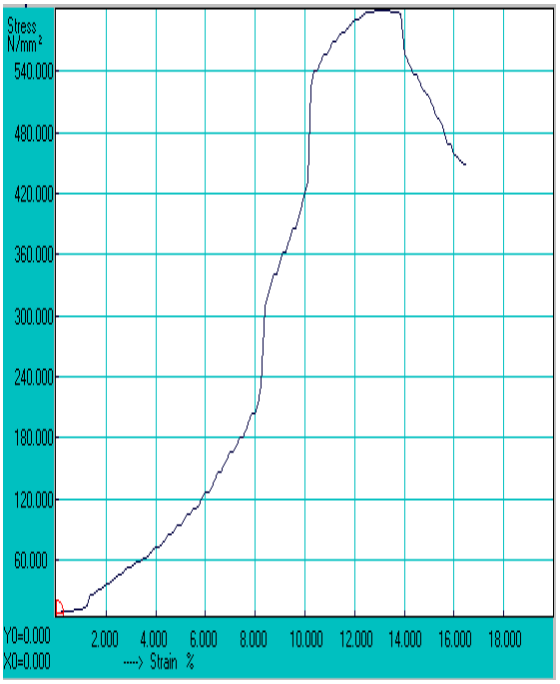

(e) Specimen No.5 with contributing factor **(Ø1, C2, D2, T2, S3, F3)**

PLOT - Load vs Displacement

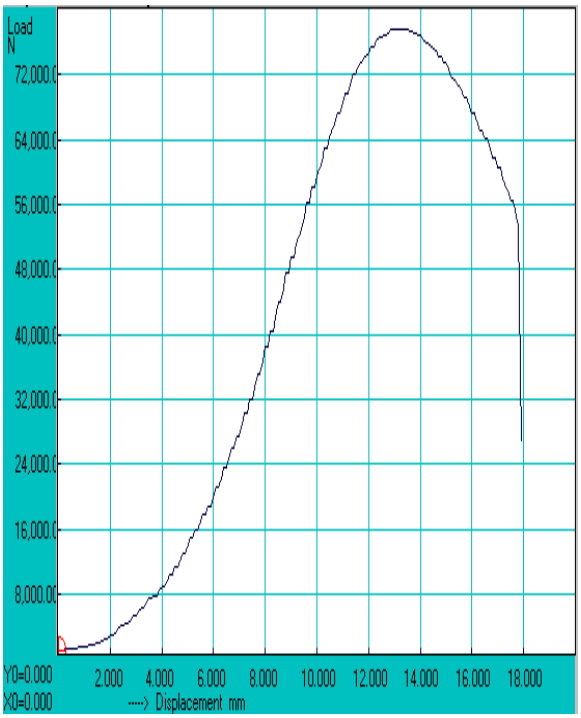

PLOT - Stress vs Strain

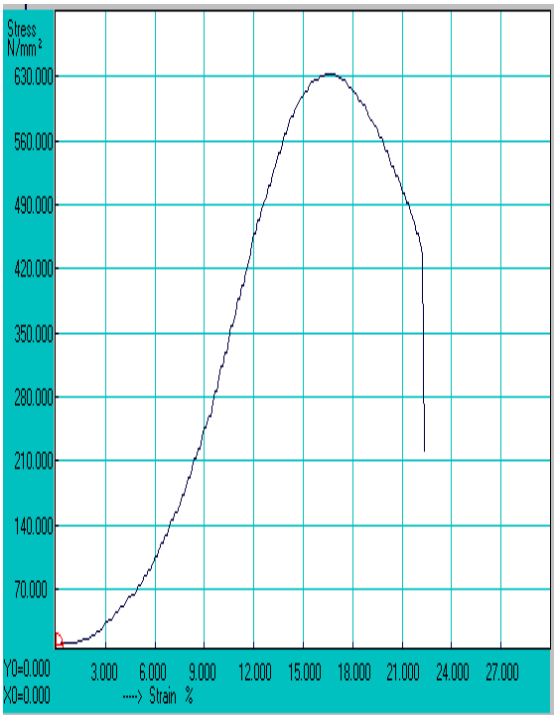

(f) Specimen No.7 with contributing factor **(Ø1, C3, D1, T2, S1, F3)**

PLOT - Load vs Displacement

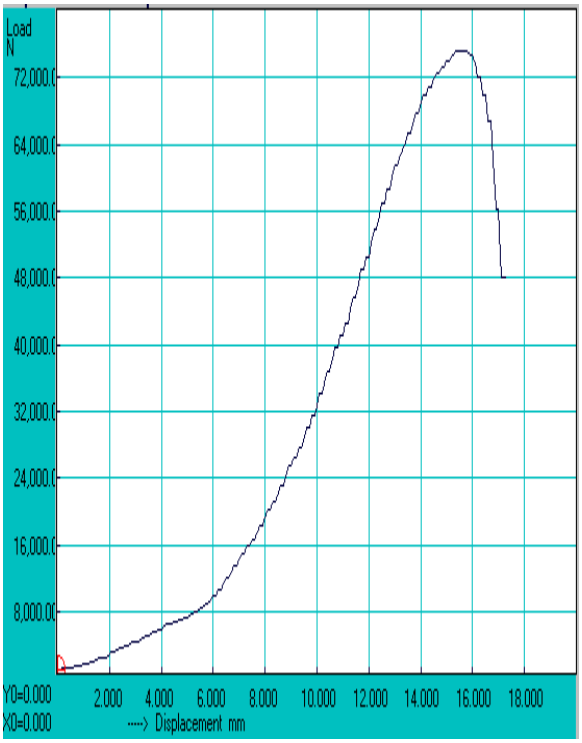

PLOT - Stress vs Strain

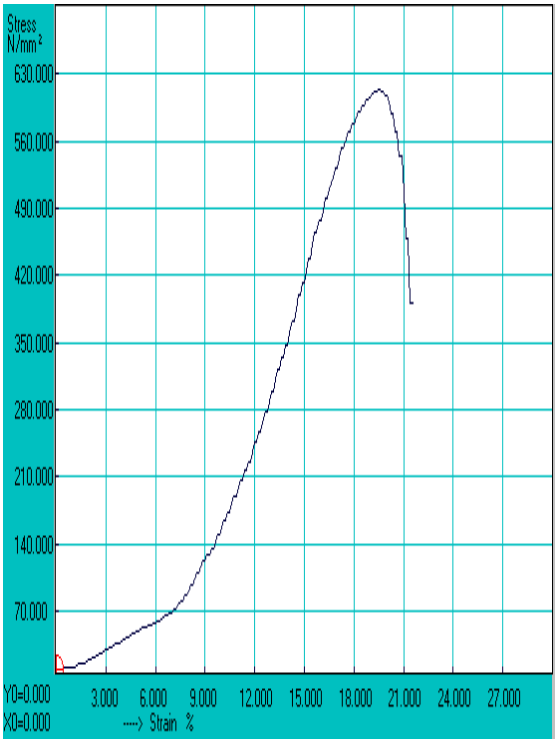

(g) Specimen No.8 with contributing factor **(Ø1, C3, D2, T3, S2, F1)**

PLOT - Load vs Displacement

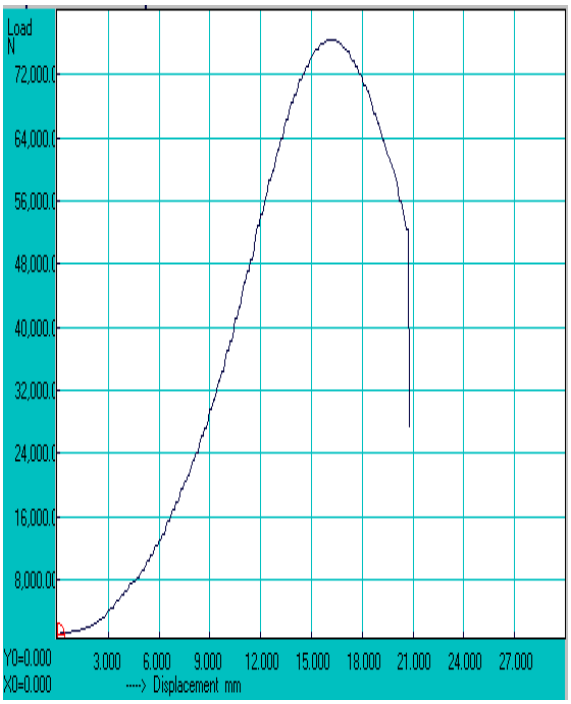

PLOT - Stress vs Strain

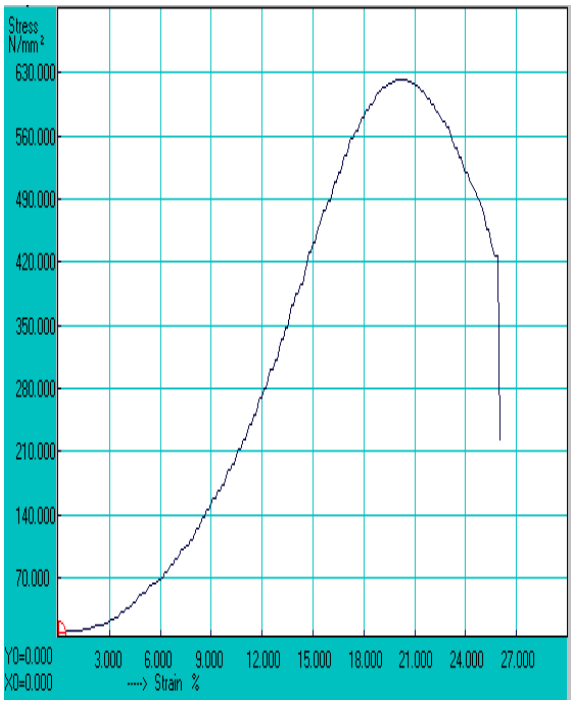

(g) Specimen No.9 with contributing factor **(Ø1, C3, D3, T1, S3, F2)**

PLOT - Load vs Displacement

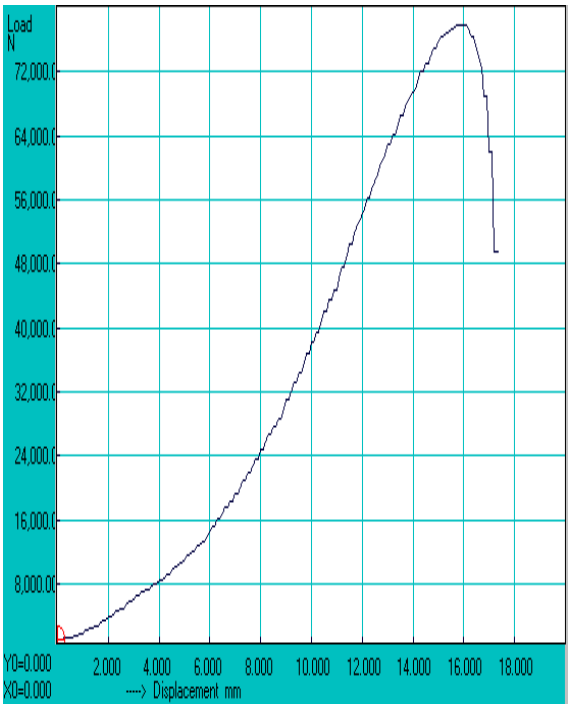

PLOT - Stress vs Strain

(i) Specimen No.10 with contributing factor **(Ø2, C1, D1, T3, S3, F2)**

PLOT - Load vs Displacement

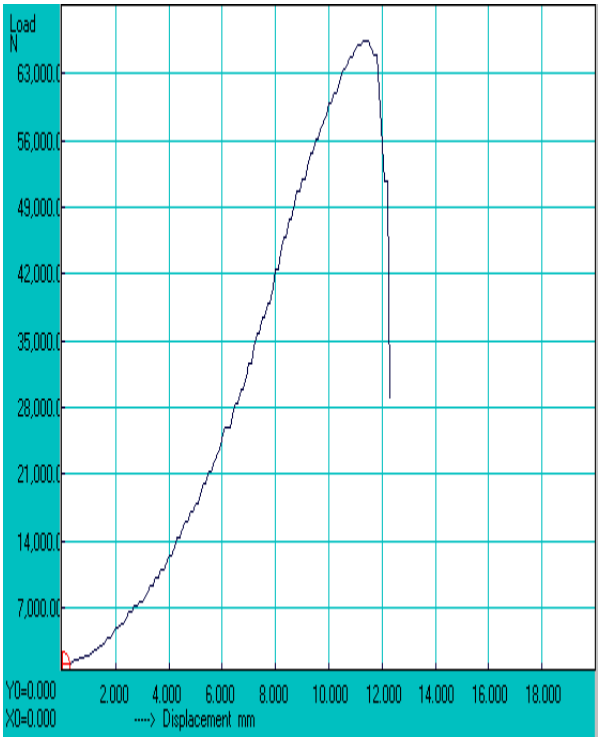

PLOT - Stress vs Strain

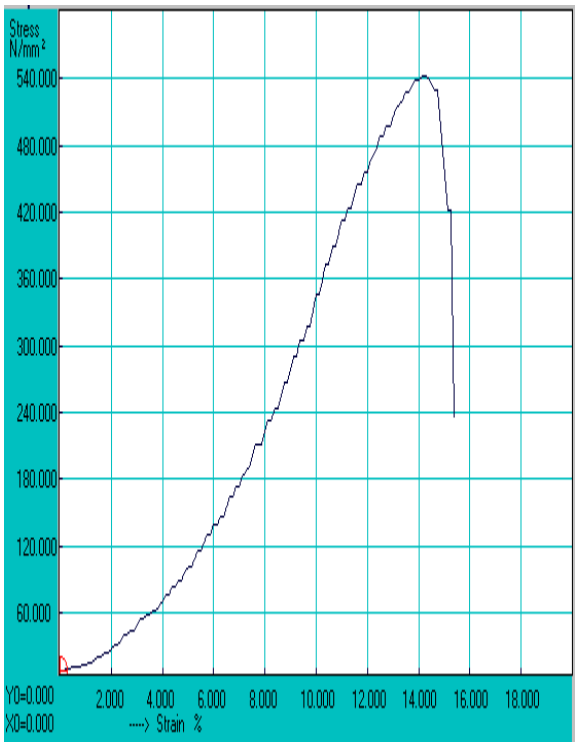

(j) Specimen No.11 with contributing factor **(Ø2, C1, D2, T1, S1, F3)**

PLOT - Load vs Displacement

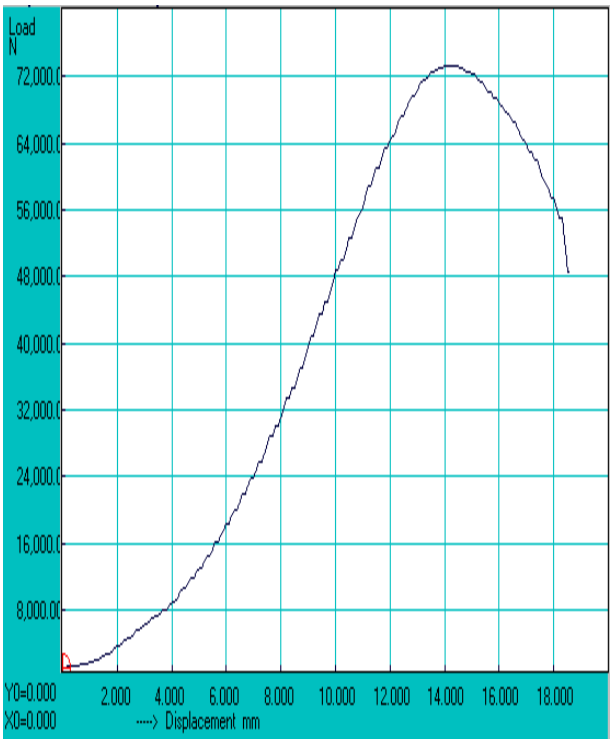

PLOT - Stress vs Strain

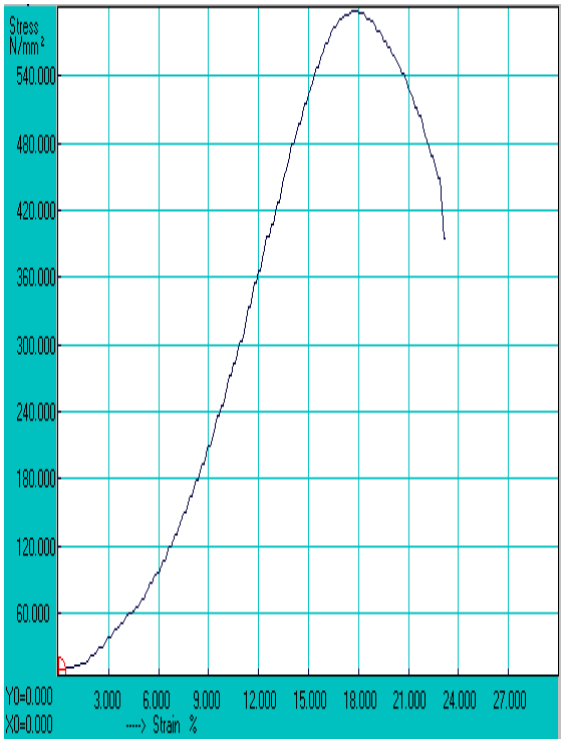

(k) Specimen No.12 with contributing factor **(Ø2, C1, D3, T2, S2, F1)**

PLOT - Load vs Displacement

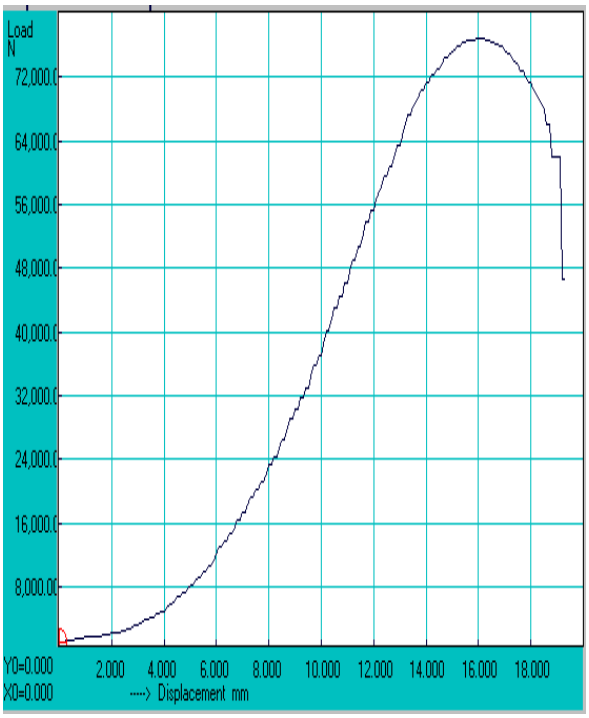

PLOT - Stress vs Strain

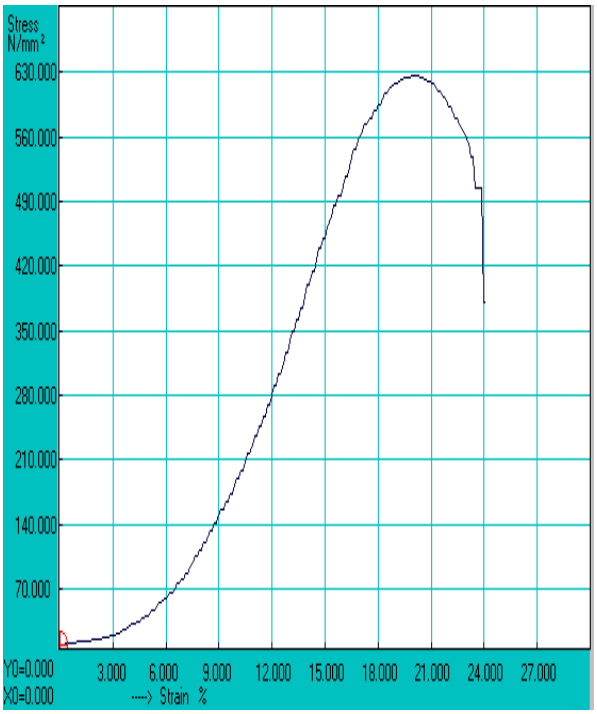

(l) Specimen No.13 with contributing factor **(Ø2, C2, D1, T2, S3, F1)**

GRAPH - Load vs Displacement

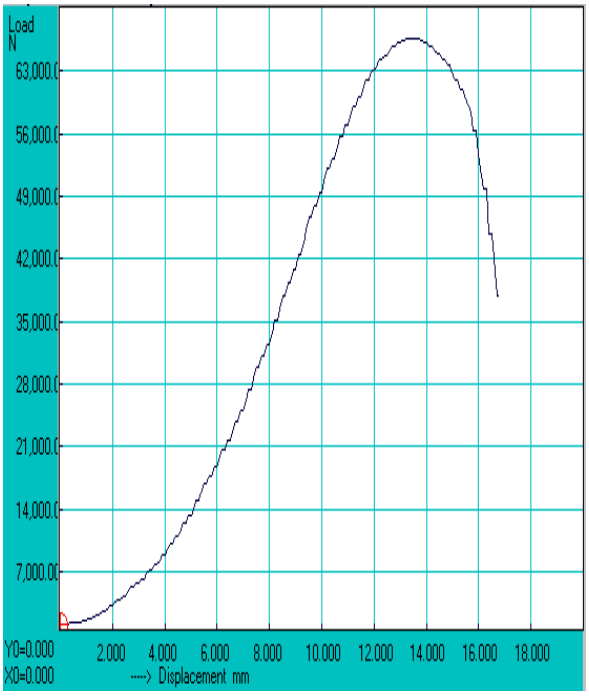

GRAPH - Stress vs Strain

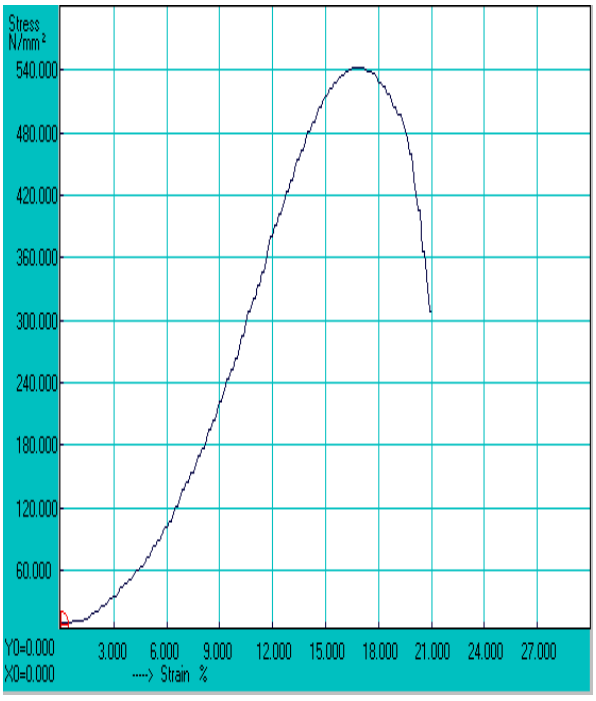

(m) Specimen No.14 with contributing factor **(Ø2, C2, D2, T3, S1, F2)**

PLOT - Load vs Displacement

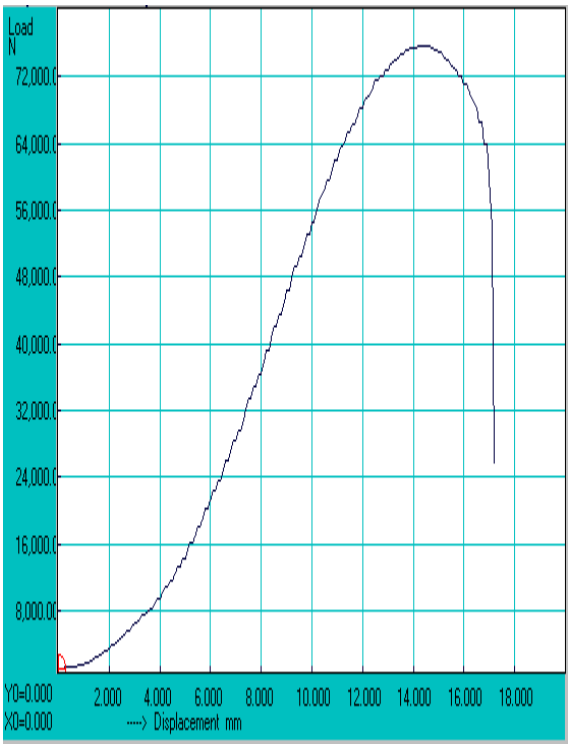

PLOT - Stress vs Strain

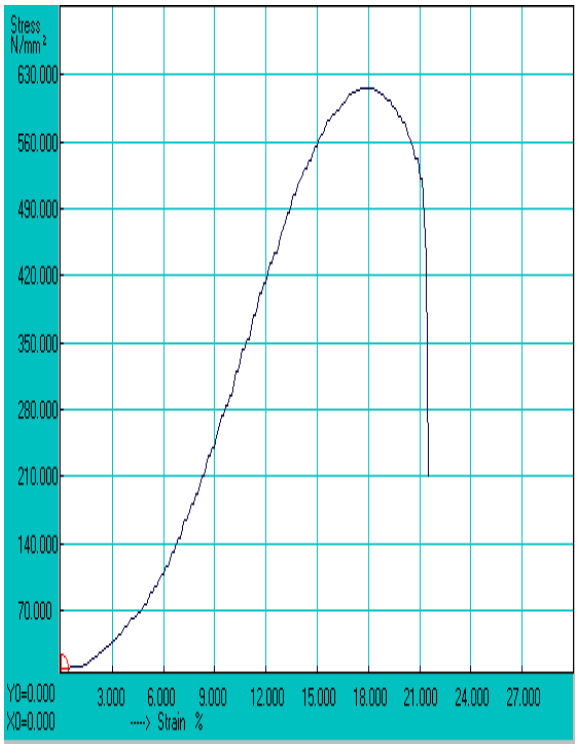

(n) Specimen No.15 with contributing factor **(Ø2, C2, D3, T1, S2, F3)**

PLOT - Load vs Displacement

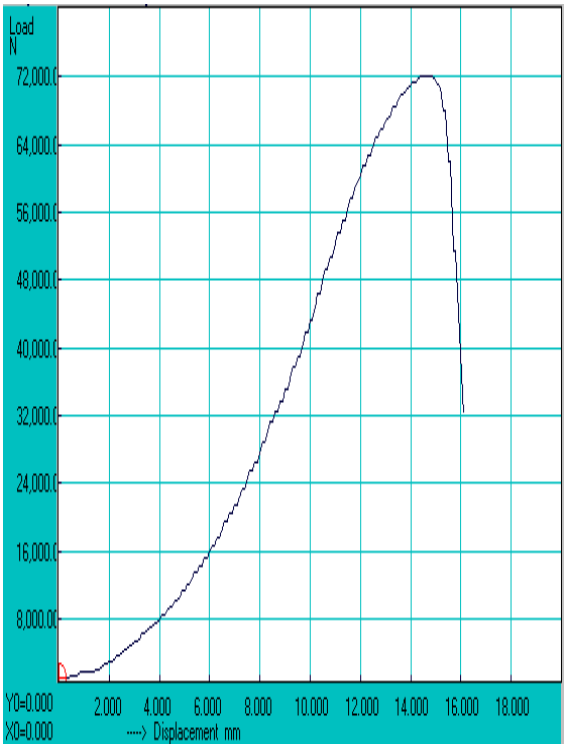

PLOT - Stress vs Strain

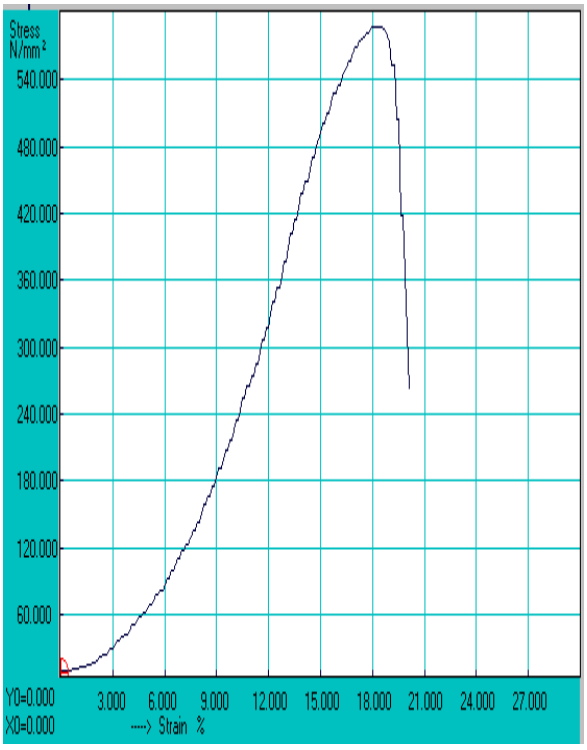

(o) Specimen No.16 with contributing factor **(Ø2, C3, D1, T3, S2, F3)**

PLOT - Load vs Displacement

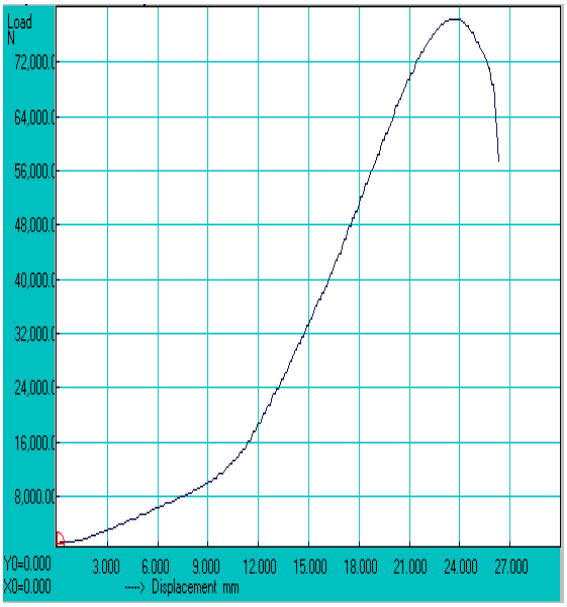

PLOT- Stress vs Strain

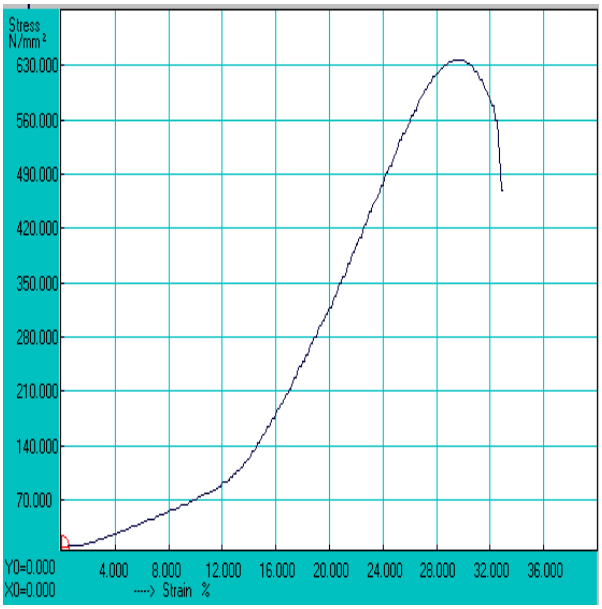

(p) Specimen No.17 with contributing factor **(Ø2, C3, D2, T1, S3, F1)**

PLOT - Load vs Displacement

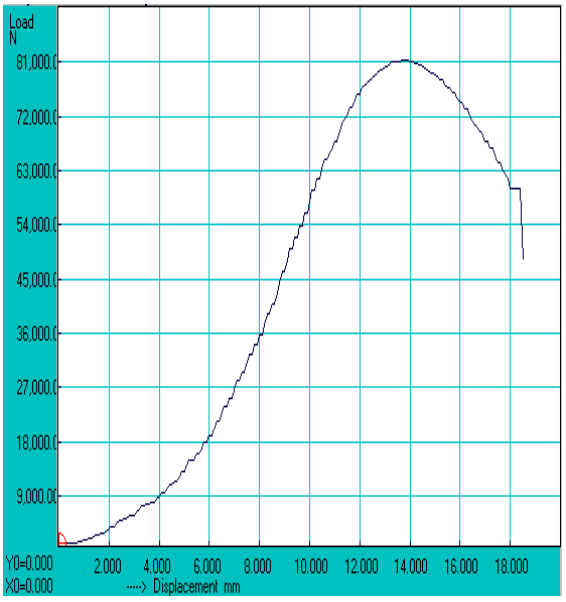

PLOT - Stress vs Strain

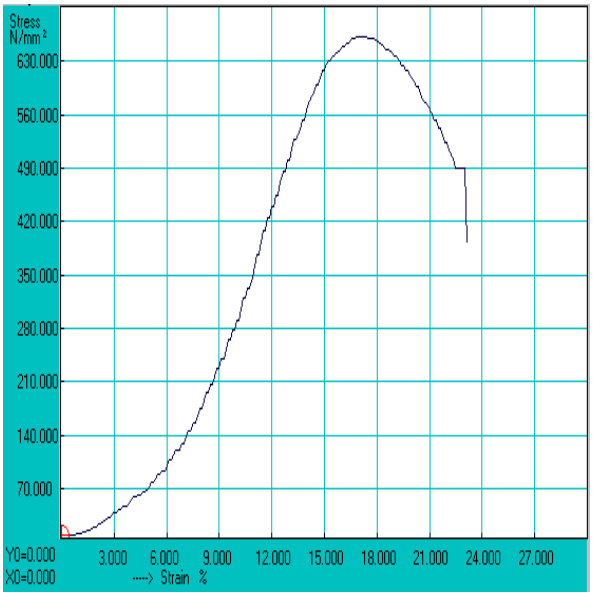

(q) Specimen No.18 with contributing factor **(Ø2, C3, D3, T2, S1, F2)**

***** Load vs Displacement and Stress vs Strain curve for tensile test of trial no. 16 was not saved due to power problem and stress vs strain for tensile test of trial no. 1 & 2 was not saved due to machine error problem.

FIGURE 4.5 (a-q) - Load vs Displacement and Stress vs Strain curve for tensile test for trial no. 1-18

4.2 ANOVA FOR TENSILE STRENGTH

Table 4.2 show that the values of tensile strength for the eighteen trials. The experimental results for tensile strength were analyzed using ANOVA and is given in the Table 4.3. The p value given in the last column of ANOVA table suggests the significance of the factors on the desired characteristics. The principle behind significance value is that the p value should be lesser than 0.05 (considering confidence level of 95%). The principle of F test is that, the F value should be large compared to e-pooled; larger the F value more is the significance of factor. An ANOVA table 4.3 show that p value for electrode diameter and current is 0.030 and 0.007 i.e. less than 0.05 indicates thereby that electrode diameter and current are the most significant factor for the tensile strength. The mean value for all six variables is given in Table 4.4. In last row of table 4.4 ranks have been given to various factors. Higher is the rank, higher is the significance. In table 4.4 welding current with the highest rank 1 and is the most significant factor and flux with its lowest rank is least significant in affecting the tensile strength. Main effect plots are shown in figure 4.4 shows the variation in the tensile strength with the change in the input factors i.e. electrode diameter, current, electrode stick-out, travel speed, preheat temperature and flux. It could be seen from the Figure 4.4 that welding current causes the most significant change in the tensile strength. Tensile strength show decreased from 400 to 450 ampere current but after 450 to 500 ampere showed vice-versa result. The change in electrode diameter and travel speed also has some effect on the variation in the tensile strength. Electrode stick-out, preheat temperature and flux have very low effect on tensile strength

TABLE 4.3 Analysis of variance for means tensile strength

Source	DF	Seq SS	Adj SS	Adj MS	F	P
Electrode Diameter (mm)	1	4292.7	4292.7	4292.7	8.05	**0.030**
Current (Ampere)	2	13884.4	13884.4	6942.2	13.03	**0.007**
Electrode Stick-Out (mm)	2	1571.9	1571.9	786.0	1.47	0.301
Preheat Temperature (^{o}C)	2	2789.8	2789.8	1394.9	2.62	0.152
Travel Speed (m/hr)	2	4923.4	4923.4	2461.7	4.62	0.061
Flux	2	376.0	376.0	188.0	0.35	0.716
Residual Error	6	3197.6	3197.6	532.9		
Total	17	31035.7				

TABLE 4.4 Response table for means of tensile strength

Level	Electrode Diameter (mm)	Current (amp)	Electrode Stick-Out (mm)	Preheat Temperature (^{o}C)	Travel Speed (m/hr)	Flux
1	580.1	577.2	602.7	583.5	576.6	592.4
2	611.0	574.6	582.4	612.7	593.2	592.3
3		634.8	601.6	590.5	616.9	602.0
Delta	30.9	60.2	20.4	29.2	40.3	9.8
Rank	**3**	**1**	**5**	**4**	**2**	**6**

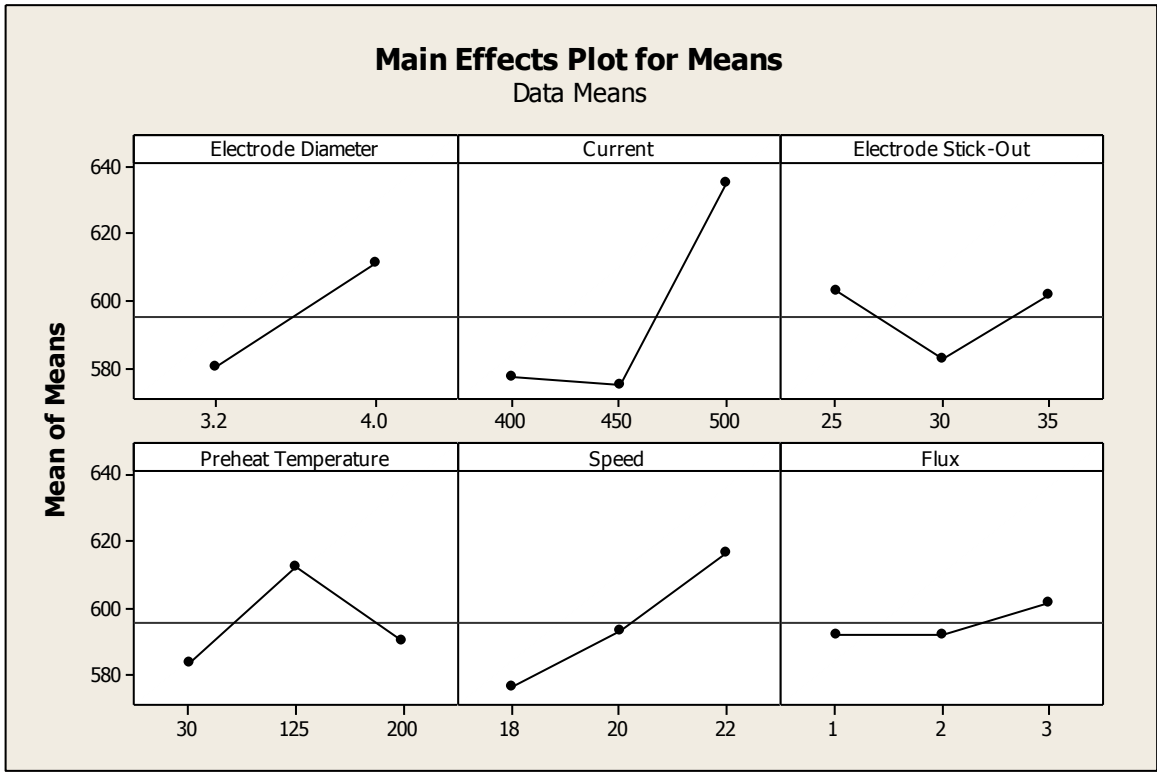

FIGURE 4.6 Main effect plot for tensile strength

4.3 OPTIMAL DESIGN FOR TENSILE STRENGTH

In this experimental analysis, the main effect plot in Figure 4.4 has been used to estimate the tensile strength in optimal conditions. From Table 4.3, it can be concluded that electrode diameter and current are two significant factors. In order to obtain maximum tensile strength, the electrode diameter should be 4 mm and welding current should be 500 Ampere.

Confidence interval predict with 95 % confidence so that value of tensile strength at optimal design conditions would be 650.23 ± 38.26 N/mm^2

Mean value of tensile strength is given by-

$\mu_{\emptyset_2 C_3} = \overline{\emptyset_2} + \overline{C_3} - 1\overline{T}$

$= 611.0 + 634.8 – (1 \times 595.57)$

$= 650.23$ N/mm^2

Confidence Interval around the estimated mean tensile strength

C.I. = $\sqrt{\frac{f\alpha:v1:v2 \; X \; Ve}{neff}}$

α = risk (0.05) confidence = 1-α

v1 = DOF for mean (which is always 1)

v2 = DOF for error = 14

Where $f\,\alpha{:}v1{:}v2 = f\,0.05{:}1{:}14$ = F ratio = 4.60

Variance = $Ve = \frac{SS\ of\ e\ pooled}{DOF\ of\ e\ pooled} = \frac{12858.6}{14} = 918.47$

n_{eff} = number of tests performed using participating factors

$n_{eff} = \frac{18}{1+\mathrm{DOF}_{\emptyset_2 C_3}} = 4.5$

C.I. = 30.64

So, the confidence interval around tensile strength is given by **650.23 ± 30.64 N/mm^2**.

4.4 DISCUSSION OF TENSILE TEST RESULTS

The effect of various process parameters i.e. current, travel speed, electrode diameter, flux composition, preheating of workpiece and electrode stick-out on ultimate tensile load and tensile strength of the welded joint were investigated. From figure 4.4, it appears that maximum tensile strength was observed for specimen no 18 i.e. 662.23 N/mm^2 and the lowest tensile strength and load was observed for specimen no. 4 i.e. 530.15 N/mm^2 and 65.05KN and the mean tensile strength using the optimal condition would be 650.23 ± 30.64 N/mm^2 with electrode diameter should be 4 mm, welding current should be 500 Ampere is used.

4.5 REGRESSION ANALYSIS FOR TENSILE TEST RESULTS

Regression table for mean tensile strength as shown below. An Regression table 4.5 show that p value for current is 0.010 less than 0.05 indicates thereby that current are the most

significant factor for the tensile strength. ANOVA for Regression of mean tensile strength is given in table 4.6 indicates the regression p value of significant factors. R^2 value given suggests the suitability of the model. In present study model is 63.3% suitable.

The regression equation is tensile Strength **= - 16 + 38.6 Electrode Diameter + 0.576 Current - 0.11 Electrode Stick-Out + 0.053 Preheat Temperature + 10.1 Speed + 4.82 Flux**

TABLE 4.5 Regression Table for Mean tensile strength

Predictor	**Coef**	**SE Coef**	**T**	**P**
Constant	-16.4	155.0	-0.11	0.917
Electrode Diameter (mm)	38.61	18.99	2.03	0.067
Current (Ampere)	0.5758	0.1861	3.09	**0.010**
Electrode Stick-Out (mm)	-0.115	1.861	-0.06	0.952
Preheat Temperature (^oC)	0.0514	0.1126	0.46	0.657
Travel Speed (m/hr)	10.077	4.652	2.17	0.053
Flux	4.819	9.303	0.52	0.615

TABLE 4.6 Analysis of Variance for Regression of Mean tensile strength

Source	**DF**	**SS**	**MS**	**F**	**P**
Regression	6	19612	3269	3.15	**0.048**
Residual Error	11	11424	1039		
Total	17	31036			

4.6 RESIDUAL ANALYSIS

The residual is the difference between the observed and fitted value of the response, there are four plots available in figure 4.7. These plots are normal probability plot, histogram, versus fits and versus order. The *x*-axis of histogram plot indicates the residuals and *y*-axis indicates the frequency of occurrence of that residual. The normal probability plot and histogram suggests approximate normal distribution of residuals. In residual plot of fits *x*-axis represent the tensile strength response and *y*-axis the residuals. Straight horizontal line residual versus fits shows the zero residual or the fitted model line. Which means all the points would have been lying on that if there is zero residual or no residual which is nearly not possible. Normal probability curve and histogram follows the approximate normal distribution curve, which is desirable. No non-random pattern occurs in residual

versus fits and residual versus order plot. The scattered points in residual versus fits show the residuals lying away from the fitted value. Absence of any particular trend of residuals in versus fitted value plot shows the good fit of the model.

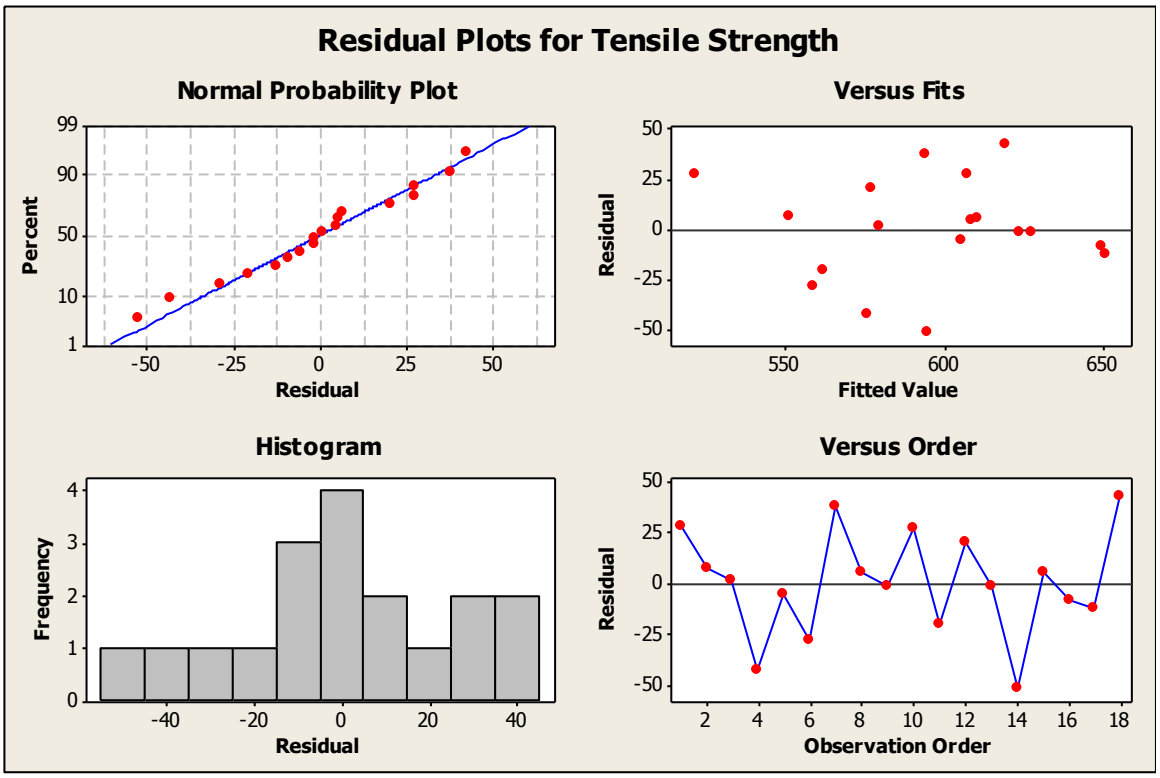

FIGURE 4.7 Residual Plots for Mean Tensile Strength

CHAPTER-5

RESULTS AND ANALYSIS OF BEAD GEOMETRY TEST

5.1 ANOVA ANALYSIS

Results obtained from the experiments were analysed using the ANOVA, which helps in predicting the significance of input parameter for any desired response function. It indicates which is the most influencing factor or parameter. A confidence interval of 95% has been taken for this analysis. Significance of all the dependent variables has been completed using statistical software MINITAB16. These dependent variables studied in this study are (1) bead height (2) bead width

5.2 ANOVA FOR BEAD HEIGHT

The results observed for the bead height is shown in the table 5.1.The table consists of the values of bead height for the eighteen trials. The mean value of the bead height is also given in table 5.2. The *p* value given in the last column of ANOVA table suggests the significance of the factors on the desired characteristics. The principle behind significance value is that the *p* value should be lesser than 0.05 (considering confidence level of 95%).The principle of F test is that, the F value should be large compared to e-pooled; larger the F value more is the significance of factor. An ANOVA table 5.2 show that p value for current and type of flux and is 0.026 and 0.029 respectively i.e. less than 0.05 indicates there by that current and flux is the most significant factor for the bead height. The response mean value for all variables is given in table 5.3. In last row of table 5.3 ranks have been given to various factors. Higher is the rank, higher is the significance. In table 5.3 current with the highest rank1 and is the most significant factor and travel speed with its lowest rank is least significant in affecting the bead height. Main effect plots are shown in figure 5.1 shows the variation in the bead height with the change in the input factors *i.e.* flux, current, travel speed, electrode diameter and electrode-stick out. It could be seen from the figure 5.1 that travel speed causes the most significant change in the bead height with change in flux. Electrode diameter and travel speed have no significant effect on the bead height.

TABLE 5.1 Results for Bead Height

Exp. No.	Contributing Factors	Bead Height Reading 1	Bead Height Reading 2	Bead Height Reading 3	Bead Height Reading 4	Avg. Bead Height (mm)	S/N Ratio
1	Ø1, C1, D1, T1,S1, F1,	2.8	2.8	2.8	2.6	2.77	-8.85
2	Ø1, C1, D2,T2,S2, F2,	3.3	2.8	3.9	3.3	3.33	-10.45
3	Ø1, C1, D3, T3,S3, F3	3.4	3.7	1.9	2.2	2.80	-8.94
4	Ø1, C2, D1, T1, S2, F2	4.1	3.9	4.7	3.0	3.90	-11.82
5	Ø1, C2, D2, T2, S3, F3	2.9	2.6	2.8	2.5	2.71	-8.64
6	Ø1, C2, D3, T3, S1, F1	5.4	5.0	2.5	2.8	3.93	-11.89
7	Ø1, C3, D1, T2, S1, F3	3.1	2.0	3.6	4.0	3.17	-10.02
8	Ø1, C3, D2, T3, S2, F1	3.4	2.8	5.1	5.2	4.13	-12.32
9	Ø1, C3, D3, T1, S3, F2	4.4	4.0	3.9	4.5	4.20	-12.45
10	Ø2, C1, D1, T3, S3,F2	2.8	3.0	3.1	3.5	3.10	-9.83
11	Ø2, C1, D2, T1, S1, F3	3.2	3.0	2.2	2.0	2.61	-8.32
12	Ø2, C1, D3, T2, S2, F1	2.7	2.5	3.0	2.8	2.75	-8.79
13	Ø2, C2, D1, T2, S3, F1	3.5	4.4	3.5	4.0	3.85	-11.71
14	Ø2, C2, D2, T3, S1, F2	4.7	3.1	3.1	3.2	3.55	-11.00
15	Ø2, C2, D3, T1, S2, F3	2.4	3.2	2.3	2.6	2.60	-8.30
16	Ø2, C3, D1, T3, S2, F3	3.2	3.8	3.6	3.4	3.50	-10.88
17	Ø2, C3, D2, T1, S3, F1	3.2	3.8	2.7	3.2	3.22	-10.16
18	Ø2, C3, D3, T2, S1, F2	5.3	4.3	5.2	3.2	4.48	-13.03

TABLE 5.2 Analysis of variance for means bead height

Source	DF	Seq SS	Adj SS	Adj MS	F	P
Electrode Diameter (mm)	1	0.08996	0.08996	0.08996	0.54	0.491
Current (Ampere)	2	2.40728	2.40728	1.20364	7.18	**0.026**
Electrode Stick-Out (mm)	2	0.12574	0.12574	0.06287	0.38	0.702
Preheat Temperature (^{o}C)	2	0.24863	0.24863	0.12432	0.74	0.515
Travel Speed (m/hr.)	2	0.03392	0.03392	0.01696	0.10	0.905
Flux	2	2.28544	2.28544	1.14272	6.82	**0.029**
Residual Error	6	1.00546	1.00546	0.16758		
Total	17	6.19644				

TABLE 5.3 Response table for means of bead height

Level	Electrode Diameter (mm)	Current (amp)	Electrode Stick-Out (mm)	Preheat Temperature (^{o}C)	Travel Speed (m/hr)	Flux
1	3.437	2.893	3.382	3.215	3.418	3.442
2	3.295	3.422	3.257	3.381	3.368	3.760
3		3.783	3.460	3.502	3.312	2.897
Delta	0.141	0.890	0.203	0.287	0.106	0.863
Rank	**5**	**1**	**4**	**3**	**6**	**2**

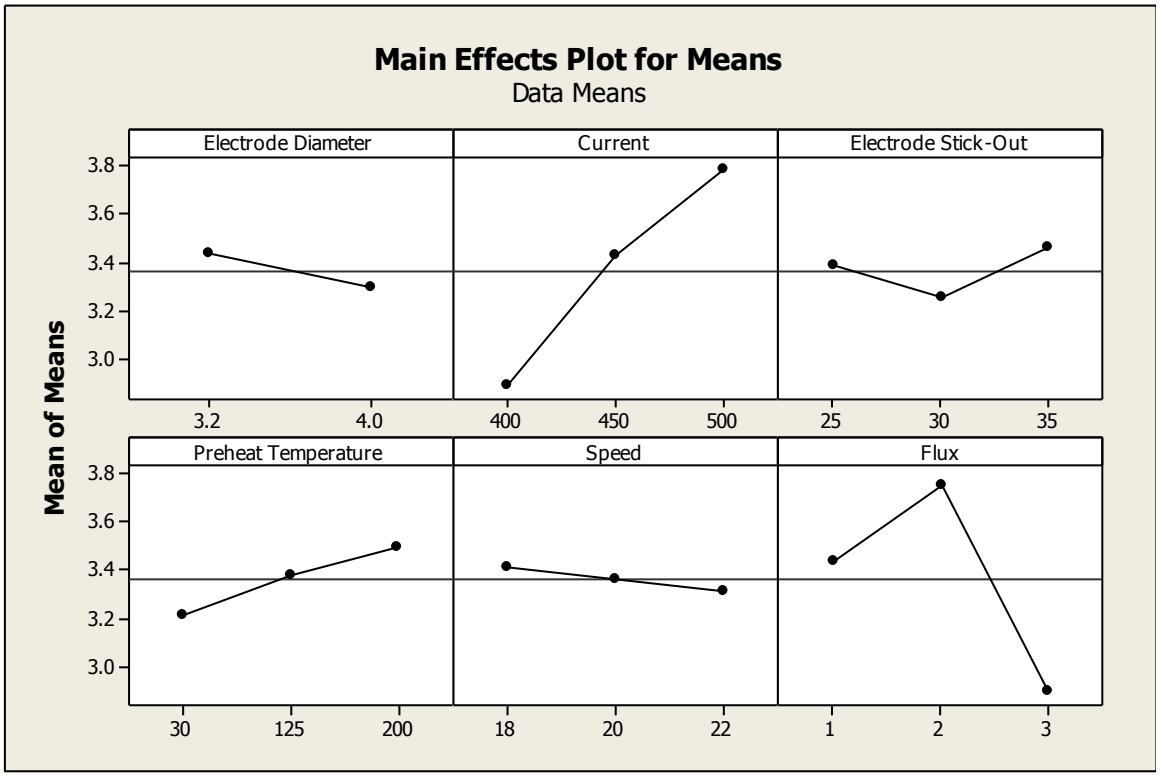

FIGURE 5.1 Main effect plot for Bead Height

5.3 OPTIMAL DESIGN FOR BEAD HEIGHT

In this experimental analysis, the main effect plot in figure 5.1 has been used to estimate the bead height in optimal conditions. From Table 5.2, it can be concluded that welding current and flux are main significant factors. In order to obtain minimum bead height, the flux should be used type 3 i.e. AUTOMELT B31 and welding current should be 400 ampere. Table 5.1 shown that trial no.15 has less value of bead height i.e. 2.60 mm. Confidence interval predict with 95 % confidence so that value of bead height at optimal design conditions would be 2.43 ± 0.3872 mm

Mean value of Bead Height is given by-

$\mu_{C_1F_3} = \overline{C_1} + \overline{F_3} - 1\overline{T}$

= 2.893+2.897- (1x3.36)

=2.43

C.I. = $\sqrt{\frac{f\alpha:v1:v2\ X\ Ve}{neff}}$; *v2* = DOF for error = 13

Where $f\,\alpha{:}v1{:}v2 = f\,0.05{:}1{:}$ 13 = 4.67

Variance = $Ve = \frac{1.50372}{13} = 0.1156$

$n_{eff} = \frac{18}{1+\mathrm{DOF}_{C_1F_3}} = 3.6$

C.I. = 0.3872

So, the confidence interval of Bead Height is given by **2.43 ± 0.3872 mm**.

5.4 ANALYSIS OF S/N RATIO FOR BEAD HEIGHT

Larger bead height is the undesirable property of the weld joint. So in case of bead height, smaller the better option has been chosen for calculation of S/N ratio. ANOVA for S/N ratio is given in table 5.4 shown that current and flux is significant. Response mean value at each level of parameters is given in table 5.5. Table 5.5 also indicates the ranks given to input parameters according to their order of significance. The main effect plot for S/N ratio is given in Figure 5.2.

TABLE 5.4 Analysis of Variance for S/N ratios

Source	DF	Seq SS	Adj SS	Adj MS	F	P
Electrode Diameter (mm)	1	0.6335	0.6335	0.63348	0.63	0.457
Current (Ampere)	2	15.8245	15.8245	7.91227	7.88	**0.021**
Electrode Stick-Out (mm)	2	0.6296	0.6296	0.31481	0.31	0.742
Preheat Temperature (^oC)	2	2.0616	2.0616	1.03082	1.03	0.414
Travel Speed (m/hr.)	2	0.1596	0.1596	0.07979	0.08	0.925
Flux	2	15.5337	15.5337	7.76685	7.73	**0.022**
Residual Error	6	6.0258	6.0258	1.00430		
Total	17	40.8684				

TABLE 5.5 Response Table for Signal to Noise Ratios
Smaller is better

Level	Electrode Diameter (mm)	Current (amp)	Electrode Stick-Out (mm)	Preheat Temperature (^oC)	Travel Speed (m/hr)	Flux
1	-10.599	-9.195	-10.518	-9.983	-10.518	-10.618
2	-10.224	-10.561	-10.148	-10.440	-10.426	-11.431
3		-11.477	-10.567	-10.811	-10.289	-9.184
Delta	0.375	2.282	0.419	0.827	0.229	2.247
Rank	**5**	**1**	**4**	**3**	**6**	**2**

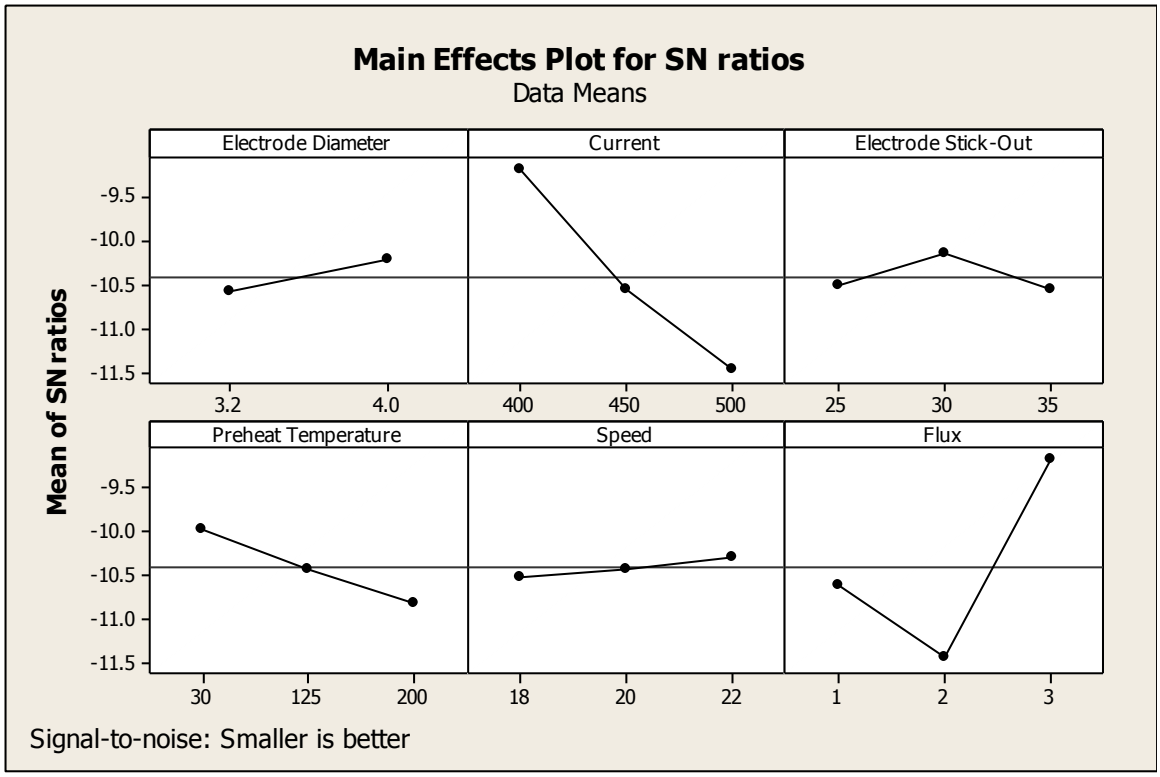

FIGURE 5.2 Main effect plot for S/N ratios of Bead Height

5.5 ANOVA for Bead Width

The results for bead width are shown in the table 5.6.The table consists of the values of bead width for the eighteen trials. Analysis of variance for means Bead width in the table 5.7. ANOVA table indicates that preheat temperature and travel speed were significant when bead width is taken as response. P value for preheat temperature and travel speed is 0.031, which is lesser than 0.05. F value for the travel speed is maximum, which indicates that it is a significant factor contributing to the response, which includes the ranks of the contributing factors. In the present study preheat temperature is the most significant factor. Main effect plots showing the variation in the bead width with change in input factors have been shown in figure 5.3. Table 5.6 shown that trial no.10 has less value of bead width i.e. 17.88 mm. It is clear from figure 5.3 that bead width decrease almost linearly with decrease travel speed.

TABLE 5.6 Results for Bead width

Exp. No.	Contributing Factors	Bead Width Reading 1	Bead Width Reading 2	Bead Width Reading 3	Bead Width Reading 4	Avg. Bead width (mm)	S/N Ratio for Bead Width
1	Ø1, C1, D1, T1,S1, F1,	24.84	24.61	24.31	24.65	24.60	-27.82
2	Ø1, C1, D2,T2,S2, F2,	26.24	24.19	21.63	20.53	23.15	-27.29
3	Ø1, C1, D3, T3,S3, F3	21.99	21.07	22.11	23.12	22.07	-26.88
4	Ø1, C2, D1, T1, S2, F2	25.82	26.69	24.28	25.3	25.52	-28.14
5	Ø1, C2, D2, T2, S3, F3	18.66	18.34	18.68	19.73	18.85	-25.51
6	Ø1, C2, D3, T3, S1, F1	27.88	24.98	23.01	21.75	24.41	-27.75
7	Ø1, C3, D1, T2, S1, F3	22.37	23.13	24.4	24.93	23.70	-27.49
8	Ø1, C3, D2, T3, S2, F1	21.86	23.79	20.71	20.86	21.81	-26.77
9	Ø1, C3, D3, T1, S3, F2	24.81	23.17	23.33	23.64	23.74	-27.51
10	Ø2, C1, D1, T3, S3,F2	17.61	16.68	18.58	18.65	17.88	-25.05
11	Ø2, C1, D2, T1, S1, F3	27.09	25.73	24.03	24.81	25.42	-28.10
12	Ø2, C1, D3, T2, S2, F1	18.23	17.82	19.76	18.04	18.46	-25.33
13	Ø2, C2, D1, T2, S3, F1	19.87	16.77	18.02	24.32	19.75	-25.91
14	Ø2, C2, D2, T3, S1, F2	21.1	24.4	23.34	21.22	22.52	-27.05
15	Ø2, C2, D3, T1, S2, F3	29.94	28.75	27.34	27.8	28.45	-29.08
16	Ø2, C3, D1, T3, S2, F3	23.54	24.45	24.16	24.74	24.22	-27.68
17	Ø2, C3, D2, T1, S3, F1	19.84	21.64	22.4	23.51	21.84	-26.79
18	Ø2, C3, D3, T2, S1, F2	23.97	23.27	24.94	25.3	24.37	-27.74

TABLE 5.7 Analysis of variance for means Bead Width

Source	DF	Seq SS	Adj SS	Adj MS	F	P
Electrode Diameter (mm)	1	1.359	1.359	1.359	0.42	0.540
Current (Ampere)	2	7.118	7.118	3.559	1.11	0.390
Electrode Stick-Out (mm)	2	5.616	5.616	2.808	0.87	0.465
Preheat Temperature (^{o}C)	2	41.802	41.802	20.901	6.50	**0.031**
Travel Speed (m/hr.)	2	41.842	41.842	20.921	6.51	**0.031**
Flux	2	11.723	11.723	5.862	1.82	0.241
Residual Error	6	19.287	19.287	3.214		
Total	17	128.747				

TABLE 5.8 Response table for means of Bead Width

Level	Electrode Diameter (mm)	Current (amp)	Electrode Stick-Out (mm)	Preheat Temperature (^{o}C)	Travel Speed (m/hr)	Flux
1	23.09	21.93	22.61	24.93	24.17	21.81
2	22.54	23.25	22.26	21.38	23.60	22.86
3		23.28	23.58	22.15	20.69	23.79
Delta	0.55	1.35	1.32	3.55	3.48	1.98
Rank	**6**	**4**	**5**	**1**	**2**	**3**

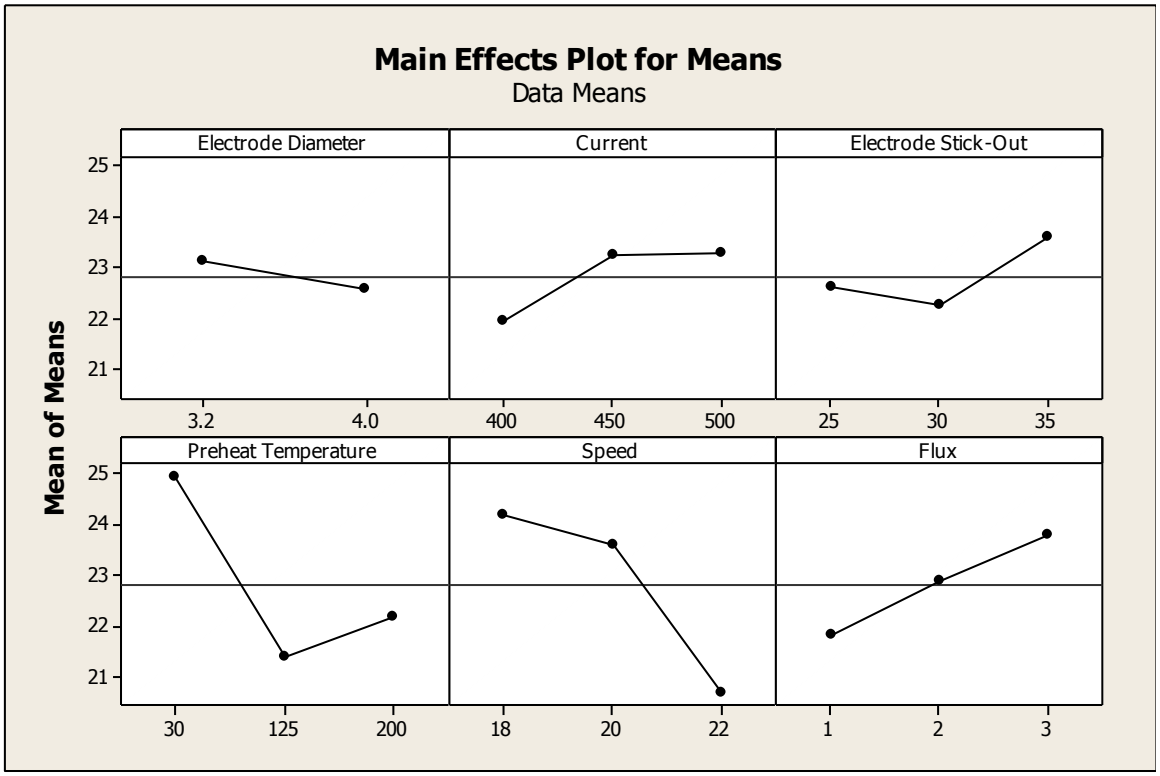

FIGURE 5.3 Main effect plot for mean of Bead Width

5.6 OPTIMAL DESIGN FOR BEAD WIDTH

In this experimental analysis, the main effect plot in figure 5.3 has been used to estimate the Bead width in optimal conditions. From table 5.7, it can be concluded that preheat temperature and travel speed are significant factor. In order to obtain minimum bead width, the preheat temperature should be 125 ^{o}C and travel speed should be 22 m/hr. Confidence interval predict with 95 % confidence so that value of Bead Width at optimal design conditions would be 19.25 $\pm$ 2.11mm.

Mean value of Bead Width is given by-

$\mu_{T_2S_3} = \overline{T_2} + \overline{S_3} - 1\overline{T}$

=21.38+20.69- (1x 22.82)

=19.25mm

$$\text{C.I.} = \sqrt{\frac{f\alpha:v1:v2\ X\ Ve}{neff}}$$

v2 = DOF for error = 13

Where $f\,\alpha{:}v1{:}v2 = f\,0.05{:}1{:}13 = 4.67$

Variancse = $Ve = \frac{45.103}{13} = 3.46$

$n_{eff} = \frac{18}{1+\text{DOF}_{T_2 S_3}} = 3.6$

C.I. = 2.11

So, the confidence interval of Bead Width is given by **19.25 ± 2.11mm**.

5.7 ANALYSIS OF S/N RATIO FOR BEAD WIDTH

Bead width, lower the better option is always chosen for ANOVA and signal to noise ratio calculations. Table 5.10 shows the response table for signal to noise ratios. Main effects plots are shown in figure 5.4.Significant change in bead width can be seen from the figure with change in the levels of preheat temperature and travel speed. ANOVA for S/N ratios table indicates that preheat temperature and travel speed were significant when bead width is taken as response. P value for preheat temperature and travel speed is 0.042 & 0.037, which is lesser than 0.05 as shown in table 5.9.

TABLE 5.9 Analysis of Variance for S/N ratios

Source	DF	Seq SS	Adj SS	Adj MS	F	P
Electrode Diameter (mm)	1	0.3294	0.3294	0.3294	0.61	0.464
Current (Ampere)	2	1.1961	1.1961	0.5981	1.11	0.389
Electrode Stick-Out (mm)	2	0.7126	0.7126	0.3563	0.66	0.551
Preheat Temperature (^oC)	2	6.0871	6.0871	3.0436	5.64	**0.042**
Travel Speed (m/hr.)	2	6.4588	6.4588	3.2294	5.99	**0.037**
Flux	2	1.6090	1.6090	0.8045	1.49	0.298
Residual Error	6	3.2372	3.2372	0.5395		
Total	17	19.6302				

TABLE 5.10 Response table for Signal to Noise Ratios

Smaller is better

Level	Electrode Diameter (mm)	Current (amp)	Electrode Stick-Out (mm)	Preheat Temperature (^{o}C)	Travel Speed (m/hr.)	Flux
1	-27.24	-26.74	-27.02	-27.91	-27.66	-26.73
2	-26.97	-27.24	-26.92	-26.54	-27.38	-27.13
3		-27.33	-27.38	-26.86	-26.27	-27.46
Delta	0.27	0.59	0.46	1.36	1.39	0.73
Rank	**6**	**4**	**5**	**1**	**2**	**3**

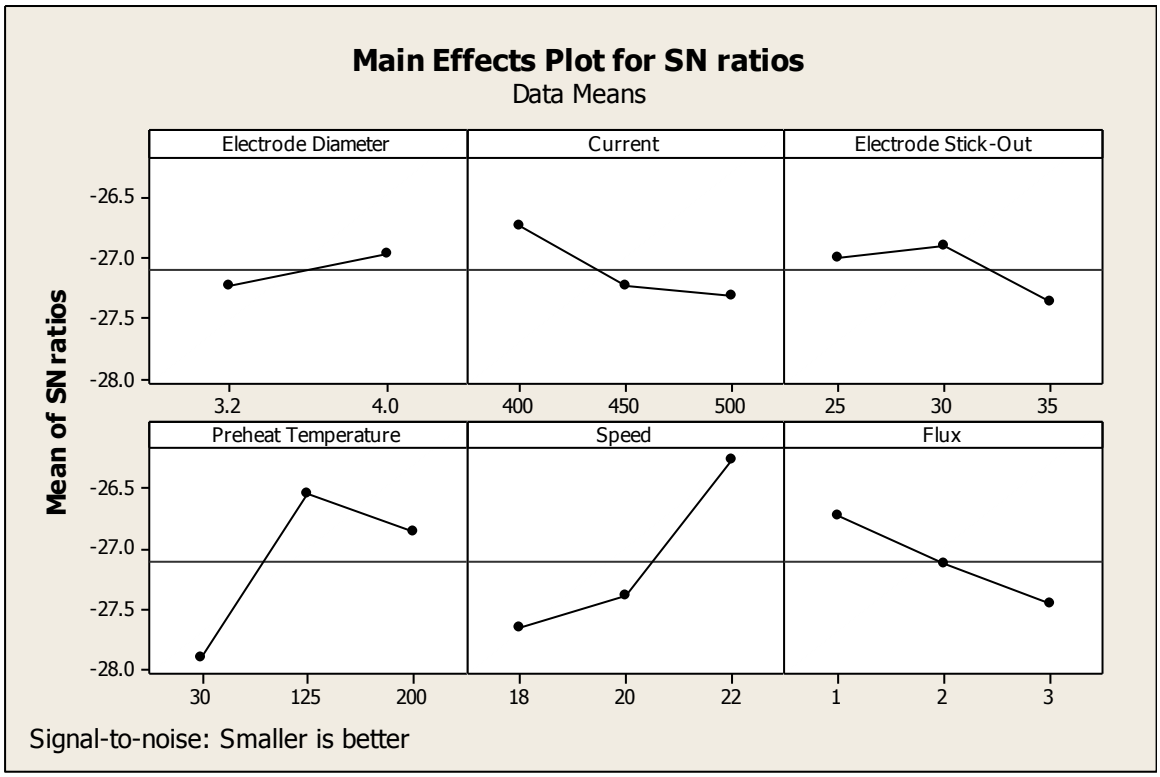

FIGURE5.4 Main effect plot for S/N ratios of Bead Width

CHAPTER 6
RESULTS OF RADIOGRAPHY TESTING

6.1 INTRODUCTION

Radiographic Testing (RT) is a non-destructive (NDT) method of inspecting materials for hidden flaws by using the ability of short wavelength electromagnetic radiation (high energy photons) to penetrate various materials. The radiation, either X-rays or gamma rays from a radioactive isotope, is absorbed as it passes through the specimen. This absorption increases as the density of the material increases so that if a photographic film is placed on the side opposite the radiation source, any less dense areas will appear as darker areas on the film as sown in figure 6.1. It gives a shadow picture of the internal features of the test sample once the film has been processed. Thus voids, porosity, slag, cracks and defects of geometry can all be identified, although planar defects normal to the beam may not be detected.Where ever there is a defect, the amount of radiation absorbed will be different and corresponding pattern will be generated**.** Detection of subsurface defects is the major advantage of this test but proper safety measures have to be taken to prevent exposure to these radiations because gamma rays are dangerous for health.

The three basic essential in producing radiography are:

(i) A source of radiation, usually X-rays or gamma rays.

(ii) The specimen to be tested

(iii) A Cassette containing the film

Radiography test was performed on the various specimens as discussed earlier and the results of the same are reported in the form of photograph of specimen after test.

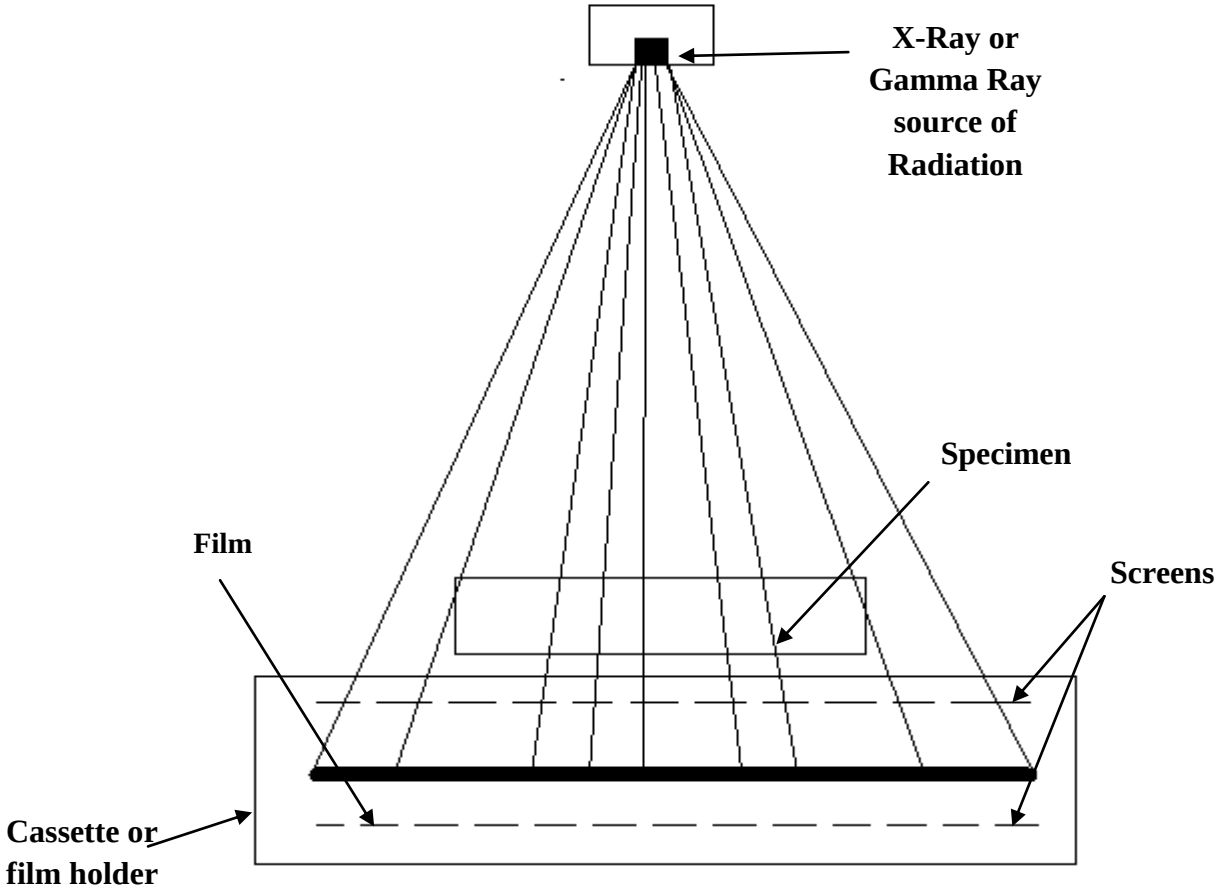

Figure 6.1 Schematic of Radiographic Testing

6.2 RADIOGRAPHY IMAGES

(a)Radiographic image of Specimen No.1 with contributing factors **(Ø1, C1, D1, T1, S1, F1)**

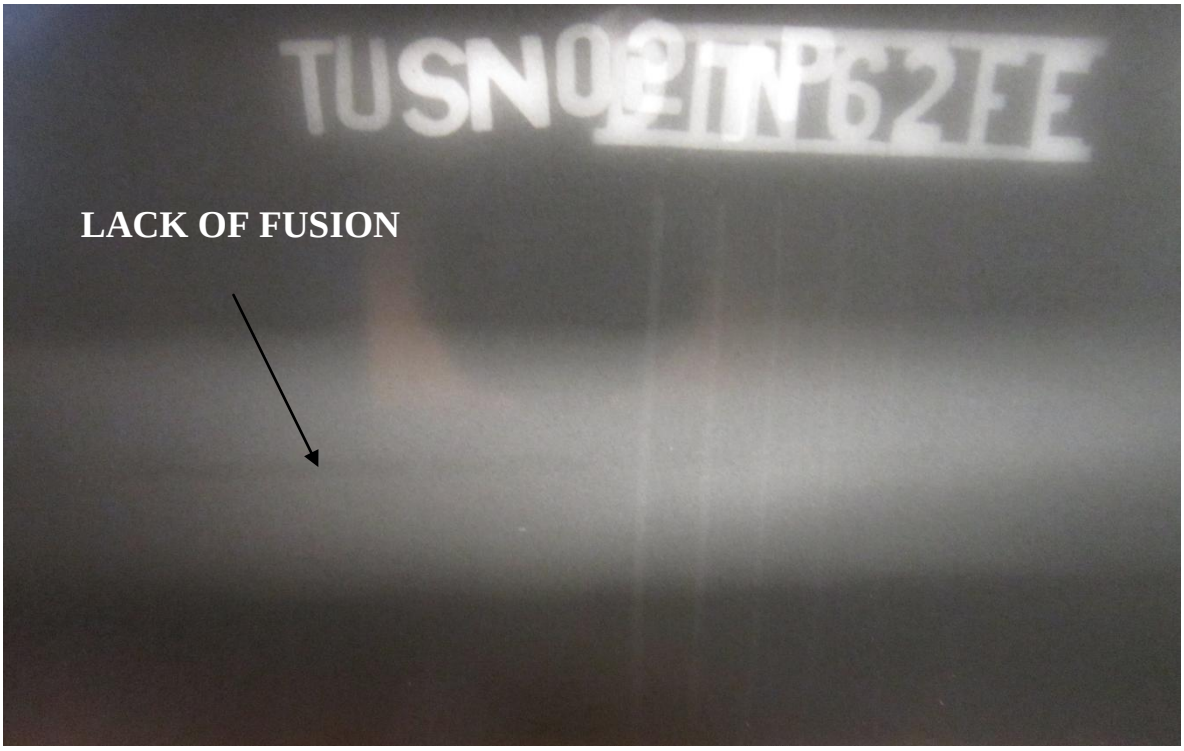

(b) Radiographic image of Specimen No.2 with contributing factors **(Ø1, C1, D2, T2, S2, F2)** revealing defect i.e. lack of fusion

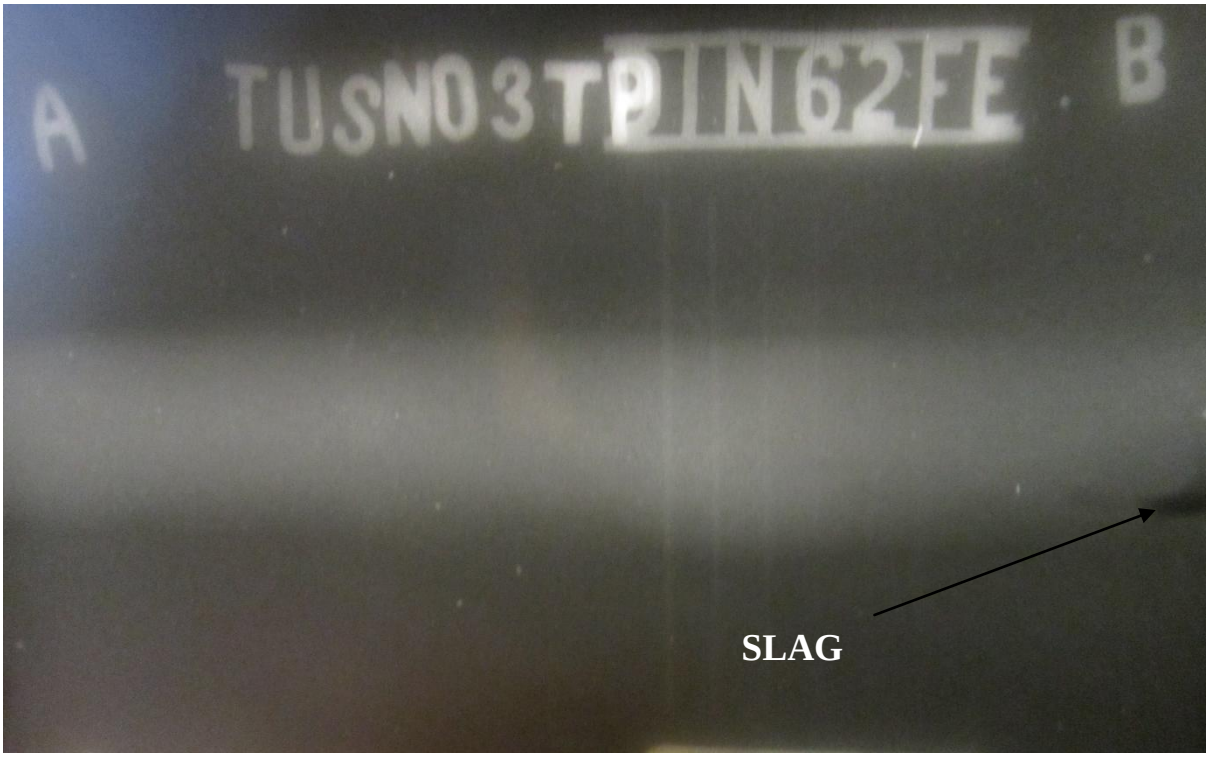

(c) Radiographic image of Specimen No.3 with contributing factors **(Ø1, C1, D3, T3, S3, F3)** revealing defect i.e. slag

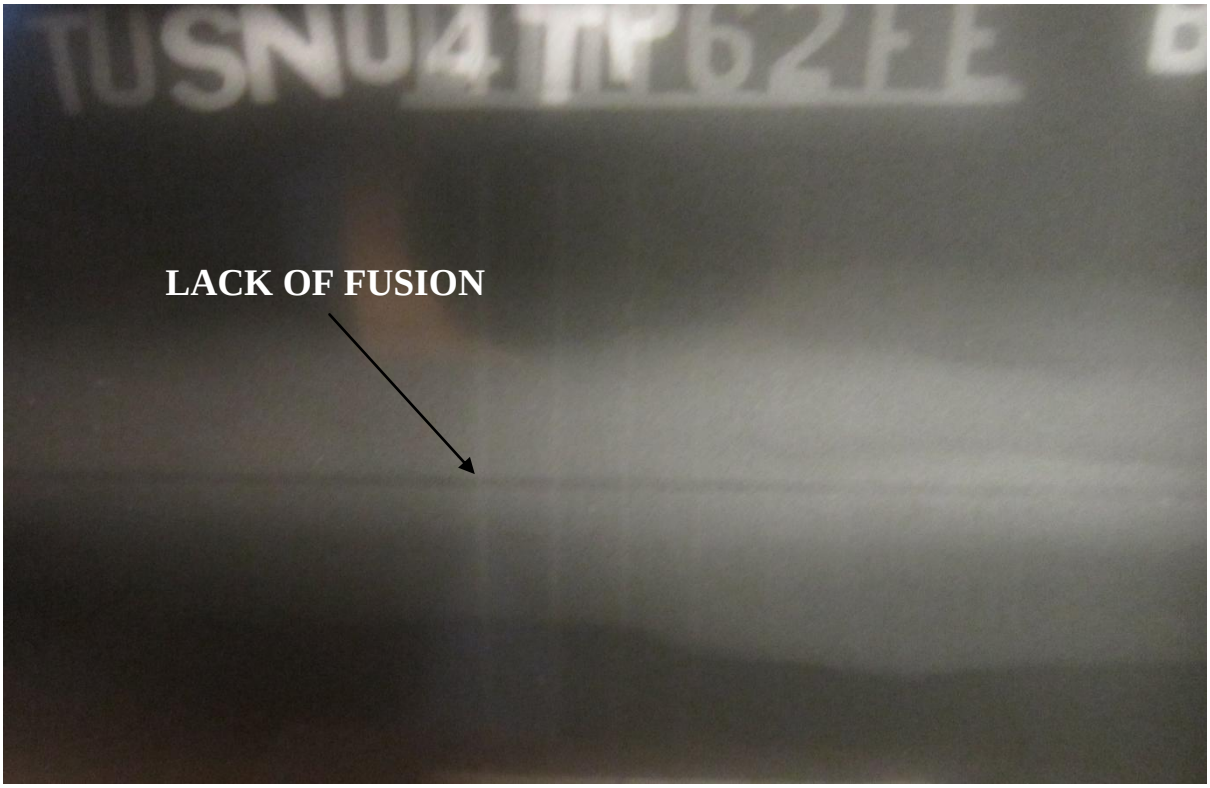

(d) Radiographic image of Specimen No.4 with contributing factors **(Ø1, C2, D1, T1, S2, F2)** revealing defect i.e. Lack of fusion

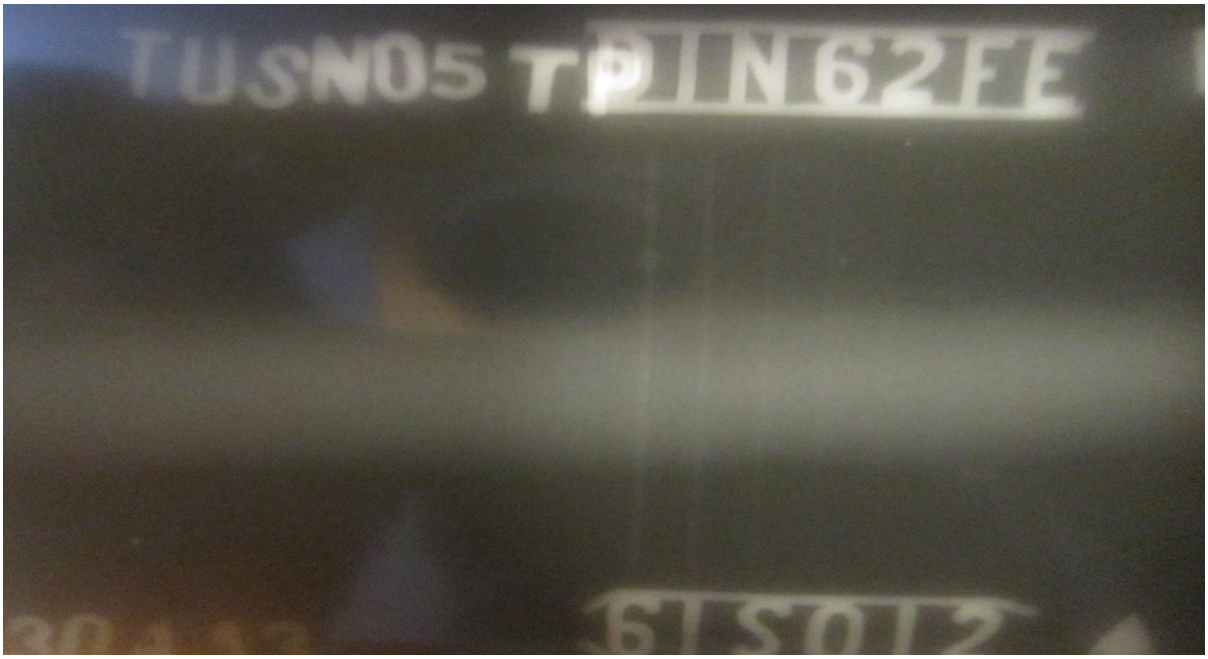

(e) Radiographic image of Specimen No.5 with contributing factors **(Ø1, C2, D2, T2, S3, F3)**

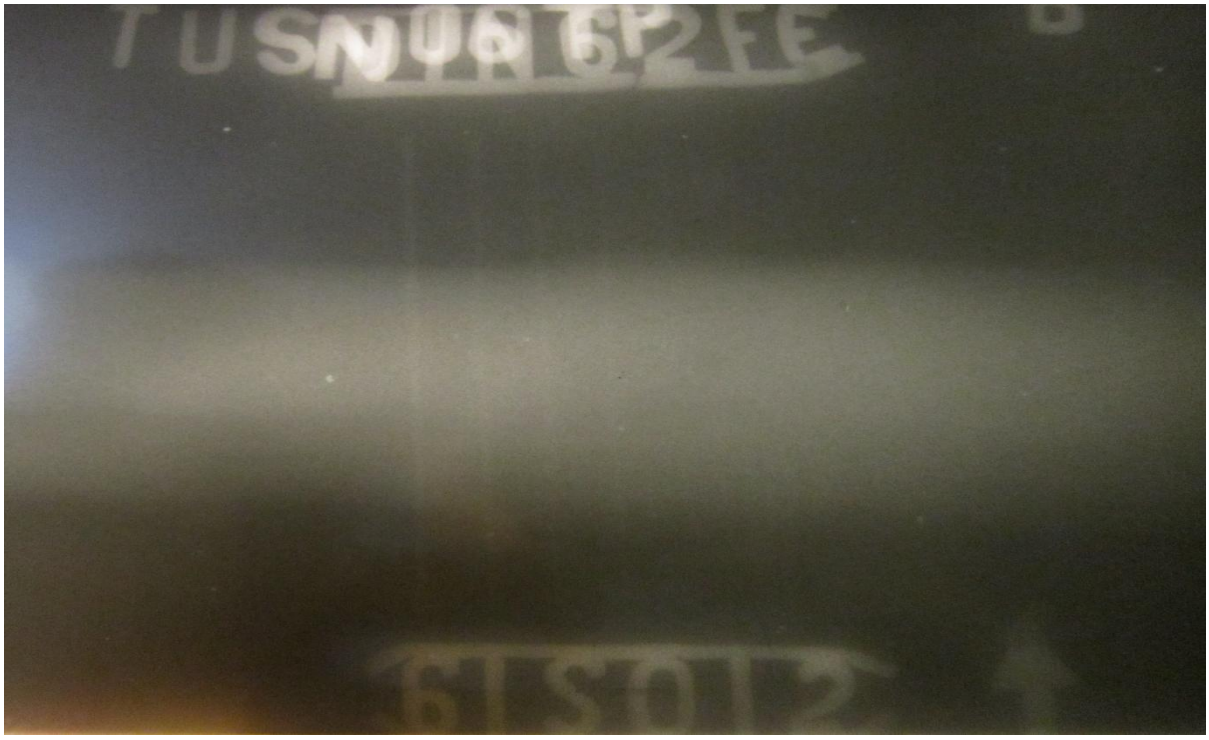

(f) Radiographic image of Specimen No.6 with contributing factors **(Ø1, C2, D3, T3, S1, F1)**

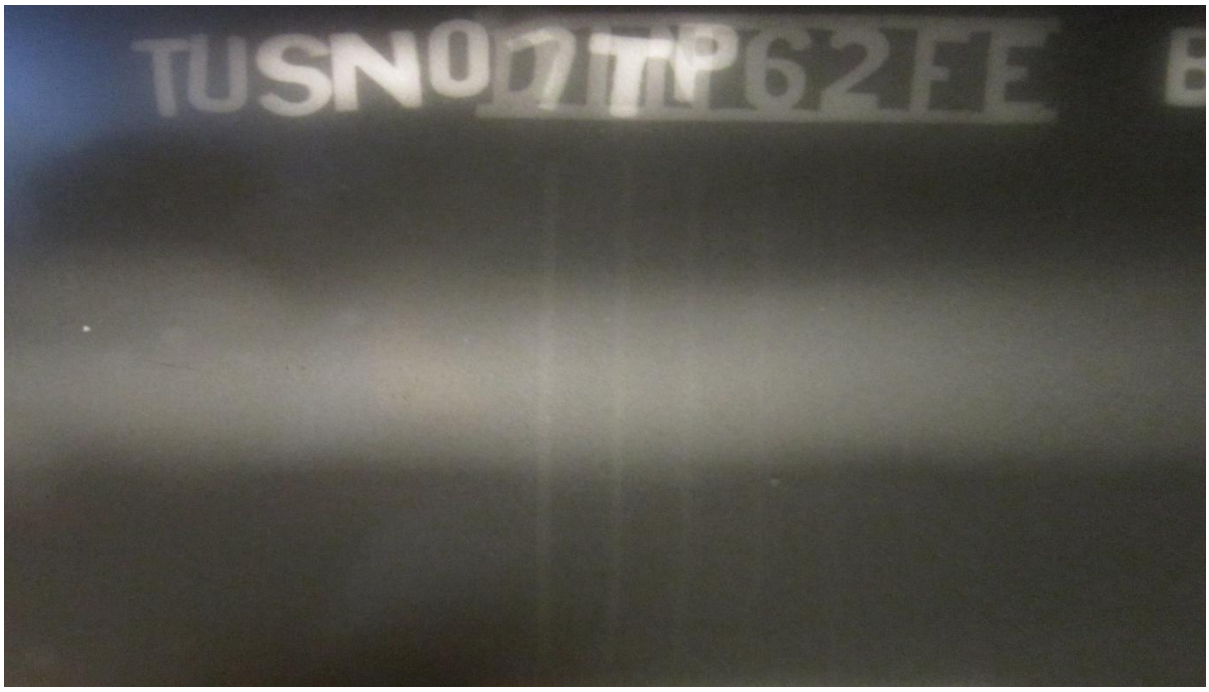

(g) Radiographic image of Specimen No.7 with contributing factors **(Ø1, C3, D1, T2, S1, F3)**

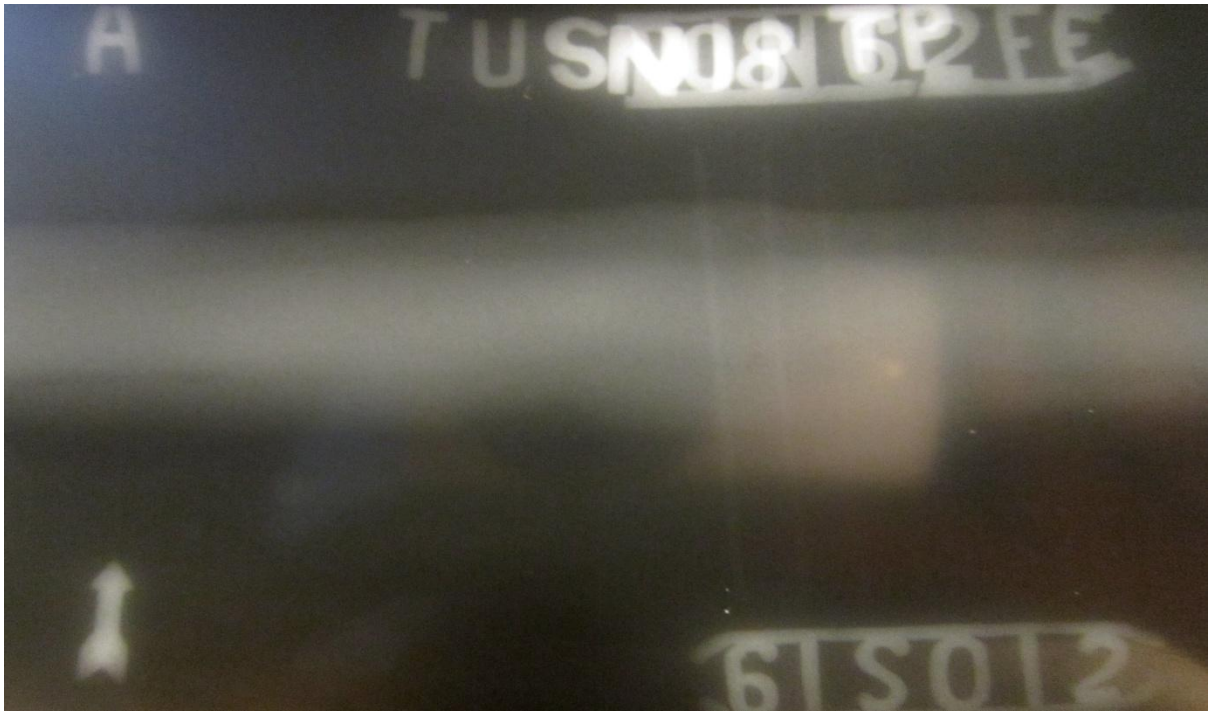

(h) Radiographic image of Specimen No.8 with contributing factors **(Ø1, C3, D2, T3, S2, F1)**

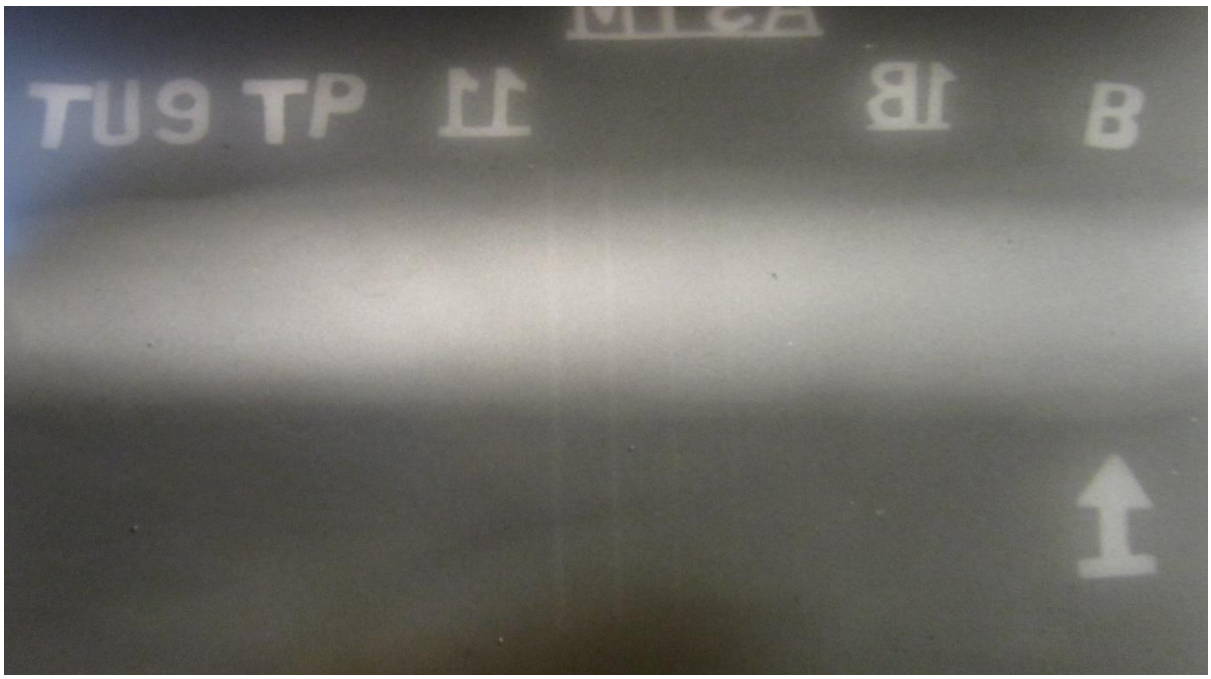

(i) Radiographic image of Specimen No.9 with contributing factors **(Ø1, C3, D3, T1, S3, F2)**

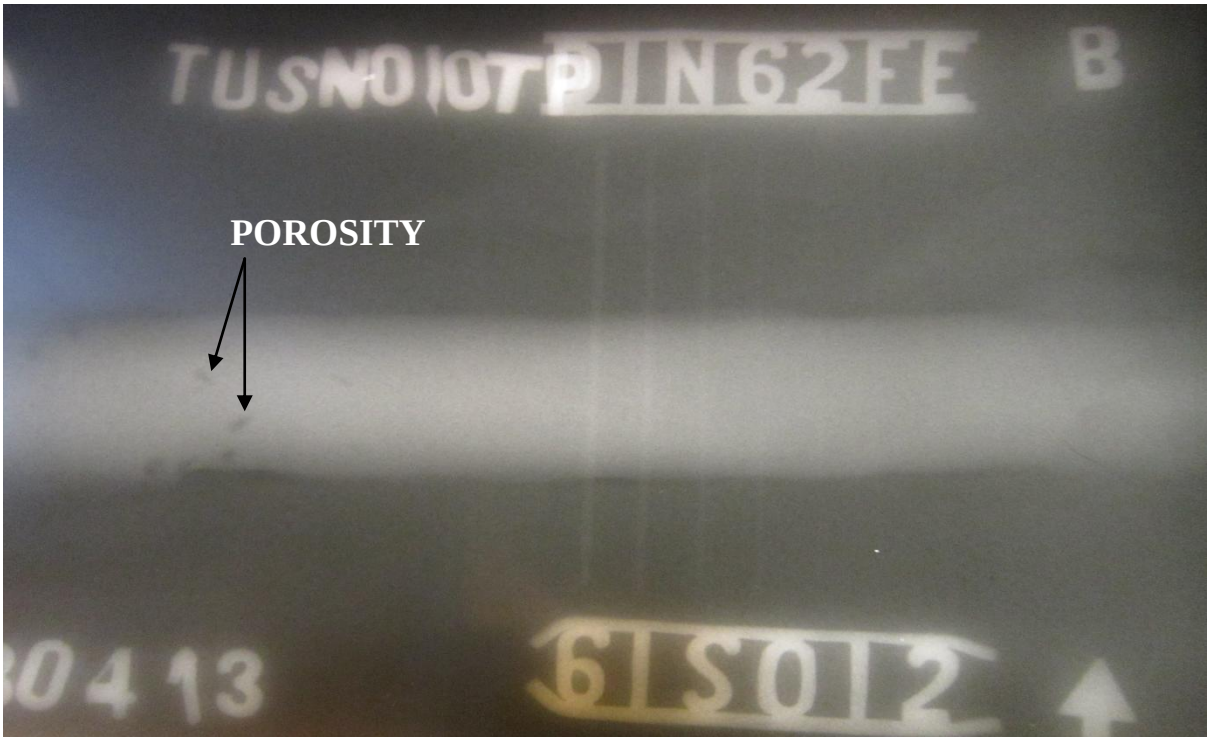

(j) Radiographic image of Specimen No.10 with contributing factors **(Ø2, C1, D1, T3, S3, F2)** revealing defect i.e. porosity

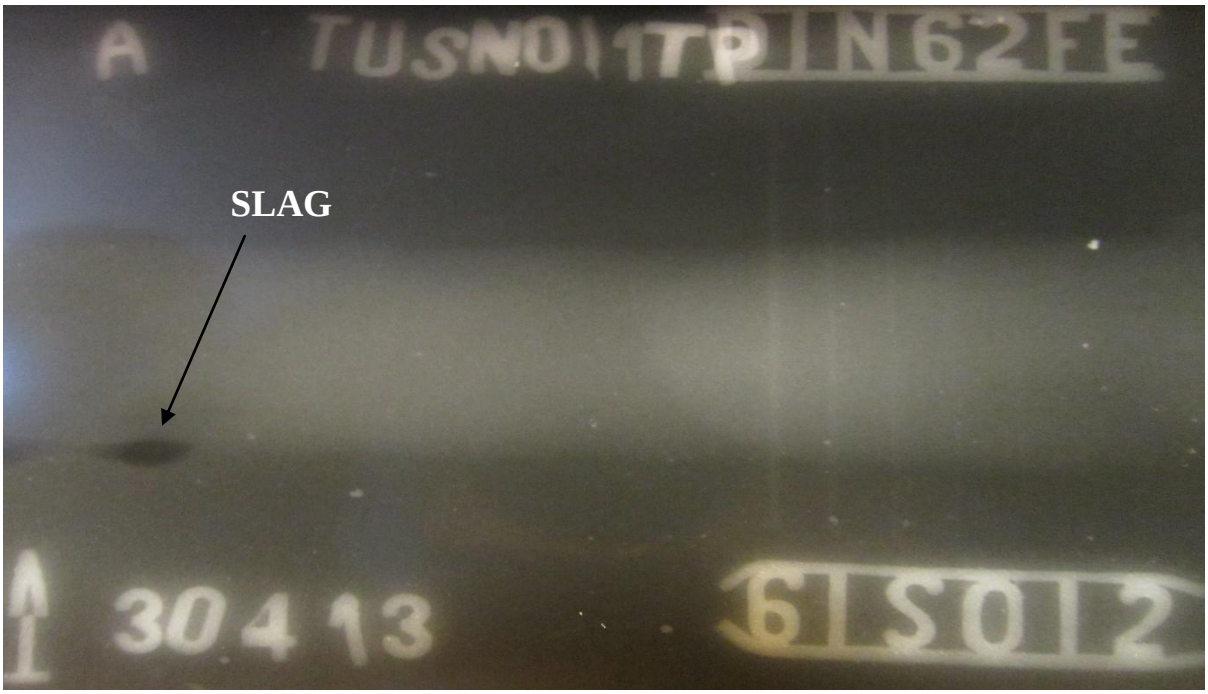

(k) Radiographic image of Specimen No.11 with contributing factors **(Ø2, C1, D2, T1, S1, F3)** revealing defect i.e. slag

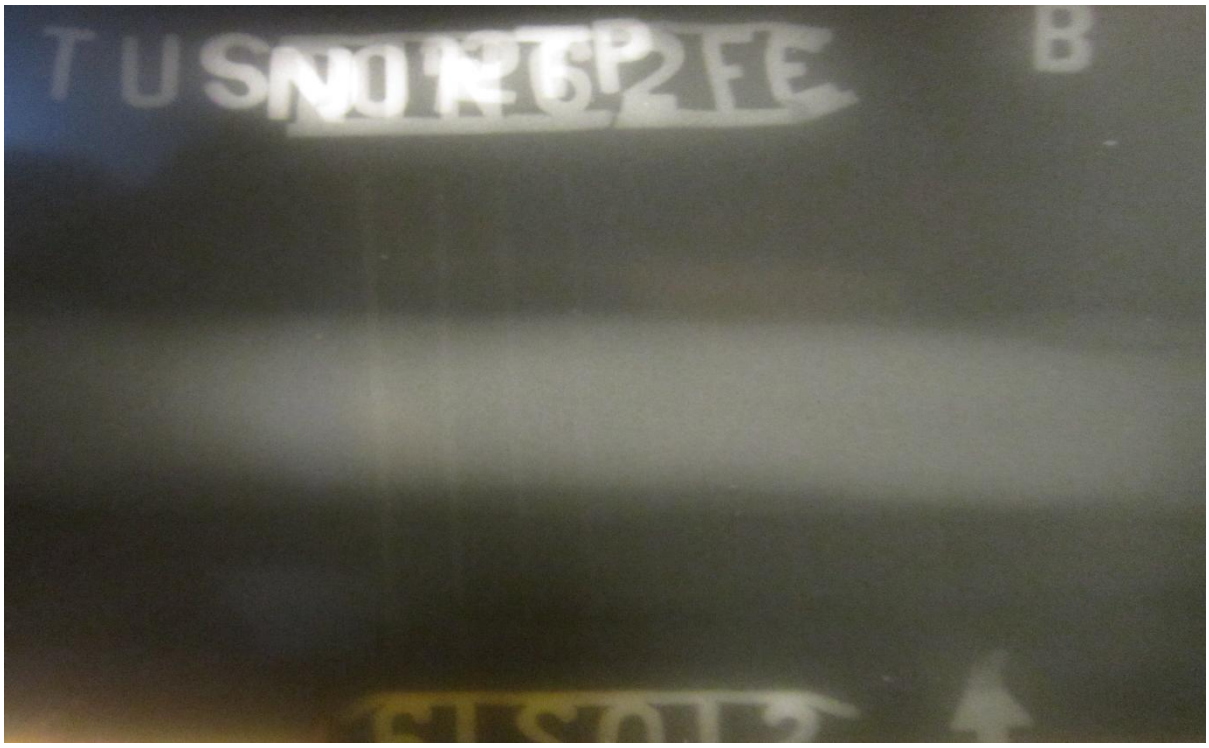

(l) Radiographic image of Specimen No.12 with contributing factors **(Ø2, C1, D3, T2, S2, F1)**

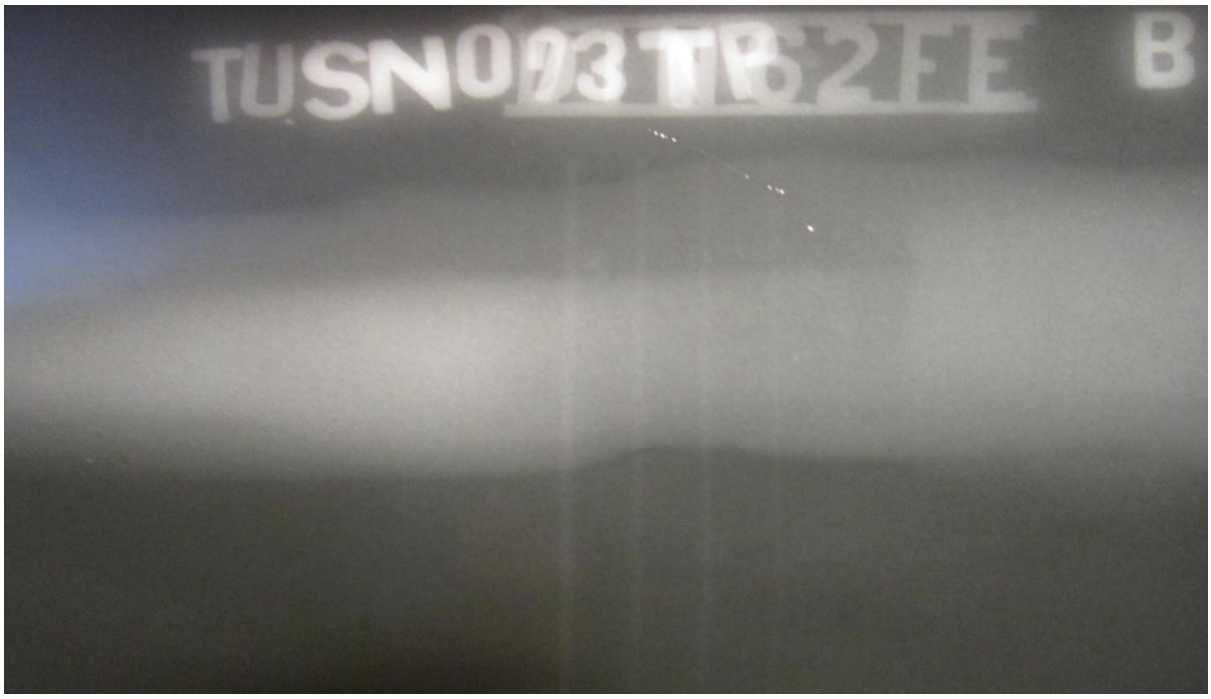

(m) Radiographic image of Specimen No.13 with contributing factors **(Ø2, C2, D1, T2, S3, F1)**

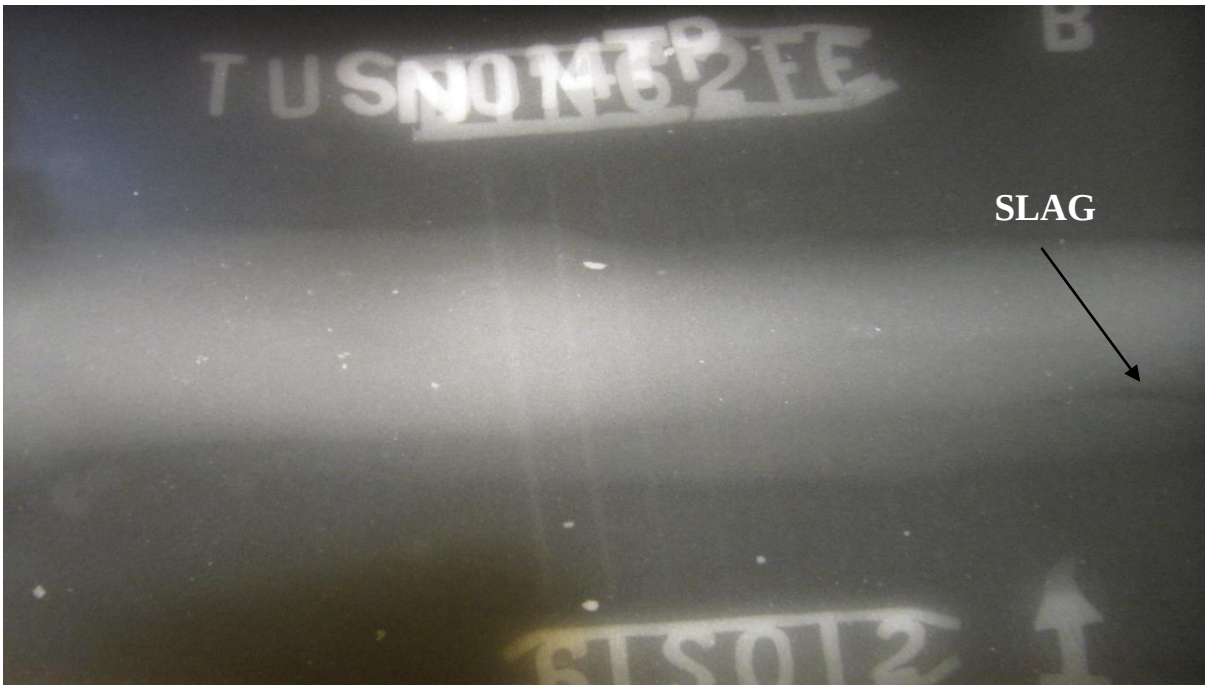

(n) Radiographic image of Specimen No.14 with contributing factors **(Ø2, C2, D2, T3, S1, F2)** revealing defect i.e. slag

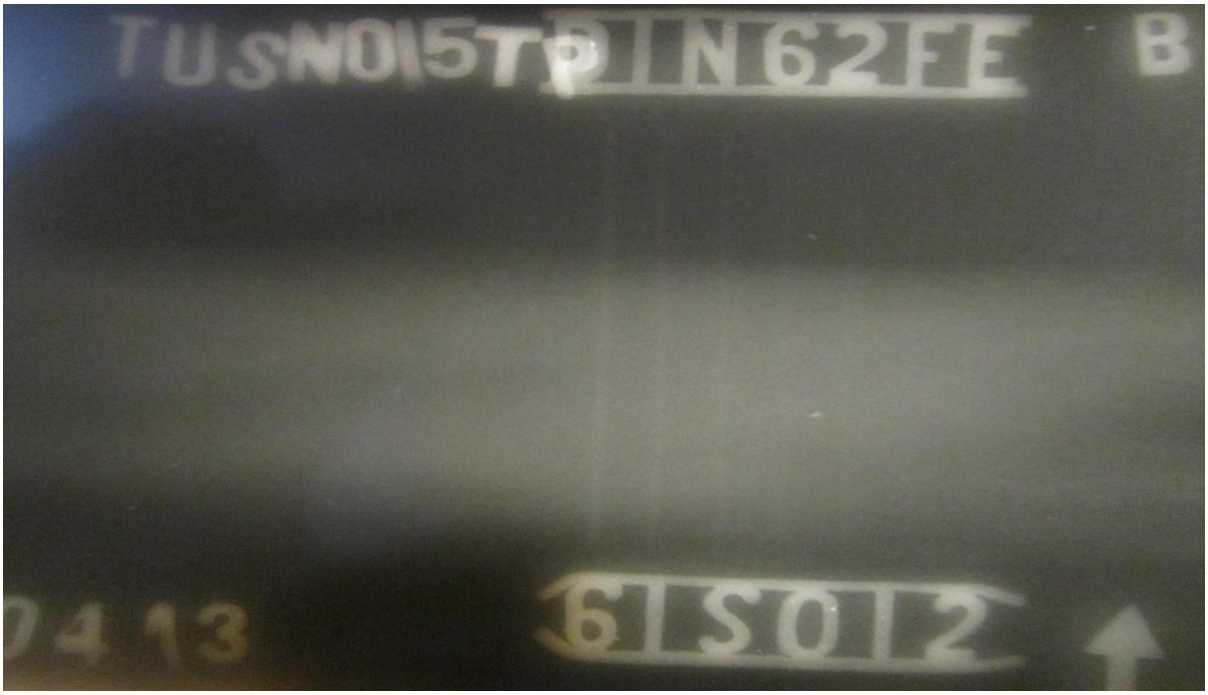

(o) Radiographic image of Specimen No.15 with contributing factors **(Ø2, C2, D3, T1, S2, F3)**

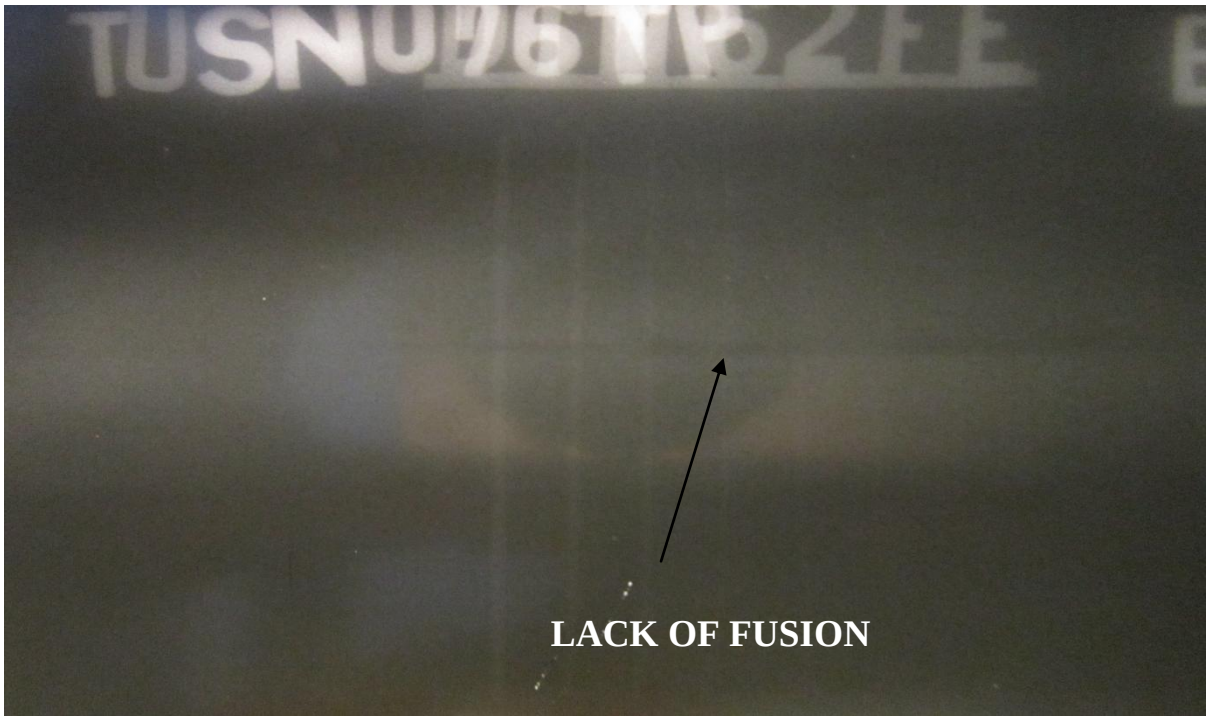

(p) Radiographic image of Specimen No.16 with contributing factors **(Ø2, C3, D1, T3, S2, F3)** revealing defect i.e. lack of fusion

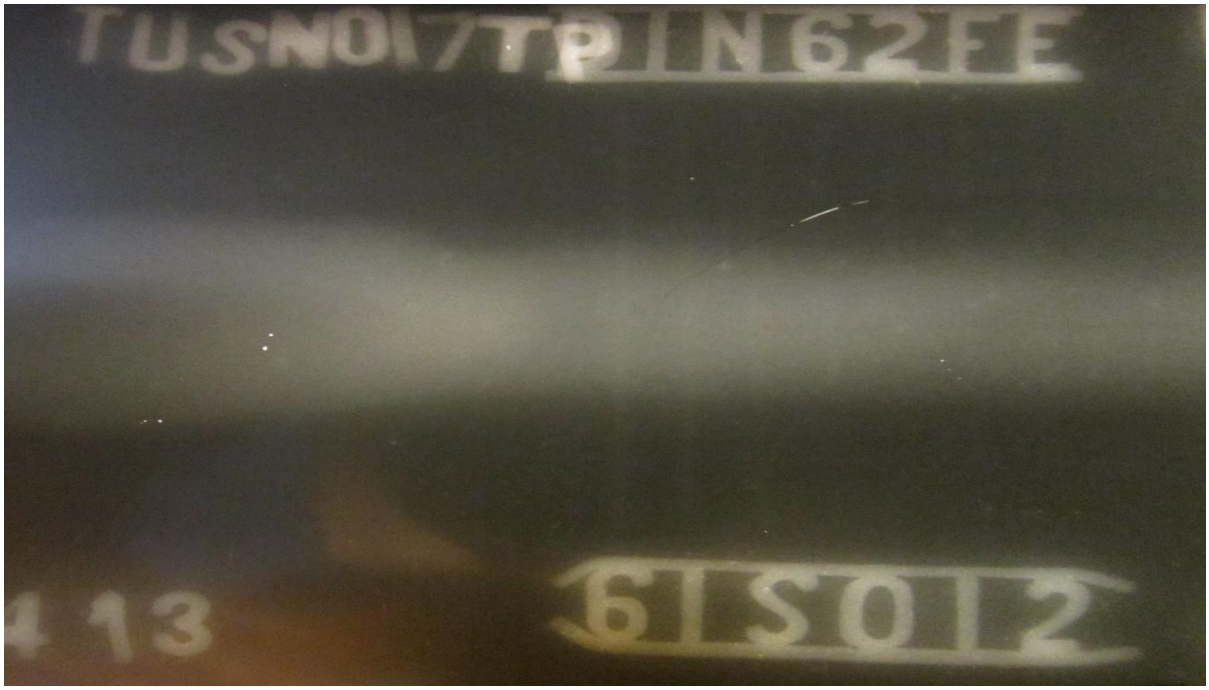

(q) Radiographic image of Specimen No.17 with contributing factors **(Ø2, C3, D2, T1, S3, F1)**

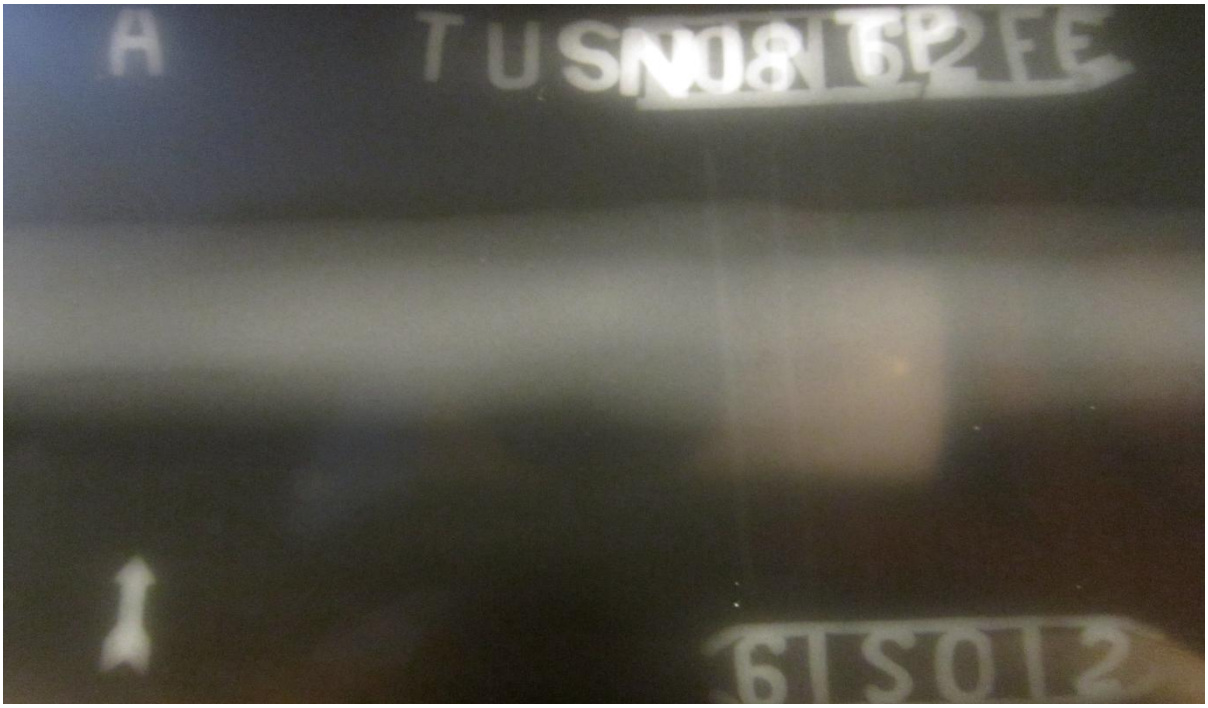

(r) Radiographic image of Specimen No.18 with contributing factors **(Ø2, C3, D3, T2, S1, F2)**

FIGURE 6.2 (a-r) Radiography image of a weld revealing defects of specimen

6.3 DISCUSSION OF RADIOGRAPHY IMAGES

Figure 6.2 (a-r) shows that welded joints have no crack defect except specimen no. 2, 4 and 16 which is having a lack of fusion defect at the centre part of the plates. Specimen no. 3, 10, 11 and 14 having minor defect like porosity, slag at the end part of the plates. Last end of plate (nearly 10-15 mm) would be rejected while cutting the plates for various mechanical testing. In overall it concluded that welded region with current 500 A having no welding imperfection i.e. surface cracks, porosity; cracks found in the specimen except no.16. Based on radiography results for better quality of joints, it suggested that should be set at its higher current (approx. 500 A) for greater than 25 mm thickness plate during submerged arc welding. Welding imperfection found in the radiography test as shown in table 6.1.

TABLE 6.1 Welding imperfection found in the radiography test

Experiment No.	**Contributing Factors**	**Types of welding imperfection found in the test**
1	Ø1, C1, D1, T1,S1, F1	No significant indication
2	Ø1, C1, D2,T2,S2, F2	Lack of Fusion
3	Ø1, C1, D3, T3,S3, F3	Slag
4	Ø1, C2, D1, T1, S2, F2	Lack of Fusion
5	Ø1, C2, D2, T2, S3, F3	No significant indication
6	Ø1, C2, D3, T3, S1, F1	No significant indication
7	Ø1, C3, D1, T2, S1, F3	No significant indication
8	Ø1, C3, D2, T3, S2, F1	No significant indication
9	Ø1, C3, D3, T1, S3, F2	No significant indication
10	Ø2, C1, D1, T3, S3,F2	Porosity
11	Ø2, C1, D2, T1, S1, F3	Slag
12	Ø2, C1, D3, T2, S2, F1	No significant indication
13	Ø2, C2, D1, T2, S3, F1	No significant indication
14	Ø2, C2, D2, T3, S1, F2	Slag
15	Ø2, C2, D3, T1, S2, F3	No significant indication
16	Ø2, C3, D1, T3, S2, F3	Lack of Fusion
17	Ø2, C3, D2, T1, S3, F1	No significant indication
18	Ø2, C3, D3, T2, S1, F2	No significant indication

CHAPTER 7

RESULTS AND DISCUSSIONS OF CHEMICAL COMPOSITION

7.1 CHEMICAL COMPOSITION OF WELD METAL

The composition of welded metal was found by using atomic absorption spectrometer. The specimen after spectroscopy are shown in Figure 7.1

FIGURE 7.1 Specimen after checking composition

Figure 7.2 (a-j) shows the variation in %age composition of different elements i.e. Iron, carbon, silicon, manganese, phosphorus, sulphur, nickel, copper, chromium and cobalt.

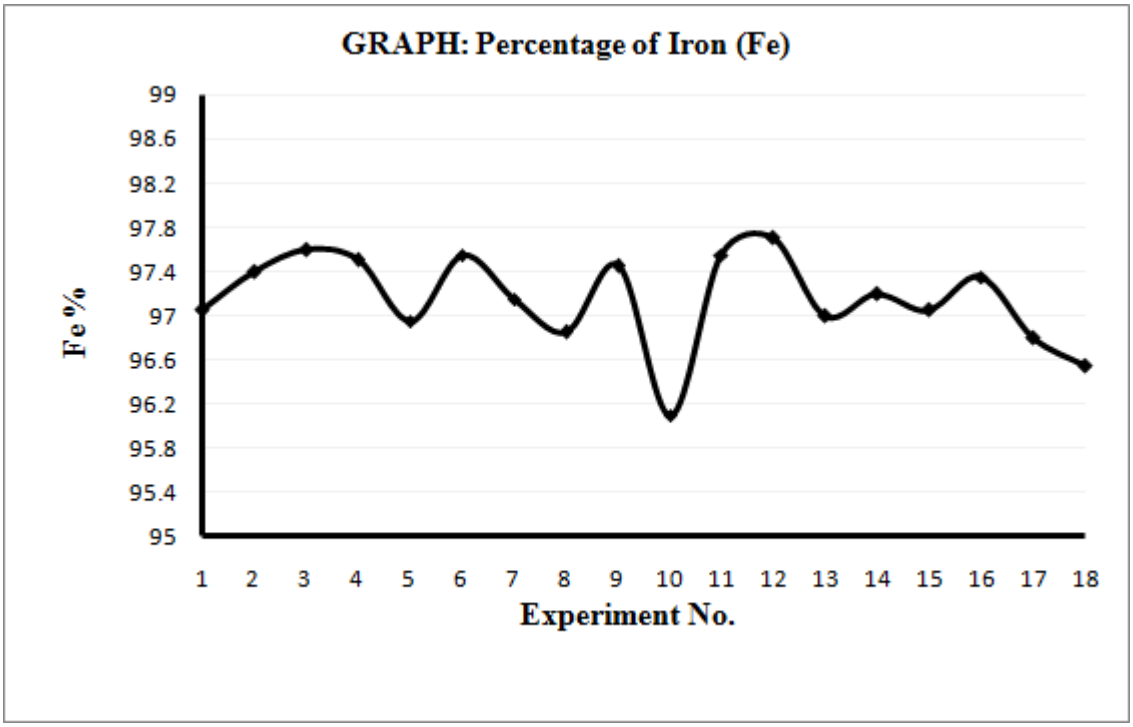

FIGURE 7.2 (a) Variation in %age composition of iron at weld centre

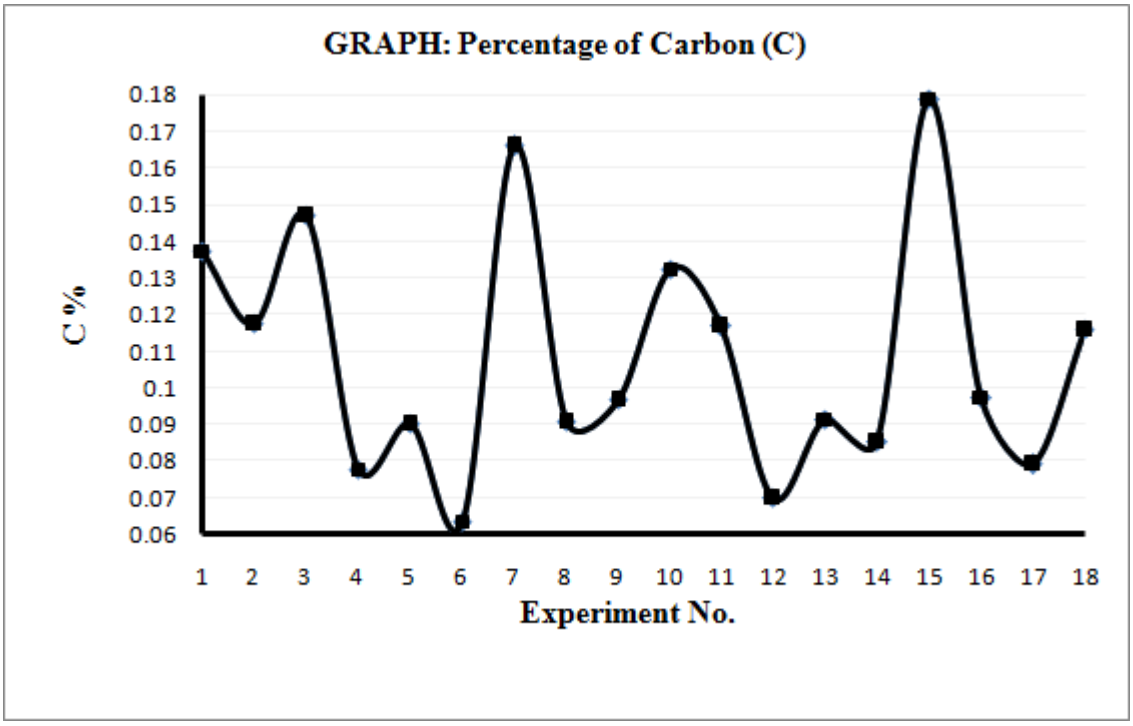

FIGURE 7.2 (b) Variation in %age composition of carbon at weld centre

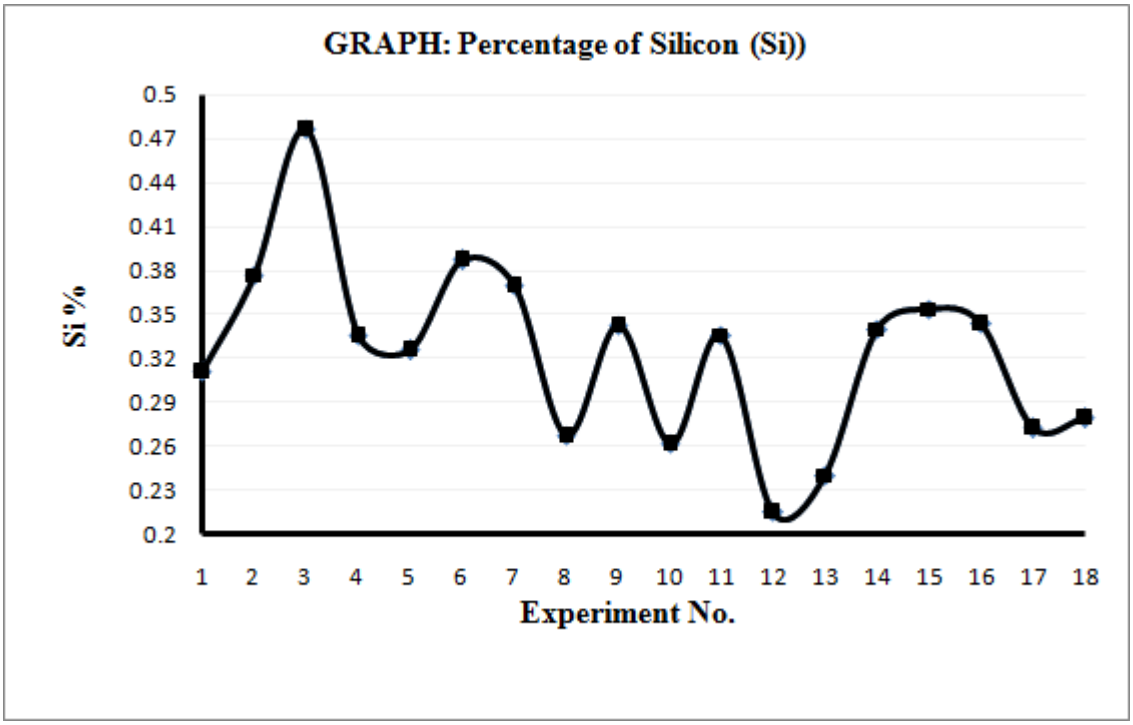

FIGURE 7.2 (c) Variation in %age composition of silicon at weld centre

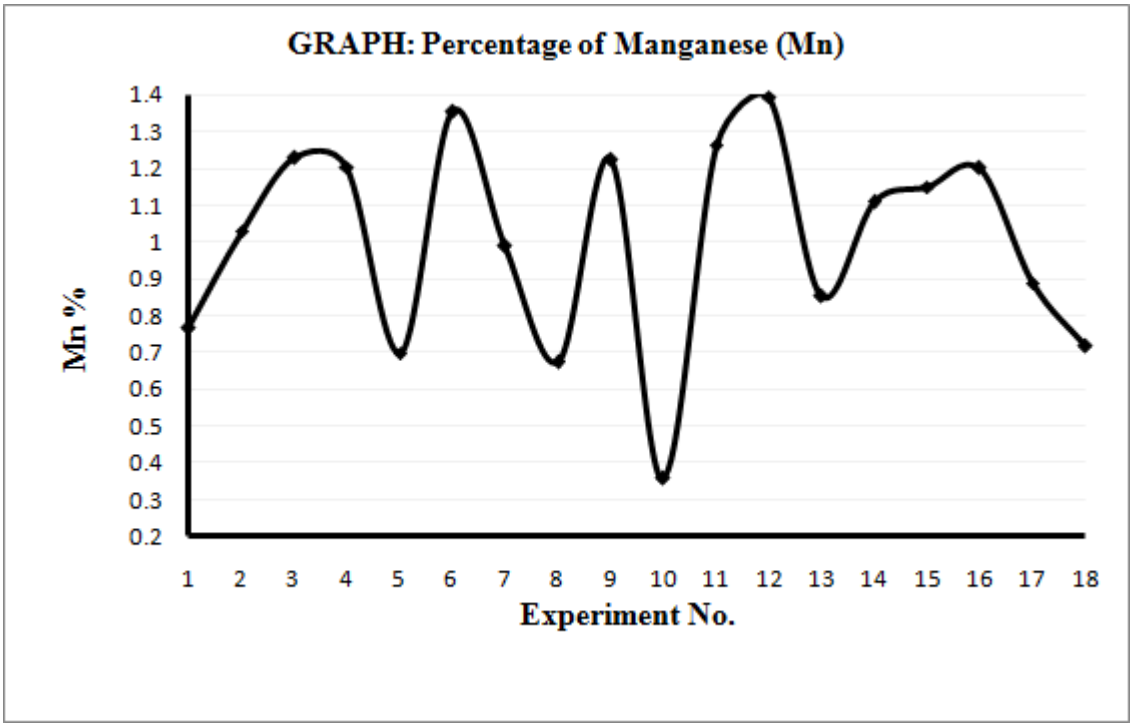

FIGURE 7.2 (d) Variation in %age composition of manganese at weld centre

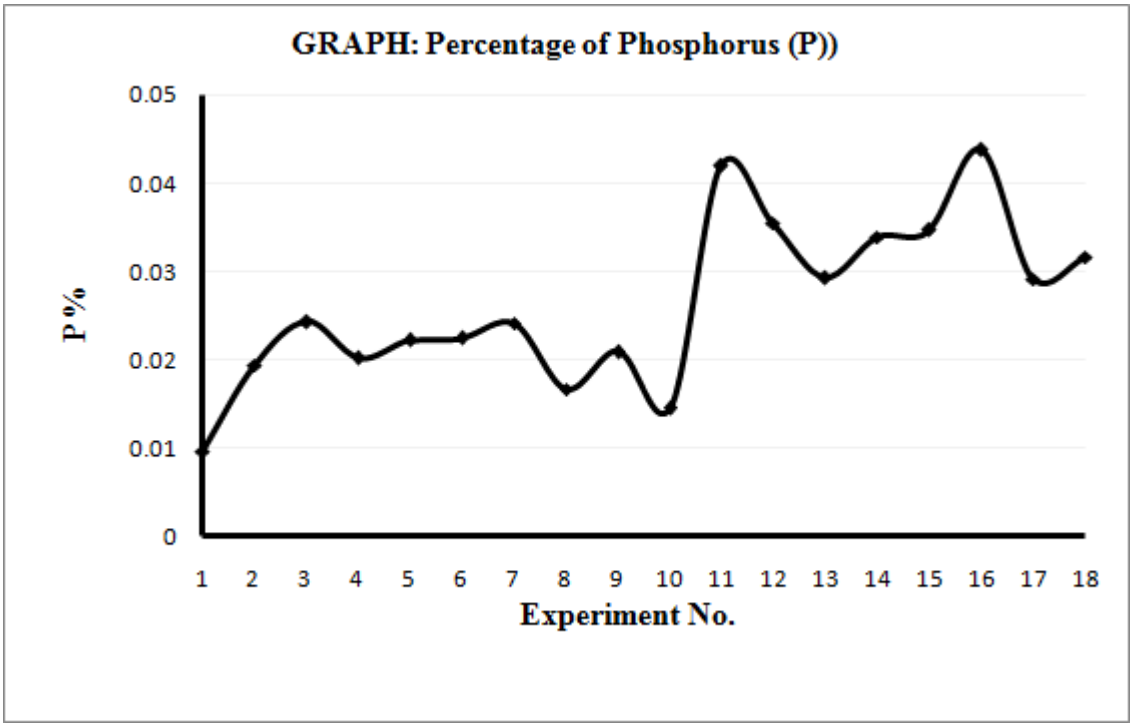

FIGURE 7.2 (e) Variation in %age composition of phosphorus at weld centre

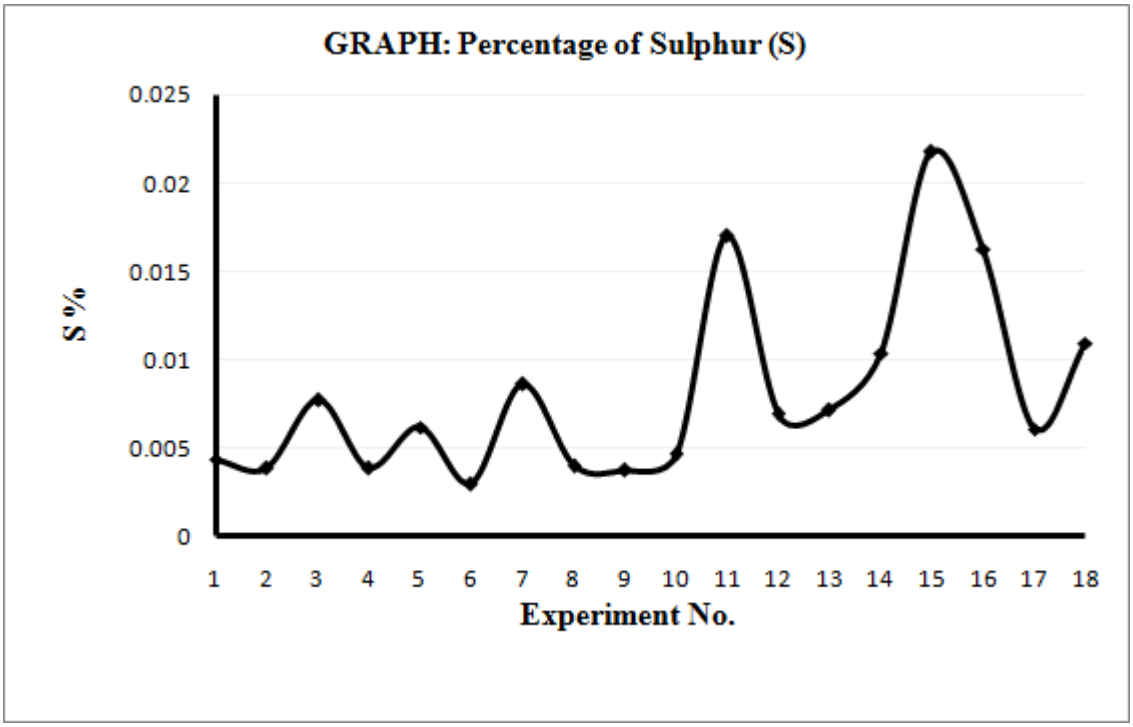

FIGURE 7.2 (f) Variation in %age composition of sulphur at weld centre

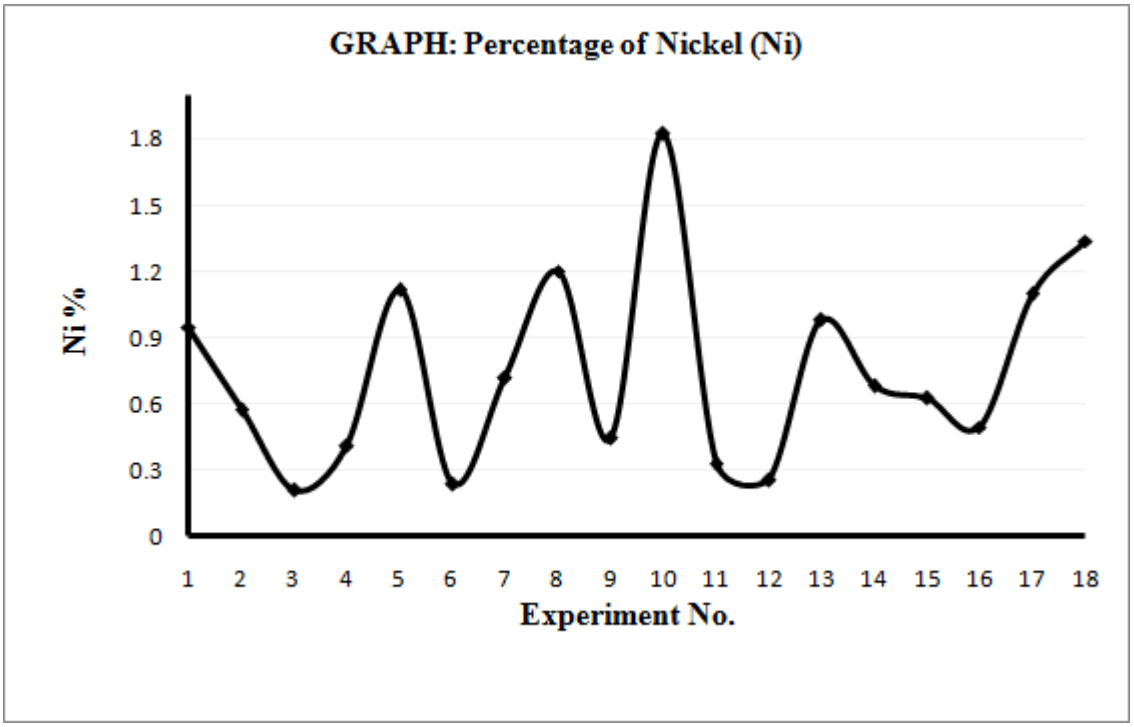

FIGURE 7.2 (g) Variation in %age composition of chromium at weld centre

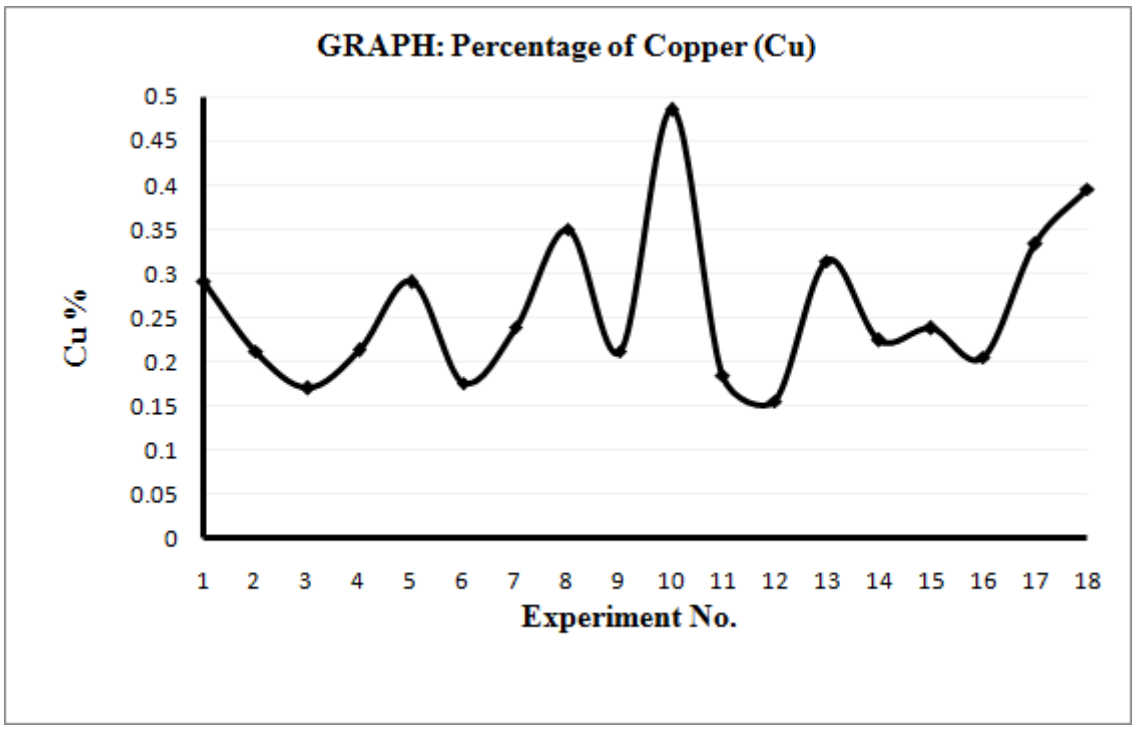

FIGURE 7.2 (h) Variation in %age composition of copper at weld centre

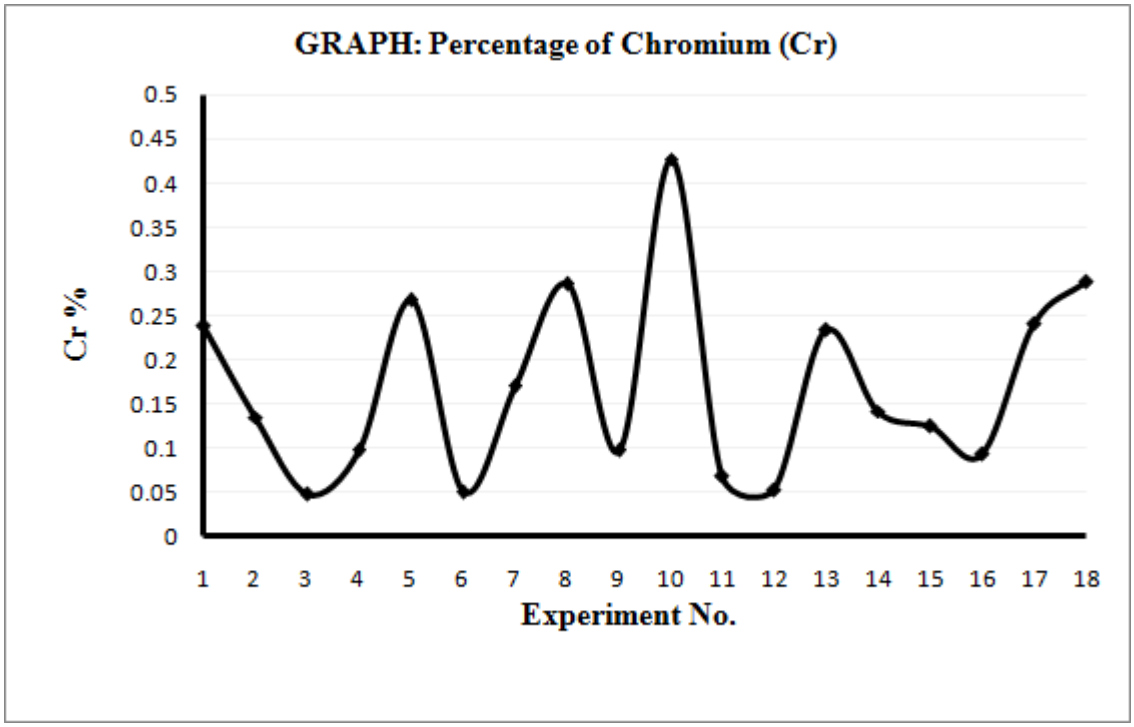

FIGURE 7.2 (i) Variation in %age composition of chromium at weld centre

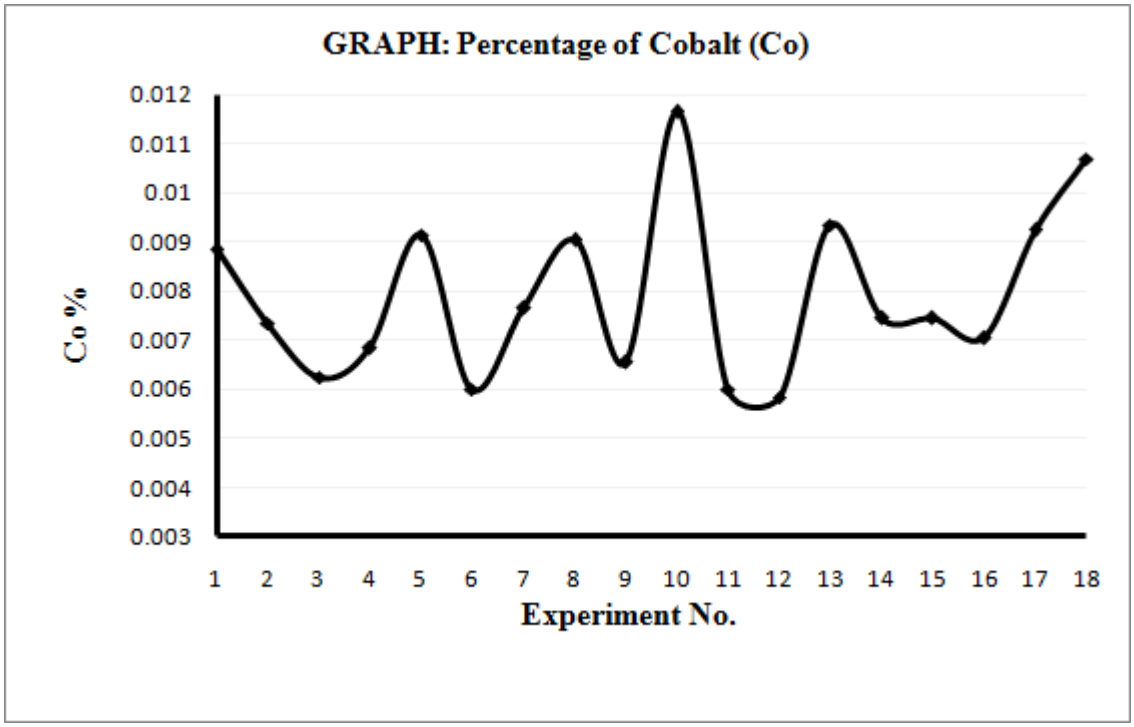

FIGURE 7.2 (j) Variation in %age composition of cobalt at weld centre

7.2 PERCENTAGE CHANGE IN CHEMICAL COMPOSITION

The Table 7.1-7.4 shows the %age difference in chemical contents after spectroscopy with the respect to base metal chemical composition.

TABLE 7.1 Percentage change in chemical composition of carbon and silicon w.r.t base metal

Exp. No.	Carbon %age (after spectroscopy)	Carbon %age in base metal	%age change in Carbon	Silicon %age (after spectroscopy)	Silicon %age in base metal	%age change in Silicon
1	0.1375	0.13	5.769	0.311	0.25	24.400
2	0.1175	0.13	-9.615	0.377	0.25	50.800
3	0.147	0.13	13.077	0.4765	0.25	90.600
4	0.0779	0.13	-40.077	0.3355	0.25	34.200
5	0.0902	0.13	-30.615	0.3255	0.25	30.200
6	0.06375	0.13	-50.962	0.387	0.25	54.800
7	0.166	0.13	27.692	0.37	0.25	48.000
8	0.09085	0.13	-30.115	0.2675	0.25	7.000
9	0.09675	0.13	-25.577	0.3425	0.25	37.000
10	0.1325	0.13	1.923	0.262	0.25	4.800
11	0.11675	0.13	-10.192	0.336	0.25	34.400
12	0.0701	0.13	-46.077	0.2155	0.25	-13.800
13	0.09145	0.13	-29.654	0.2405	0.25	-3.800
14	0.0853	0.13	-34.385	0.3405	0.25	36.200
15	0.179	0.13	37.692	0.354	0.25	41.600
16	0.0976	0.13	-24.923	0.344	0.25	37.600
17	0.0791	0.13	-39.154	0.2725	0.25	9.000
18	0.116	0.13	-10.769	0.2795	0.25	11.800

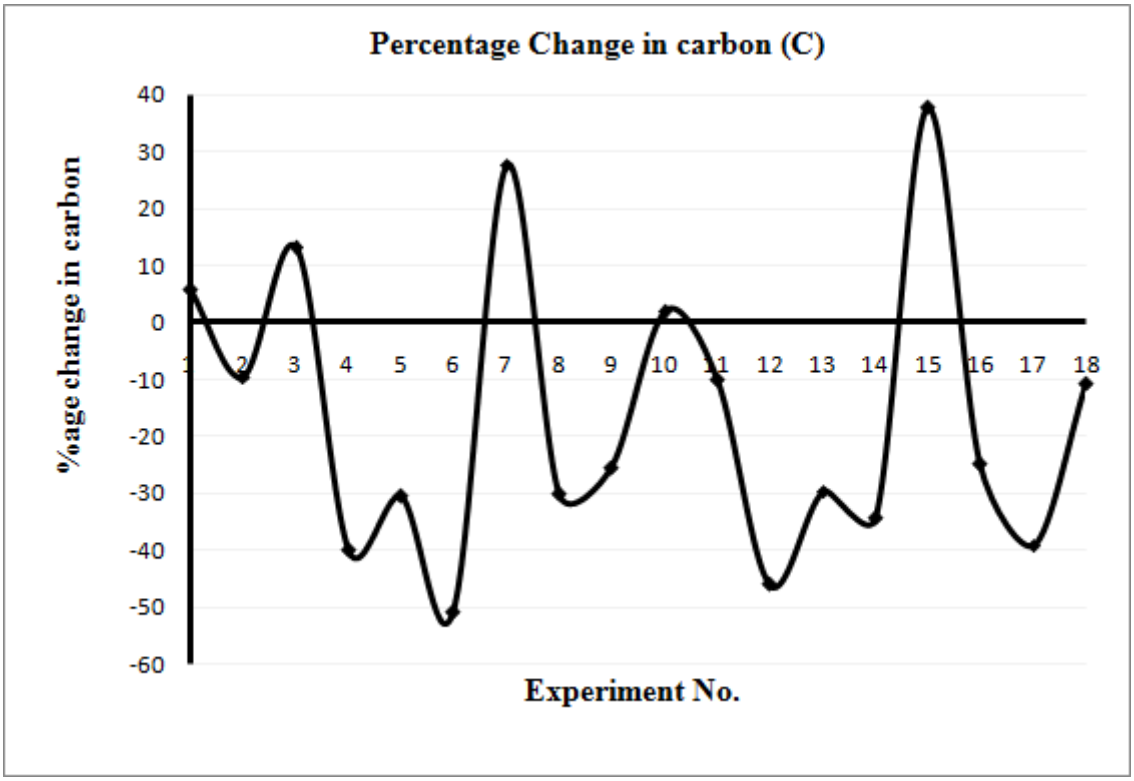

FIGURE 7.3 (a) Variation in %age change in composition of carbon at weld centre

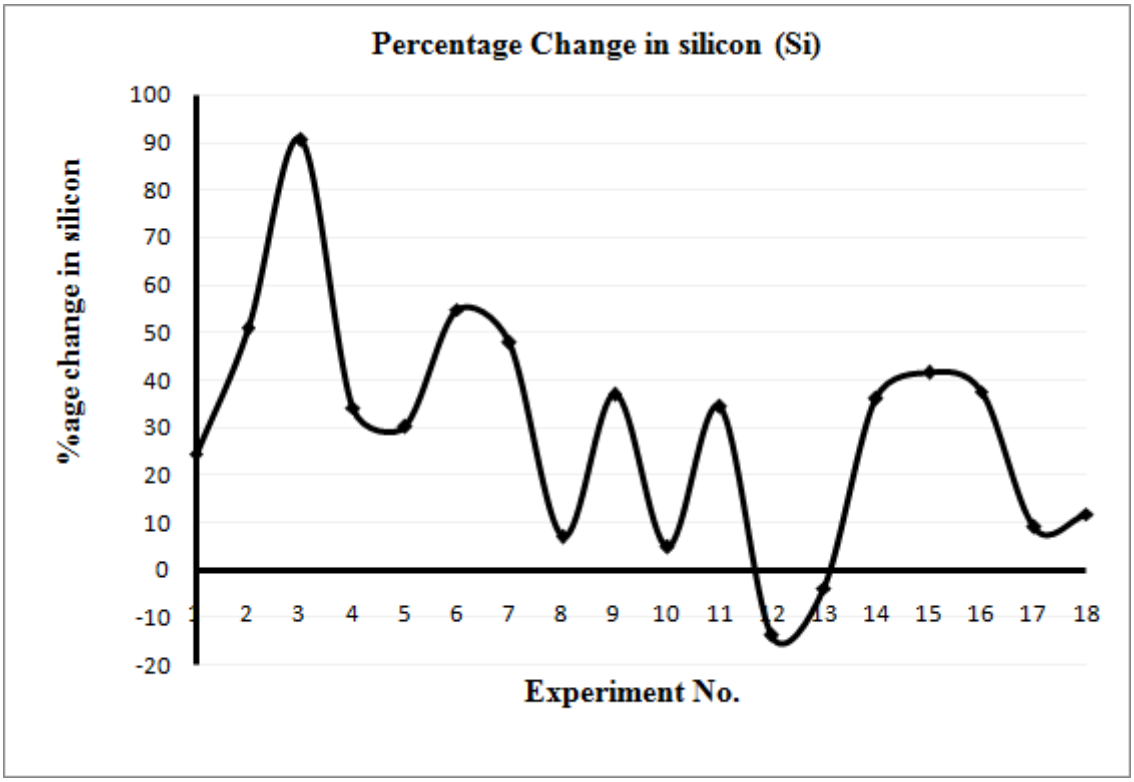

FIGURE 7.3 (b) Variation in % age change in composition of silicon at weld centre

TABLE 7.2 Percentage change in chemical composition of manganese and phosphorus w.r.t base metal

Exp. No.	Manganese %age (after spectroscopy)	Manganese %age in base metal	%age change in Manganese	Phosphorus %age (after spectroscopy)	Phosphorus %age in base metal	%age change in Phosphorus
1	0.765	0.39	96.154	0.0097	0.003	223.333
2	1.0305	0.39	164.231	0.01945	0.003	548.333
3	1.23	0.39	215.385	0.02435	0.003	711.667
4	1.205	0.39	208.974	0.02015	0.003	571.667
5	0.699	0.39	79.231	0.0222	0.003	640.000
6	1.355	0.39	247.436	0.02245	0.003	648.333
7	0.9905	0.39	153.974	0.02415	0.003	705.000
8	0.674	0.39	72.821	0.0167	0.003	456.667
9	1.225	0.39	214.103	0.02095	0.003	598.333
10	0.358	0.39	-8.205	0.0146	0.003	386.667
11	1.265	0.39	224.359	0.04195	0.003	1298.333
12	1.395	0.39	257.692	0.0355	0.003	1083.333
13	0.8535	0.39	118.846	0.02935	0.003	878.333
14	1.11	0.39	184.615	0.03395	0.003	1031.667
15	1.15	0.39	194.872	0.03465	0.003	1055.000
16	1.2	0.39	207.692	0.0438	0.003	1360.000
17	0.8895	0.39	128.077	0.0292	0.003	873.333
18	0.718	0.39	84.103	0.03165	0.003	955.000

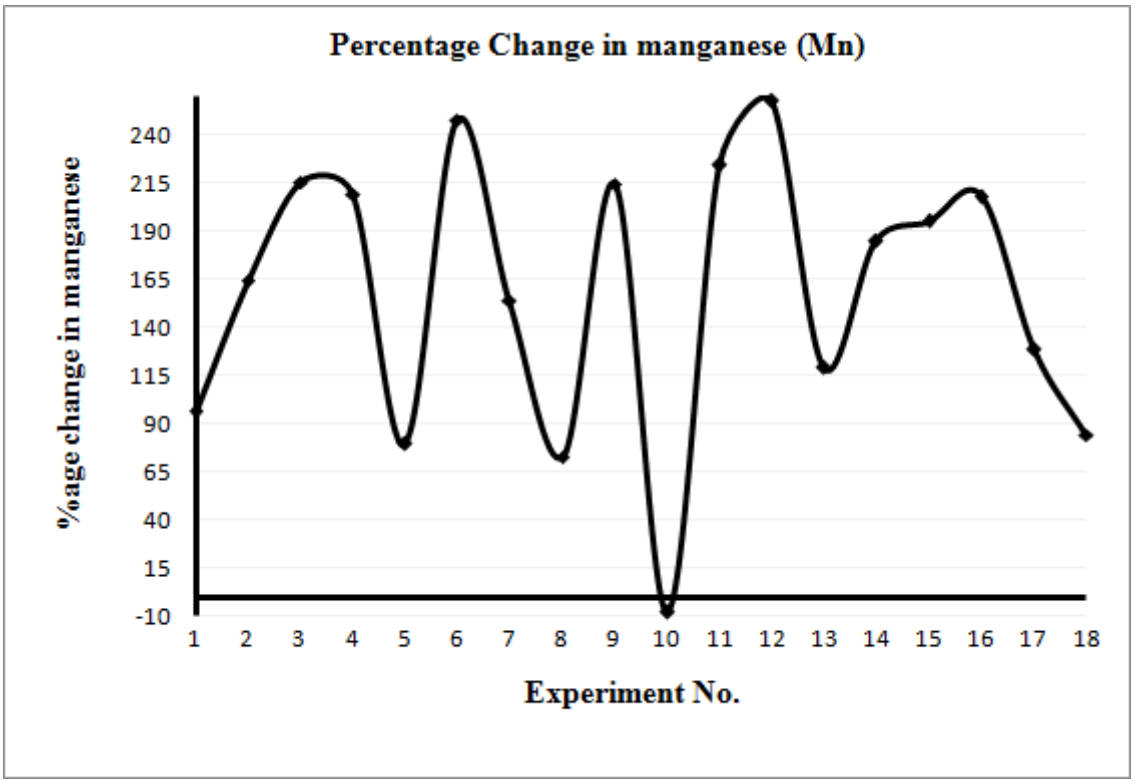

FIGURE 7.3 (c) Variation in % age change in composition of manganese at weld centre

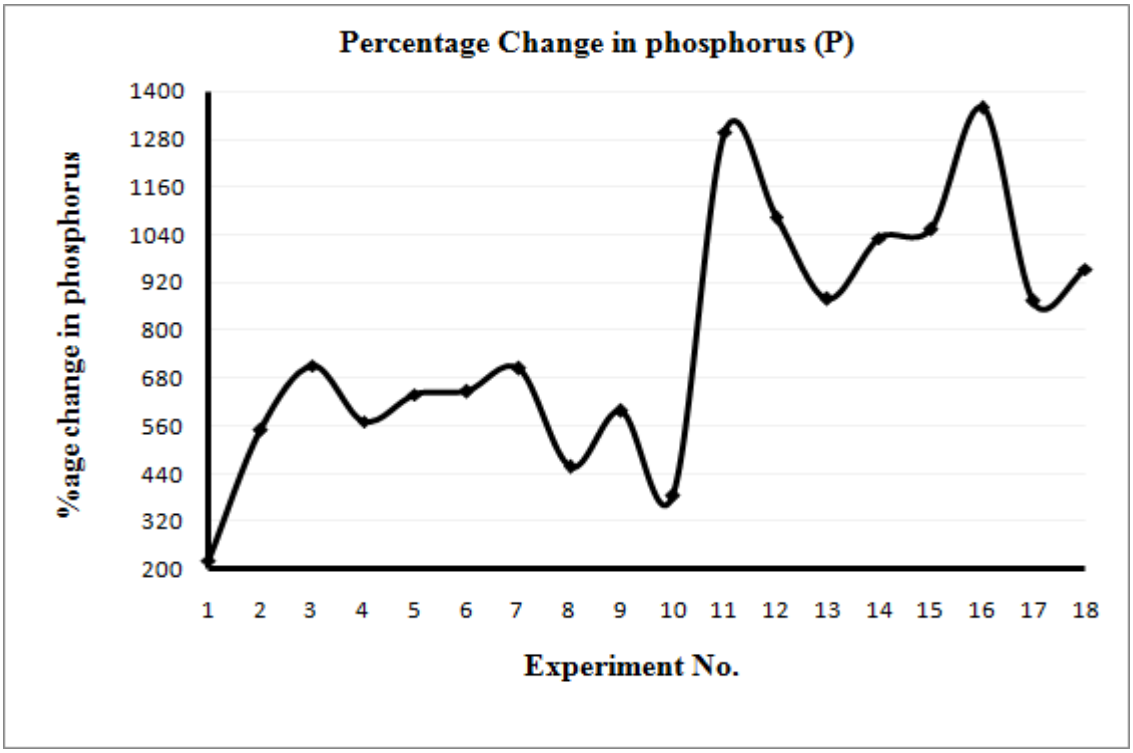

FIGURE 7.3 (d) Variation in % age change in composition of phosphorus at weld centre

TABLE 7.3 Percentage change in chemical composition of sulphur and nickel w.r.t base metal

Exp. No.	Sulphur %age (after spectroscopy)	Sulphur %age in base metal	%age change in Sulphur	Nickel %age (after spectroscopy)	Nickel %age in base metal	%age change in Nickel
1	0.0044	0.01	-56.00	0.948	1.76	-46.136
2	0.0039	0.01	-61.00	0.574	1.76	-67.386
3	0.0077	0.01	-23.00	0.211	1.76	-88.011
4	0.0039	0.01	-61.00	0.411	1.76	-76.648
5	0.0062	0.01	-38.00	1.1165	1.76	-36.563
6	0.003	0.01	-70.00	0.24	1.76	-86.364
7	0.0086	0.01	-14.00	0.7155	1.76	-59.347
8	0.004	0.01	-60.00	1.2025	1.76	-31.676
9	0.00375	0.01	-62.50	0.4465	1.76	-74.631
10	0.00465	0.01	-53.50	1.825	1.76	3.693
11	0.01705	0.01	70.50	0.327	1.76	-81.420
12	0.0069	0.01	-31.00	0.2585	1.76	-85.313
13	0.0072	0.01	-28.00	0.9785	1.76	-44.403
14	0.0104	0.01	4.00	0.68	1.76	-61.364
15	0.02175	0.01	117.50	0.626	1.76	-64.432
16	0.0163	0.01	63.00	0.495	1.76	-71.875
17	0.0061	0.01	-39.00	1.0985	1.76	-37.585
18	0.01095	0.01	9.50	1.338	1.76	-23.977

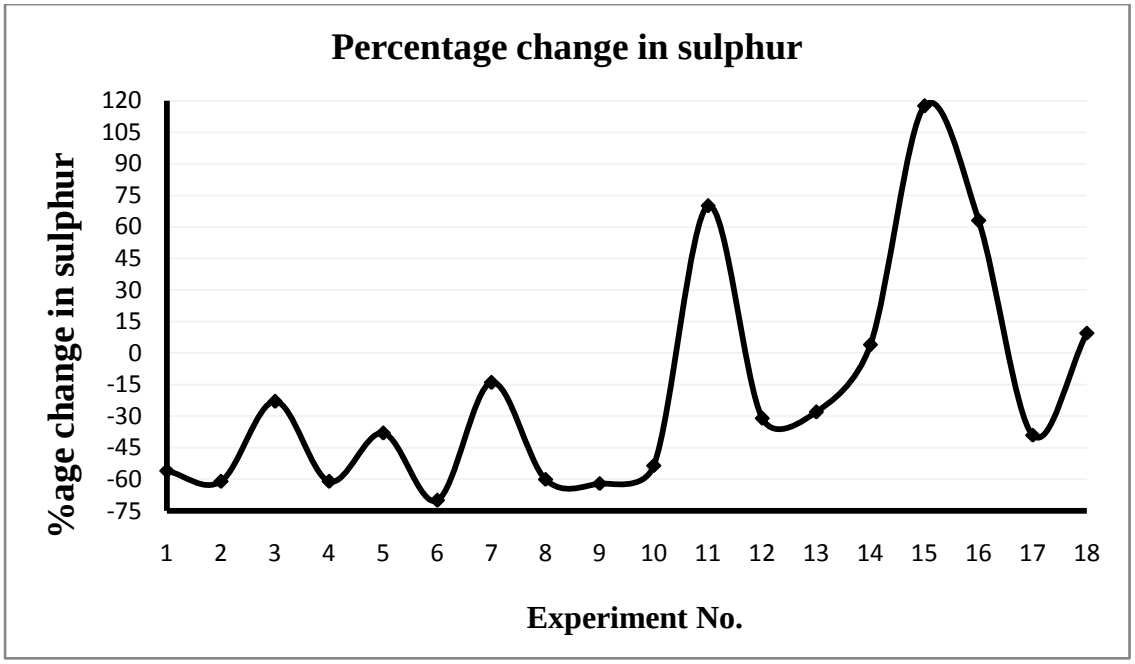

FIGURE 7.3 (e) Variation in %age change in composition of sulphur at weld centre

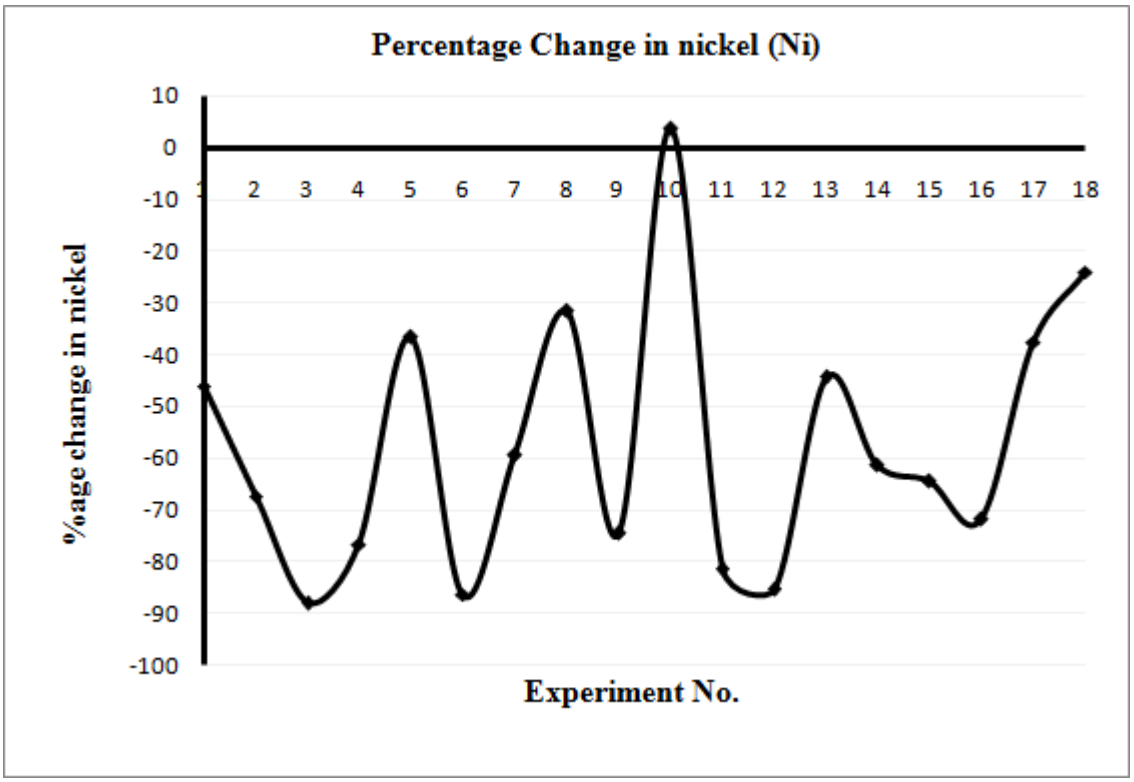

FIGURE 7.3 (f) Variation in %age change in composition of nickel at weld centre

TABLE 7.4 Percentage change in chemical composition of copper and chromium w.r.t base metal

Exp. No.	Copper %age (after spectroscopy)	Copper %age in base metal	%age change in Copper	Chromium %age (after spectroscopy)	Chromium %age in base metal	%age change in Chromium
1	0.2915	0.5	-41.700	0.239	0.41	-41.707
2	0.2125	0.5	-57.500	0.135	0.41	-67.073
3	0.171	0.5	-65.800	0.0477	0.41	-88.366
4	0.213	0.5	-57.400	0.0972	0.41	-76.293
5	0.2905	0.5	-41.900	0.268	0.41	-34.634
6	0.176	0.5	-64.800	0.0501	0.41	-87.780
7	0.2395	0.5	-52.100	0.1705	0.41	-58.415
8	0.3505	0.5	-29.900	0.2855	0.41	-30.366
9	0.212	0.5	-57.600	0.098	0.41	-76.098
10	0.4855	0.5	-2.900	0.4275	0.41	4.268
11	0.1855	0.5	-62.900	0.06815	0.41	-83.378
12	0.1555	0.5	-68.900	0.05255	0.41	-87.183
13	0.3145	0.5	-37.100	0.2335	0.41	-43.049
14	0.225	0.5	-55.000	0.142	0.41	-65.366
15	0.2385	0.5	-52.300	0.125	0.41	-69.512
16	0.2055	0.5	-58.900	0.09285	0.41	-77.354
17	0.3335	0.5	-33.300	0.2405	0.41	-41.341
18	0.3955	0.5	-20.900	0.2885	0.41	-29.634

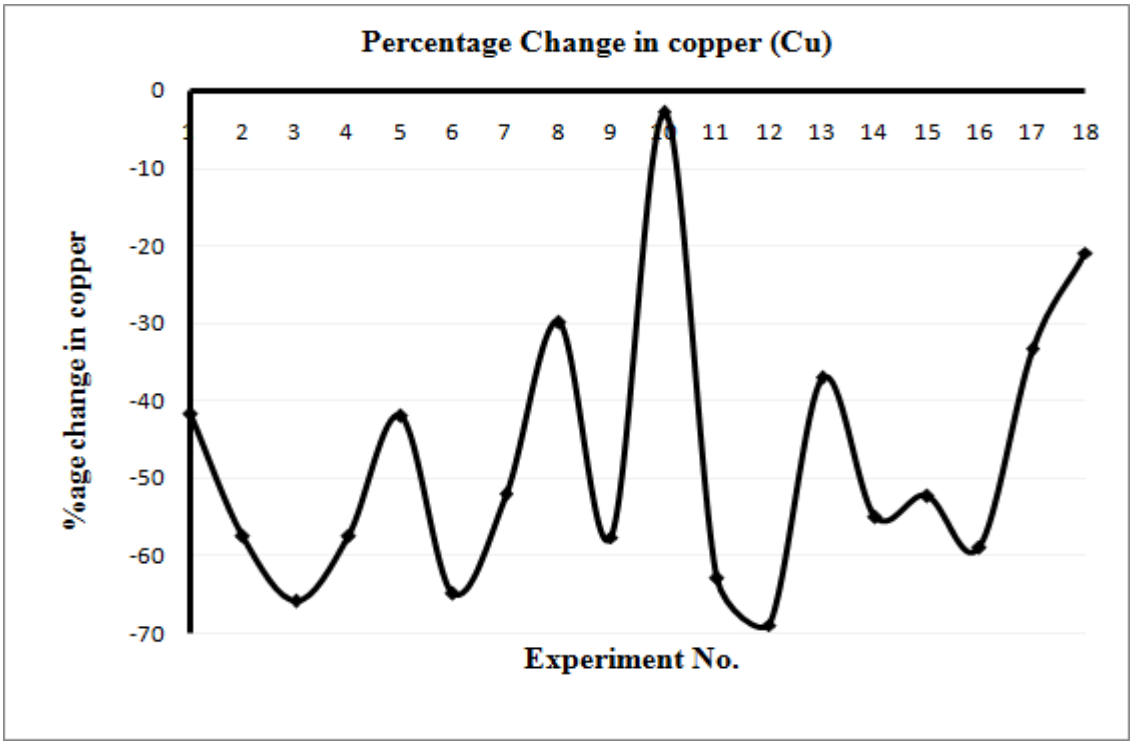

FIGURE 7.3 (g) Variation in %age change in composition of copper at weld centre

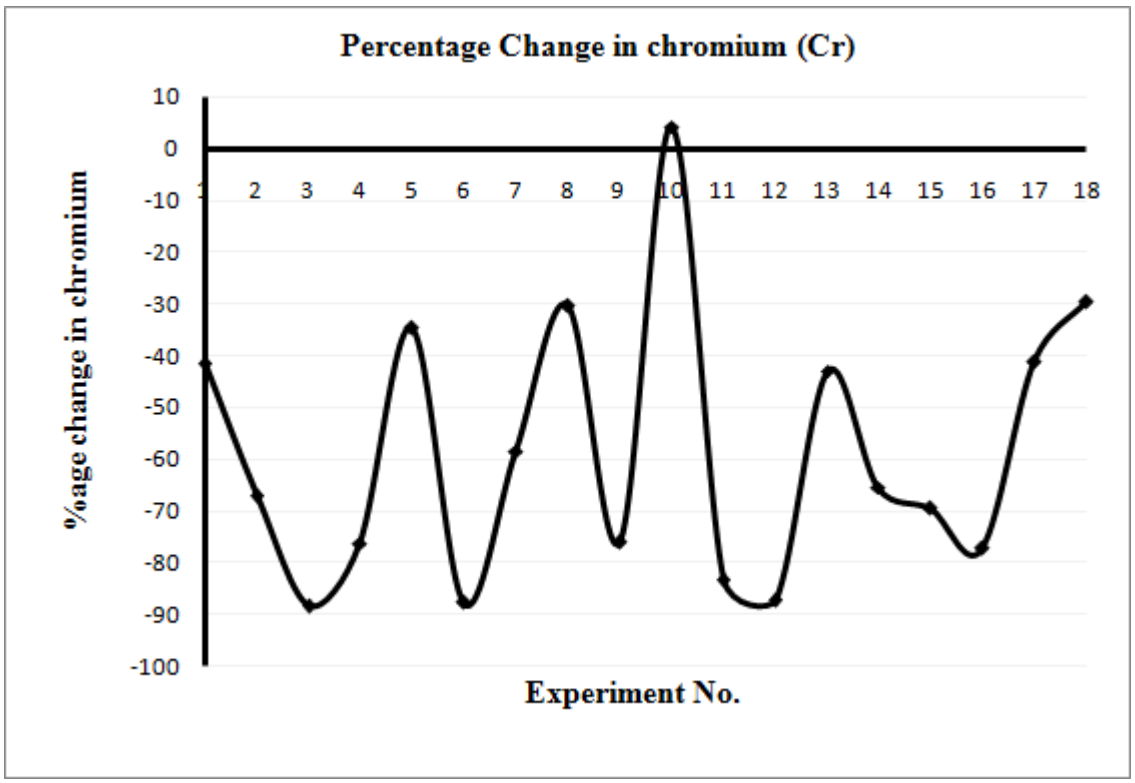

FIGURE 7.3 (h) Variation in %age change in composition of chromium at weld centre

7.3 DISCUSSION OF CHEMICAL COMPOSITION

It is concluded that from figure 7.3 (a-h) that percentage change in phosphorous and manganese, silicon were increasing in weld region but nickel, copper and chromium contents were decreasing whereas for sulphur and carbon shows the mixed trend. So, it concludes that some compounds transfer into the weld region by external source i.e. flux, filler wire and electrode wire.

CHAPTER 8
MICROSTRUCTURAL ANALYSIS

8.1 INTRODUCTION

Metallurgical analysis is basically based on the microstructure; phase and composition study of the parent and weld samples. The present study was carried out to study the effect of current, electrode stick-out, travel speed, preheat temperature, electrode diameter and flux on the microstructure analysis with EDAX of the work material during submerged arc welding. Effect of various input factors on the micro structure were analyzed on the weld. In metal alloys, microstructure is characterized by the type and shape of the grain structure, their proportions, and the manner in which they are distributed or arranged. During welding, the metal converts into molten weld pool. Due to high temperature of molten metal, re-crystallization of the metal grains takes place. Upon cooling of the heated material, a change in microstructure takes place due to the raised temperature and subsequent cooling. The heat input or input factor and cooling rate decides the grain shape, size and its properties. The heat input has been varied by changing the input factors value. The present study focuses on the composition change that have occurred in ferrite, carbide, bainite and pearlite structure and including the changes in the grain shape of the work material after the submerged arc welding. The term phase equilibrium is often used, in the context of microstructure. This term applies to situation when one or more phase of single material exists. Hence analysis of metallurgical aspects of machining is done on SEM (Scanning Electron Microscope) for microstructure analysis, EDX (Energy Dispersive X-ray) for phase and composition analysis.

8.2 MICROSTUCTURE ANALYSIS

Microstructure analysis was carried out on eighteen samples with base metal sample on SEM, model-LEO 435 VP, SEMTech Solutions, USA to study change in microstructure after submerged arc welding. SEM is mainly used for imaging the surface and detecting small surface features. These images have been taken after etching of specimen with 3% nital solution; with an optical microscope at 200×, 500× and 1000× magnification. The micrographs of welding zone shown below have been taken at the half of width of welding zone. Figure 8.1 shows the microstructure of the parent metal and Figures 8.2 to 8.19 shows the microstructure of welding region of different specimen at varied input conditions as per the treatment with EDX composition analysis.

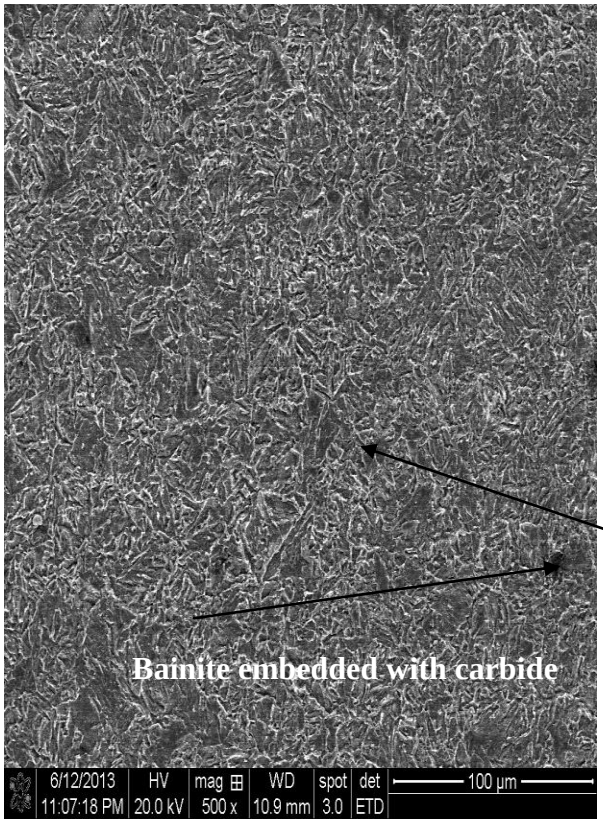

(i)

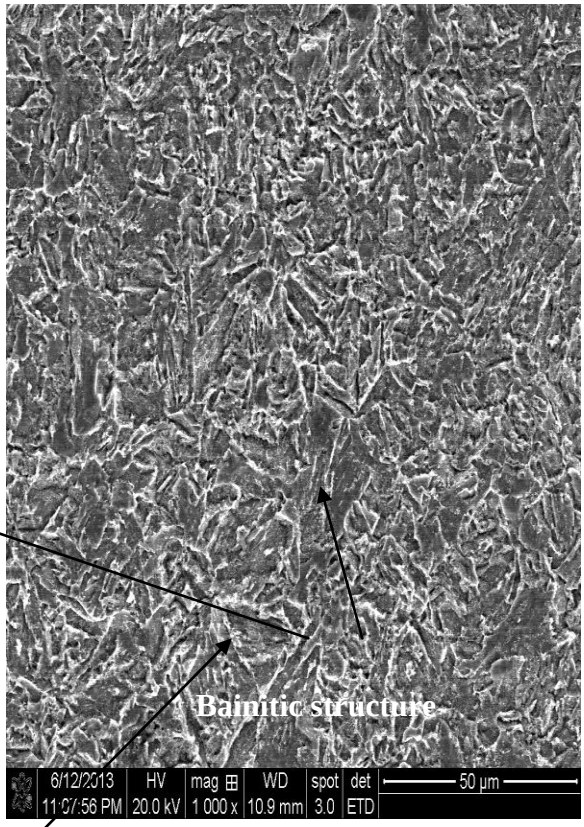

(ii)

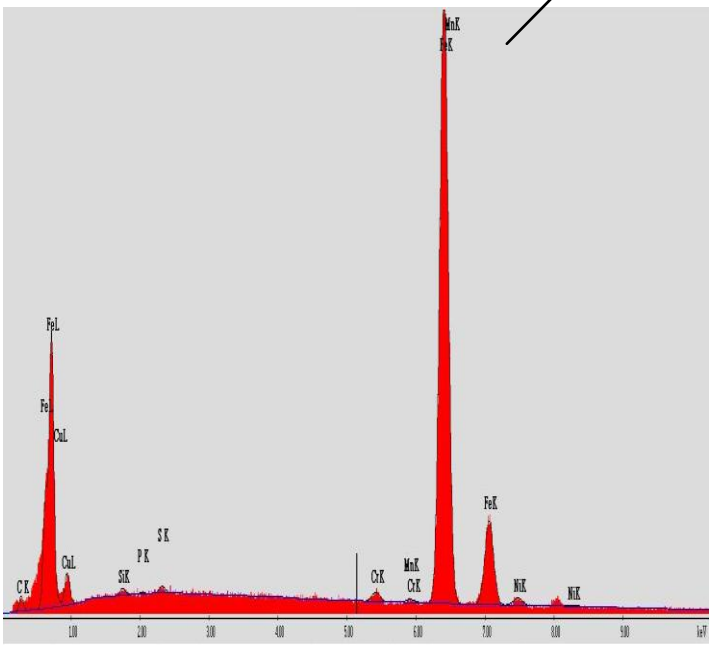

(iii)

Element	Weight%	Atomic%
C K	2.87	12.14
Cu K	8.59	6.87
SiK	0.36	0.65
PK	0.06	0.10
SK	0.28	0.44
CrK	0.74	0.72
MnK	0.29	0.26
Fe K	85.15	77.38
NiK	1.66	1.43

(iv)

FIGURE 8.1 SEM & EDX micrograph of Parent metal (i) 500× (ii) 1000× (iii) EDX image of parent metal (iv) Chemical composition of parent metal resulting from EDX analysis

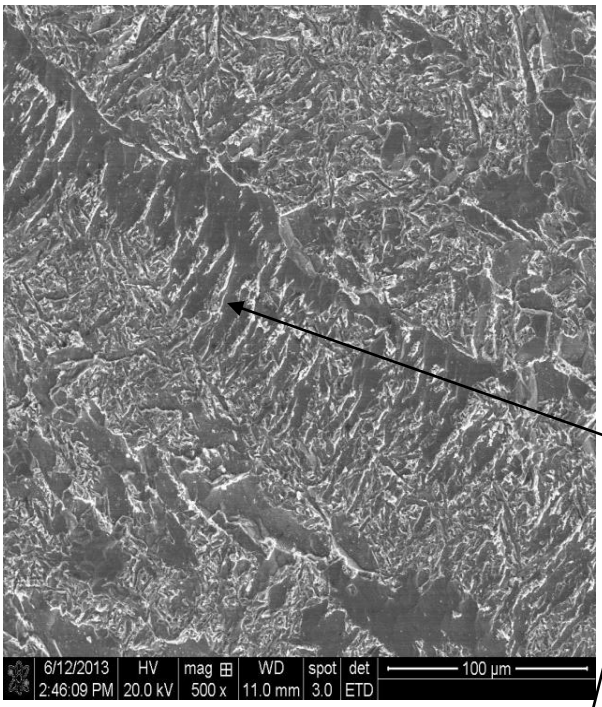

(i)

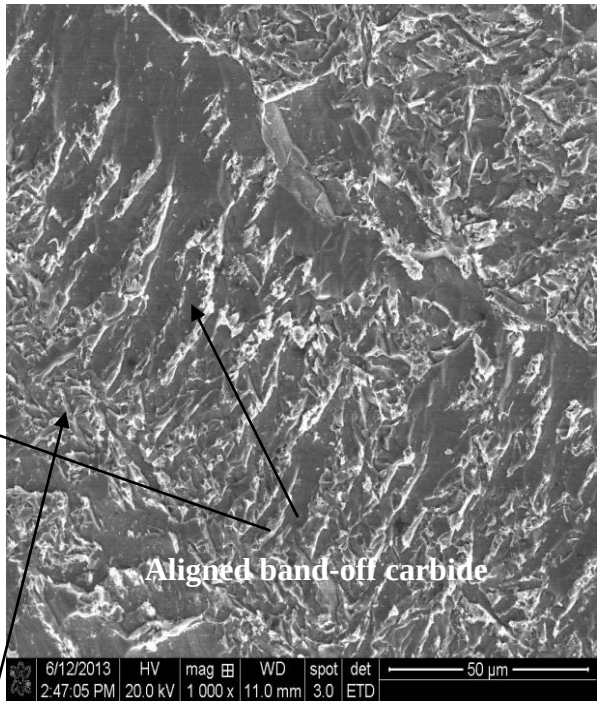

(ii)

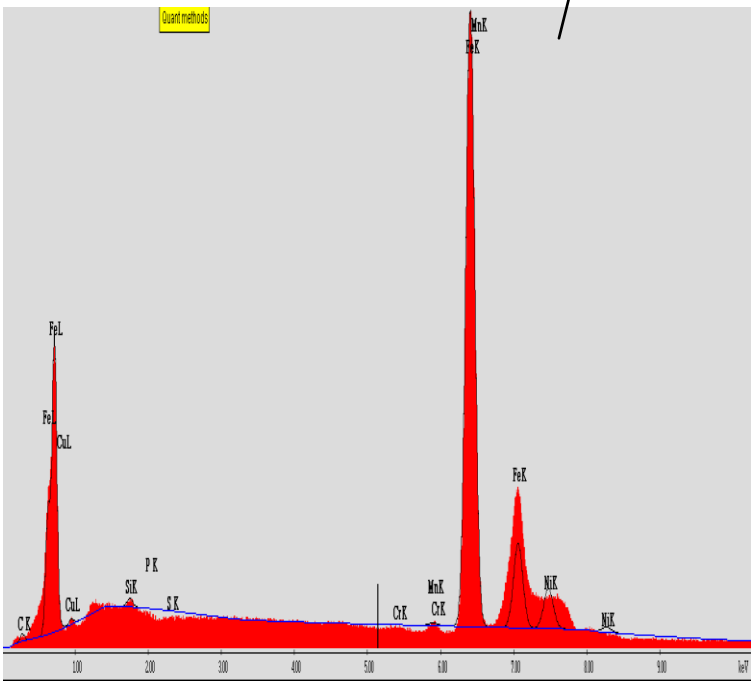

(iii)

Element	Weight%	Atomic %
C K	1.44	6.39
Cu K	1.55	1.30
SiK	0.47	0.89
PK	0.00	0.00
SK	0.00	0.00
CrK	0.00	0.00
MnK	0.39	0.37
Fe K	86.74	82.53
NiK	9.41	8.51

(iv)

FIGURE 8.2 SEM & EDX micrograph of welding region with trial no.1[Electrode Diameter 3.2,Current 400 A, electrode stick-out 25 mm, No preheat temperature, travel speed 18m/hr, Flux1] (i) 500× (ii) 1000× (iii) EDX image of trial no.1 (iv) Chemical composition of trial no.1 resulting from EDX analysis

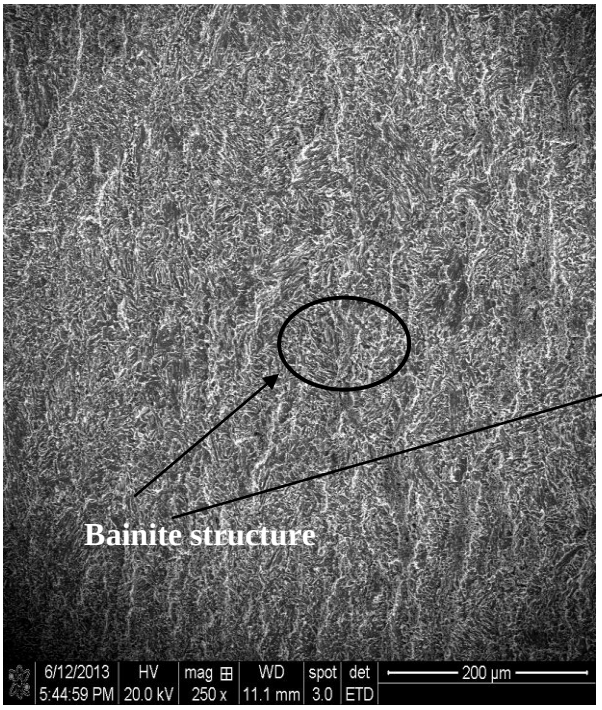

(i)

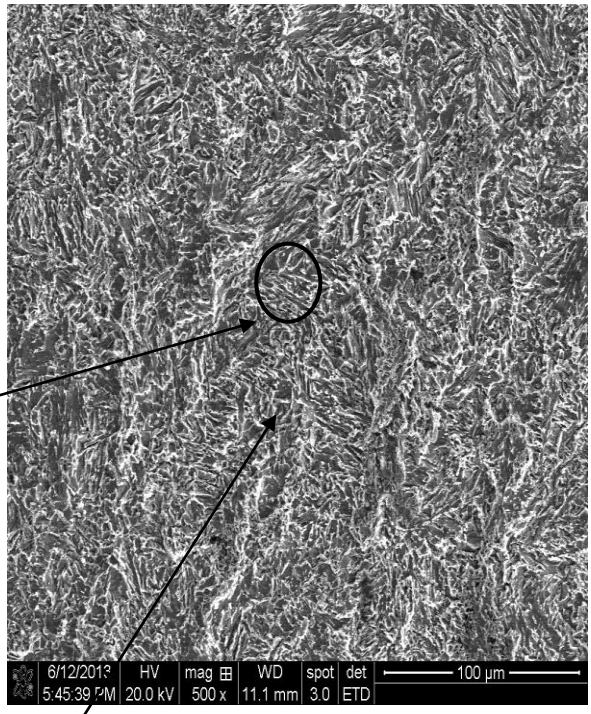

(ii)

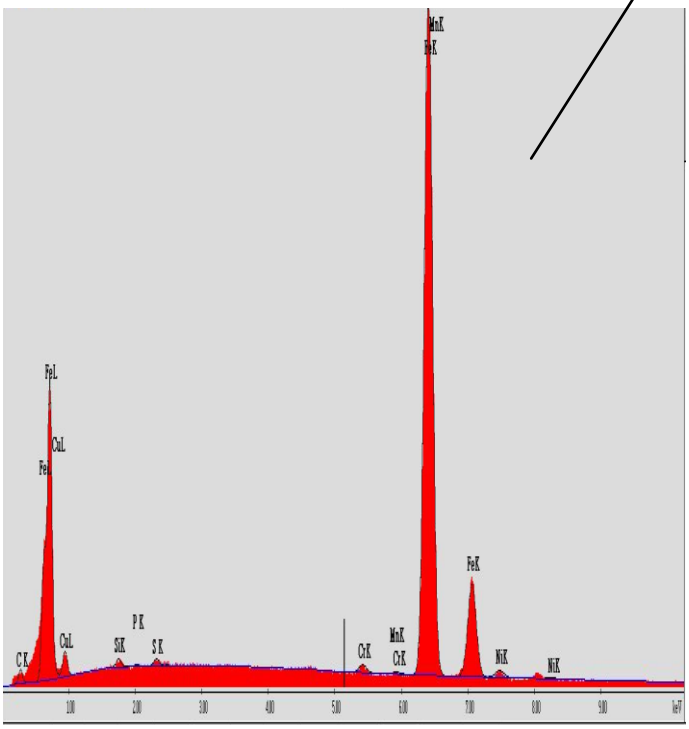

(iii)

Element	Weight%	Atomic%
C K	2.60	11.07
Cu K	6.36	5.11
SiK	0.41	0.75
PK	0.08	0.12
SK	0.27	0.43
CrK	0.56	0.55
MnK	0.11	0.10
Fe K	88.11	80.56
NiK	1.50	1.31

(iv)

FIGURE 8.3 SEM & EDX micrograph of welding region with trial no.2 [Electrode Diameter 3.2,Current 400 A, electrode stick-out 30 mm, preheat temperature 125°C, travel speed 20m/hr, Flux2] (i) 250× (ii) 500× (iii) EDX image of trial no.2 (iv) Chemical composition of trial no.2 resulting from EDX analysis

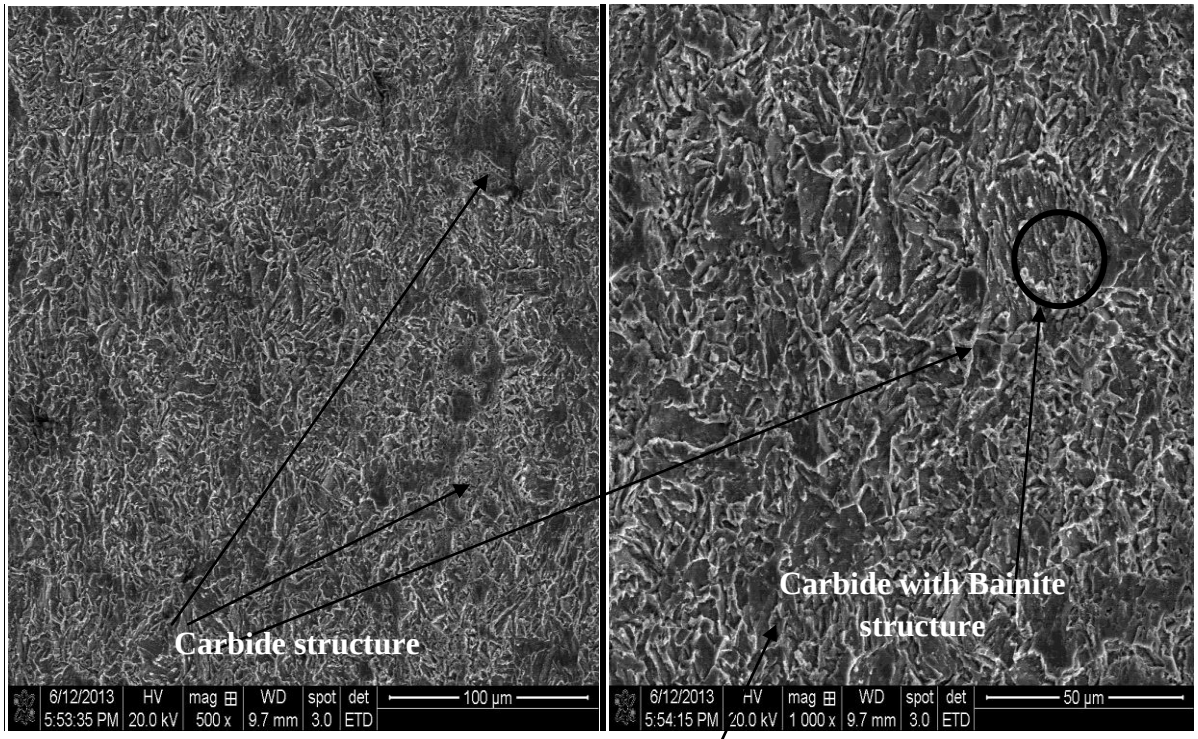

(i) (ii)

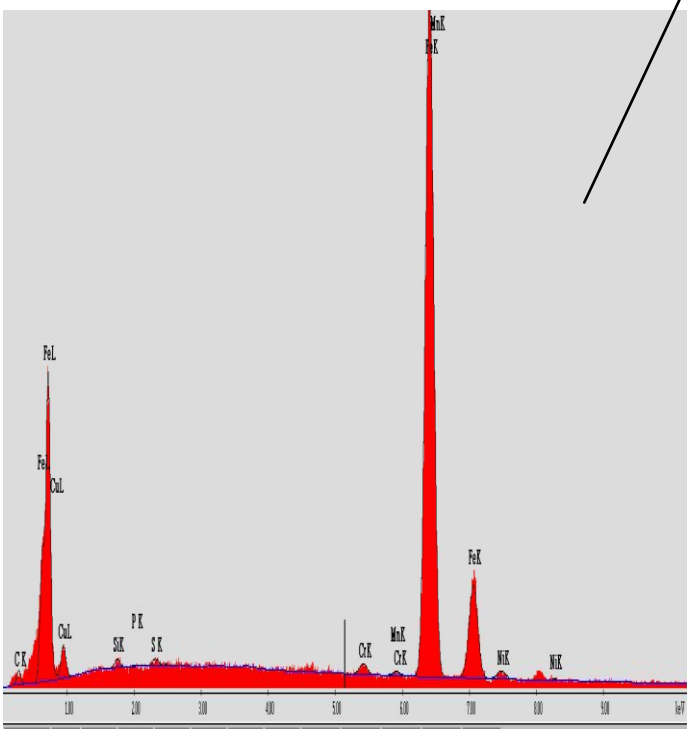

Element	Weight%	Atomic%
C K	2.61	11.12
Cu K	8.06	6.49
SiK	0.41	0.75
PK	0.05	0.08
SK	0.26	0.42
CrK	0.74	0.73
MnK	0.34	0.32
Fe K	85.84	78.63
NiK	1.69	1.47

(iii) (iv)

FIGURE 8.4 SEM & EDX micrograph of welding region with trial no.3 [Electrode Diameter 3.2,Current 400 A, electrode stick-out 35 mm, preheat temperature 200°C, travel speed 22 m/hr, Flux3] (i) 500× (ii) 1000× (iii) EDX image of trial no.3 (iv) Chemical composition of trial no.3 resulting from EDX analysis

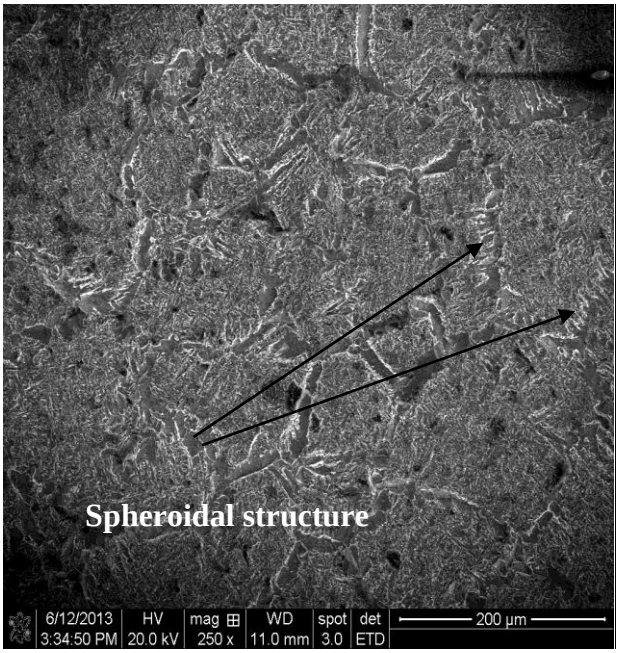

(i)

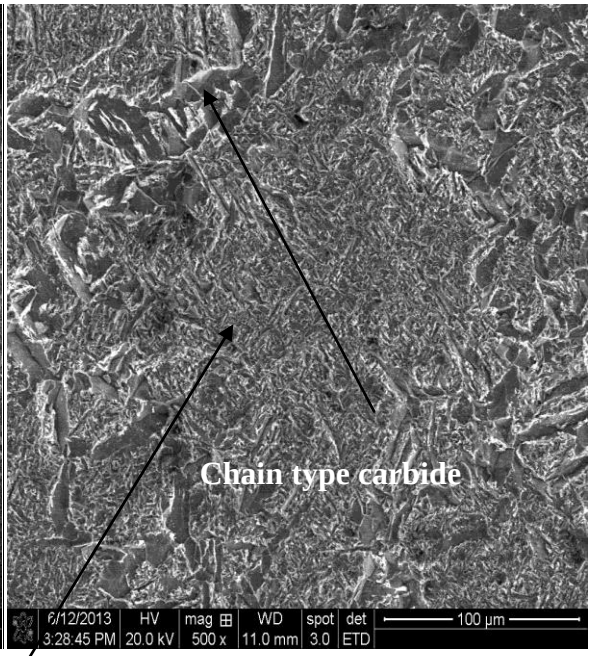

(ii)

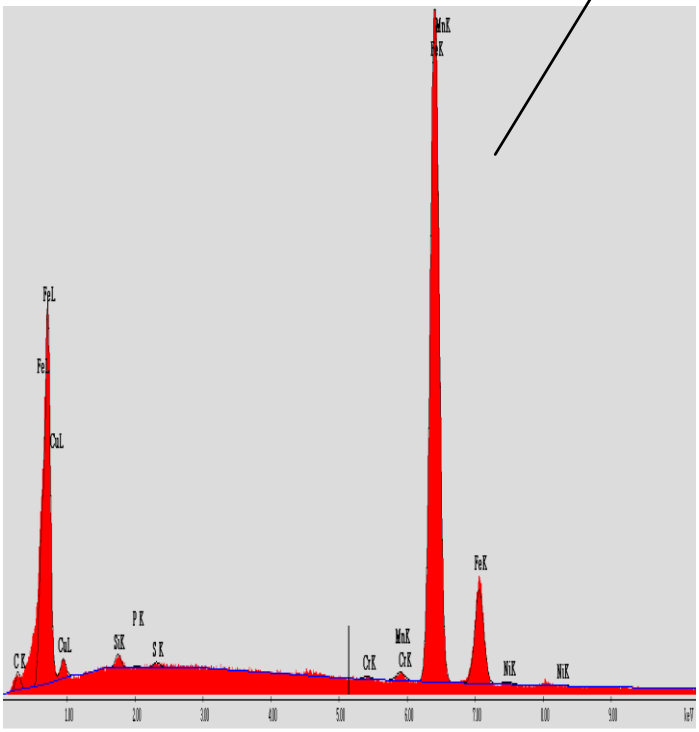

(iii)

Element	Weight%	Atomic%
C K	3.33	13.78
Cu K	5.19	4.06
SiK	0.67	1.18
PK	0.08	0.13
SK	0.22	0.34
CrK	0.20	0.19
MnK	0.90	0.81
Fe K	88.85	79.03
NiK	0.55	0.47

(iv)

FIGURE 8.5 SEM & EDX micrograph of welding region with trial no.4 [Electrode Diameter 3.2,Current 450 A, electrode stick-out 25 mm, No preheat temperature, travel speed 20 m/hr, Flux2] (i) 250× (ii) 500× (iii) EDX image of trial no.4 (iv) Chemical composition of trial no.4 resulting from EDX analysis

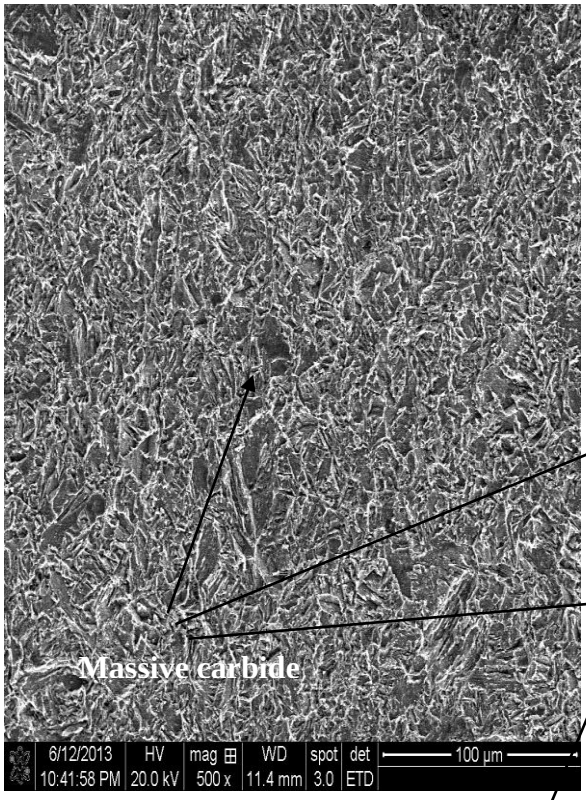

(i)

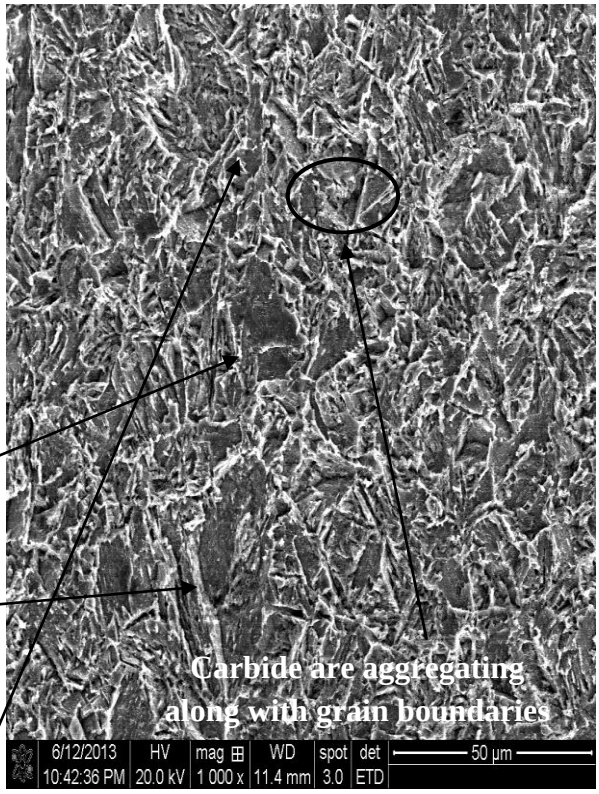

(ii)

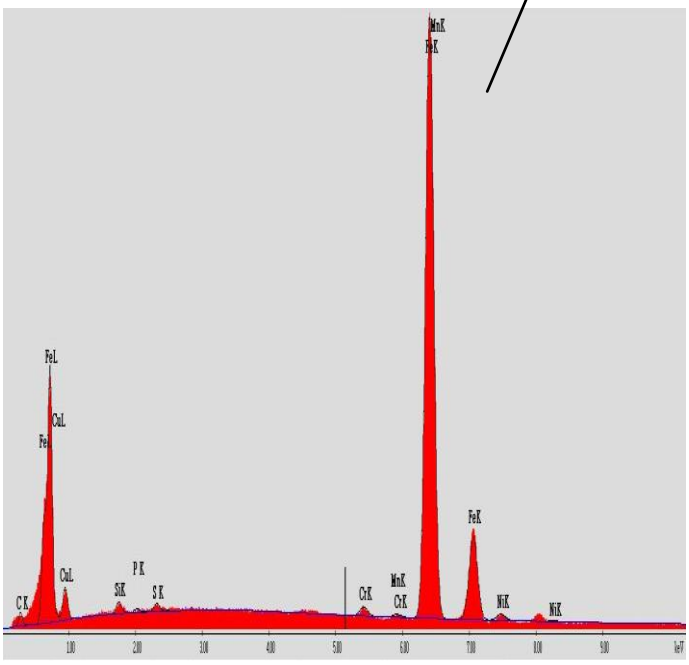

(iii)

Element	Weight%	Atomic%
C K	2.65	11.25
Cu K	8.54	6.84
SiK	0.64	1.16
PK	0.18	0.30
SK	0.35	0.56
CrK	0.70	0.69
MnK	0.24	0.22
Fe K	85.26	77.74
NiK	1.43	1.24

(iv)

FIGURE 8.6 SEM & EDX micrograph of welding region with trial no.5 [Electrode Diameter 3.2,Current 400 A, electrode stick-out 35 mm, preheat temperature 200°C, travel speed 22 m/hr, Flux3] (i) 500× (ii) 1000× (iii) EDX image of trial no.5 (iv) Chemical composition of trial no.5 resulting from EDX analysis

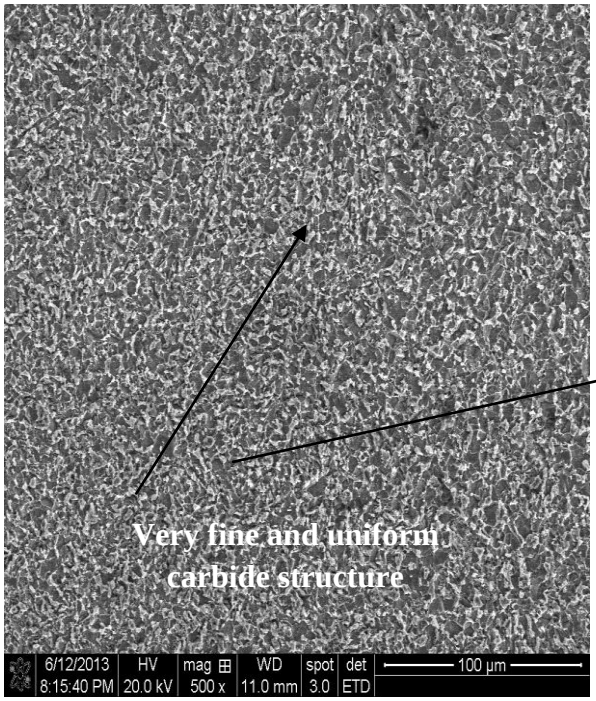

(i)

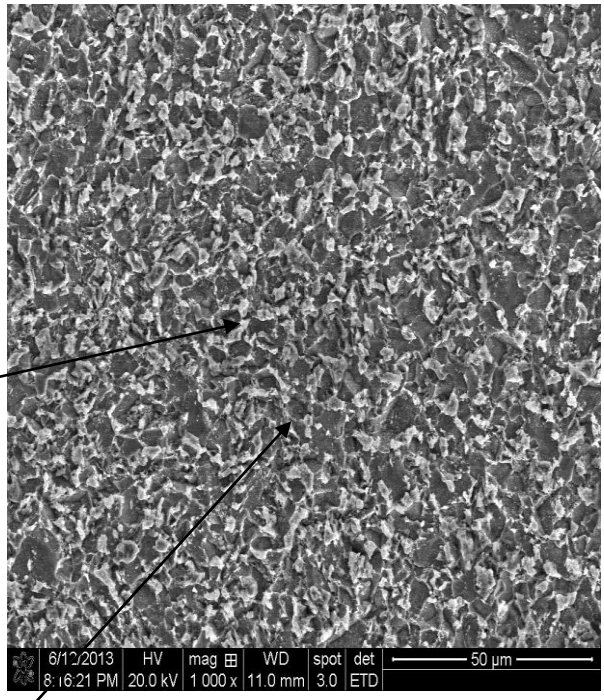

(ii)

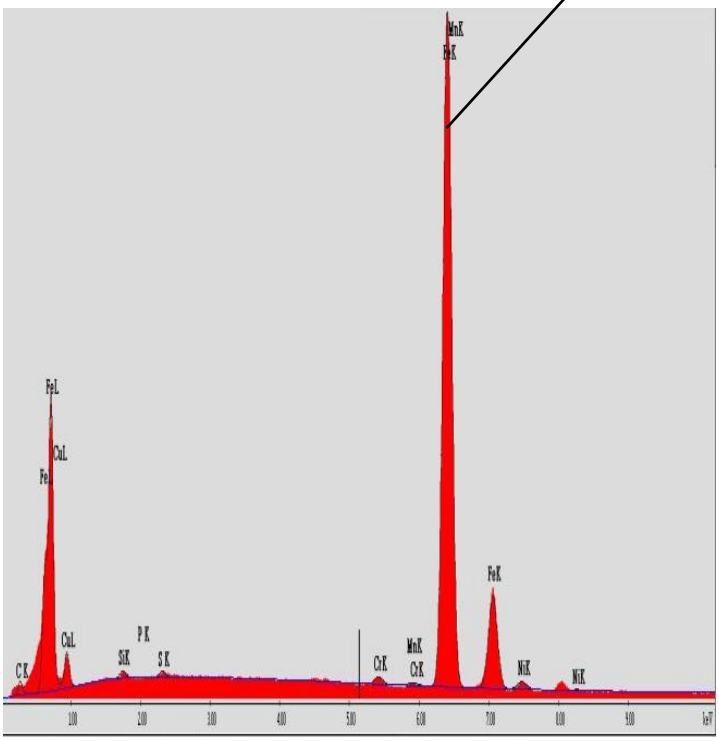

(iii)

Element	Weight%	Atomic%
C K	2.46	10.57
Cu K	8.56	6.94
SiK	0.36	0.65
PK	0.00	0.00
SK	0.24	0.38
CrK	0.53	0.53
MnK	0.25	0.24
Fe K	86.07	79.36
NiK	1.52	1.34

(iv)

FIGURE 8.7 SEM & EDX micrograph of welding region with trial no.6 [Electrode Diameter 3.2,Current 450 A, electrode stick-out 35 mm, preheat temperature 200°C, travel speed 18 m/hr, Flux1] (a) 500× (b) 1000× (iii) EDX image of trial no.6 (iv) Chemical composition of trial no.6 resulting from EDX analysis

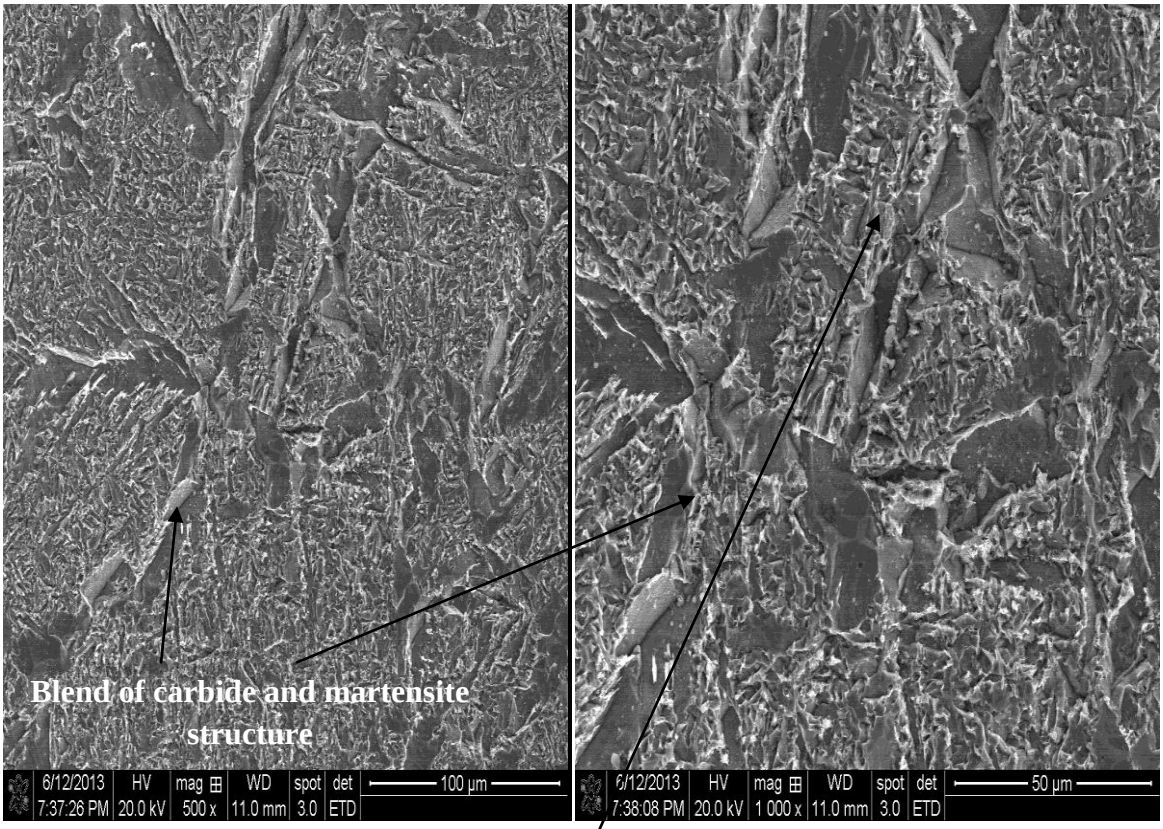

(i) (ii)

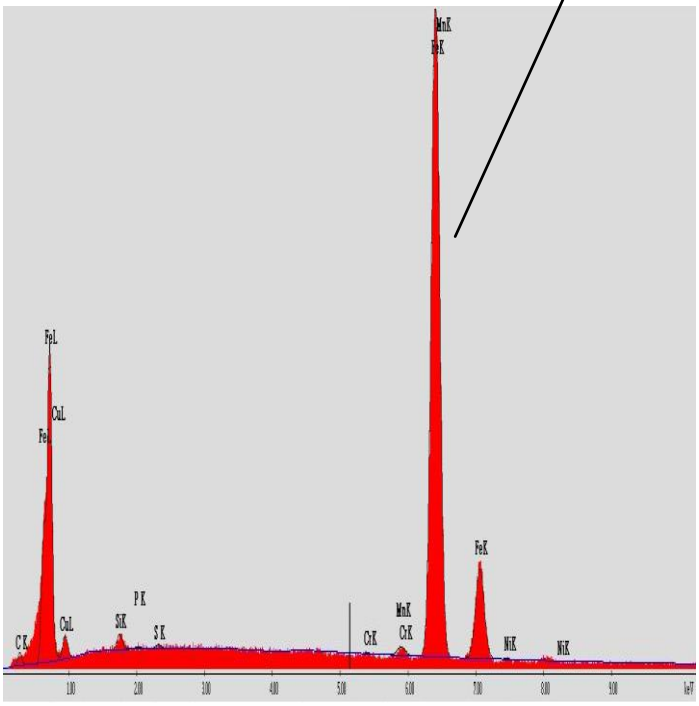

Element	Weight%	Atomic%
C K	2.45	10.44
Cu K	6.21	5.00
SiK	0.80	1.46
PK	0.11	0.18
SK	0.15	0.23
CrK	0.04	0.04
MnK	1.01	0.94
Fe K	89.13	81.62
NiK	0.10	0.09

(iii) (iv)

FIGURE 8.8 SEM & EDX micrograph of welding region with trial no.7 [Electrode Diameter 3.2,Current 500 A, electrode stick-out 25 mm, preheat temperature 125°C, travel speed 18 m/hr, Flux3] (i) 500× (ii) 1000× (iii) EDX image of trial no.7 (iv) Chemical composition of trial no.7 resulting from EDX analysis

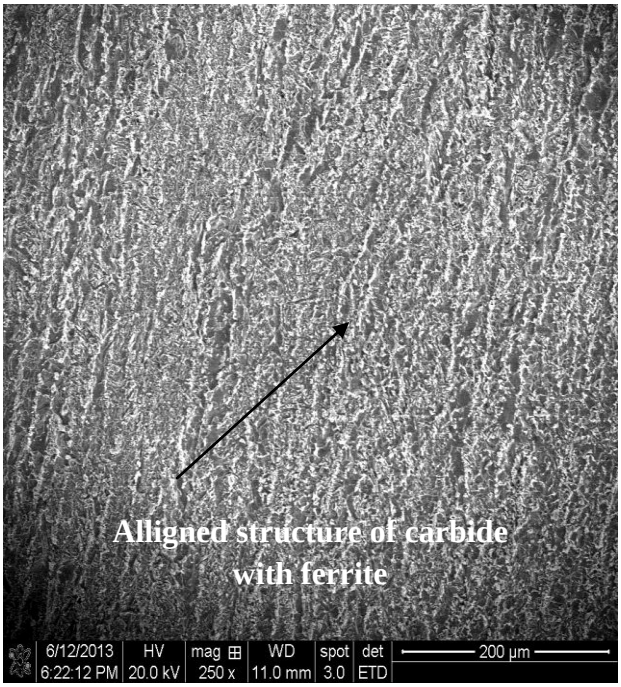

(i)

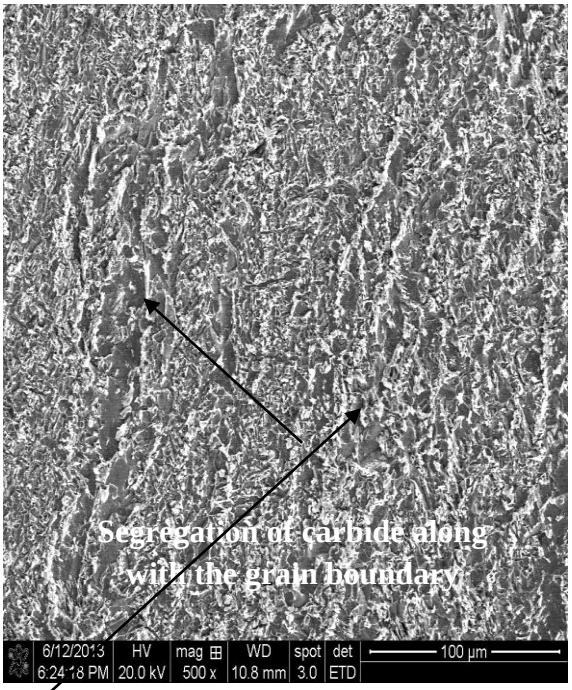

(ii)

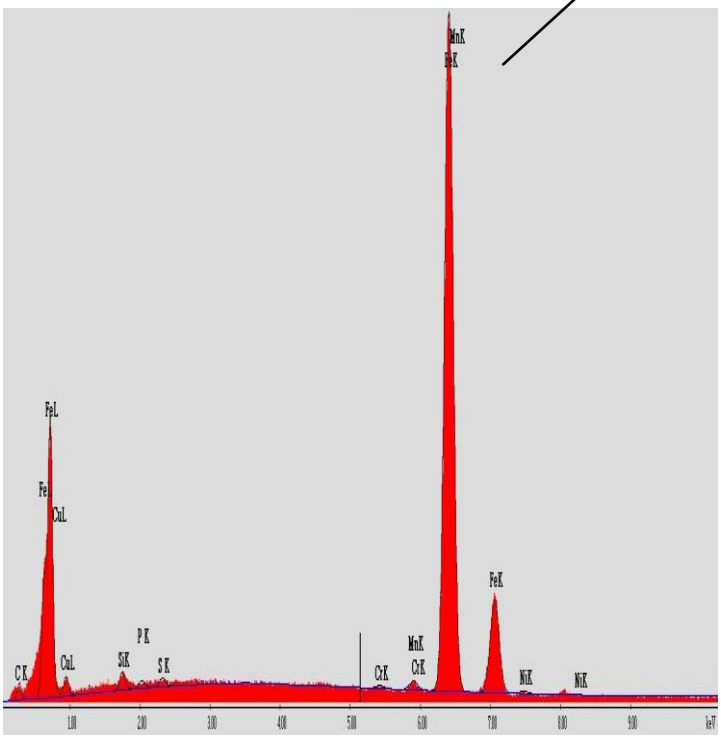

(iii)

Element	Weight%	Atomic%
C K	3.10	12.87
Cu K	5.01	3.92
SiK	0.91	1.61
PK	0.32	0.51
SK	0.34	0.53
CrK	0.21	0.20
MnK	0.98	0.89
Fe K	88.64	79.04
NiK	0.48	0.41

(iv)

FIGURE 8.9 SEM & EDX micrograph of welding region with trial no.8 [Electrode Diameter 3.2,Current 500 A, electrode stick-out 30 mm, preheat temperature 200°C, travel speed 20 m/hr, Flux1] (i) 250× (ii) 500× (iii) EDX image of trial no.8 (iv) Chemical composition of trial no.8 resulting from EDX analysis

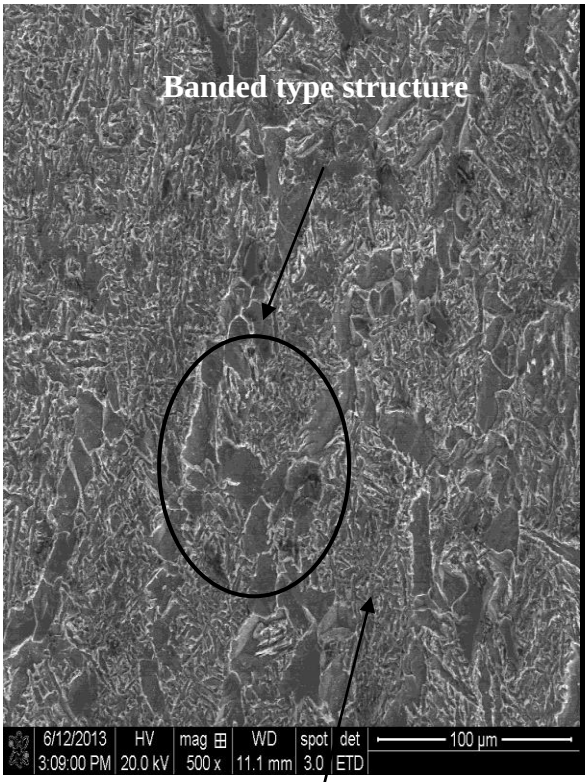

(i)

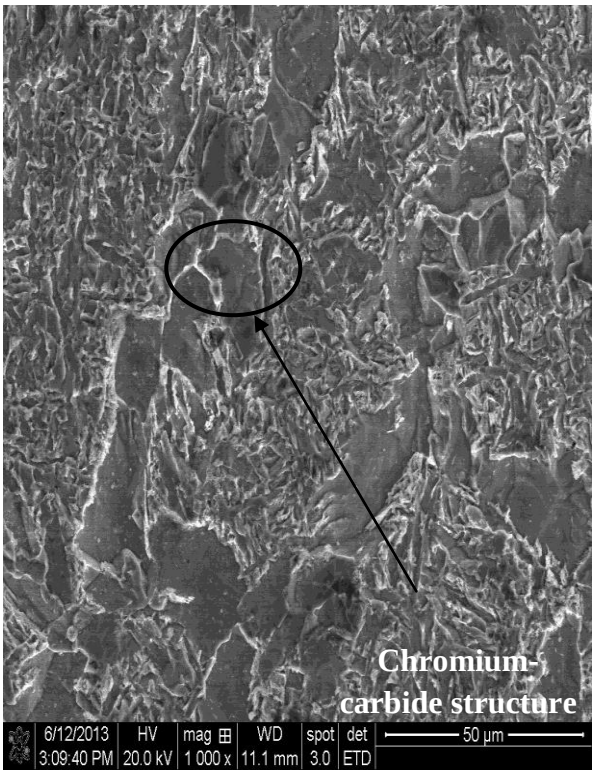

(ii)

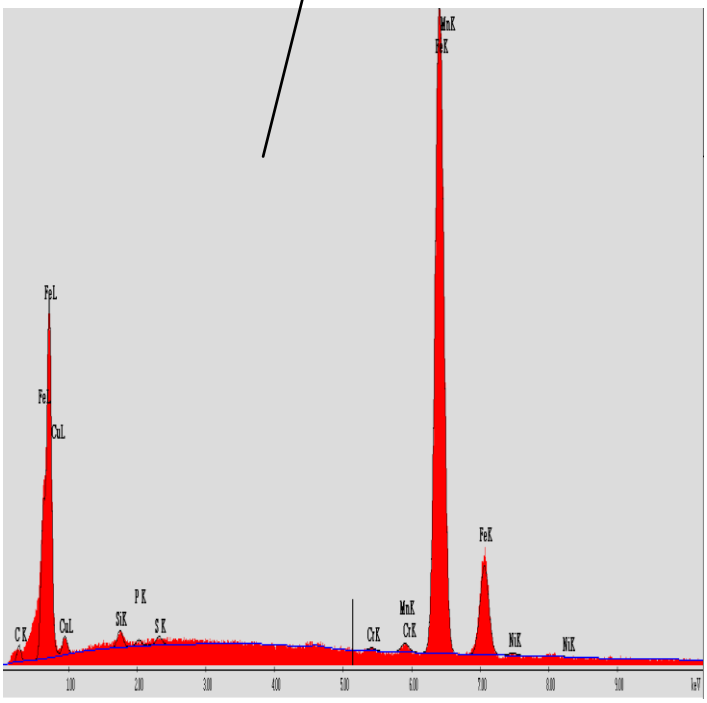

(iii)

Element	Weight%	Atomic%
C K	3.11	12.91
Cu K	4.80	3.76
SiK	0.88	1.55
PK	0.29	0.46
SK	0.37	0.57
CrK	0.21	0.20
MnK	0.98	0.89
Fe K	88.88	79.24
NiK	0.49	0.41

(iv)

FIGURE 8.10 SEM & EDX micrograph of welding region with trial no.9 [Electrode Diameter 3.2,Current 500 A, electrode stick-out 35 mm, No preheat temperature, travel speed 20 m/hr, Flux1] (a) 500× (b) 1000× (iii) EDX image of trial no.9 (iv) Chemical composition of trial no.9 resulting from EDX analysis

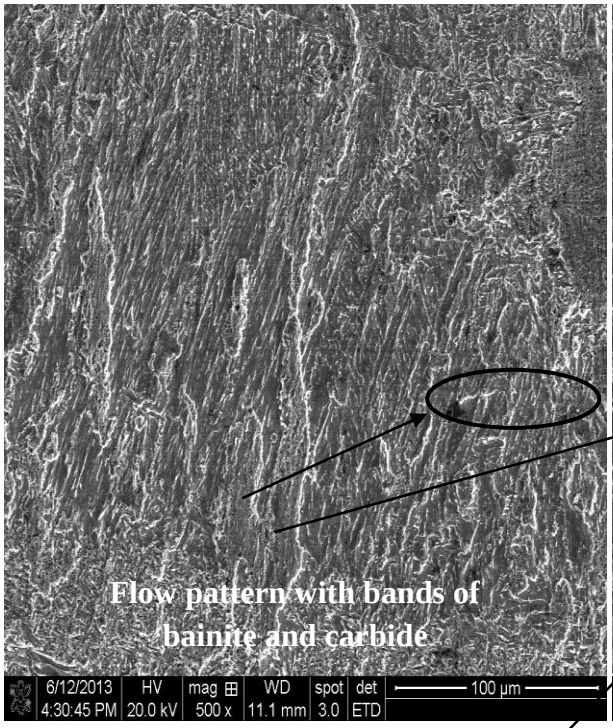

(i)

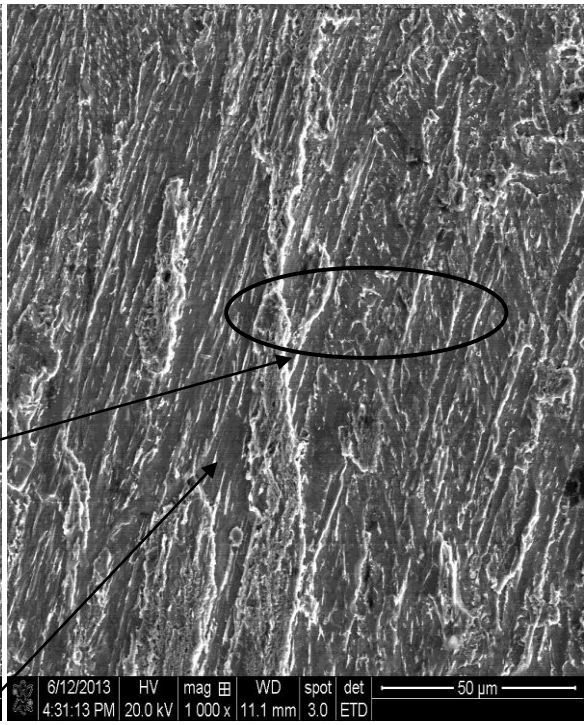

(ii)

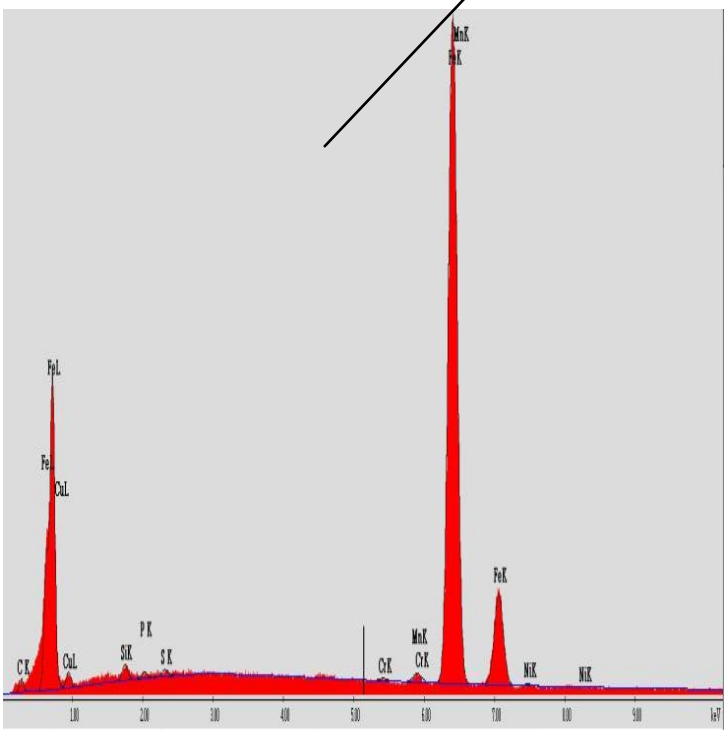

(iii)

Element	Weight%	Atomic%
C K	2.60	10.96
Cu K	4.05	3.23
SiK	0.80	1.45
PK	0.28	0.46
SK	0.28	0.44
CrK	0.18	0.18
MnK	1.01	0.93
Fe K	90.44	82.04
NiK	0.35	0.30

(iv)

FIGURE 8.11 SEM & EDX micrograph of welding region with trial no.10 [Electrode Diameter 4,Current 400 A, electrode stick-out 25 mm, preheat temperature 200 ºC, travel speed 22 m/hr, Flux2] (a) 500× (b) 1000× (iii) EDX image of trial no.10 (iv) Chemical composition of trial no.10 resulting from EDX analysis

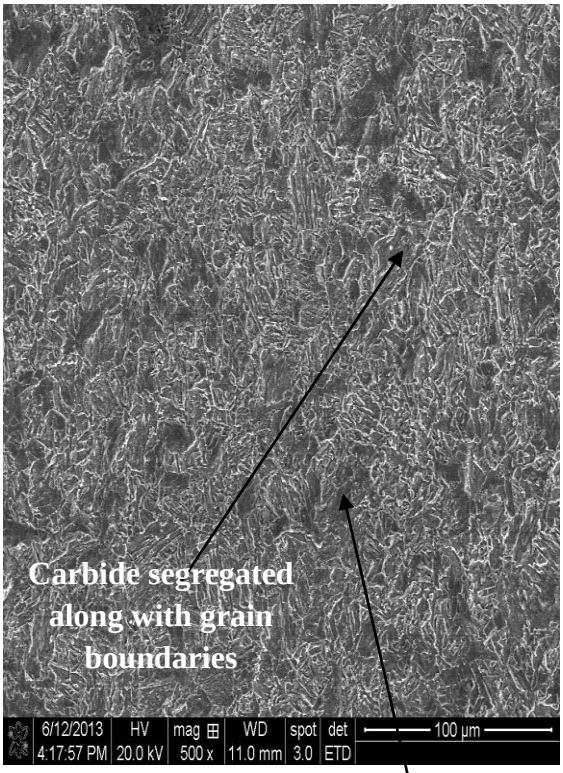

(i)

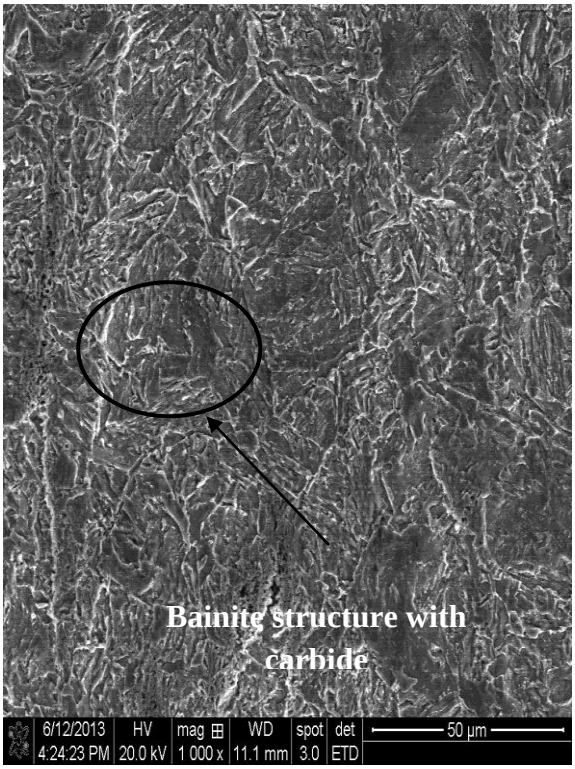

(ii)

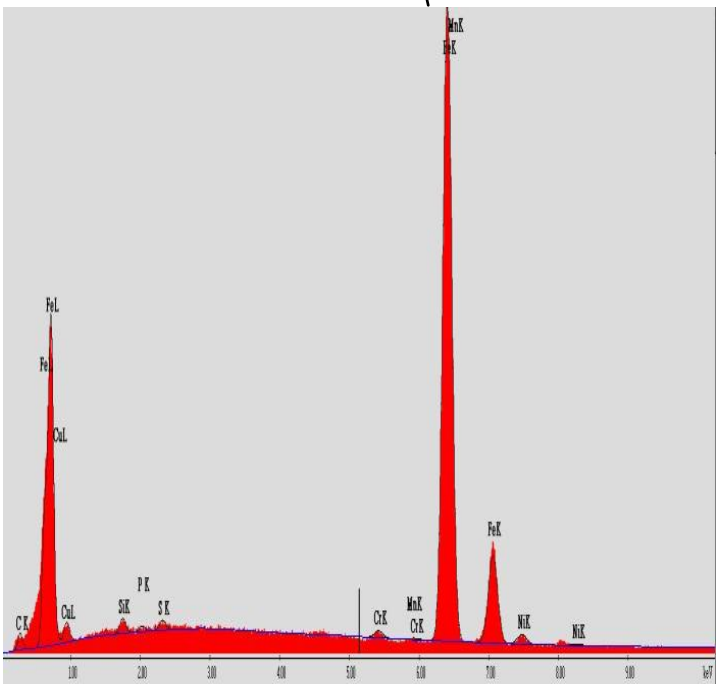

(iii)

Element	Weight%	Atomic%
C K	3.22	13.32
Cu K	5.69	4.46
SiK	0.79	1.40
PK	0.25	0.40
SK	0.44	0.68
CrK	0.51	0.49
MnK	0.08	0.08
Fe K	86.94	77.41
NiK	2.07	1.76

(iv)

FIGURE 8.12 SEM & EDX micrograph of welding region with trial no.11 [Electrode Diameter 4,Current 400 A, electrode stick-out 30 mm, No preheat temperature, travel speed 18 m/hr, Flux3] (a) 500× (b) 1000× (iii) EDX image of trial no.11 (iv) Chemical composition of trial no.11 resulting from EDX analysis

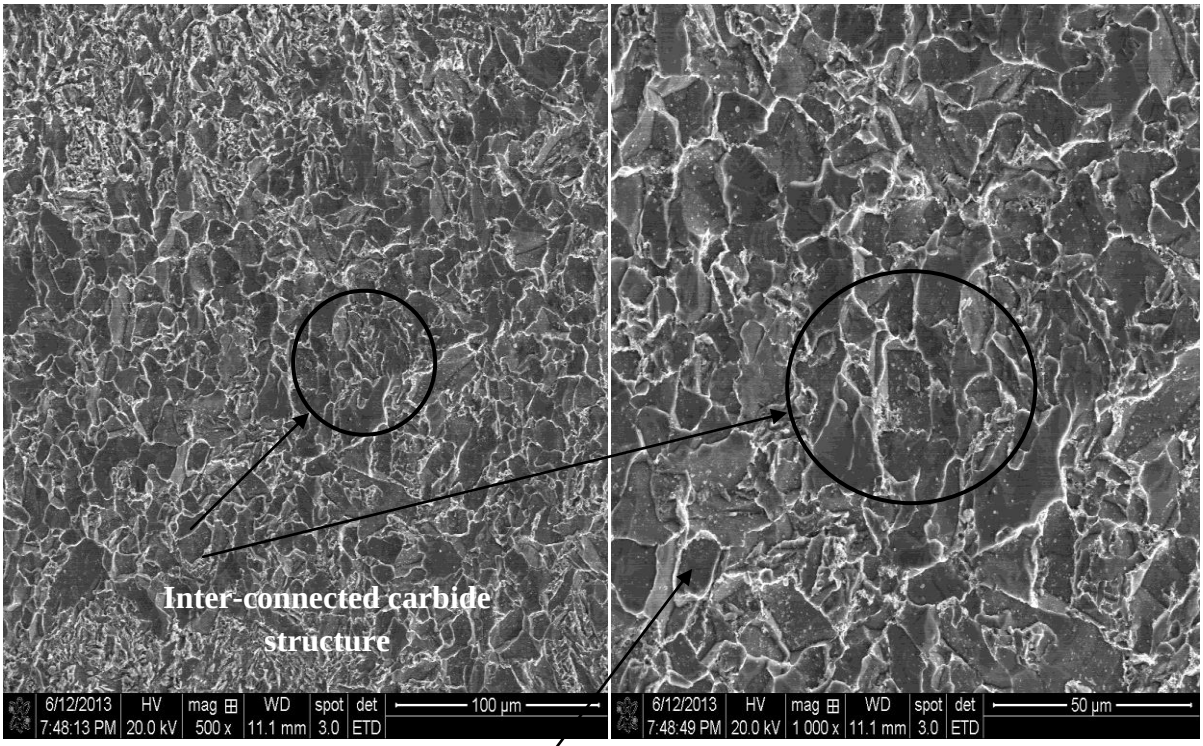

(i) (ii)

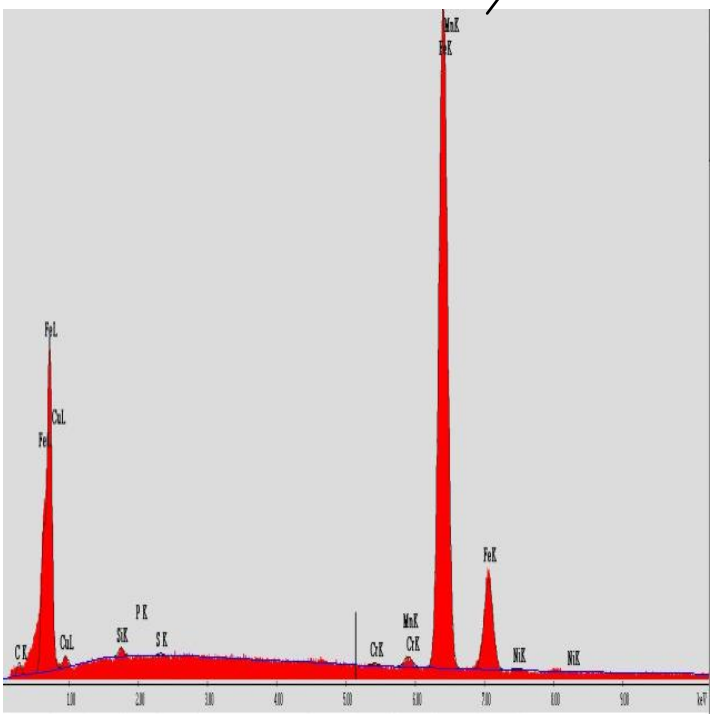

Element	Weight%	Atomic%
C K	2.53	10.75
Cu K	3.22	2.59
SiK	0.46	0.83
PK	0.00	0.00
SK	0.11	0.17
CrK	0.18	0.17
MnK	1.23	1.15
Fe K	91.77	83.89
NiK	0.51	0.44

(iii) (iv)

FIGURE 8.13 SEM & EDX micrograph of welding region with trial no.12 [Electrode Diameter 4,Current 400 A, electrode stick-out 35 mm, preheat temperature 125 ºC, travel speed 20 m/hr, Flux1] (i) 500× (ii) 1000× (iii) EDX image of trial no.12 (iv) Chemical composition of trial no.12 resulting from EDX analysis

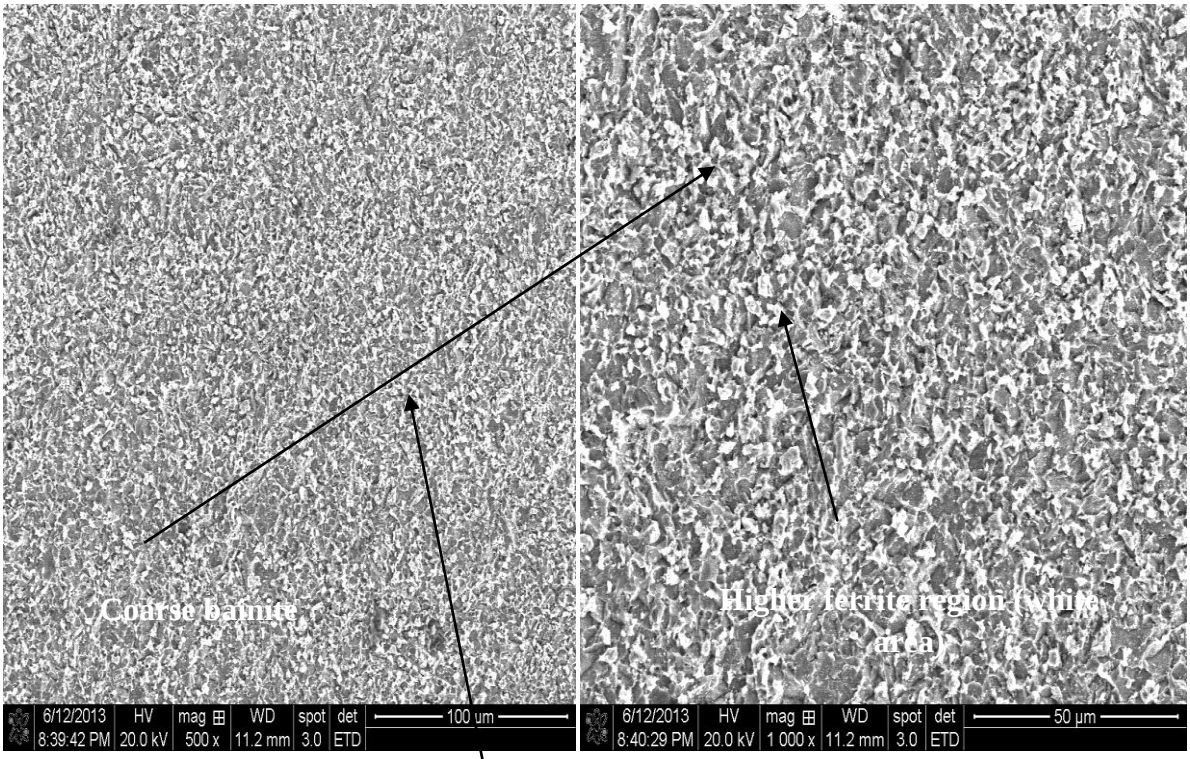

(i) (ii)

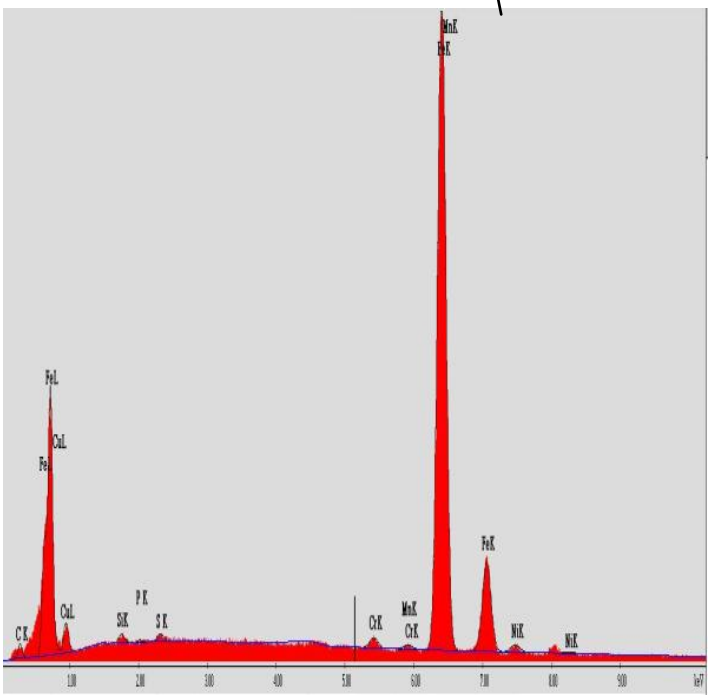

(iii)

Element	Weight%	Atomic%
C K	2.77	11.72
Cu K	7.65	6.12
SiK	0.43	0.79
PK	0.08	0.13
SK	0.33	0.53
CrK	0.78	0.76
MnK	0.36	0.34
Fe K	85.98	78.23
NiK	1.61	1.39

(iv)

FIGURE 8.14 SEM & EDX micrograph of welding region with trial no.13 [Electrode Diameter 4,Current 450 A, electrode stick-out 25 mm, preheat temperature 125 ºC, travel speed 22 m/hr, Flux1] (i) 500× (ii) 1000× (iii) EDX image of trial no.13 (iv) Chemical composition of trial no.13 resulting from EDX analysis

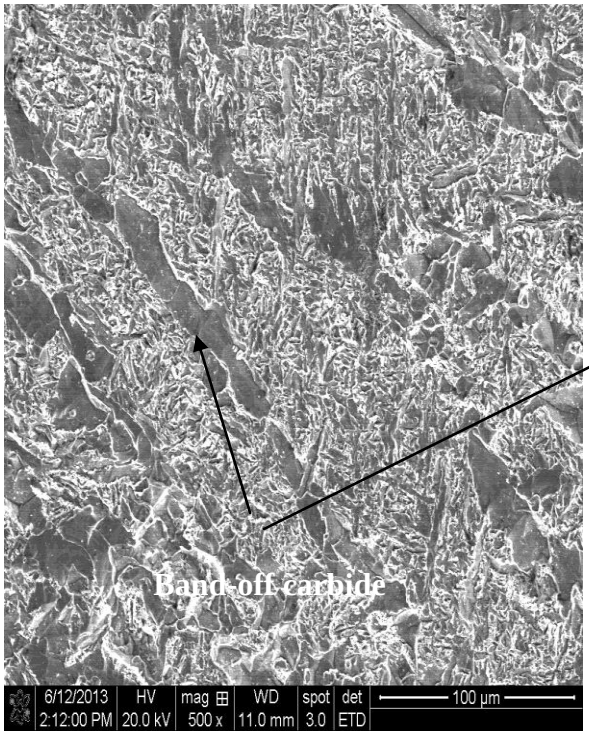

(i)

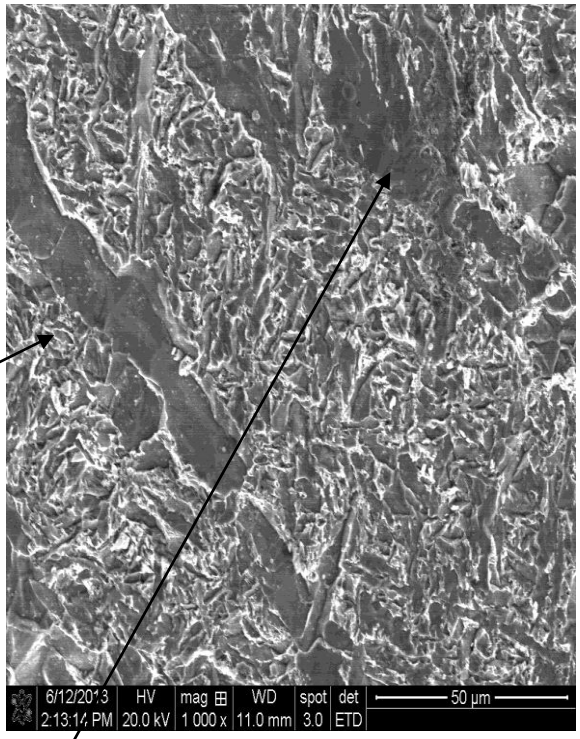

(ii)

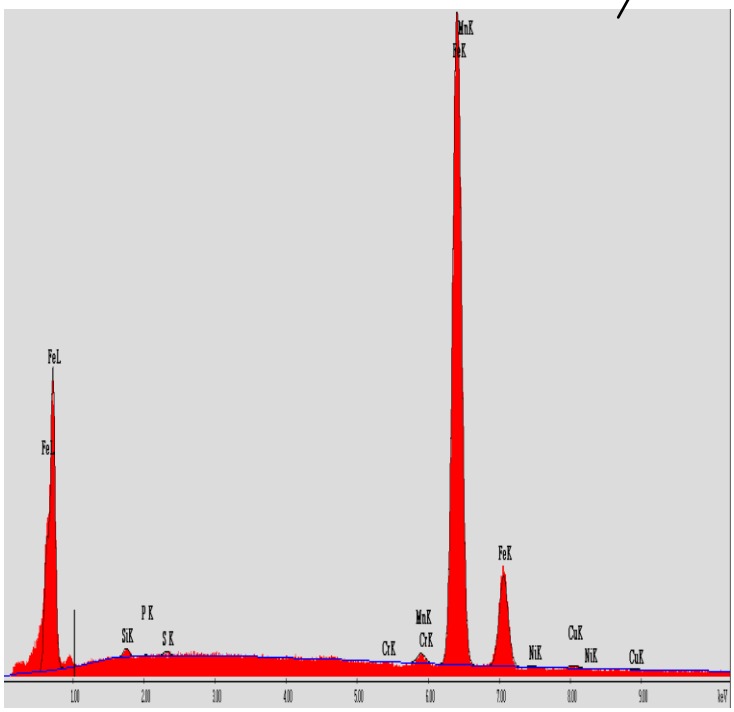

(iii)

Element	Weight%	Atomic%
Cu K	0.88	0.77
SiK	0.47	0.93
PK	0.05	0.10
SK	0.20	0.35
CrK	0.04	0.04
MnK	1.25	1.26
Fe K	96.88	96.33
NiK	0.23	0.22

(iv)

FIGURE 8.15 SEM & EDX micrograph of welding region with trial no.14 [Electrode Diameter 4,Current 450 A, electrode stick-out 30 mm, preheat temperature 200 ºC, travel speed 18 m/hr, Flux2] (a) 500× (b) 1000× (iii) EDX image of trial no.14 (iv) Chemical composition of trial no.14 resulting from EDX analysis

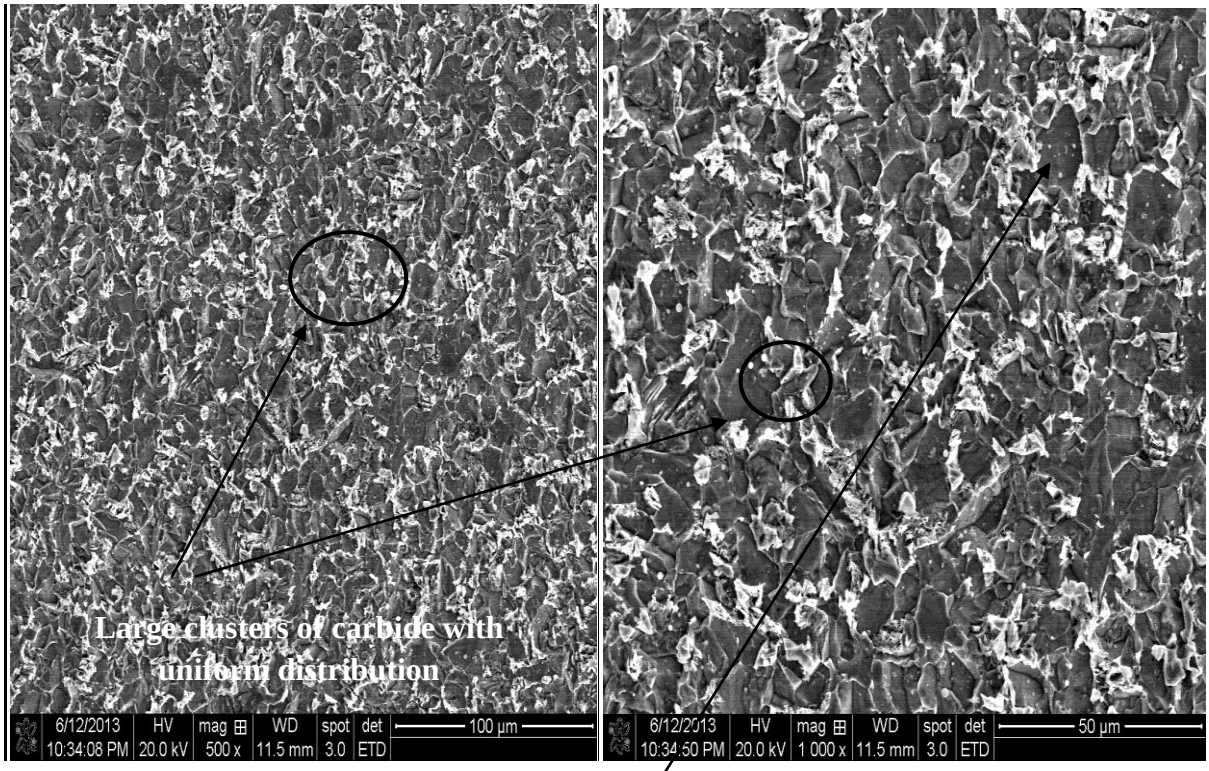

(i) (ii)

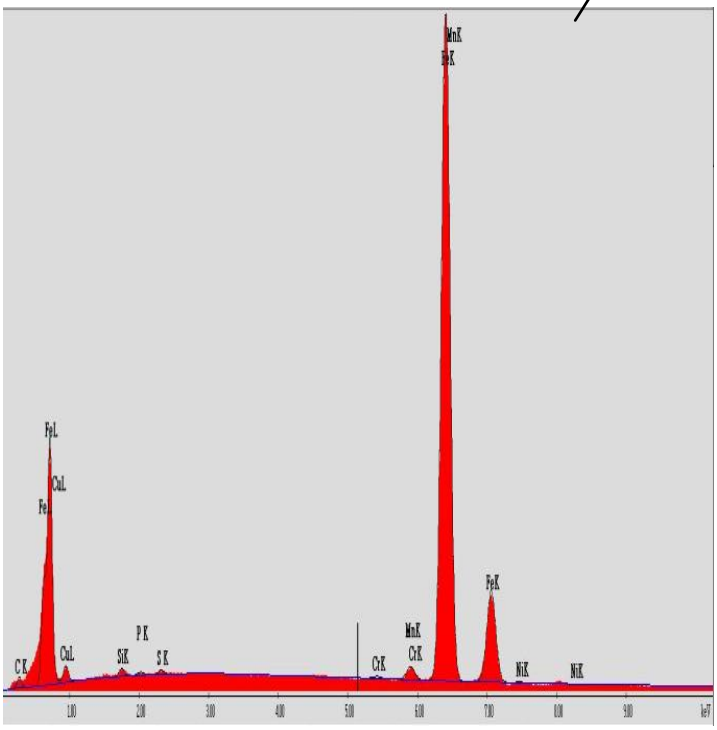

Element	Weight%	Atomic%
C K	2.07	8.94
Cu K	4.42	3.60
SiK	0.41	0.75
PK	0.15	0.25
SK	0.17	0.28
CrK	0.16	0.16
MnK	1.52	1.44
Fe K	90.97	84.46
NiK	0.14	0.12

(iii) (iv)

FIGURE 8.16 SEM & EDX micrograph of welding region with trial no.15 [Electrode Diameter 4,Current 450 A, electrode stick-out 35 mm, No preheat temperature, travel speed 20 m/hr, Flux3] (a) 500× (b) 1000× (iii) EDX image of trial no.15 (iv) Chemical composition of trial no.15 resulting from EDX analysis

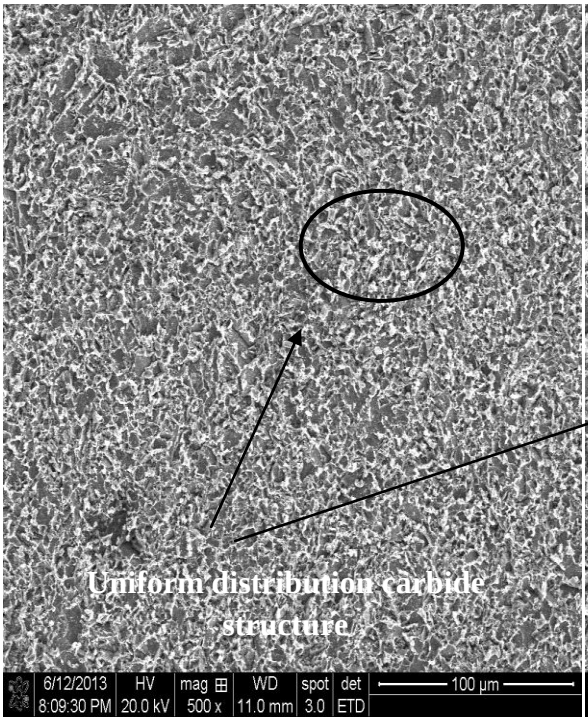

(i)

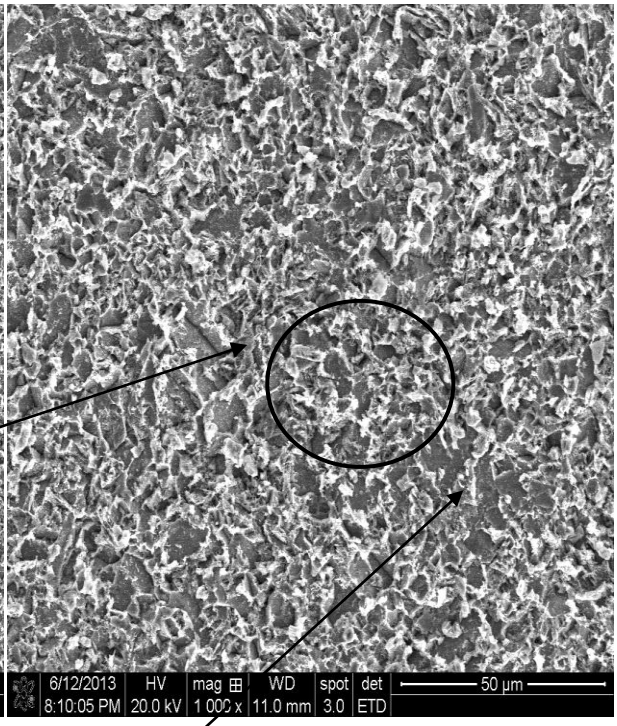

(ii)

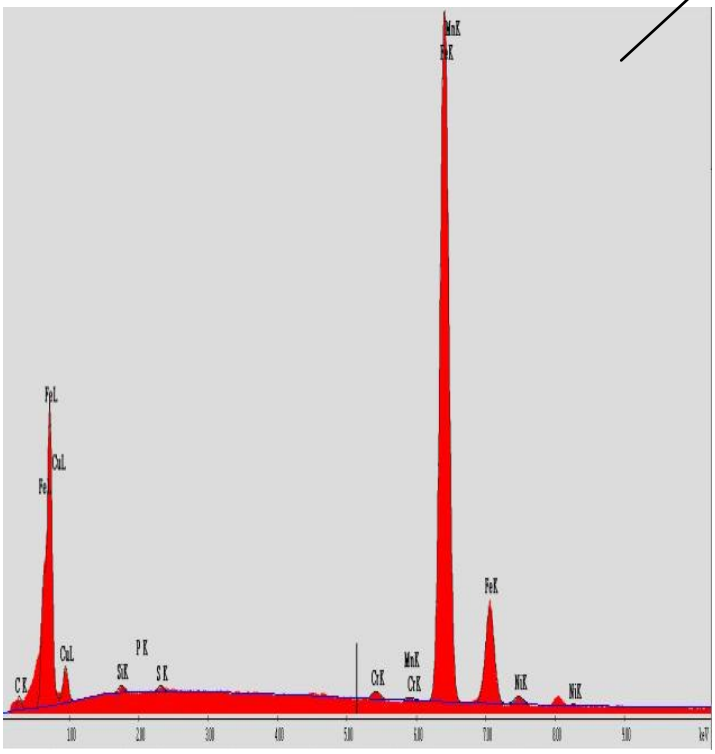

(iii)

Element	Weight%	Atomic%
C K	2.46	10.57
Cu K	8.56	6.94
SiK	0.36	0.65
PK	0.00	0.00
SK	0.24	0.38
CrK	0.53	0.53
MnK	0.25	0.24
Fe K	86.07	79.36
NiK	1.52	1.34

(iv)

FIGURE 8.17 SEM & EDX micrograph of welding region with trial no.16 [Electrode Diameter 4,Current 500 A, electrode stick-out 25 mm, preheat temperature 200 °C, travel speed 20 m/hr, Flux3] (a) 500× (b) 1000× (iii) EDX image of trial no.16 (iv) Chemical composition of trial no.16 resulting from EDX analysis

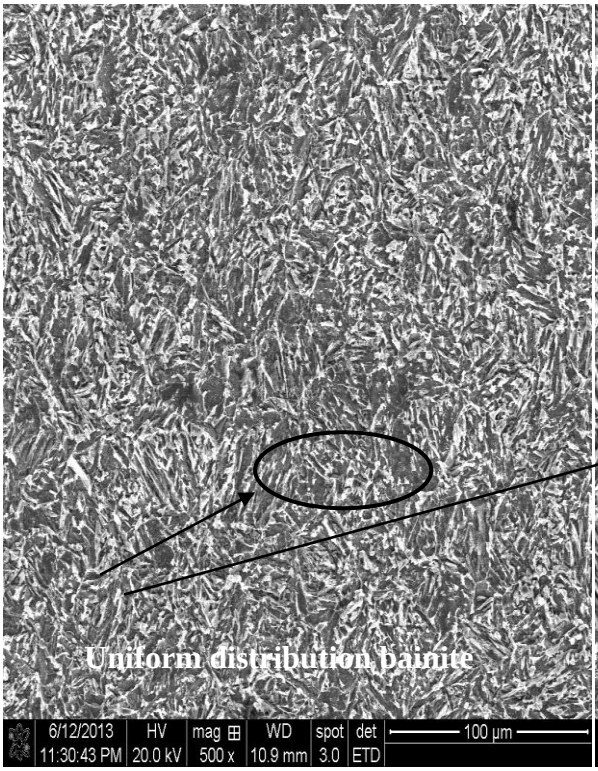

(i)

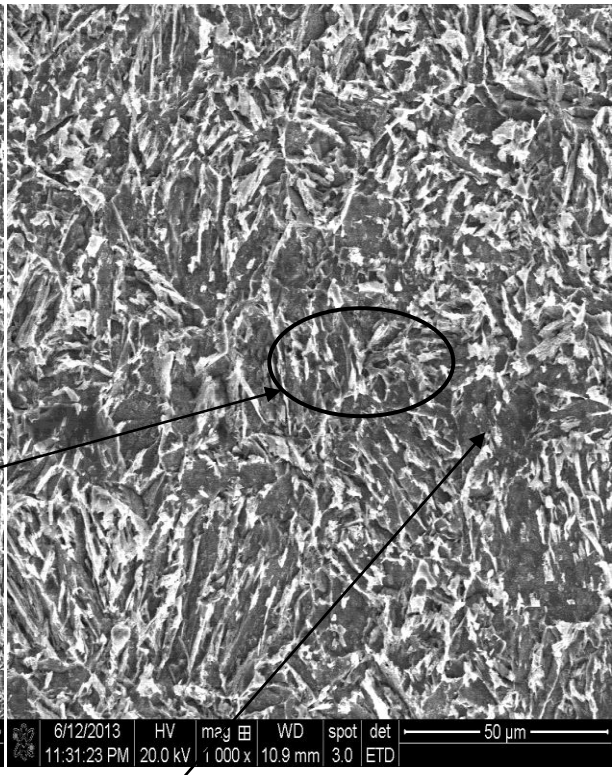

(ii)

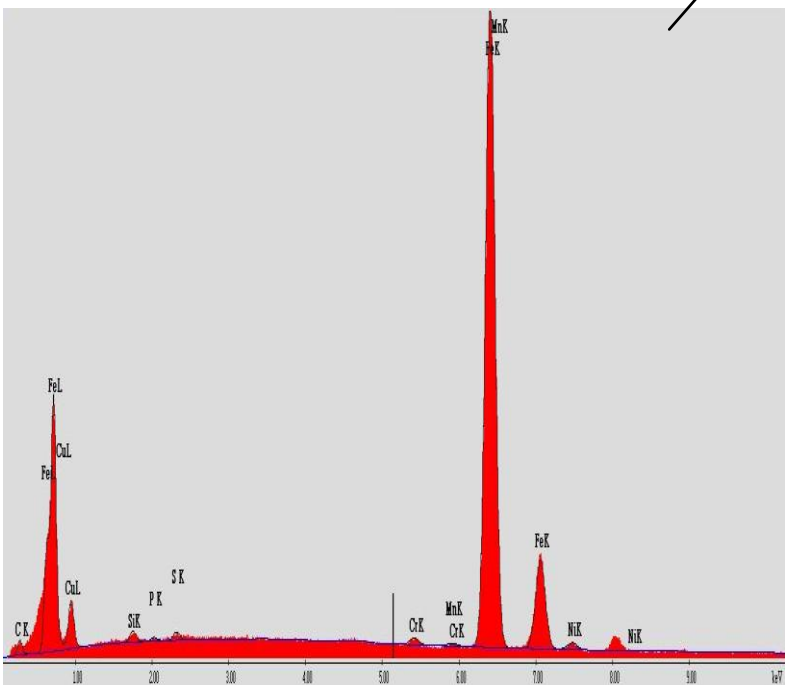

(iii)

Element	Weight%	Atomic%
C K	2.81	11.92
Cu K	11.39	9.12
SiK	0.55	1.00
PK	0.17	0.27
SK	0.33	0.53
CrK	0.48	0.47
MnK	0.25	0.23
Fe K	82.58	75.22
NiK	1.43	1.24

(iv)

FIGURE 8.18 SEM & EDX micrograph of welding region with trial no.17 [Electrode Diameter 4,Current 500 A, electrode stick-out 30 mm, No preheat temperature, travel speed 22 m/hr, Flux1] (a) 500× (b) 1000× (iii) EDX image of trial no.17 (iv) Chemical composition of trial no.17 resulting from EDX analysis

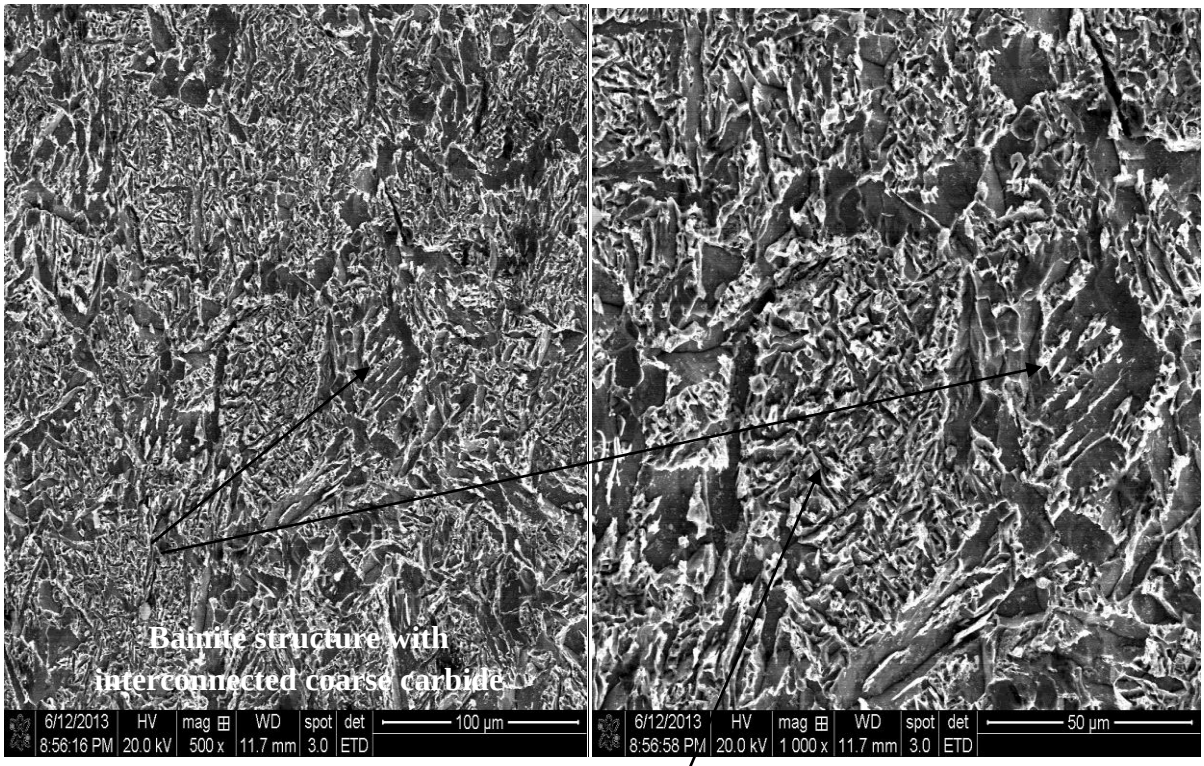

(i) (ii)

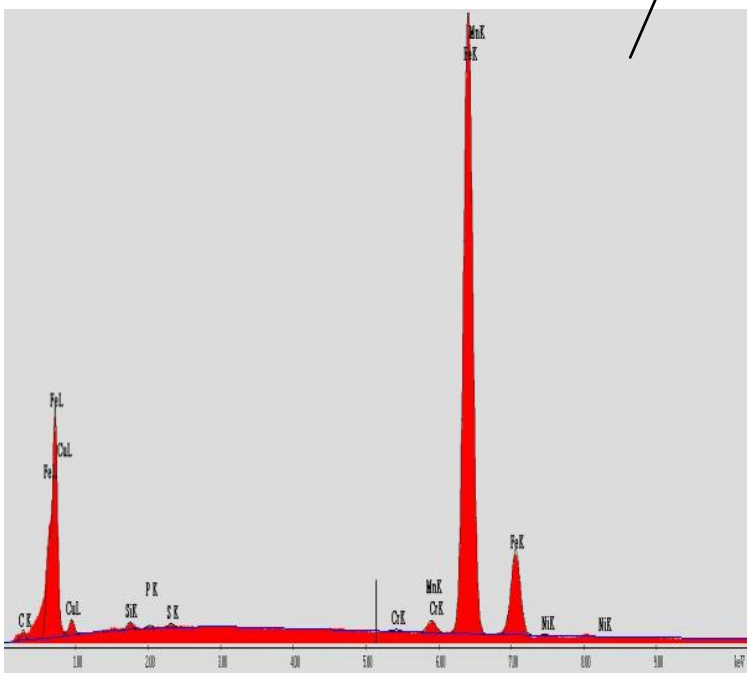

Element	Weight%	Atomic%
C K	2.07	8.94
Cu K	4.42	3.60
SiK	0.41	0.75
PK	0.15	0.25
SK	0.17	0.28
CrK	0.16	0.16
MnK	1.52	1.44
Fe K	90.97	84.46
NiK	0.14	0.12

(ii) (iv)

FIGURE 8.19 SEM & EDX micrograph of welding region with trial no.18 [Electrode Diameter 4,Current 500 A, electrode stick-out 35 mm, preheat temperature 125 ºC, travel speed 18 m/hr, Flux 2] (a) 500× (b) 1000× (iii) EDX image of trial no.18 (iv) Chemical composition of trial no.18 resulting from EDX analysis

8.3 DISCUSSION

Figure 8.1 shows the microstructure of the base metal at a magnification of 500 x and 1000 x. Two constituents are visible in the micrograph which is white and black in colour. The white and black colour indicates the presence of ferrite phase *(α-iron)* and iron carbide respectively. The microstructure of bainite consists of ferrite and cementite phases, and thus diffusion processes are involved. In figure 8.1 shows the bainite embedded with carbide at 500x, which resulted have higher strength (687.06 N/mm^2).Energy dispersive x-ray (EDX) shows the chemical composition analysis at weld region. Figure 8.2 shows the micrograph of HSLA steel welding region after welding at first trial input factors with 400 A current with travel speed 18 m/hr and no preheat temperature is used. Figure 8.2 shows the aligned band-off carbide with no uniform distribution of two phases.EDX shows the high percentage of nickel (9.41%), which resulted have in higher toughness (176.085 *J*). Figure 8.3 shows the micrograph of welding region after second trial. It shows the large cluster of ferrite and cementite and traces of bainitic structure in the field. EDX shows the low percentage of nickel (1.50%) than previous one, which resulted have in lower toughness (139.30 *J*) at room temperature is observed. It also shows the lower tensile strength (558.56 N/mm^2) in trial no.2 than the base metal due to less percentage of chromium (0.56%). SEM micrograph for welding region with preheat temperature 200^oC at 400 *A* current and travel speed 22 *m/hr* on time at two different magnifications is shown in Figure 8.4.It shows the needle-shaped structure present in the field indicate formation of bainite with carbide structure, which results have maximum hardness was obtained i.e.77.5 *hvn*. Due to bainite cluster it has observed high micro hardness. EDX shows the high percentage of nickel (1.69%), which has results high toughness (177.07 *J*), was observed. Figure 8.5 shows the micrograph at 450 *A* with no preheat temperature at two magnification was observed. Chain type carbide with spheroidal structure was observed with non-uniform distribution of two regions, which have results lower tensile strength (533.12 N/mm^2). The percentage of Si (0.67%) is maximum than trial no.3, which resulted have higher toughness (190.805 *J*) than trial no. 3. Figure 8.6 shows the micrograph at 400*A* with preheat temperature 200^oC was observed higher strength (599.91 N/mm^2) than the previous trial due to the presence of massive carbide structure. It was observed that carbide is aggregating along with grain boundaries. EDX indicate the copper percentage is high (8.54%), which have promotes tenacious oxide film to aid atmospheric corrosion resistance. Figure 8.7 shows the very uniform and fine carbide structure was observed at electrode diameter 3.2, current 450

A, electrode stick-out 35 *mm*, preheat temperature 200 *°C*, travel speed 18 *m/hr*, Flux1with two magnifications is used. Due to high Ni and Si percentage, which results have higher toughness (193.255 *J*) was observed. SEM micrograph for HSLA steel welding with parameter is used i.e. electrode diameter 3.2 *mm*, current 500 *A*, electrode stick-out 25 *mm*, preheat temperature 125*°C*, travel speed 18 *m/hr*, Flux 3 is shown in figure 8.8. Figure shows the blend of carbide and martensite structure. Ni (0.10 *%*) concentration was observed by EDX, which have resulted in lower toughness (152.544 *J*) at room temperature. It also showed the chain type carbide structure and very less percentage of ferrite (white region) was observed in micrograph. High tensile strength is observed even at very high current value. This is a condition of very high heat input, that is why the ferrite percentage of this welded region is lesser than previous one. Figure 8.9 shows the welded region at maximum heat input. Due to high current is observed the aligned structure of carbide with ferrite in 250 x magnification. In 500 x magnifications is observed segregation of carbide along with grain boundaries. High-ferrite count is observed, which have resulted in tensile strength also reduced than the previous trial. Figure 8.10 shows at different parameter i.e. electrode diameter 3.2, current 500 *A*, electrode stick-out 35 *mm*, no preheat temperature, travel speed 20 *m/hr*, flux1 shows the banded type chromium carbide structure. It also shows the low percentage of ferrite count. High tensile strength and toughness is observed as Ni, Si and Cr element concentration is more. Figure 8.11 shows the welded region at 400 *A* and 4.0 *mm* electrode diameter respectively. The picture shows the flow pattern with bands of bainite and carbide in whole matrix. The hardness of welded region was observed to be 73.69 *hvn* which is quite higher than previous trial with flux 2 which could be the presence of bainite structure and higher tensile strength (634.53 N/mm^2) is observed among all the trial due to flow pattern of bainite and carbide. Figure 8.12 observations for the micrograph at electrode diameter 4, current 400 *A*, electrode stick-out 30 *mm*, no preheat temperature, travel speed 18 *m/hr* and Flux 3 shows the bainite structure with carbide at 1000 x magnification. In picture it also observed that carbide segregated along with grain boundaries. By EDX study shows the higher concentration of Ni content was observed with 2.07*%*, which resulted have toughness value at room temperature with 202.572 *J* is maximum than previous trials. Figure 8.13 shows the inter-connected carbide structure at 400 *A* current is used. It also observed low-ferrite count with uniform distribution of structure due to high concentration of Mn (1.23*%*) in welded region. In general, higher Mn concentration promotes uniform austenite grain structure. Figure 8.14 shows the higher ferrite region is observed at 450 *A* current with higher travel speed (*22m/hr*) respectively. In picture shows the uniform distribution of carbide,

bainite and ferrite, which resulted have high mechanical properties was observed among all the experiment except micro hardness. Figure 8.15 shows the welded region micrograph at electrode diameter 4,current 450 *A*, electrode stick-out 30 *mm*, preheat temperature 200 *°C*, travel speed 18 *m/hr*, Flux 2 with band-off carbide is observed. Due to higher ferrite count with no-uniform distribution structure have found less micro hardness 62.67 *hvn* at weld region among all the previous trial except trial no.7 & 9. Figure 8.16 shows the microstructure at 450 *A* with large cluster of uniform distributed carbide with segregated grain boundary by ferrite structure. Uniform distribution of grain boundary is observed due to higher Mn (1.52*%*) concentration in welded region leading to a hardness value i.e. 71.72*hvn*. Figure 8.17 shows microstructure of HSLA welding region with electrode diameter 4, current 500 *A*, electrode stick-out 25 *mm*, preheat temperature 200 *°C*, travel speed 20 *m/hr* and Flux 3. Uniform carbide structure is observed with leading to a moderate tensile strength (640.70 N/mm^2) and toughness at room temperature i.e.198.65 *J*. Figure 8.18 shows microstructure with maximum heat input. Uniform distribution of bainite structure is observed leading to hardness value i.e. 65.37 *hvn.* Due to moderate content of Ni and Si in welding region, which resulted have Maximum toughness at room temperature (212.38 *J*) is observed amongst all the trial except trial no.13. Figure 8.19 observed the micrograph with 500 *A* current and travel speed 18m/hr is used. It shows the bainitic structure with interconnected coarse carbide, which resulted have strength and toughness are 662.23 N/mm^2 and 73.0 *J* respectively.

CHAPTER-9

RESULTS AND ANALYSIS OF TOUGHNESS RESULTS

9.1 TOUGHNESS TEST

The ability of a metal to rapidly distribute within itself due to both the stress and strain caused by a suddenly applied load or the ability of a material to withstand shock loading. It is the exact opposite of "brittleness" which carries the implication of sudden failure. The tested specimen after toughness test is shown in Figure 9.1 for 18 sets of experiment.

FIGURE 9.1 Specimen after toughness test at -40^{o}C & room temperature (twice study for each temperature)

The toughness test details for base metal are shown in Table 9.1.

TABLE 9.1 Toughness values of base metal

	Charpy Test at -40 ^{o}C (J)	**Charpy Test at Room Temp. (J)**
Base Metal	125	210

For all the 18 sets of experiment, the toughness test summery is shown in table 9.2 and corresponding plot at room temperature are shown below sequentially in figure 9.3.

TABLE9.2 Toughness values at room temperature

Exp. No.	**Contributing Factors**	**Charpy Test at Room Temp. (J) Reading 1**	**Charpy Test at Room Temp. (J) Reading 2**	**Average value of charpy test at Room Temp.**
1	Ø1, C1, D1, T1,S1, F1,	176.580	175.590	176.085
2	Ø1, C1, D2,T2,S2, F2,	132.430	146.169	139.300
3	Ø1, C1, D3, T3,S3, F3	170.694	183.447	177.070
4	Ø1, C2, D1, T1, S2, F2	183.447	198.162	190.805
5	Ø1, C2, D2, T2, S3, F3	145.188	147.150	146.169
6	Ø1, C2, D3, T3, S1, F1	206.010	180.500	193.255
7	Ø1, C3, D1, T2, S1, F3	154.998	150.090	152.544
8	Ø1, C3, D2, T3, S2, F1	166.770	151.074	158.922
9	Ø1, C3, D3, T1, S3, F2	186.390	184.420	185.405
10	Ø2, C1, D1, T3, S3,F2	179.520	195.219	187.370
11	Ø2, C1, D2, T1, S1, F3	210.915	194.230	202.572
12	Ø2, C1, D3, T2, S2, F1	181.485	161.865	171.675
13	Ø2, C2, D1, T2, S3, F1	211.896	230.535	221.215
14	Ø2, C2, D2, T3, S1, F2	201.105	212.870	206.988
15	Ø2, C2, D3, T1, S2, F3	188.352	200.614	194.483
16	Ø2, C3, D1, T3, S2, F3	177.561	219.744	198.653
17	Ø2, C3, D2, T1, S3, F1	201.105	223.668	212.387
18	Ø2, C3, D3, T2, S1, F2	199.143	160.884	180.013

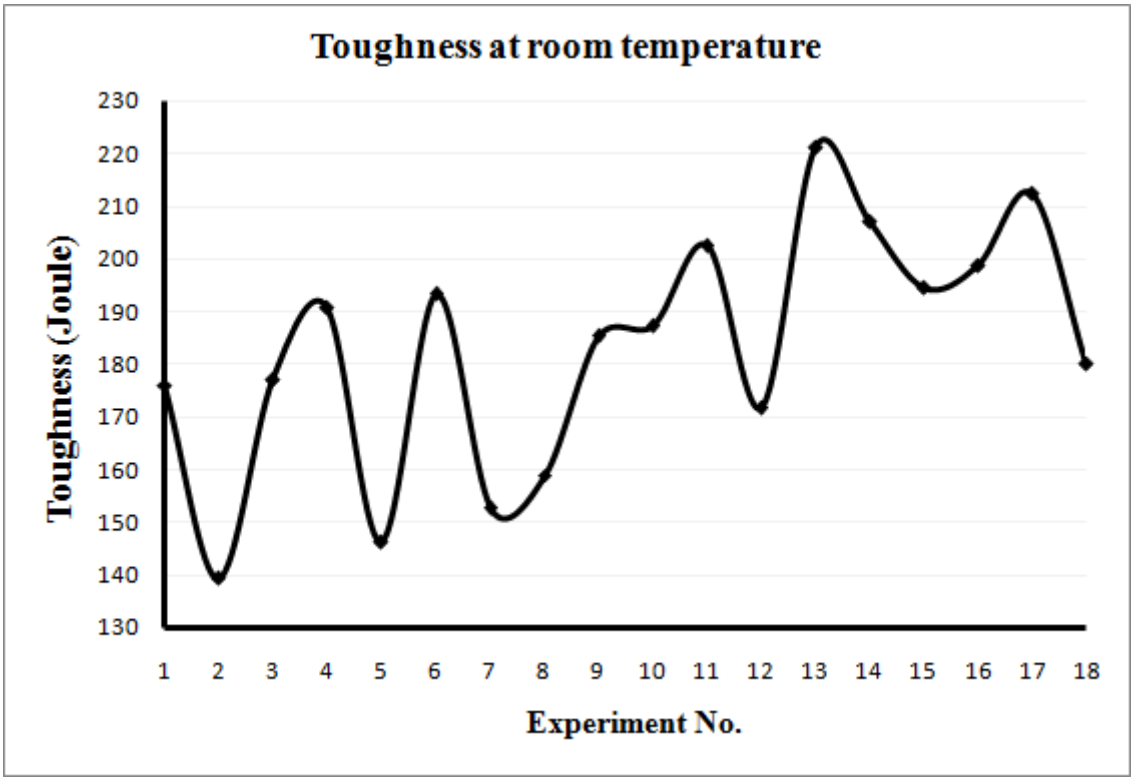

FIGURE 9.2 Variation in toughness at room temperature

9.2 ANOVA FOR TOUGHNESS AT ROOM TEMPERATURE

Table 9.3, column no. 6 consists of the values of toughness at room temperature for the eighteen trials. The experimental results for toughness are analyzed using ANOVA and is given in the table 9.3. An ANOVA table 9.3 shows that p value for electrode diameter and preheats temperature is 0.005and 0.048 respectively are the most significant or dependent factor for the toughness at room temperature. In table 9.4 electrode diameters with the highest rank 1 and is the most significant factor and electrode stick-out with its lowest rank is least significant in affecting the toughness at room temperature. Main effect plots are shown in figure 9.2 shows the variation in the toughness at room temperature with the change in the input factors i.e. electrode diameter, current, electrode stick-out, travel speed, preheat temperature, and flux. It could be seen from the figure 9.2 that electrode diameter causes the most significant change in the toughness. The change in preheat temperature also has some effect on the variation in the toughness at room temperature. Current, electrode stick-out, flux and travel speed does not have any significant effect on toughness at room temperature.

TABLE 9.3 Analysis of variance for means toughness at room temperature

Source	DF	Seq SS	Adj SS	Adj MS	F	P
Electrode Diameter (mm)	1	3635.2	3635.2	3635.2	18.78	**0.005**
Current (Ampere)	2	841.1	841.1	420.5	2.17	0.195
Electrode Stick-Out (mm)	2	306.6	306.6	153.3	0.79	0.495
Preheat Temperature (^{o}C)	2	2039.0	2039.0	1019.5	5.27	**0.048**
Travel Speed (m/hr)	2	521.8	521.8	260.9	1.35	0.329
Flux	2	338.6	338.6	169.3	0.87	0.464
Residual Error	6	1161.7	1161.7	193.6		
Total	17	8844.0				

TABLE 9.4 Response table for means of toughness at room temperature

Level	Electrode Diameter (mm)	Current (amp)	Electrode Stick-Out (mm)	Preheat Temperature (^{o}C)	Travel Speed (m/hr)	Flux
1	168.8	175.7	187.8	193.6	185.2	188.9
2	197.3	192.2	177.7	168.5	175.6	181.6
3		181.3	183.7	187.0	188.3	178.6
Delta	28.4	16.5	10.1	25.1	12.6	10.3
Rank	**1**	**3**	**6**	**2**	**4**	**5**

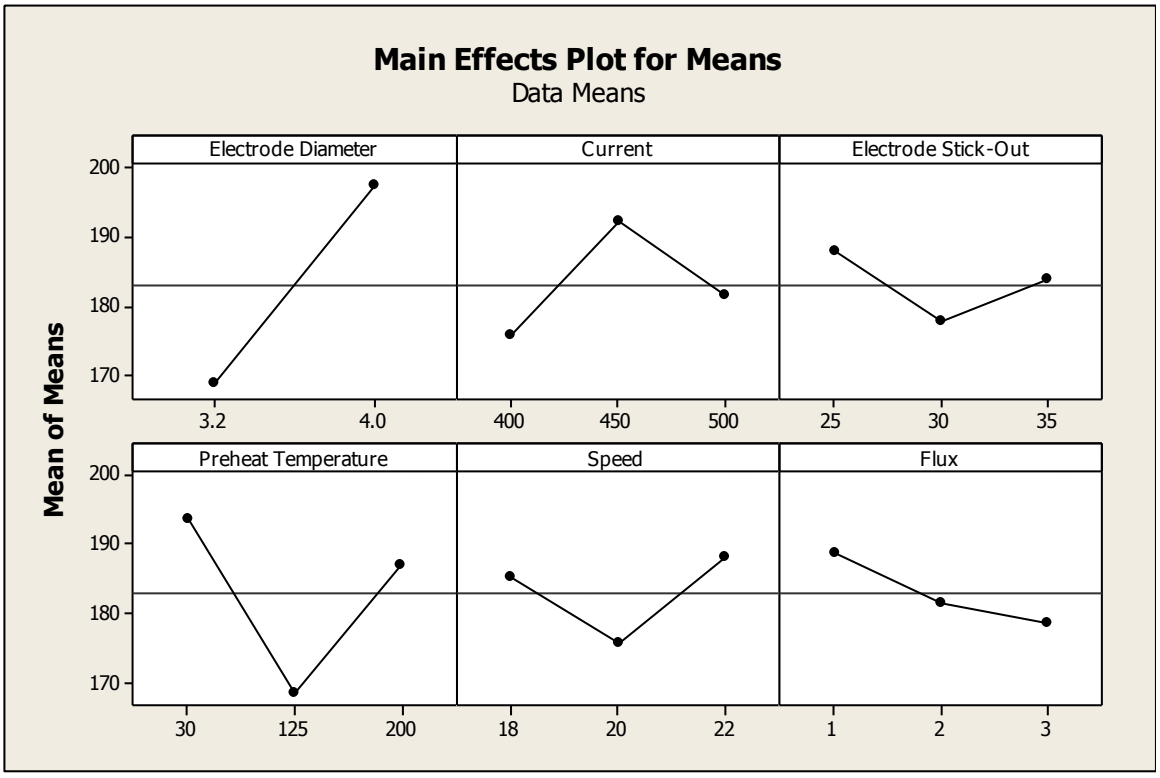

FIGURE 9.3 Main effect plot for tensile test at room temperature

9.3 OPTIMAL DESIGN FOR TOUGHNESS AT ROOM TEMPERATURE

In this experimental analysis, the main effect plot in figure 9.3 has been used to estimate the toughness in optimal conditions. From table 9.3, it can be concluded that electrode diameter and preheat temperature are the most significant factors. In order to obtain maximum toughness at room temperature, the electrode diameter should be 4mm, preheat temperature should be 30^{o}C i.e. No preheat temperature has been chosen. Confidence interval predict with 95 % confidence so that value of toughness at room temperature at optimal design conditions would be 207.85 ± 15.210 J.

Mean value of toughness at Room Temperature is given by-

$\mu_{\emptyset_1 T_1} = \overline{\emptyset_2} + \overline{T_1} - 1\overline{T}$

= 197.3+193.6- (1x183.050)

=207.85 J

C.I. = $\sqrt{\frac{f\alpha : v1 : v2 \; X \; Ve}{neff}}$

v2 = DOF for error = 14

Where $f\,\alpha{:}v1{:}v2 = f\,0.05{:}1{:}14 = 4.60$

Variance = $Ve = \frac{3168.5}{14} = 226.32$

$n_{eff} = \frac{18}{1+\mathrm{DOF}_{\emptyset_2 T_1}} = 4.5$

C.I. = 15.210

So, the confidence interval around toughness at room temperature is given by **207.85 ± 15.210 J.**

9.4 ANOVA FOR TOUGHNESS AT -40^{o}C

Table 9.5, column no. 5 consists of the average values of toughness at -40^{o}C for the eighteen trials with two repetitions. The experimental results for toughness were analyzed using ANOVA and is given in the Table 9.5. An ANOVA table 9.6 show that p value for current is 0.033 and value of electrode stick-out is 0.028 i.e. less than 0.05 indicates thereby that current and electrode stick-out are the most significant factor for the toughness at -40^{o}C. In last row of table 9.7 have been ranks for various factors. In table 9.7 current with the highest rank 1 and is the most significant factor and electrode diameter with its lowest rank is least significant in affecting the toughness at -40^{o}C. Main effect plots are shown in figure 9.5 shows the variation in the toughness at -40^{o}C. It could be seen from the figure 9.5 that current causes the most significant change in the toughness with change in electrode stick-out. Electrode diameter, preheat temperature, flux and travel speed have very low effect on toughness at -40^{o}C.Figure 9.4 shows that trial no.17 has maximum toughness at -40^{o}C due to high value of current.

TABLE 9.5 Toughness values at -40^{o}C temperature

Exp. No.	Contributing Factors	Charpy Test at -40 ^{o}C Temp. (J) Reading 1	Charpy Test at -40 ^{o}C Temp. (J) Reading 2	Average value of charpy test at -40 ^{o}C Temp.
1	Ø1, C1, D1, T1,S1, F1,	137.340	127.530	132.435
2	Ø1, C1, D2,T2,S2, F2,	137.340	109.872	123.606
3	Ø1, C1, D3, T3,S3, F3	107.910	100.062	103.986
4	Ø1, C2, D1, T1, S2, F2	166.770	172.656	169.713
5	Ø1, C2, D2, T2, S3, F3	127.530	93.195	110.363
6	Ø1, C2, D3, T3, S1, F1	140.283	109.872	125.077
7	Ø1, C3, D1, T2, S1, F3	149.112	129.492	139.302
8	Ø1, C3, D2, T3, S2, F1	142.245	159.903	151.074
9	Ø1, C3, D3, T1, S3, F2	127.530	147.150	137.340
10	Ø2, C1, D1, T3, S3,F2	168.732	107.910	138.321
11	Ø2, C1, D2, T1, S1, F3	132.435	109.872	121.154
12	Ø2, C1, D3, T2, S2, F1	100.062	119.682	109.872
13	Ø2, C2, D1, T2, S3, F1	166.770	186.390	176.580
14	Ø2, C2, D2, T3, S1, F2	117.720	88.290	103.005
15	Ø2, C2, D3, T1, S2, F3	132.435	139.302	135.868
16	Ø2, C3, D1, T3, S2, F3	156.960	196.200	176.580
17	Ø2, C3, D2, T1, S3, F1	171.675	196.200	183.938
18	Ø2, C3, D3, T2, S1, F2	143.226	119.682	131.454

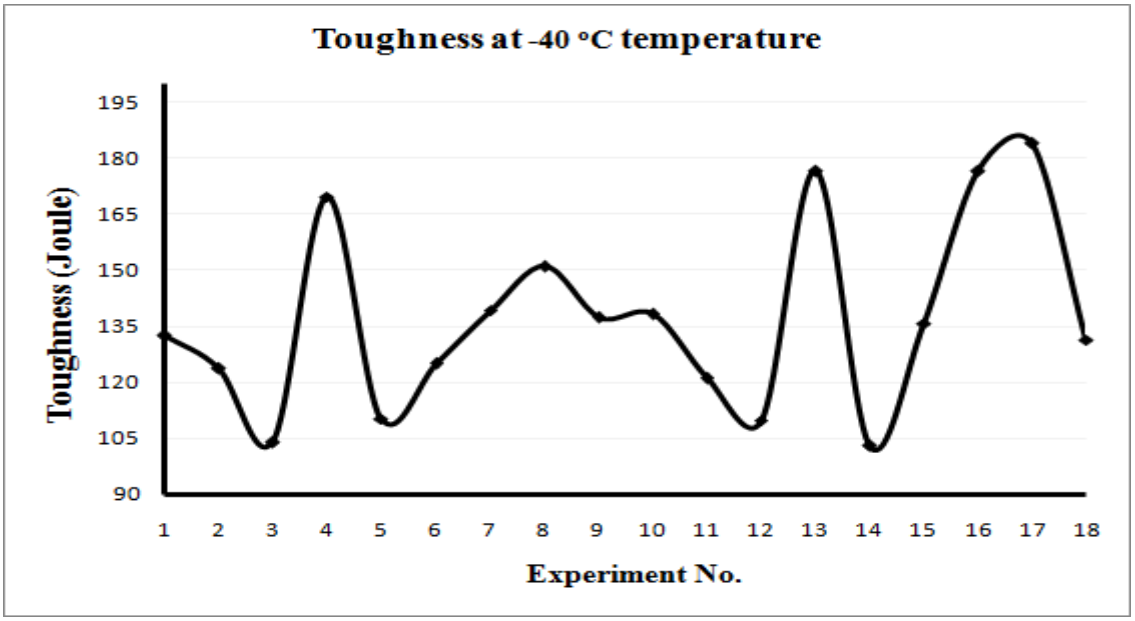

FIGURE 9.4 Variation in toughness at -40 ^{o}C

TABLE 9.6 Analysis of variance for means toughness at -40^{o}C

Source	DF	Seq SS	Adj SS	Adj MS	F	P
Electrode Diameter (mm)	1	390.8	390.8	390.8	1.67	0.244
Current (Ampere)	2	3020.0	3020.0	1510.0	6.44	**0.032**
Electrode Stick-Out (mm)	2	3213.5	3213.5	1606.8	6.85	**0.028**
Preheat Temperature (^{o}C)	2	822.6	822.6	411.3	1.75	0.251
Travel Speed (m/hr)	2	1274.8	1274.8	637.4	2.72	0.144
Flux	2	798.9	798.9	399.5	1.70	0.259
Residual Error	6	1406.8	1406.8	234.5		
Total	17	10927.5				

TABLE 9.7 Response table for means of toughness at -40 ^{o}C

Level	Electrode Diameter (mm)	Current (amp)	Electrode Stick-Out (mm)	Preheat Temperature (^{o}C)	Travel Speed (m/hr)	Flux
1	132.5	121.6	155.5	146.7	125.4	146.5
2	141.9	136.8	132.2	131.9	144.5	133.9
3		153.3	123.9	133.0	141.8	131.2
Delta	9.3	31.7	31.6	14.9	19.0	15.3
Rank	**6**	**1**	**2**	**5**	**3**	**4**

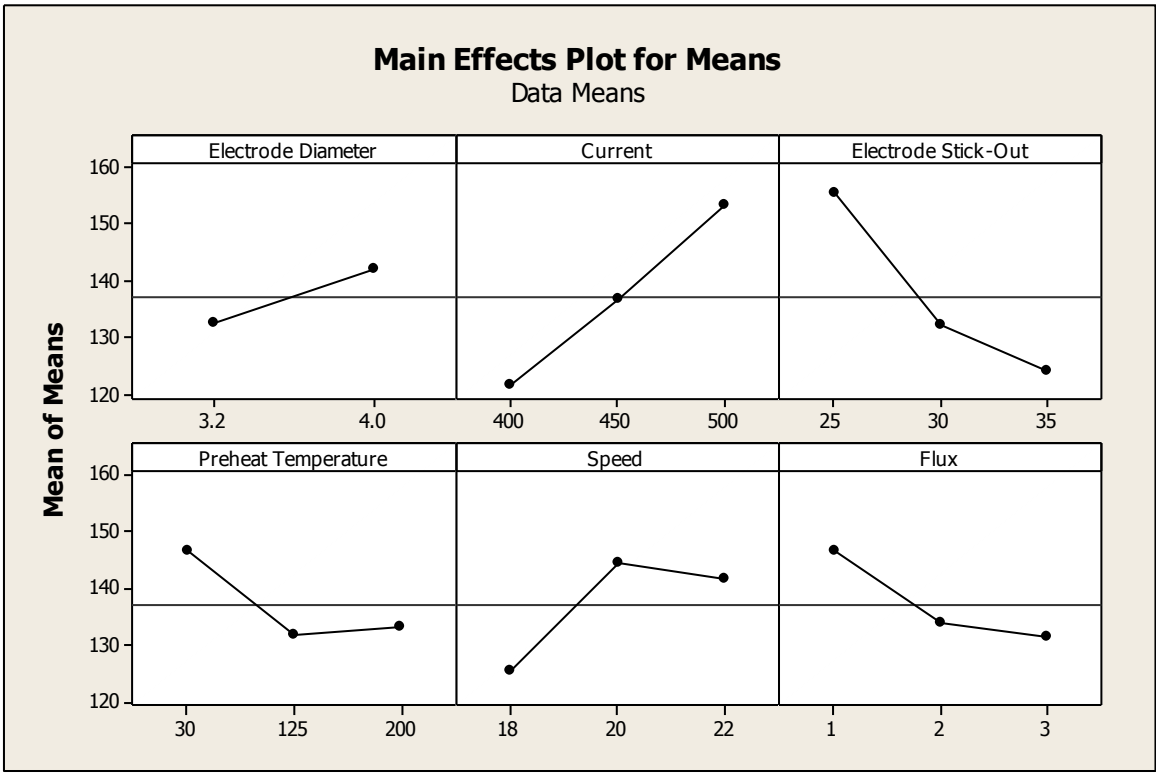

FIGURE 9.5 Main effect plot for mean at -40 ^{o}C

9.5 OPTIMAL DESIGN FOR TOUGHNESS AT -40 ^{O}C

In this experimental analysis, the main effect plot in Figure 9.5 has been used to estimate the toughness in optimal conditions. From table 9.6, it can be concluded that current and electrode stick-out is the two most significant factors. In order to obtain maximum toughness at -40^{o}C, current should be 500 A and electrode stick-out should be 25 mm has been chosen. Confidence interval predict with 95 % confidence so that value of toughness at -40 ^{o}C at optimal design conditions would be 171.597 ± 21.642 J.

Mean value of toughness at -40 ^{o}C is given by-

$\mu_{C_3D_1} = \overline{C_3} + \overline{D_1} - 1\overline{T}$

= 153.3+155.5-(1x137.203)

= 171.597

Confidence Interval around the estimated mean toughness

C.I. = $\sqrt{\frac{f\alpha:v1:v2\ X\ Ve}{neff}}$

v2 = DOF for error = 13

Where $f\,\alpha{:}v1{:}v2$ = 4.67

Variance = $Ve = \frac{4694}{13} = 361.07$

$n_{eff} = \frac{18}{1+\mathrm{DOF}_{C_3D_1}} = 3.6$

C.I=21.642

So, the confidence interval around toughness at -40 ^{o}C is given by **171.597 ± 21.642 J**.

9.6 DISCUSSION OF TOUGHNESS TEST RESULTS

It is clear from Figure 9.2 that maximum toughness at room temperature is obtained from specimen no. 13 i.e. 221.215 J. It is concluded that at room temperature specimen no. 13 has maximum toughness value. The mean toughness at room temperature using the optimal condition would be 207.85 ± 15.210 J with electrode diameter should be 4 mm, preheat temperature should be 30 ^{o}C .

It is clear from Figure 9.4 that maximum toughness at -40 ^{o}C is obtained from specimen no. 17 i.e. 131 J. It is concluded that at room temperature specimen no. 17 enhances toughness value. The mean toughness at -40 ^{o}C using the optimal condition would be 171.597 ± 21.642 J with current should be 500 A and electrode stick-out should be 25 mm.

CHAPTER-10

RESULTS AND ANALYSIS OF MICROHARDNESS TEST

10.1 MICROHARDNESS TEST

The microhardness test details for base metal are shown in table 10.1 and corresponding plots is shown in figure 10.1 for comparison.

TABLE 10.1 Microhardness values of base metal at different region

Base Metal	Indent Load (gm)	Dwell Time (sec)	Hardness Value at -10 mm from Centre (HVN)	Hardness Value at -5 mm from Centre (HVN)	Hardness Value at Centre (HVN)	Hardness Value at 5 mm from Centre (HVN)	Hardness Value at 10 mm from Centre (HVN)
	1000	20	74.50	76.05	78.15	75.05	77.70

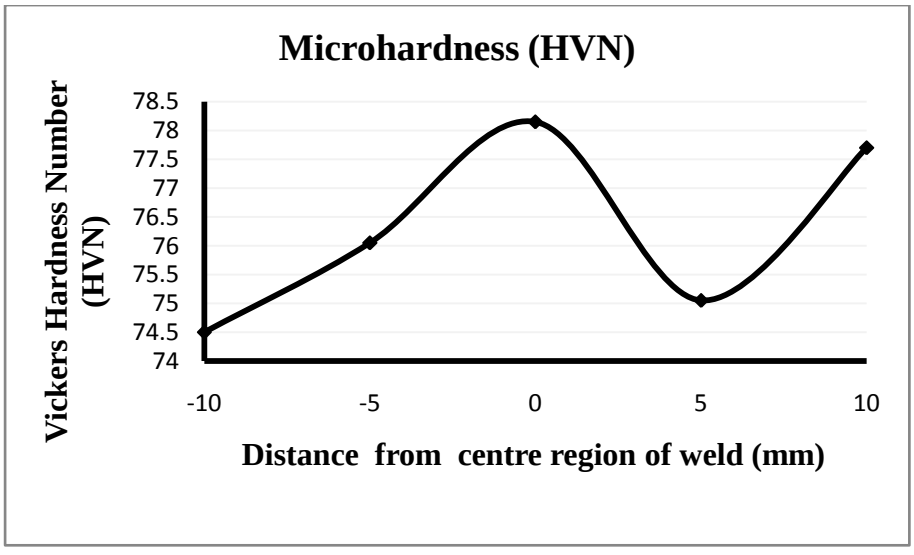

FIGURE 10.1 Microhardness of base metal

For all the 18 sets of experiment, the microhardness test summery is shown in table 10.2 and corresponding plots at different region are shown below sequentially in figure 10.2 (i-xviii).

TABLE 10.2 Microhardness values at weld region (indent load 1 kg and dwell time 20 s)

Exp No.	Contributing Factors	Hardness Value at -10 mm from Weld Centre (HVN)	Hardness Value at -5 mm from Weld Centre (HVN)	Hardness Value at Weld Centre (HVN)	Hardness Value at 5 mm from Weld Centre (HVN)	Hardness Value at 10 mm from Weld Centre (HVN)
1	Ø1, C1, D1, T1,S1, F1	65.31	63.22	77.05	68.34	65.08
2	Ø1, C1, D2,T2,S2, F2	66.39	60.315	78.08	83.17	83.55
3	Ø1, C1, D3, T3,S3, F3	71.79	78.95	80.93	77.53	78.77
4	Ø1, C2, D1, T1, S2, F2	66.8	66.89	65.28	73.05	68.07
5	Ø1, C2, D2, T2, S3, F3	70.97	65.15	66.71	73.124	74.39
6	Ø1, C2, D3, T3, S1, F1	75	75.42	65.35	62.36	66.75
7	Ø1, C3, D1, T2, S1, F3	63.22	59.38	63.24	59.26	62
8	Ø1, C3, D2, T3, S2, F1	67.12	69.49	68.91	73.12	71.88
9	Ø1, C3, D3, T1, S3, F2	64.16	58.45	62.86	59.6	61.02
10	Ø2, C1, D1, T3, S3,F2	64.37	75.74	72.71	77.42	78.22
11	Ø2, C1, D2, T1, S1, F3	78.95	71.64	63.37	68.7	65.71
12	Ø2, C1, D3, T2, S2, F1	66.71	73.12	65.31	64.98	64.03
13	Ø2, C2, D1, T2, S3, F1	71.25	66.94	71.05	76.24	62.76
14	Ø2, C2, D2, T3, S1, F2	60.55	61.87	66.122	60.31	64.52
15	Ø2, C2, D3, T1, S2, F3	72.71	71.28	71.42	73.917	69.28
16	Ø2, C3, D1, T3, S2, F3	61.63	61.38	60.67	62.35	65.62
17	Ø2, C3, D2, T1, S3, F1	63.88	64.87	68.34	63.01	66.75
18	Ø2, C3, D3, T2, S1, F2	74.28	78.45	70.22	70.44	73.7

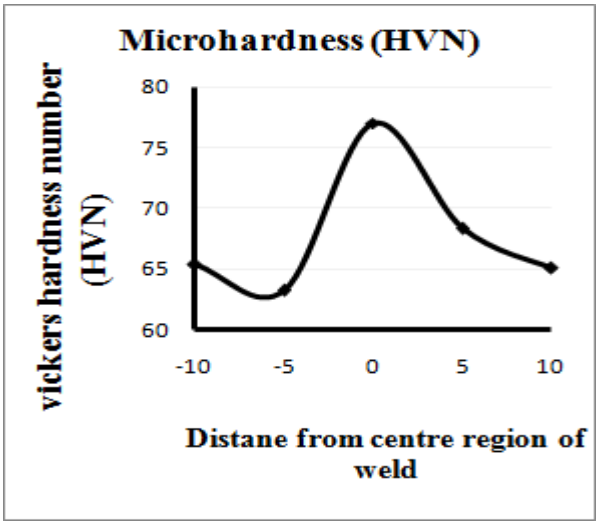

(i) Trial No. 1

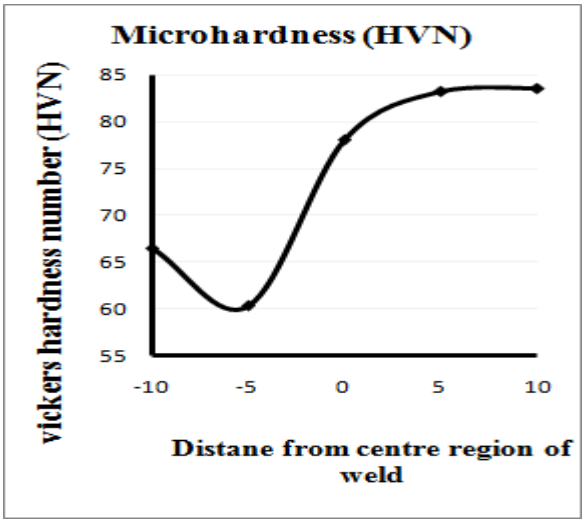

(ii) Trial No. 2

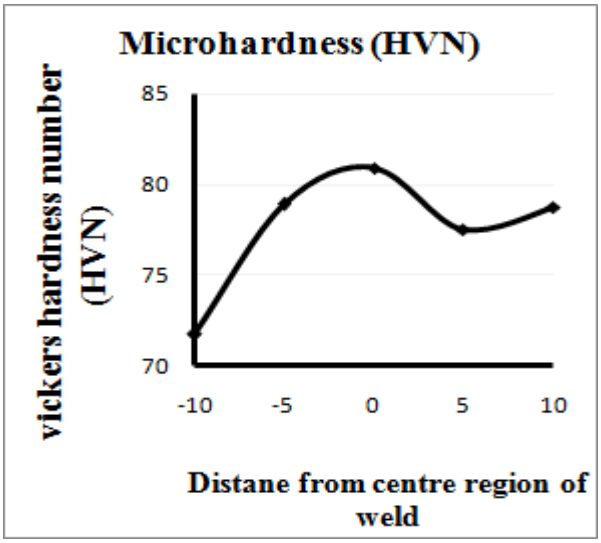

(iii) Trial No. 3

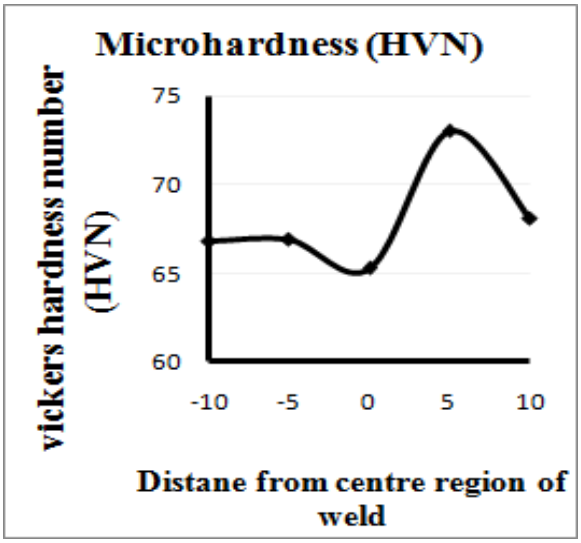

(iv) Trial No. 4

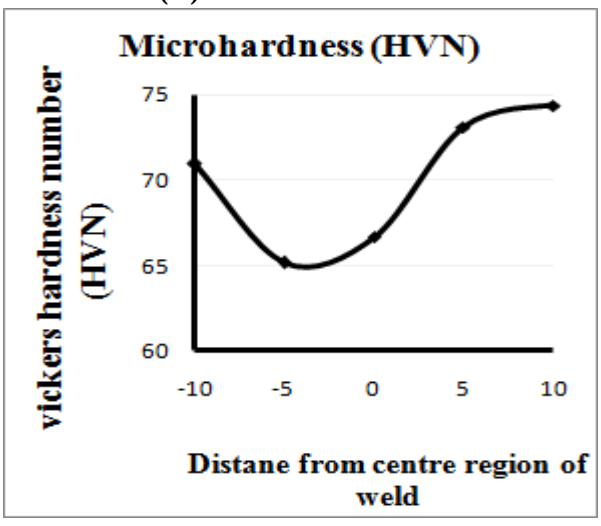

(v) Trial No. 5

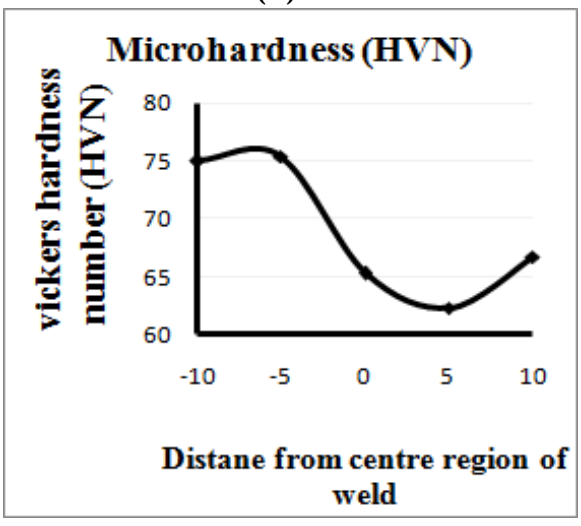

(Vi) Trial No. 6

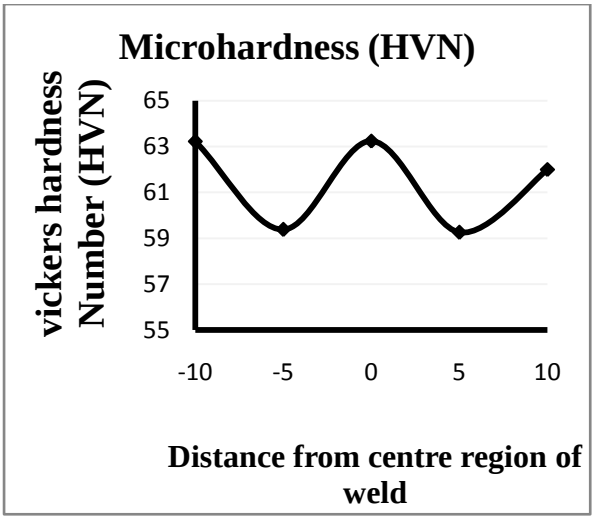

(vii) Trial No. 7

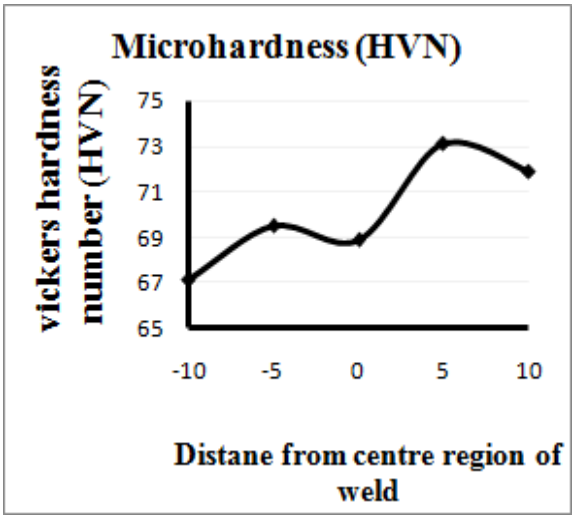

(Viii) Trial No. 8

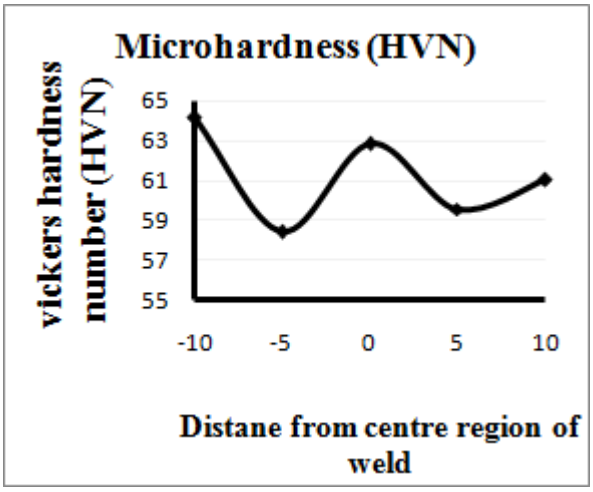

(ix) Trial No. 9

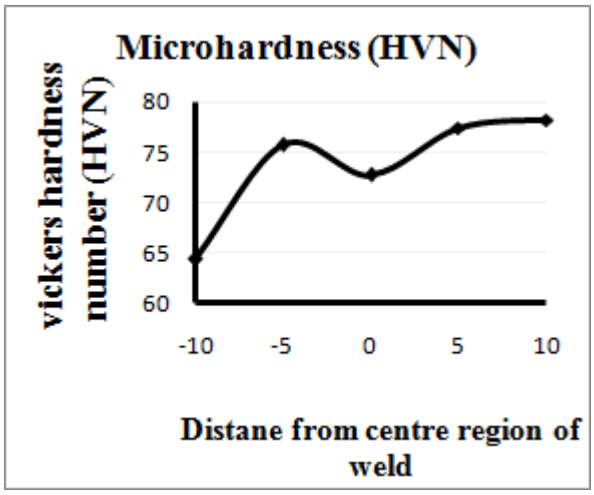

(x) Trial No. 10

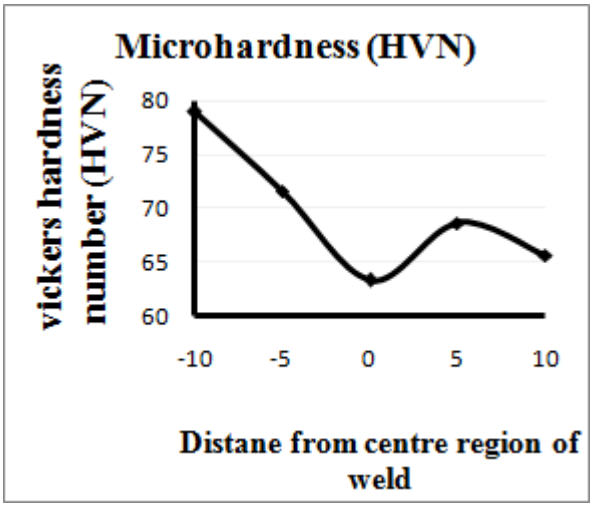

(xi) Trial No. 11

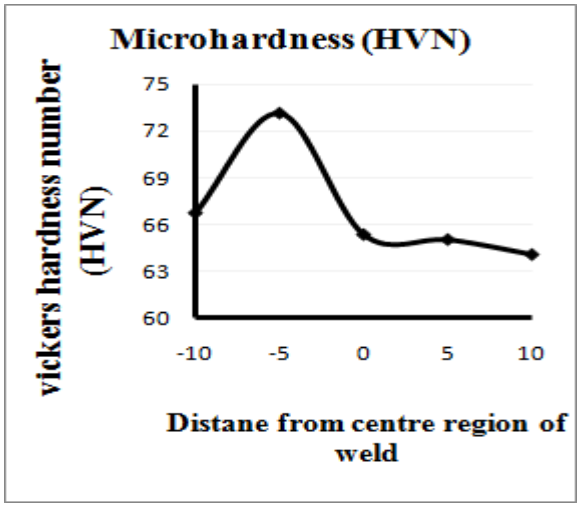

(xii) Trial No. 12

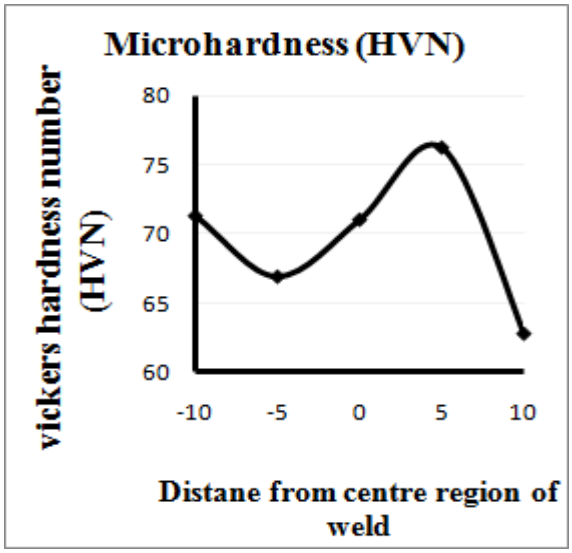

(xiii) Trial No. 13

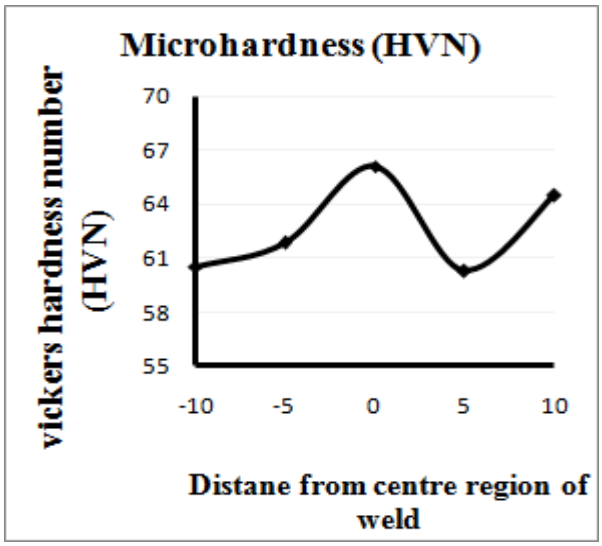

(xiv) Trial No. 14

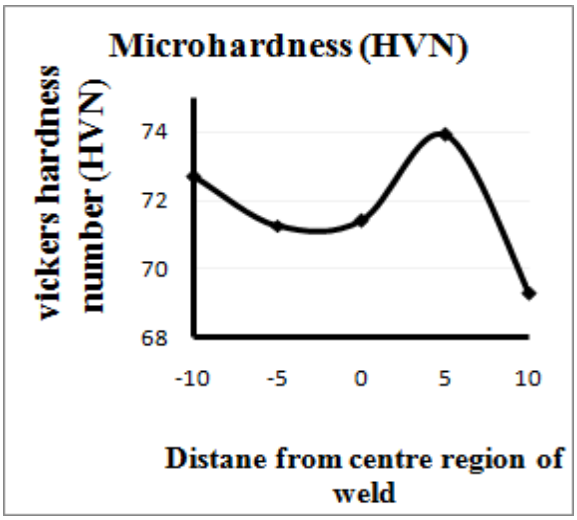

(xv) Trial No. 15

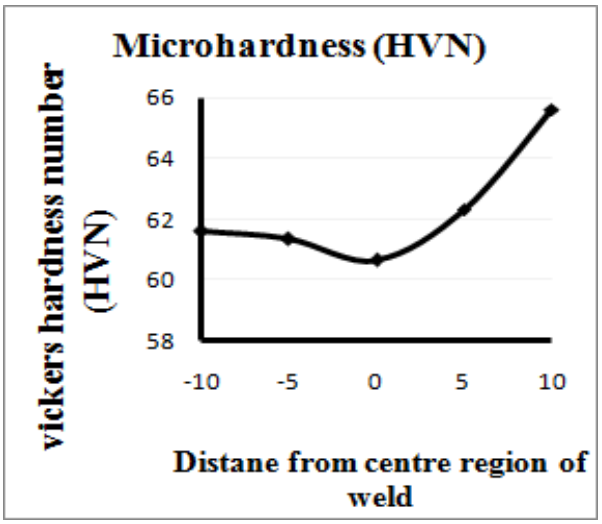

(xvi) Trial No. 16

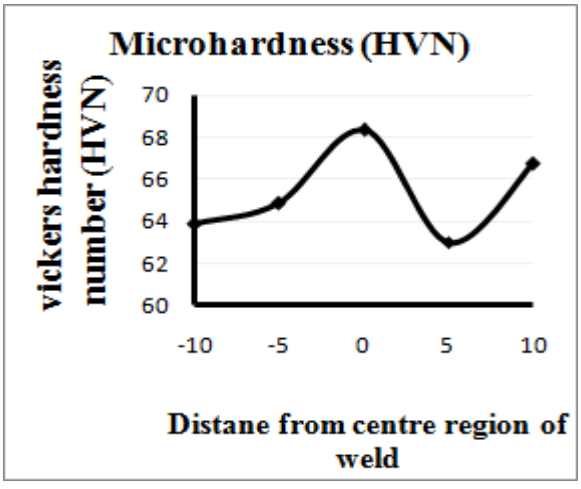

(xvii) Trial No. 17

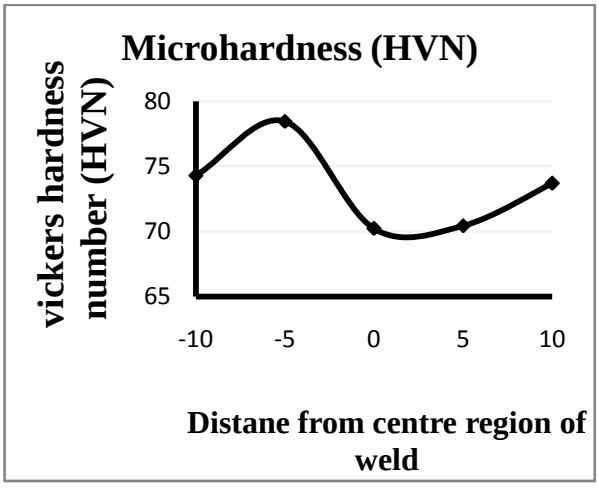

(xviii) Trial No. 18

FIGURE 10.2 Variation of microhardness of different trials (i-xviii) at weld region

In order to summarize the results of microhardness test, for all 18 sets of experiments, the variation in microhardness value at centre, 5 mm, -5 mm, 10 mm and -10 mm from weld centre is shown in table 10.2.

From table 10.2, it was observed that

- At weld centre, maximum microhardness of 80.93 HVN was obtained from specimen no. 3 and minimum microhardness of 60.67 HVN was obtained from specimen no. 16.
- At 5 mm from weld centre, maximum microhardness of 83.17 HVN was obtained from specimen no. 2 and minimum microhardness of 59.6 HVN was obtained from specimen no. 9.
- At -5 mm from weld centre, maximum microhardness of 78.95 HVN was obtained from specimen no. 3 and minimum microhardness of 58.45 HVN was obtained from specimen no. 9.
- At 10 mm from weld centre, maximum microhardness of 83.55 HVN was obtained from specimen no. 2 and minimum microhardness of 62.0 HVN was obtained from specimen no. 7.
- At -10 mm from weld centre, maximum microhardness of 78.95 HVN was obtained from specimen no. 11 and minimum microhardness of 60.55 HVN was obtained from specimen no. 14.

10.2 ANOVA FOR MICROHARDNESS AT WELD REGION

Table 10.2, column no. 5 consists of the values of microhardness at weld region for the eighteen trials. The experimental results for microhardness at weld region were analyzed using ANOVA and the response value for all six variables is given in table 10.3. In table 10.3 welding current with the highest rank 1 and is the most significant factor and electrode diameter with its lowest rank is least significant in affecting the microhardness. Main effect plots are shown in Figure 10.3 shows the variation in the microhardness with the change in the input factors i.e. electrode diameter, current, electrode stick-out, travel speed, preheat temperature and flux. It could be seen from the Figure 10.3 that welding current causes the most significant change in the microhardness with change in current. As the welding current increases from 400 Ampere to 500 Ampere, microhardness will also decrease. As the electrode stick-out increases from 25 to 35 mm, microhardness will increase. The change in

speed and preheat temperature also has some effect on the variation in the microhardness. Electrode diameter and flux have very minor effect on microhardness.

TABLE 10.3 Response table for mean of microhardness at weld region

Level	Electrode Diameter (mm)	Current (amp)	Electrode Stick-Out (mm)	Preheat Temperature (^{o}C)	Travel Speed (m/hr)	Flux
1	68.83	71.65	67.15	67.30	67.33	68.12
2	68.37	68.52	68.70	69.28	68.88	68.89
3		65.64	69.96	69.23	69.60	68.80
Delta	0.46	6.01	2.81	1.98	2.27	0.77
Rank	**6**	**1**	**2**	**4**	**3**	**5**

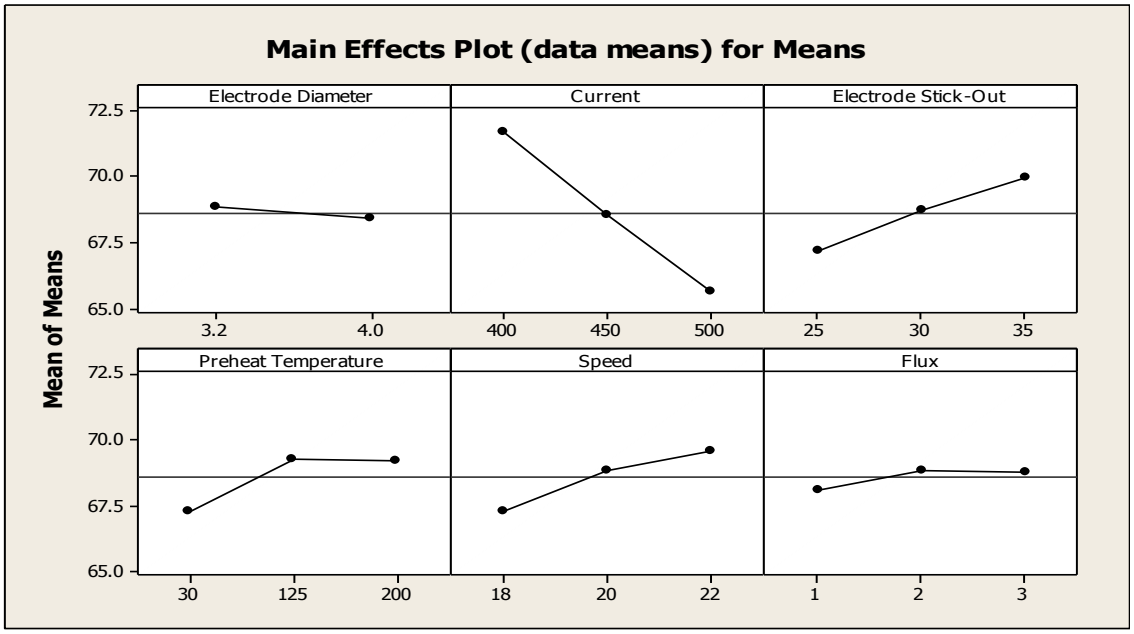

FIGURE 10.3 Main effect plot for microhardness at weld region

10.3 DISCUSSION OF MICROHARDNESS

There are five readings at different location were taken and analysis was done at the average of weld region. It is clear from table 10.2 that maximum microhardness (Vickers hardness number) in weld centre is obtained from specimen no. 3 i.e. 80.93 hvn. The microhardness would be maximum when, flux should be of type 2 i.e. GEE FLUX 544 (Basic), current should be 400 Ampere, speed should be 22m/hr and electrode stick-out should be 35 mm.

CHAPTER-11

SUMMARY, CONCLUSIONS AND FUTURE SCOPE

11.1 RESULTS

The effect of six input factors was studied on the bead geometry, tensile strength, toughness, microhardness, radiography testing, metallurgical behaviour and chemical composition using the L18 Taguchi experimental design.

TABLE 11.1 Table for mean value of results

Experiment No.	Mean Tensile Strength (N/mm^2)	Mean Bead Height (mm)	Mean Bidth width (mm)	Mean Toughness at room temperature (J)	Mean Toughness at -40 ^oC (J)	Mean value of Microhardness at weld region (HVN)
1	550.22	2.77	24.60	176.085	132.435	67.8000
2	558.56	3.33	23.15	139.300	123.606	74.3010
3	581.18	2.80	22.07	177.070	103.986	77.5940
4	533.12	3.90	25.52	190.805	169.713	68.0180
5	599.91	2.71	18.85	146.169	110.363	70.0688
6	530.15	3.93	24.41	193.255	125.077	68.9760
7	632.50	3.17	23.70	152.544	139.302	61.4200
8	613.35	4.13	21.81	158.922	151.074	70.1040
9	622.31	4.20	23.74	185.405	137.340	61.2180
10	634.53	3.10	17.88	187.370	138.321	73.6920
11	541.67	2.61	25.42	202.572	121.154	69.6740
12	597.47	2.75	18.46	171.675	109.872	66.8300
13	625.57	3.85	19.75	221.215	176.580	69.6480
14	542.90	3.55	22.52	206.988	103.005	62.6744
15	616.20	2.60	28.45	194.483	135.868	71.7214
16	640.70	3.50	24.22	198.653	176.580	62.3300
17	637.79	3.22	21.84	212.387	183.938	65.3700
18	662.23	4.48	24.37	180.013	131.454	73.4180

Bead geometry, tensile strength, toughness at room temperature, toughness at -40 ^{o}C and microhardness at weld region were measured as the response parameters. ANOVA was completed for all the responses to analyze the significance of the input factors. Regression equation was developed to predict the relationship amongst the dependent and independent variables for tensile strength. Main effect plots for mean values has been developed and analyzed. Table 11.1 shows the value of responses measured.

11.1.1 Tensile Strength

- Welding current and electrode diameter was found as the most significant factor with p value of 0.007 and 0.030 respectively. Another factor did not show any significant effect on tensile strength. Highest and lower value of tensile strength was observed for experiment no. 18 and 6 respectively.
- The mean tensile strength using the optimal condition would be 650.23 ± 30.64 N/mm^2 with electrode diameter should be 4 mm, welding current should be 500 Ampere and travel speed should be 15 m/hr.
- Regression analysis and equation has been developed for tensile strength.

11.1.2 Bead width

- For bead width preheat temperature and travel speed would be used to be the most significant factor with both has same p value of 0.031. Highest value of bead width was found for experiment no. 15 and lower value of bead width was found for experiment no. 17.
- ANOVA for S/N ratio for bead width also shows the significance of preheat temperature and travel speed with p value of 0.042 and 0.037 respectively.
- The predicted value of bead width with 95% confidence in optimal design,(preheat temperature 125 ^{o}C and travel speed should be 22m/hr) was 19.25 $\pm$ 2.11mm.

11.1.3 Bead height

- For bead height current and flux would be used to be the most significant factor with p value of 0.026 and 0.029 respectively. Highest value of bead height was found for experiment no. 18 and lower value of bead height was found for experiment no. 15.
- ANOVA for S/N ratio for bead height also shows the significance of current and flux with p value of 0.021and 0.022 respectively.

- The predicted value of bead width with 95% confidence in optimal design,(400 ampere and flux should be type 3 i.e. AUTOMELT B31) was 2.43 ± 0.3872 mm.

11.1.4 Toughness at Room Temperature

- Electrode diameter and preheat temperature was found as the most significant factor with p value of 0.005and 0.048 respectively. Highest and lower value of toughness at room temperature was observed for experiment no. 13 and 2 respectively
- The mean toughness at room temperature using the optimal condition would be 207.85 ± 15.210 J with electrode diameter should be 4 mm, preheat temperature should be 30^{o}C i.e. no preheat temperature.

11.1.5 Toughness at -40 ^{o}C

- Current and electrode stick-out was found as a most significant factor with p value of 0.032 and 0.028. Highest value of toughness at -40 ^{o}C temperature was observed for experiment no. 13 and 16 respectively
- The mean toughness at -40 ^{o}C temperature was estimated be 171.597 ± 21.642 J at 95% confidence.
- For optimal value of toughness at -40 ^{o}C temperature, current should be set higher current at 500 ampere and electrode stick-out should be 25 mm.

11.1.6 Microhardness at weld region

- Current and electrode stick-out was found as the most significant factors that affect microhardness at weld region.
- As the welding current increases from 400 to 500 A, microhardness will also decrease. As the electrode stick-out increases from 25 to 35mm, microhardness will increase.
- The microhardness would be maximum for experiment no.3 when, electrode diameter should be 3.2 mm, preheat temperature should be 200 ^{o}C, flux should be of type 3 i.e. AUTOMELT B31 (Neutral), current should be 400 Ampere, travel speed should be 22m/hr and electrode stick-out should be 25 mm.

11.1.7 Chemical Composition

- The percentage change in phosphorous and manganese, silicon were increasing in weld region but nickel, copper and chromium contents were decreasing whereas for sulphur and carbon shows the mixed trend in weld region**.**

11.1.8 Radiography Testing

- In overall it observed that welded region with current 500 Ampere having no welding imperfection i.e. surface cracks, porosity; cracks found in the specimen except no.16. Based on radiography results for better quality of joints, it suggested that should be set at its higher current for greater than 25mm thickness plate during submerged arc welding for improving the quality of weld region.

11.1.9 Micro structural study

- Microstructure with EDAX for welding zone has been taken for all the eighteen samples and effects of all the input parameters have been studied and results have been compiled in chapter 8 with detailed description of every trial condition with chemical composition in section 8.3.

11.2 CONCLUSIONS

The present study was carried out to study the effect of process parameters on weld joint quality during submerged arc welding of HSLA steel. The process parameters that has been considered for changing are current, travel speed, electrode diameter, flux composition, pre heating of workpiece and electrode stick-out were varied at different levels to optimize the process parameters. The following conclusions have been drawn from the experimental study:

- Welding current was found to be the most significant factor that affects the tensile strength, bead height toughness at -40 ^{o}C, quality of weld region and microhardness but did not show any significant affect on toughness at room temperature.
- Bead width is mainly affected by preheat temperature and travel speed and bead height is affected by current and flux.
- Tensile strength is majorly affected by current and electrode diameter, but did not show any significant effect on bead width. Tensile strength also had a significant effect on the microstructure.

- The flux composition did not show any significant affect on tensile strength, toughness, bead width and microhardness but had a major effect on bead height.
- Travel speed but had a major effect on bead width but did not show any significant effect on other process parameters.
- Preheating of workpiece did show significant effect on bead width, toughness at room temperature and electrode diameter was observed to have a direct relation to tensile strength and toughness at room temperature.
- Electrode stick-out has a significant effect on toughness at -40 ^{o}C and microhardness but did not show any significant effect on tensile strength and bead geometry.

11.3 FUTURE SCOPE

Following are some of the future recommendations on the basic of present study:

- Corrosion test, bending and reverse bending test etc. may also be carried along with other non-destructive tests like ultrasonic testing, liquid penetrate testing etc.
- Multi-Response optimization and empirical modelling technique could be used for optimization during submerged arc welding.
- Effect of flux with different grade or basicity index, filler wire on the mechanical properties and chemical composition of welded joints may be carried out.
- Effect of post weld heat treatment (PWHT) has been studied by many researchers for various grades of steels. Same may also be carried out for HSLA steel.
- Study the Effect of metal powder addition in order to increase the mechanical properties by using tabular electrode.
- Modeling of submerged arc welding process can be carried out by using finite element packages or ANSYS software.

CHAPTER-12
REFERENCES

[1] **S. V. Nadkarni (1988),** "Modern arc welding technology", Advani-Oerlikon limited.

[2] www.weldguru.com/images/fig09-48.gif, downloaded on Dated-Feb, 10-2013.

[3] **R. S. Parmar (2008),** "Welding processes and technology", 2th Ed.

[4] **Larry Jeffus (2004),**"Welding Principles and Application", *Thomsom Delmer Learning.*

[5] **Jonathan S. Ogborn, Lincoln Electric Company (1993)**,"Welding, Brazing and Soldering", ASM Handbook, Volume-6, pp. 618-641, ISBN 0-87170-377-7(V.1)

[6] **Vincent Van Der Mee, Fred Neessen (2007)**,"Development of High Strength Steel Consumables from Project to Product", Lincoln Smitweld, Netherlands.

[7] **Kanjilal P., Pal T.K., and Majumdar S.K. (2006),**"Combined effect of flux and welding parameters on chemical composition and mechanical properties of submerged arc weld metal". *Journal of Materials Processing Technology*, Vol.171, pp. 223–231.

[8] **Prasad K. and Dwivedi D.K. (2006),**"Some investigations on microstructure and mechanical properties of submerged arc welded HSLA steel joints*", Journal of Advanced Manufacturing Technology*, Vol.198, pp. 475-483.

[9] **Paniagua-Mercado Ana Ma., Lopez-Hirata Victor M. and Munoz Maribel L. Saucedo (2005),**"Influence of the chemical composition of flux on the microstructure and tensile properties of submerged-arc welds", *Journal of Materials Processing Technology*, Vol.169, pp. 346–351.

[10] **Karaoglu S. and Secgin A. (2008),**"Sensitivity analysis of submerged arc welding process parameter", *Journal of materials processing technology,*Vol.202, pp. 500–507

[11] **Lee C.S., Chandel R.S. and Seow H.P. (2000),**"Effect of Welding Parameters on the Size of Heat Affected Zone of Submerged Arc Welding", *Materials and Manufacturing Processes,* Vol. 15, No.5, pp. 649-666.

[12] **Bhole S.D., Nemade J.B, Collins L. and Liu Cheng (2006),**"Effect of nickel and molybdenum additions on weld metal toughness in a submerged arc welded HSLA line-pipe steel", *Journal of Materials Processing Technology,* Vol.173, pp. 92–100.

[13] **Sahni V., Singh Kulwant and Pandey S. (2009),** "Waste to Wealth: Reuse of Slag as a Flux in Submerged Arc Welding" *Asian Journal of Chemistry* Vol. 21, No. 10 S072-075.

[14] **Nowacki J. and Rybicki Pawel (2005),**"The influence of welding heat input on submerged arc welded duplex steel joints imperfections" *Journal of Materials Processing Technology,* Vol.164–165, pp.1082–1088.

[15] **Shen S., Oguocha I.N.A. and Yannacopoulos S. (2011),**"Effect of heat input on weld bead geometry of submerged arc welded ASTM A709 Grade 50 steel joints", *Journal of Materials Processing Technology*, Vol.120-131, pp. 1043– 1049.

[16] **Beidokhti B., Koukabi A.H. and Dolati A. (2009),**"Effect of titanium addition on the microstructure and inclusion formation in submerged arc welded HSLA pipeline steel." *Journal of Materials Processing Technology*, Vol.209, pp. 4027–4035.

[17] **Yayla P., Kaluc E. and Ural K. (2007),**"Effects of welding processes on the mechanical properties of HY 80 steel weldment", *Materials and Design* ,Vol.28, pp. 1898–1906

[18] **Tuseka J. and Suban M. (2003), "**High-productivity multiple-wire submerged-arc welding and cladding with metal-powder addition", *Journal of Materials Processing Technology*, Vol.133, pp. 207–213

[19] **Gulenc Behcet and Kahraman Nizamettin (2003**), "Wear behaviour of bulldozer rollers welded using a submerged arc welding process", *Materials and Design,* Vol. 130, pp. 537–542.

[20] **Ravi S., Balasubramaniana V. and Nasser S. N. (2005),**"Influences of post weld heat treatment on fatigue life prediction of strength mis-matched HSLA steel welds", *International Journal of Fatigue*, Vol. 27, pp. 547–553

[21] **Lua S.P, Kwon O.Y, Kima T.B. and Kima K.H. (2004), "**Microstructure and wear property of Fe–Mn–Cr–Mo–V alloy cladding by submerged arc welding", *Journal of Materials Processing Technology*, Vol.147, pp. 191–196

[22] **Pandey N.D. and Bharti A. (1994),**"Effect of submerged arc welding parameters and fluxes on element transfer behaviour and weld-metal chemistry", *Journal of Materials Processing Technology,* Vol. 40, pp. 195-211.

[23] **Kumaresh babu S.P. and Natranjan S. (2008),"**Influence of heat input on high temperature weldment in submerged arc welded power plant steel", *Material and design*, Vol. 29, pp. 1036-1042.

[24] **Datta S., Bandyopadhyay A. and Pal P.K. (2008),** "Modelling and optimization of features of bead geometry including percentage dilution in submerged arc welding using mixture of fresh flux and fused slag", *Int. Journal Adv. Manufacturing Technology*, Vol.36, pp. 1080–1090.

[25] **Chandel R. S., Seow H. P. and Cheong F. L. (1998),**"Effect of metal powder addition on mechanical properties of submerged arc welds", *Journal of Materials Science Letters*, Vol. 17, pp. 1785-1786.

[26] **Bang K.S., Park C., Jung H.C. and Lee J.B. (2009),**"Effects of Flux Composition on the Element Transfer and Mechanical Properties of Weld Metal in Submerged Arc Welding" *Met. Mater. Int.,* Vol. 15, pp. 471-477.

[27] **Lucia O. B. Vera, Voorwald H.J.C., Neves N.D. and Bott I.S. (2001),**"Effects of a Postweld Heat Treatment on a Submerged Arc Welded ASTM A537 Pressure Vessel Steel", *JMEPEG, Vol.* 10, pp. 249–257.

[28] **Kumar V., Mohan N. and Khamba J.S. (2009),**"Development Of Cost Effective Agglomerated Fluxes From Waste Flux Dust For Submerged Arc Welding" *Proceedings of the world congress on engineering*,vol.1 WCE 2009, London, U.K.

[29] **Zrilic M., Grabulov V., Burzic Z., Arsic M. and Sedmak S. (2007),** "Static and impact crack properties of a high-strength steel welded joint" *International Journal of Pressure Vessels and Piping,* Vol. 84, pp. 139–150.

[30] **Kumar P., Batish A., Bhattacharya A., and R K Duvedi (2010), "**Effect of process parameters on micro hardness and microstructure of heat affected zone in submerged arc welding", *Proceedings of the Institution of Mechanical Engineers,* Part B: *Journal of Engineering Manufacture,* Vol. 225, pp. 711-721.

[31] **Ma C.,Yun P. and Zhiling Tian (2002),**"Microstructure and Properties of Welding Heat-affected Zone of HCM12A Steel", *State Key Laboratory of Advanced Steel Processes and Products China Iron & Steel Research Institute Group,* Beijing 100081, China.

[32] **Singh K. and Pandey S. (2009),**"Recycling of slag act as in Submerged Arc Welding," *Resources, Conservation and Recycling,* Vol. 53, pp. 552-558.

[33] **Shafeek H.I.,Gadelmawla E.S., Abdel-Shafy A.A. and Elewa I.M. (2004),** "Assessment of welding defects for gas pipeline radiographs using computer vision," *NDT&E International,* Vol.37, pp. 291-299.

[34] **ASTM standard E8/E8M**-11,"Standard testing methods and definitions for mechanical testing of steel products, *ASTM International.*

[35] **Nandre S.J., Shitole S.J. and Ahire R.R (2012)**, "Study of Growth, EDAX, Optical properties and Surface Morphology of Zinc Tartrate Crystals",*Journal of Nano and Electronic Physics*,Vol.4, No4,04013 (4pp).

[36] **Ross, P.J. (1995),** "*Taguchi technique for quality engineering*," McGraw Hill publication.